

AMERICAN UNIVERSITY OF BEIRUT

EDGE FORCES IN METAL CUTTING: FUNDAMENTAL
ANALYSIS AND EXPERIMENTAL VERIFICATION

by
RIMAH SAMI AL ARIDI

A thesis
submitted in partial fulfillment of the requirements
for the degree of Master of Engineering
to the Department of Mechanical Engineering
of the Faculty of Architecture and Engineering
at the American University of Beirut

Beirut, Lebanon
December 2019

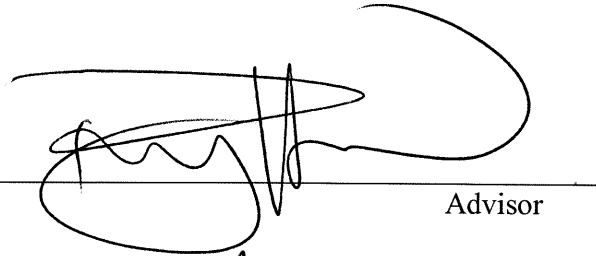
AMERICAN UNIVERSITY OF BEIRUT

EDGE FORCES IN METAL CUTTING: FUNDAMENTAL
ANALYSIS AND EXPERIMENTAL VERIFICATION

by
RIMAH SAMI AL ARIDI


Approved by:

Dr. Ramsey Hamade
Professor, Mechanical Engineering



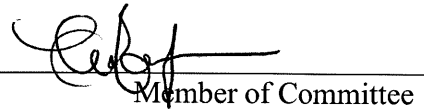
Advisor

Dr. Mu'Tasem Shehadeh
Associate Professor, Mechanical Engineering



Member of Committee

Dr. Elsa Maalouf
Associate Professor, Chemical Engineering



Member of Committee

Date of thesis defense: December 20, 2019

AMERICAN UNIVERSITY OF BEIRUT

THESIS, DISSERTATION, PROJECT RELEASE FORM

Student Name: Al Aridi Rimah Sami
Last First Middle

Master's Thesis Master's Project Doctoral

I authorize the American University of Beirut to: (a) reproduce hard or electronic copies of my thesis, dissertation, or project; (b) include such copies in the archives and digital repositories of the University; and (c) make freely available such copies to third parties for research or educational purposes.

I authorize the American University of Beirut, to: (a) reproduce hard or electronic copies of it; (b) include such copies in the archives and digital repositories of the University; and (c) make freely available such copies to third parties for research or educational purposes

after : **One ---- year from the date of submission of my thesis, dissertation, or project.**

Two ---- years from the date of submission of my thesis, dissertation, or project.

Three ---- years from the date of submission of my thesis, dissertation, or project.



10/02/2020

Signature

Date

ACKNOWLEDGEMENTS

Deepest thanks to Prof. Hamade for his unwavering support and guidance, his constant drive to research and innovates is genuinely inspiring. A special thanks to the thesis committee members Prof. Mu'Tasem Shehadeh and Prof. Elsa Maalouf for their insight and feedback. Thank you to the Engineering Faculty and Mechanical Engineering Department.

The author would like to thank the Engineering Shops, the biomedical laboratory and the Central Research Science Laboratory (CRSL), for their technical help.

The author acknowledges the financial support of the University Research Board (URB) at the American University of Beirut.

A special thanks to my family, friends and my Fiancée, without which none of my academic achievements would have been possible, supporting me through it all to become the man I am today.

AN ABSTRACT OF THE THESIS OF

Rimah Sami Al Aridi for

Master of Engineering
Major: Mechanical Engineering

Title: EDGE FORCES IN METAL CUTTING: FUNDAMENTAL ANALYSIS AND
EXPERIMENTAL VERIFICATION

In metal cutting, some of the generated forces do not contribute to chip formation and where chip is not developed per the classical cutting mechanics. Such forces are referred to as parasitic or plowing forces and are induced mainly as a result of the finite sharpness of the tool (cutting edge radius) and the tool's land (flank). Determining the magnitude of parasitic forces is essential to developing a better understanding of the mechanics and the physics in such applications that involve cutting at very small feed values (e.g., micro-machining and vibration-assisted- micro-machining). It is well recognized that plowing forces increase with tool wear.

This research estimates these forces while employing analytical and numerical simulations. Extensive experimental is utilized to verify the simulated values of these parasitic forces where an experiment is designed to measure these forces as function of several cutting parameters. The developed analytical model relates the parasitic forces to geometric and process parameters such as cutting-edge radius, feed, and speed

CONTENTS

ACKNOWLEDGEMENTS	V
ABSTRACT	VI
CONTENTS	VII
ILLUSTRATIONS	X
TABLES	XIX
NOMENCLATURE	XX
Chapter	Page
I. INTRODUCTION.....	1
II. METHODOLOGY	18
A. Experimental	18
1. Tool Setup and Force Measurements	18
2. Tool scanning and verification	21
3. Temperature Measurements	22
4. Process Parameters	22
a. Cutting Speeds	24
b. Test Matrix.....	24
B. Analytical solutions (using Matlab).....	27
1. Cutting regions & Force Diagram:	27
2. Region 1: Rubbing Phase	28
3. Region 2: Plowing Phase.....	30
4. Cutting Edge Radius and Tool wear:.....	37

C.	Numerical Modeling (FEM)	39
1.	Pre-Simulation	39
a.	Modeling of Shear Behavior:.....	39
b.	Tool Geometry:.....	39
c.	Parameters:.....	40
d.	Mesh size	41
e.	Cutting Edge Radius	42
2.	Post Simulation.....	43
a.	Forces.....	43
b.	Stresses and Strains.....	44
III.	RESULTS	45
A.	Experimental.....	45
1.	Influence of Cutting Speed on Frictional forces.....	45
2.	Influence of uncut chip thickness on plowing forces.	50
3.	Influence of cutting speed on plowing forces.....	75
4.	Temperature Measurements:	77
5.	Tool Scanning:.....	84
B.	Analytical.....	85
1.	Region 1.....	85
2.	Region 2.....	86
a.	Constant Cutting-Edge Radius.....	88
b.	Variable Cutting Edge Radius	94
C.	Numerical.....	106
1.	Stagnation Point.....	106
2.	Forces	107
3.	Temperature.....	118
IV.	DISCUSSION	126
V.	CONCLUSION	133
BIBLIOGRAPHY	134	

APPENDIX 137

ILLUSTRATIONS

Figure		Page
1.	New force diagram containing the force P which is due to the plowing force [9]	3
2.	The complete force diagram of the orthogonal cutting process after the addition of land forces [9].	4
3.	Tool forces, dependent upon the uncut chip thickness t, illustrate the development of components P1 and P2 of the plowing force P with increasing t up to a certain stage when P remains practically constant with a further increase of t [9].	5
4.	The influence of cutting edge radius CER on plowing force components in the direction of cutting (left) and direction of feed motion (right) [10]	8
5.	Influence of cutting speed V on forces in turning Ti–Al6–V4 with different feeds f and various cutting edge radii rn, standardized to a cutting width of b = 1 mm [10].	8
6.	Influence of cutting edge radius on plowing force in turning Ti–6Al–4V at different cutting speeds, forces are standardized to a cutting width of b = 1mm [10].	9
7.	Pz and Pxy vs. Wear Area Width h [15].	10
8.	Effect of radius of tool edge on mode of deformation in cutting (a = 30 deg, t1 = 50 μm, μ = 0.5, mF = 0.5, v = 1 μm/sec) [21].	13
9.	Effect of Cutting Edge Radius on Tangential and Longitudinal forces respectively	14
10.	Cutting with material separation point on edge with 3 recovery scenarios [24]	15
11.	Cutting with a stable build-up on edge [24]	15
12.	Observed and predicted plowing forces using cylinder indenter model for (a) r, = 0.7938 mm thrust direction (b) re .7938 mm cutting direction (c) re .3969 mm thrust .7938 mm cutting direction (c) re .3969 mm thrust direction and (d) re .396 [24]	16
13.	Observed and predicted plowing forces using blunt indenter model for (a) r, = 0.7938 mm thrust direction (b) re .7938 mm cutting direction (c) re .3969 mm thrust .7938 mm cutting direction (c) re .3969 mm thrust direction and (d) re .3969 mm cutting direction [24]	17
14.	Setup design on CREO	19
15.	The final design manufactured and used in the experiments	19
16.	Forces on the Cutting-Edge Radius	19
17.	Forces in metal cutting: (a) forces acting on the chip in orthogonal cutting, and (b) forces acting on the tool that can be measured	20
18.	Portion of the tool scanned under the microscope. (The Cutting-Edge Radius)	21
19.	Cutting Edge Radius scanned under the microscope	21

20.	Thermal Camera	22
21.	(a) AZ31 Workpiece	23
22.	Cutting Regions	28
23.	Forces acting in Region 1. (Phase 1)	29
24.	Forces acting in Region 1 and Region 2. (Phase 2).....	31
25.	Calculation of angle theta	32
26.	Projection of Friction force 2 on x and z	33
27.	Projection of Normal 2 on x and z	34
28.	Half space model [24].....	35
29.	Deform Friction Coefficient Input	41
30.	(a) Fine Mesh of the tool	42
31.	(a) CER of 5 μm	42
32.	(a) Xload vs. Time	43
	(b) Yload vs. Time.....	43
33.	Effective Stresses	44
34.	Effective Strain	44
35.	Forces vs. time at Cutting speed 30 m/min.....	45
36.	Forces vs. time at Cutting speed 60 m/min	46
37.	Forces vs. time at Cutting speed 90 m/min.....	46
38.	Forces vs. time at Cutting speed 120 m/min.....	47
39.	Forces vs. time at Cutting speed 150 m/min.....	47
40.	Frictional Forces vs. Cutting Speed.....	49
41.	Normal Forces vs. Cutting Speed	50
42.	Typical cutting forces (RPM = 720, Cutting speed= 30 m/min, feed = 0.0005 mm/rev OR Feed rate of mm/min = N. $F = 720 * 0.0005 \text{ mm/rev} = 0.36 \text{ mm/min}$).	51
43.	Typical cutting forces (RPM = 720, Cutting speed= 30 m/min, feed = 0.005 mm/rev OR Feed rate of mm/min = N. $F = 720 * 0.005 \text{ mm/rev} = 3.6 \text{ mm/min}$).	52
44.	Typical cutting forces (RPM = 720, Cutting speed= 30 m/min, feed = 0.01 mm/rev OR Feed rate of mm/min = N. $F = 720 * 0.01 \text{ mm/rev} = 7.2 \text{ mm/min}$).	53
45.	Typical cutting forces (RPM = 720, Cutting speed= 90 m/min, feed = 0.0005 mm/rev OR Feed rate of mm/min = N. $F = 720 * 0.0005 \text{ mm/rev} = 0.36 \text{ mm/min}$).	54
46.	Typical cutting forces (RPM = 720, Cutting speed= 90 m/min, feed = 0.005 mm/rev OR Feed rate of mm/min = N. $F = 720 * 0.005 \text{ mm/rev} = 3.6 \text{ mm/min}$).	55
47.	Typical cutting forces (RPM = 720, Cutting speed= 90 m/min, feed = 0.01 mm/rev OR Feed rate of mm/min = N. $F = 720 * 0.01 \text{ mm/rev} = 7.2 \text{ mm/min}$).	56
48.	Typical cutting forces (RPM = 720, Cutting speed= 150 m/min, feed = 0.0005 mm/rev OR Feed rate of mm/min = N. $F = 720 * 0.0005 \text{ mm/rev} = 0.36 \text{ mm/min}$).	57

49.	Typical cutting forces (RPM = 720, Cutting speed= 150 m/min, feed = 0.005 mm/rev OR Feed rate of mm/min = $N. F = 720 * 0.005 \text{ mm/rev} = 3.6 \text{ mm/min}$).	58
50.	Typical cutting forces (RPM = 720, Cutting speed= 150 m/min, feed = 0.01 mm/rev OR Feed rate of mm/min = $N. F = 720 * 0.01 \text{ mm/rev} = 7.2 \text{ mm/min}$).	59
51.	Plowing Coefficient vs. Uncut Chip Thickness at Speed 30 m/min.....	65
52.	Plowing Coefficient vs. Uncut Chip Thickness at Speed 60 m/min.....	66
53.	Plowing Coefficient vs. Uncut Chip Thickness at Speed 90 m/min.....	67
54.	Plowing Coefficient vs. Uncut Chip Thickness at Speed 120 m/min.....	68
55.	Plowing Coefficient vs. Uncut Chip Thickness at Speed 150 m/min.....	69
56.	Thrust Coefficient vs. Uncut Chip Thickness at Speed 30 m/min	71
57.	Thrust Coefficient vs. Uncut Chip Thickness at Speed 60 m/min	72
58.	Thrust Coefficient vs. Uncut Chip Thickness at Speed 90 m/min	73
59.	Thrust Coefficient vs. Uncut Chip Thickness at Speed 120 m/min	74
60.	Thrust Coefficient vs. Uncut Chip Thickness at Speed 150 m/min	75
61.	Plowing Coefficient vs. Uncut Chip Thickness at different Cutting Speeds.....	76
62.	Thermal Photos of experiments at Speed 90 m/min and feed 0.005 mm	77
63.	Thermal Photos of experiments at Speed 150 m/min and feed 0.005 mm.	77
64.	Temperature vs. Uncut Chip Thickness at Speed 30 m/min	79
65.	Temperature vs. Uncut Chip Thickness at Speed 60 m/min	80
66.	Temperature vs. Uncut Chip Thickness at Speed 90 m/min	81
67.	Temperature vs. Uncut Chip Thickness at Speed 120 m/min	82
68.	Temperature vs. Uncut Chip Thickness at Speed 150 m/min	83
69.	Length of contact	84
70.	Analytical Values.....	88
71.	Analytical vs. Experimental Corrected Values for Speed 30 m/min.....	89
72.	Analytical vs. Experimental Values for Speed 60 m/min.....	90
73.	Analytical vs. Experimental Values for Speed 90 m/min.....	91
74.	Analytical vs. Experimental Values for Speed 120 m/min.....	92
75.	Analytical vs. Experimental Values for Speed 150 m/min.....	93
76.	Damaged Cutting-Edge Radius	94
77.	Analytical Values.....	95
78.	Analytical vs. Experimental values in the x direction for a variable CER at Speed 30 m/min.	96
79.	Analytical vs. Experimental values in the x direction for a variable CER at Speed 60 m/min.	97
80.	Analytical vs. Experimental values in the x direction for a variable CER at Speed 90 m/min.	98
81.	Analytical vs. Experimental values in the x direction for a variable CER at Speed 120 m/min.	99
82.	Analytical vs. Experimental values in the x direction for a variable CER at Speed 150 m/min.	100
83.	Analytical vs. Experimental values in the z direction for a variable CER at Speed 30 m/min.	101

84.	Analytical vs. Experimental values in the z direction for a variable CER at Speed 60 m/min.	102
85.	Analytical vs. Experimental values in the z direction for a variable CER at Speed 90 m/min.	103
86.	Analytical vs. Experimental values in the z direction for a variable CER at Speed 120 m/min.	104
87.	Analytical vs. Experimental values in the z direction for a variable CER at Speed 150 m/min.	105
88.	Stagnation Point.....	106
89.	Numerical vs. Analytical vs. Experimental values for different feeds at Speed of 30 m/min for Forces in the x direction	109
90.	Numerical vs. Analytical vs. Experimental values for different feeds at Speed of 60 m/min for Forces in the x direction	110
91.	Numerical vs. Analytical vs. Experimental values for different feeds at Speed of 90 m/min for Forces in the x direction.	111
92.	Numerical vs. Analytical vs. Experimental values for different feeds at Speed of 120 m/min for Forces in the x direction	112
93.	Numerical vs. Analytical vs. Experimental values for different feeds at Speed of 150 m/min for Forces in the x direction	113
94.	Numerical vs. Analytical vs. Experimental values for different feeds at Speed of 30 m/min for Forces in the z direction.....	114
95.	Numerical vs. Analytical vs. Experimental values for different feeds at Speed of 60 m/min for Forces in the z direction.....	115
96.	Numerical vs. Analytical vs. Experimental values for different feeds at Speed of 90 m/min for Forces in the z direction.....	116
97.	Numerical vs. Analytical vs. Experimental values for different feeds at Speed of 120 m/min for Forces in the z direction.....	117
98.	Numerical vs. Analytical vs. Experimental values for different feeds at Speed of 150 m/min for Forces in the z direction.....	118
99.	Temperature distrubtion from deform	119
100.	Temperature vs. Feed for different cutting speeds.	120
101.	Analytical vs. Experimental for Speed of 30 m/min	121
102.	Analytical vs. Experimental for Speed of 60 m/min	122
103.	Analytical vs. Experimental for Speed of 90 m/min	123
104.	Analytical vs. Experimental for Speed of 120 m/min	124
105.	Analytical vs. Experimental for Speed of 150 m/min	125
106.	Experimental versus theoretical force components for Al2024 cutting tests [27]	127
107.	Kne and Kte for the cutting edge only shown plotted along the length of the lip. Values correspond to cutting speed of 50 m/min [29].....	128
108.	Plowing Coefficient at Cutting Speed of 60 m/min.....	129
109.	Influence of cutting edge radius on plowing force in turning Ti-6Al-4V at different cutting speeds, forces are standardized to a cutting width of $b = 1\text{mm}$ [10].....	130

110. Comparison between the analytical model of this research and the predicted values of [38].	131
111. Conventional Grinding vs. Laser-assisted Grinding [39]	132
112. Typical cutting forces (RPM = 720, Cutting speed= 30 m/min, feed = 0.0005 mm/rev OR Feed rate of mm/min = $N. F = 720 * 0.0005 \text{ mm/rev} = 0.36 \text{ mm/min}$).	137
113. Typical cutting forces (RPM = 720, Cutting speed= 30 m/min, feed = 0.001mm/rev OR Feed rate of mm/min = $N. F = 720 * 0.001 \text{ mm/rev} = 0.72 \text{ mm/min}$).	137
114. Typical cutting forces (RPM = 720, Cutting speed= 30 m/min, feed = 0.0015 mm/rev OR Feed rate of mm/min = $N. F = 720 * 0.0015 \text{ mm/rev} = 1.08 \text{ mm/min}$).	138
115. Typical cutting forces (RPM = 720, Cutting speed= 30 m/min, feed = 0.002 mm/rev OR Feed rate of mm/min = $N. F = 720 * 0.002 \text{ mm/rev} = 1.44 \text{ mm/min}$).	138
116. Typical cutting forces (RPM = 720, Cutting speed= 30 m/min, feed = 0.0025 mm/rev OR Feed rate of mm/min = $N. F = 720 * 0.0025 \text{ mm/rev} = 1.8 \text{ mm/min}$).	139
117. Typical cutting forces (RPM = 720, Cutting speed= 30 m/min, feed = 0.003 mm/rev OR Feed rate of mm/min = $N. F = 720 * 0.003 \text{ mm/rev} = 2.16 \text{ mm/min}$).	139
118. Typical cutting forces (RPM = 720, Cutting speed= 30 m/min, feed = 0.0035 mm/rev OR Feed rate of mm/min = $N. F = 720 * 0.0035 \text{ mm/rev} = 2.52 \text{ mm/min}$).	140
119. Typical cutting forces (RPM = 720, Cutting speed= 30 m/min, feed = 0.004 mm/rev OR Feed rate of mm/min = $N. F = 720 * 0.004 \text{ mm/rev} = 2.88 \text{ mm/min}$).	140
120. Typical cutting forces (RPM = 720, Cutting speed= 30 m/min, feed = 0.0045 mm/rev OR Feed rate of mm/min = $N. F = 720 * 0.0045 \text{ mm/rev} = 3.24 \text{ mm/min}$).	141
121. Typical cutting forces (RPM = 720, Cutting speed= 30 m/min, feed = 0.005 mm/rev OR Feed rate of mm/min = $N. F = 720 * 0.005 \text{ mm/rev} = 3.6 \text{ mm/min}$).	141
122. Typical cutting forces (RPM = 720, Cutting speed= 30 m/min, feed = 0.006 mm/rev OR Feed rate of mm/min = $N. F = 720 * 0.006 \text{ mm/rev} = 4.32 \text{ mm/min}$).	142
123. Typical cutting forces (RPM = 720, Cutting speed= 30 m/min, feed = 0.007 mm/rev OR Feed rate of mm/min = $N. F = 720 * 0.007 \text{ mm/rev} = 5.04 \text{ mm/min}$).	142
124. Typical cutting forces (RPM = 720, Cutting speed= 30 m/min, feed = 0.008 mm/rev OR Feed rate of mm/min = $N. F = 720 * 0.008 \text{ mm/rev} = 5.76 \text{ mm/min}$).	143
125. Typical cutting forces (RPM = 720, Cutting speed= 30 m/min, feed = 0.009 mm/rev OR Feed rate of mm/min = $N. F = 720 * 0.009 \text{ mm/rev} = 6.48 \text{ mm/min}$).	143

126. Typical cutting forces (RPM = 720, Cutting speed= 30 m/min, feed = 0.01 mm/rev OR Feed rate of mm/min = N. $F = 720 * 0.01 \text{ mm/rev} = 7.2 \text{ mm/min}$).	144
127. Typical cutting forces (RPM = 720, Cutting speed= 60 m/min, feed = 0.0005 mm/rev OR Feed rate of mm/min = N. $F = 720 * 0.0005 \text{ mm/rev} = 0.36 \text{ mm/min}$).	144
128. Typical cutting forces (RPM = 720, Cutting speed= 60 m/min, feed = 0.001 mm/rev OR Feed rate of mm/min = N. $F = 720 * 0.001 \text{ mm/rev} = 0.72 \text{ mm/min}$).	145
129. Typical cutting forces (RPM = 720, Cutting speed= 60 m/min, feed = 0.0015 mm/rev OR Feed rate of mm/min = N. $F = 720 * 0.0015 \text{ mm/rev} = 1.08 \text{ mm/min}$).	145
130. Typical cutting forces (RPM = 720, Cutting speed= 60 m/min, feed = 0.002 mm/rev OR Feed rate of mm/min = N. $F = 720 * 0.002 \text{ mm/rev} = 1.44 \text{ mm/min}$).	146
131. Typical cutting forces (RPM = 720, Cutting speed= 60 m/min, feed = 0.0025 mm/rev OR Feed rate of mm/min = N. $F = 720 * 0.0025 \text{ mm/rev} = 1.8 \text{ mm/min}$).	146
132. Typical cutting forces (RPM = 720, Cutting speed= 60 m/min, feed = 0.003 mm/rev OR Feed rate of mm/min = N. $F = 720 * 0.003 \text{ mm/rev} = 2.16 \text{ mm/min}$).	147
133. Typical cutting forces (RPM = 720, Cutting speed= 60 m/min, feed = 0.0035 mm/rev OR Feed rate of mm/min = N. $F = 720 * 0.0035 \text{ mm/rev} = 2.52 \text{ mm/min}$).	147
134. Typical cutting forces (RPM = 720, Cutting speed= 60 m/min, feed = 0.004 mm/rev OR Feed rate of mm/min = N. $F = 720 * 0.004 \text{ mm/rev} = 2.88 \text{ mm/min}$).	148
135. Typical cutting forces (RPM = 720, Cutting speed= 60 m/min, feed = 0.0045 mm/rev OR Feed rate of mm/min = N. $F = 720 * 0.0045 \text{ mm/rev} = 3.24 \text{ mm/min}$).	148
136. Typical cutting forces (RPM = 720, Cutting speed= 60 m/min, feed = 0.005 mm/rev OR Feed rate of mm/min = N. $F = 720 * 0.005 \text{ mm/rev} = 3.6 \text{ mm/min}$).	149
137. Typical cutting forces (RPM = 720, Cutting speed= 60 m/min, feed = 0.006 mm/rev OR Feed rate of mm/min = N. $F = 720 * 0.006 \text{ mm/rev} = 4.32 \text{ mm/min}$).	149
138. Typical cutting forces (RPM = 720, Cutting speed= 60 m/min, feed = 0.007 mm/rev OR Feed rate of mm/min = N. $F = 720 * 0.007 \text{ mm/rev} = 5.04 \text{ mm/min}$).	150
139. Typical cutting forces (RPM = 720, Cutting speed= 60 m/min, feed = 0.008 mm/rev OR Feed rate of mm/min = N. $F = 720 * 0.008 \text{ mm/rev} = 5.76 \text{ mm/min}$).	150
140. Typical cutting forces (RPM = 720, Cutting speed= 60 m/min, feed = 0.009 mm/rev OR Feed rate of mm/min = N. $F = 720 * 0.009 \text{ mm/rev} = 6.48 \text{ mm/min}$).	151

141. Typical cutting forces (RPM = 720, Cutting speed= 60 m/min, feed = 0.01 mm/rev OR Feed rate of mm/min = N. $F = 720 * 0.01 \text{ mm/rev} = 7.2 \text{ mm/min}$).	151
142. Typical cutting forces (RPM = 720, Cutting speed= 90 m/min, feed = 0.0005 mm/rev OR Feed rate of mm/min = N. $F = 720 * 0.0005 \text{ mm/rev} = 0.36 \text{ mm/min}$).	152
143. Typical cutting forces (RPM = 720, Cutting speed= 90 m/min, feed = 0.001 mm/rev OR Feed rate of mm/min = N. $F = 720 * 0.001 \text{ mm/rev} = 0.72 \text{ mm/min}$).	152
144. Typical cutting forces (RPM = 720, Cutting speed= 90 m/min, feed = 0.0015 mm/rev OR Feed rate of mm/min = N. $F = 720 * 0.0015 \text{ mm/rev} = 1.08 \text{ mm/min}$).	153
145. Typical cutting forces (RPM = 720, Cutting speed= 90 m/min, feed = 0.002 mm/rev OR Feed rate of mm/min = N. $F = 720 * 0.002 \text{ mm/rev} = 1.44 \text{ mm/min}$).	153
146. Typical cutting forces (RPM = 720, Cutting speed= 90 m/min, feed = 0.0025 mm/rev OR Feed rate of mm/min = N. $F = 720 * 0.0025 \text{ mm/rev} = 1.8 \text{ mm/min}$).	154
147. Typical cutting forces (RPM = 720, Cutting speed= 90 m/min, feed = 0.003 mm/rev OR Feed rate of mm/min = N. $F = 720 * 0.003 \text{ mm/rev} = 2.16 \text{ mm/min}$).	154
148. Typical cutting forces (RPM = 720, Cutting speed= 90 m/min, feed = 0.0035 mm/rev OR Feed rate of mm/min = N. $F = 720 * 0.0035 \text{ mm/rev} = 2.52 \text{ mm/min}$).	155
149. Typical cutting forces (RPM = 720, Cutting speed= 90 m/min, feed = 0.004 mm/rev OR Feed rate of mm/min = N. $F = 720 * 0.004 \text{ mm/rev} = 2.88 \text{ mm/min}$).	155
150. Typical cutting forces (RPM = 720, Cutting speed= 90 m/min, feed = 0.0045 mm/rev OR Feed rate of mm/min = N. $F = 720 * 0.0045 \text{ mm/rev} = 3.24 \text{ mm/min}$).	156
151. Typical cutting forces (RPM = 720, Cutting speed= 90 m/min, feed = 0.005 mm/rev OR Feed rate of mm/min = N. $F = 720 * 0.005 \text{ mm/rev} = 3.6 \text{ mm/min}$).	156
152. Typical cutting forces (RPM = 720, Cutting speed= 90 m/min, feed = 0.006 mm/rev OR Feed rate of mm/min = N. $F = 720 * 0.006 \text{ mm/rev} = 4.32 \text{ mm/min}$).	157
153. Typical cutting forces (RPM = 720, Cutting speed= 90 m/min, feed = 0.007 mm/rev OR Feed rate of mm/min = N. $F = 720 * 0.007 \text{ mm/rev} = 5.04 \text{ mm/min}$).	157
154. Typical cutting forces (RPM = 720, Cutting speed= 90 m/min, feed = 0.008 mm/rev OR Feed rate of mm/min = N. $F = 720 * 0.008 \text{ mm/rev} = 5.76 \text{ mm/min}$).	158
155. Typical cutting forces (RPM = 720, Cutting speed= 90 m/min, feed = 0.009 mm/rev OR Feed rate of mm/min = N. $F = 720 * 0.009 \text{ mm/rev} = 6.48 \text{ mm/min}$).	158

156. Typical cutting forces (RPM = 720, Cutting speed= 90 m/min, feed = 0.01 mm/rev OR Feed rate of mm/min = N. $F = 720 * 0.001 \text{ mm/rev} = 7.2 \text{ mm/min}$).	159
157. Typical cutting forces (RPM = 720, Cutting speed= 120 m/min, feed = 0.0005 mm/rev OR Feed rate of mm/min = N. $F = 720 * 0.0005 \text{ mm/rev} = 0.36 \text{ mm/min}$).	159
158. Typical cutting forces (RPM = 720, Cutting speed=120 m/min, feed = 0.001 mm/rev OR Feed rate of mm/min = N. $F = 720 * 0.001 \text{ mm/rev} = 0.72 \text{ mm/min}$).	160
159. Typical cutting forces (RPM = 720, Cutting speed=120 m/min, feed = 0.0015 mm/rev OR Feed rate of mm/min = N. $F = 720 * 0.0015 \text{ mm/rev} = 1.08 \text{ mm/min}$).	160
160. Typical cutting forces (RPM = 720, Cutting speed=120 m/min, feed = 0.002 mm/rev OR Feed rate of mm/min = N. $F = 720 * 0.002 \text{ mm/rev} = 1.44 \text{ mm/min}$).	161
161. Typical cutting forces (RPM = 720, Cutting speed=120 m/min, feed = 0.0025 mm/rev OR Feed rate of mm/min = N. $F = 720 * 0.0025 \text{ mm/rev} = 1.8 \text{ mm/min}$).	161
162. Typical cutting forces (RPM = 720, Cutting speed=120 m/min, feed = 0.003 mm/rev OR Feed rate of mm/min = N. $F = 720 * 0.003 \text{ mm/rev} = 2.16 \text{ mm/min}$).	162
163. Typical cutting forces (RPM = 720, Cutting speed=120 m/min, feed = 0.0035 mm/rev OR Feed rate of mm/min = N. $F = 720 * 0.0035 \text{ mm/rev} = 2.52 \text{ mm/min}$).	162
164. Typical cutting forces (RPM = 720, Cutting speed=120 m/min, feed = 0.004 mm/rev OR Feed rate of mm/min = N. $F = 720 * 0.004 \text{ mm/rev} = 2.88 \text{ mm/min}$).	163
165. Typical cutting forces (RPM = 720, Cutting speed=120 m/min, feed = 0.0045 mm/rev OR Feed rate of mm/min = N. $F = 720 * 0.0045 \text{ mm/rev} = 3.24 \text{ mm/min}$).	163
166. Typical cutting forces (RPM = 720, Cutting speed=120 m/min, feed = 0.005 mm/rev OR Feed rate of mm/min = N. $F = 720 * 0.005 \text{ mm/rev} = 3.6 \text{ mm/min}$).	164
167. Typical cutting forces (RPM = 720, Cutting speed=120 m/min, feed = 0.006 mm/rev OR Feed rate of mm/min = N. $F = 720 * 0.006 \text{ mm/rev} = 4.32 \text{ mm/min}$).	164
168. Typical cutting forces (RPM = 720, Cutting speed=120 m/min, feed = 0.007 mm/rev OR Feed rate of mm/min = N. $F = 720 * 0.007 \text{ mm/rev} = 5.04 \text{ mm/min}$).	165
169. Typical cutting forces (RPM = 720, Cutting speed=120 m/min, feed = 0.008 mm/rev OR Feed rate of mm/min = N. $F = 720 * 0.008 \text{ mm/rev} = 5.76 \text{ mm/min}$).	165
170. Typical cutting forces (RPM = 720, Cutting speed=120 m/min, feed = 0.009 mm/rev OR Feed rate of mm/min = N. $F = 720 * 0.009 \text{ mm/rev} = 6.48 \text{ mm/min}$).	166

171. Typical cutting forces (RPM = 720, Cutting speed=120 m/min, feed = 0.01 mm/rev OR Feed rate of mm/min = $N \cdot F = 720 * 0.01 \text{ mm/rev} = 7.2 \text{ mm/min}$).	166
172. Typical cutting forces (RPM = 720, Cutting speed=150 m/min, feed = 0.0005 mm/rev OR Feed rate of mm/min = $N \cdot F = 720 * 0.0005 \text{ mm/rev} = 0.36 \text{ mm/min}$).	167
173. Typical cutting forces (RPM = 720, Cutting speed=150 m/min, feed = 0.001 mm/rev OR Feed rate of mm/min = $N \cdot F = 720 * 0.001 \text{ mm/rev} = 0.72 \text{ mm/min}$).	168
174. Typical cutting forces (RPM = 720, Cutting speed=150 m/min, feed = 0.0015 mm/rev OR Feed rate of mm/min = $N \cdot F = 720 * 0.0015 \text{ mm/rev} = 1.08 \text{ mm/min}$).	168
175. Typical cutting forces (RPM = 720, Cutting speed=150 m/min, feed = 0.002 mm/rev OR Feed rate of mm/min = $N \cdot F = 720 * 0.002 \text{ mm/rev} = 1.44 \text{ mm/min}$).	169
176. Typical cutting forces (RPM = 720, Cutting speed=150 m/min, feed = 0.0025 mm/rev OR Feed rate of mm/min = $N \cdot F = 720 * 0.0025 \text{ mm/rev} = 1.8 \text{ mm/min}$).	169
177. Typical cutting forces (RPM = 720, Cutting speed=150 m/min, feed = 0.003 mm/rev OR Feed rate of mm/min = $N \cdot F = 720 * 0.003 \text{ mm/rev} = 2.16 \text{ mm/min}$).	170
178. Typical cutting forces (RPM = 720, Cutting speed=150 m/min, feed = 0.0035 mm/rev OR Feed rate of mm/min = $N \cdot F = 720 * 0.0035 \text{ mm/rev} = 2.52 \text{ mm/min}$).	170
179. Typical cutting forces (RPM = 720, Cutting speed=150 m/min, feed = 0.004 mm/rev OR Feed rate of mm/min = $N \cdot F = 720 * 0.004 \text{ mm/rev} = 2.88 \text{ mm/min}$).	171
180. Typical cutting forces (RPM = 720, Cutting speed=150 m/min, feed = 0.0045 mm/rev OR Feed rate of mm/min = $N \cdot F = 720 * 0.0045 \text{ mm/rev} = 3.24 \text{ mm/min}$).	171
181. Typical cutting forces (RPM = 720, Cutting speed=150 m/min, feed = 0.005 mm/rev OR Feed rate of mm/min = $N \cdot F = 720 * 0.005 \text{ mm/rev} = 3.6 \text{ mm/min}$).	172
182. Typical cutting forces (RPM = 720, Cutting speed=150 m/min, feed = 0.006 mm/rev OR Feed rate of mm/min = $N \cdot F = 720 * 0.006 \text{ mm/rev} = 4.32 \text{ mm/min}$).	172
183. Typical cutting forces (RPM = 720, Cutting speed=150 m/min, feed = 0.007 mm/rev OR Feed rate of mm/min = $N \cdot F = 720 * 0.007 \text{ mm/rev} = 5.04 \text{ mm/min}$).	173
184. Typical cutting forces (RPM = 720, Cutting speed=150 m/min, feed = 0.008 mm/rev OR Feed rate of mm/min = $N \cdot F = 720 * 0.008 \text{ mm/rev} = 5.76 \text{ mm/min}$).	173
185. Typical cutting forces (RPM = 720, Cutting speed=150 m/min, feed = 0.009 mm/rev OR Feed rate of mm/min = $N \cdot F = 720 * 0.009 \text{ mm/rev} = 6.48 \text{ mm/min}$).	174

186. Typical cutting forces (RPM = 720, Cutting speed=150 m/min, feed = 0.01 mm/rev OR Feed rate of mm/min = N. $F = 720 * 0.01 \text{ mm/rev} = 7.2 \text{ mm/min}$).
..... 174

TABLES

Table	Page
1. Cutting Speeds	24
2. Experimental test matrix covering all feeds and RPMs.....	25
3. Experimental test matrix covering all feeds and RPMs.....	26
4. Machining time meter	27
5. Parameters for AZ31B	39
6. Tool Geometry	40
7. Forces acting in Region 1.....	48
8. Plowing Coefficient at different feeds and RPMs.....	60
9. Thrust Coefficient at different feeds and RPMs.	61
10. Corrected Plowing Coefficients for all feeds and speeds.....	63
11. Corrected Thrust Coefficient at different feeds and speeds.	64
12. Temperature Measurements	78
13. AZ31B Material Properties	87
14. Force z Numerical values obtained by DEFORM for all speeds and feeds.....	107
15. Force z Numerical values obtained by DEFORM for all speeds and feeds.....	108

NOMENCLATURE

E : Modulus of Elasticity

ν : Poisson's Ratio

CER : Cutting Edge Radius

α : Normal rake angle

V : Cutting Speed

t_c : Uncut Chip Thickness

δ : Plowing layer thickness

l_1 : Contact length in Region 1

l_2 : Contact length in Region 2

T : Temperature at the tool chip interface

F_c : Cutting Force measured experimentally

F_{f1} : Friction Force in Region 1

F_{f2} : Friction Force in Region 2

N_1 : Normal Force in Region 1

N_2 : Normal Force in Region 2

F_p : Plowing Force in Region 2

F_t : Thrust Force in Region 2

R_1 : Resultant Force in Region 1

R_2 : Resultant Force in Region 2

Q : Shearing Force (N)

Q_1 : Component of force Q in the direction of tool motion

Q_2 : Component of force Q perpendicular to the direction of tool motion

Q_n : Normal component of force Q

Q_f : Frictional component of force Q

Q_f : Frictional component of force Q

S : Total force on the shear plane

S_S : Component of S in the direction of shearing at the shear plane

μ : Coefficient of friction

τ_s : Mean shear stress on the shear plane

$\mu_Q := \frac{Q_F}{Q_n} = \tan(\tau_Q)$ Coefficient of friction on chip-tool interface

τ_Q : Friction angle corresponding to Coefficient of friction μ_Q

$\mu_r = \frac{P_F}{P_n} = \tan(\tau_r)$ = Coefficient of friction on sharpness rounding of cutting edge

τ_r : Friction angle corresponding to the coefficient of friction μ_1

$\mu_L := \frac{L_1}{L_2} \tan(\tau_L)$ = coefficient of friction on wear land of tool flank

$\tau_L := \frac{L_1}{L_2} = \tan(\tau_L)$ = Friction angle corresponding to coefficient μ_L

CHAPTER I

INTRODUCTION

Developments in the theory of cutting processes have been present since the last century to determine all forces present during metal cutting. Identifying forces helps in monitoring, designing, and selecting cutting tools. The recent revelation of the plowing force helps in the understanding of the mechanics of 2D orthogonal cutting. The plowing force is instigated by the finite sharpness of the tool edge radius, and it is caused mainly by flank wear happening during the cutting process.

Micromachining of hard materials presents further complications associated with tool wear, tool failure, low stiffness of the micro tools. Although micromachining incorporates characteristics of the conventional machining process, the size effect plays in role in modifying the mechanism of material removal. Thus, the rules of similarity do not apply when going from macro to micromachining [1].

The ratio of the depth of cut to the cutting-edge radius significantly affects micromachining processes. A small change in the uncut thickness causes a significant influence on the cutting process. The smaller the uncut chip thickness, the higher the impacts on the tool wear and cutting force. This ratio defines the active material removal mechanism such as cutting, plowing, or sliding and thus the resulting surface quality. When the thickness of the material to be removed is of the same order of magnitude as the tool edge radius, the notion of size effect is introduced [2].

In conventional machining, cutting tool edge is assumed to be ideally sharp, and the contact between the tool's clearance face and the machined surface is assumed to be nonexistence. Chip is then formed mainly by shearing of the material in front of the tooltip. However, in micromachining, the tool edge radius is usually on the same order as the chip thickness. Another difference between macro and micromachining is the location of shearing. In Macro-machining, shear takes place along the shear plane, while in micromachining, the material is deformed and pushed instead sheared. The shear stress in micromachining is found to acting continuously around the cutting edge [3] [5][6][7].

Cutting force in micromachining is also significantly influenced by problems that are generally minor in macro-domain such as tool wear, unbalance (run-out), and instability (chatter) [2][3][4] [8].

In his work Albrecht [9] proposes an extension to the theoretical sharp tool machining model proposed by Merchant. Albrecht also added land forces, which are the force present on the wear land of the tool flank illustrated in *Figure 2*. The new force diagram shown in *Figure 1* shows force Q as the shearing force acting on the straight portion of the tool, while force P represents the plowing force which is the force acting

on the rounded part of the tool.

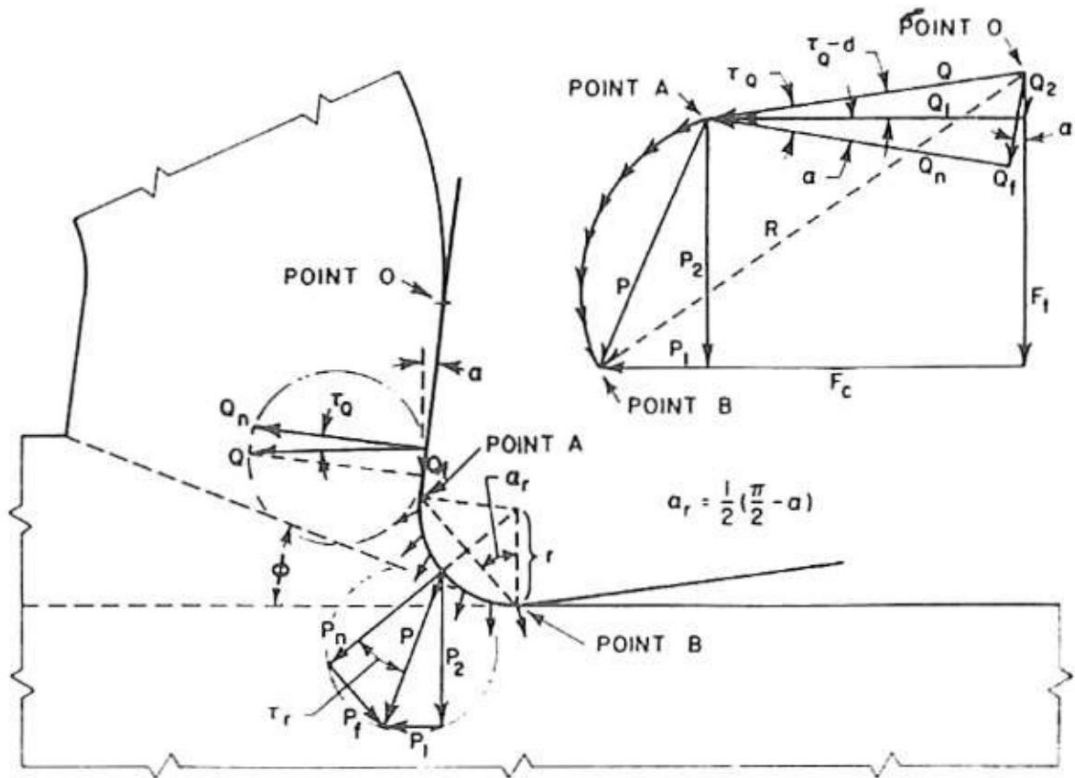


Figure 1: New force diagram containing the force P which is due to the plowing force [9]

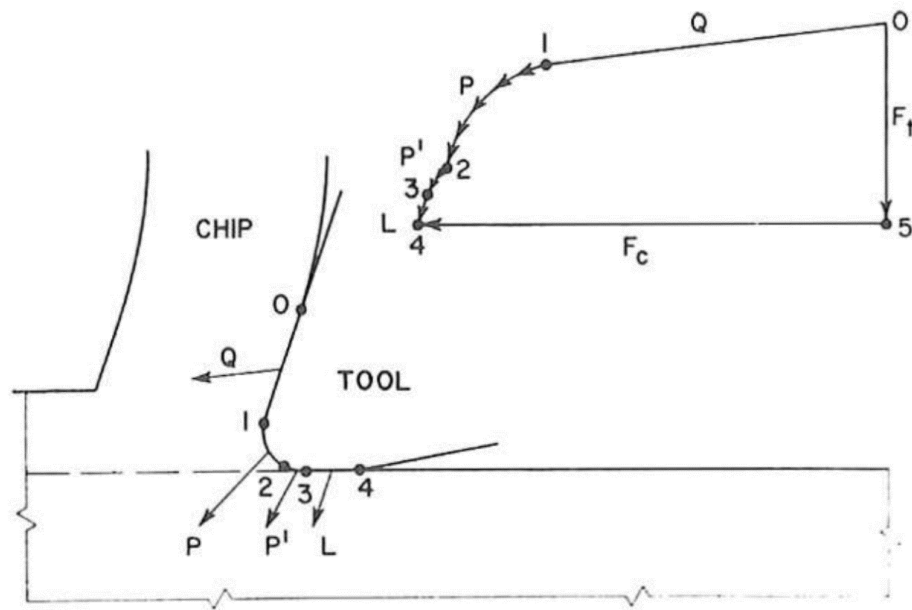


Figure 2: The complete force diagram of the orthogonal cutting process after the addition of land forces [9].

Defining actual coefficients of friction in a cutting process could be possible by determining and separating the plowing forces from the total forces, providing a better insight of tool wear and shearing process. Cutting Forces are mainly divided into shearing and plowing forces [10]. Shearing Forces are the main contributors of chip formation, while the plowing forces have no contribution at all. The plowing force represents the effect coming from the drifting of the tool from the ideal sharpness; it is denoted as the zero-feed force. It is the force before chip formation [11].

A series of orthogonal cutting experiments were made by varying the rake angle, the nose radius, and the uncut chip thickness. Results are shown in Figure 3. For small uncut chip thickness, both Q and P varies with the uncut thickness (feed), but for large thickness P is constant, and Q is proportional to uncut thickness.

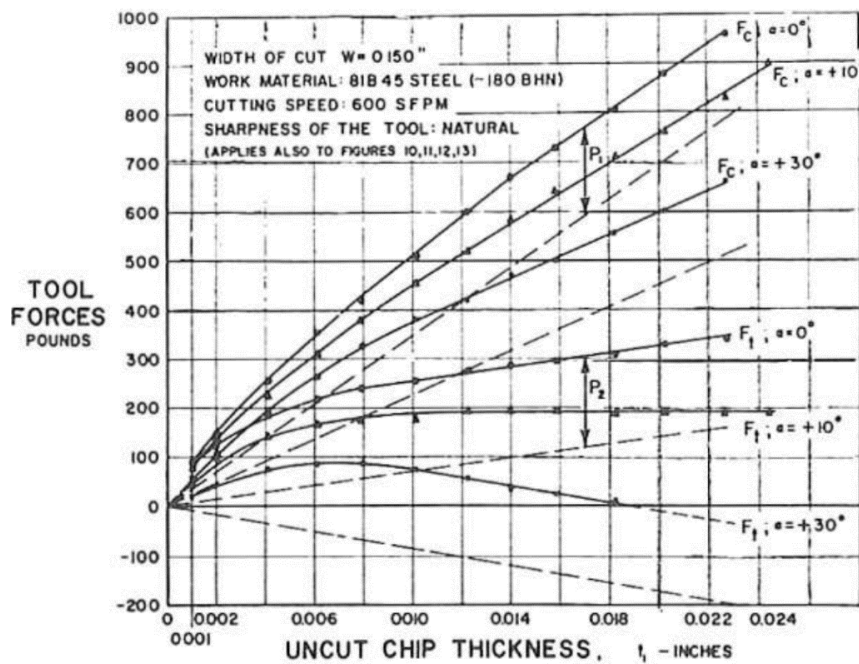


Figure 3: Tool forces, dependent upon the uncut chip thickness t , illustrate the development of components P_1 and P_2 of the plowing force P with increasing t up to a certain stage when P remains practically constant with a further increase of t [9].

The coefficient of friction is found by the equation:

$$\mu_Q = \frac{(F_t - P_2) + (F_c - P_1) \tan \alpha}{(F_c - P_1) - (F_t - P_2) \tan \alpha} \quad (1)$$

Also, Albrecht added the effect of cutting speed on shearing force Q . The cutting speed only affects the plowing force in the thrust forces. The plowing force increases with increasing velocity but only at lower ranges of cutting rates. The forces keep increasing until reaching a maximum and then decreasing until reaching a level off. The effect of cutting speed on the force has been found due to the development of the built-up edge [9].

One of the main methods to determine edge forces is the extrapolation method. The extrapolation method is plotting the force vs. feed then extrapolating into zero feed. So, the non-zero intercept is the plowing force. This method has been followed by [9], [11], and [13] to obtain the plowing force.

Stevenson [11] interpreted the legitimacy of the non-zero method by comparing the calculated shear flow stress to uncut chip thickness, experimental data, and the positivity of the shear strain rate. Stevenson also plotted the cutting force and thrust force versus wear land and noticed that both follow the same trend [11]. However, researchers have shown that this method doesn't confirm in orthogonal cutting since a cyclic force pattern doesn't appear before the cutting tool disengages. It only appears on a specific uncut thickness [12].

Guo, Y. B. et al. [12] followed another method which comprises of comparing the calculated flow stress data to conventional compression test data without extrapolation and to model predictions. Guo, Y. B. also characterized the measured forces versus time, determined magnitudes of the plowing force at different cutting speeds, studied the strain rate sensitivity of the flow stress and investigated the calculated material flow stress versus uncut chip thickness. The results showed that the method followed by Stevenson [11] isn't preferred since the cyclic pattern wasn't observed. The appearance of a cyclic pattern in only a single uncut thickness determines that the cyclic force pattern is due to a periodic chip interaction with the cutting tool after steady state cutting. The calculated flow stresses based on the corrected force data were found to be more uniform against the uncut chip thickness than those based on the measured force data. Comparing the corrected flow stresses with the extrapolated

compression test data revealed agreement. Thus, and according to [12], the determination of the plowing force could be accomplished by the extrapolation method, keeping in mind the dependence on the cutting speed with a possible nonlinear manner.

Other parameters, such as cutting speeds and temperature, also affect the process. Wyen, C.-F. a. et al. [10] stated that to determine the plowing force, it is assumed that total force increases linearly with increasing feed while plowing forces are independent of feed forces. After measuring Force values, plowing force is obtained by extrapolation for $t=0$. Afterward, the friction coefficient is calculated by deducting plowing force from the total force. The results of [10] experiments displayed in Figure 4 indicates that both force components increase with increasing cutting edge radius, but the cutting forces are less sensitive to CER than the feed forces. The results in Figure 5 and Figure 6 also showed that as cutting speed increases, cutting forces decreases, whereas for feed forces, the values depend on the cutting edge radius. Opposite effects of cutting speed on deformation resistance and thermal softening might be the reason behind the interdependency noticed, but this needs further analysis. It was also stated that no uniform influence exists by the cutting speeds on plowing forces [10].

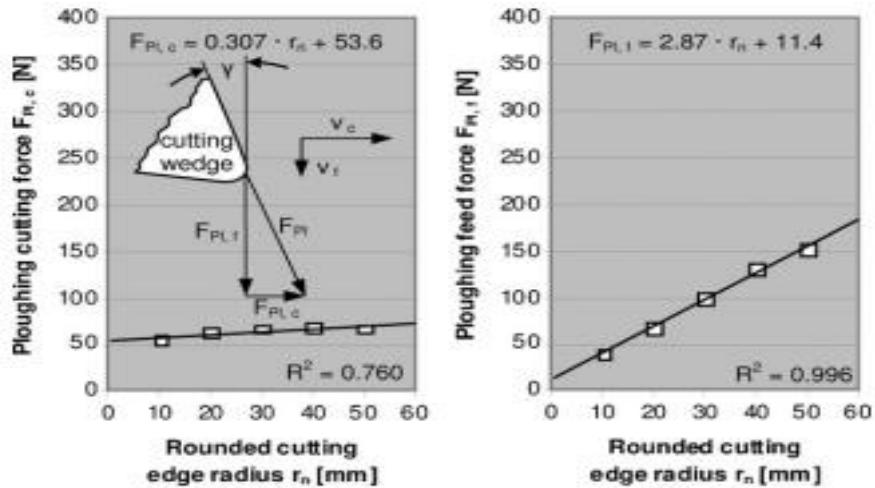


Figure 4: The influence of cutting edge radius CER on plowing force components in the direction of cutting (left) and direction of feed motion (right) [10]

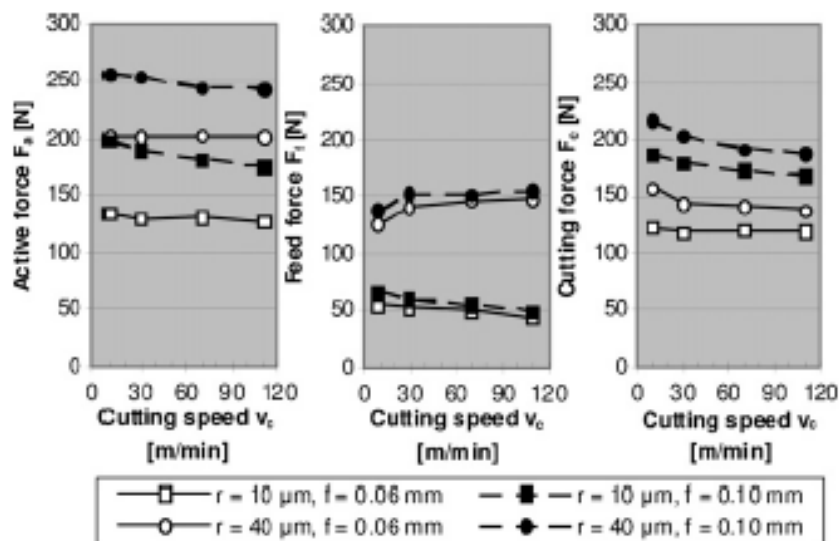


Figure 5: Influence of cutting speed V on forces in turning Ti-Al6-V4 with different feeds f and various cutting edge radii r_n , standardized to a cutting width of $b = 1 \text{ mm}$ [10].

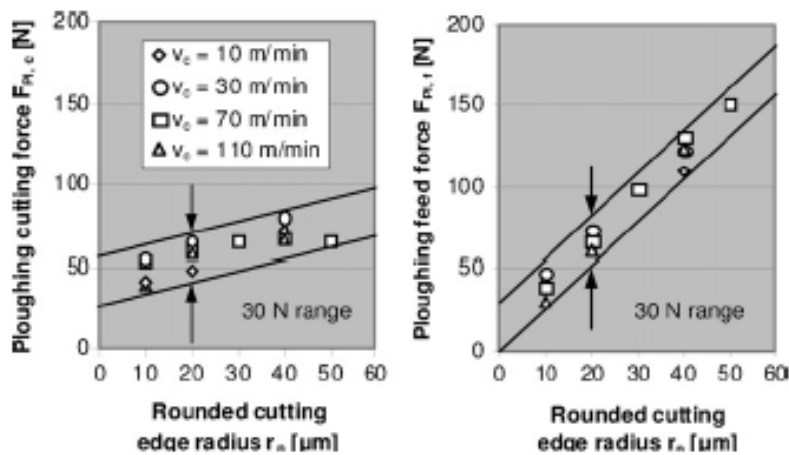


Figure 6: Influence of cutting edge radius on plowing force in turning Ti-6Al-4V at different cutting speeds, forces are standardized to a cutting width of $b = 1$ mm [10].

As a conclusion of the research done by [10], thermal softening might be the reason behind the interdependency noticed in the behavior of forces vs. cutting speeds. No further analysis has been done in this area.

In other pieces of research, Popov et al. [14] claimed that it is impossible to use the direct measurement method in determining plowing forces because of the rigidity influence of the technological system. As a result of this, the comparison method of total forces at different flank wears is followed to determine the plowing forces by multiple researchers. The method is based on the idea that if all cutting conditions are constant, with only increasing flank wear, chip forming along the force acting on the front surface remains constant. So, the increase in total forces noticed should be assumed to be as a result of increasing plowing forces, since and due to increasing flank wear, the plowing force is increased at the contact area between the tool flank surface and the processed material. The results obtained confirm the conclusion that the

extrapolation method on zero uncut thickness cannot be used to determine the plowing forces [14].

Lipatov, A. et al. [15] considered another approach which is an extrapolation to zero wear area. In the proposed methodology, the cutting tool has different width h_x of the wear area at the rear surface. The cutting force components and are determined experimentally. As shown in Figure 7, nonlinear behavior was obtained.

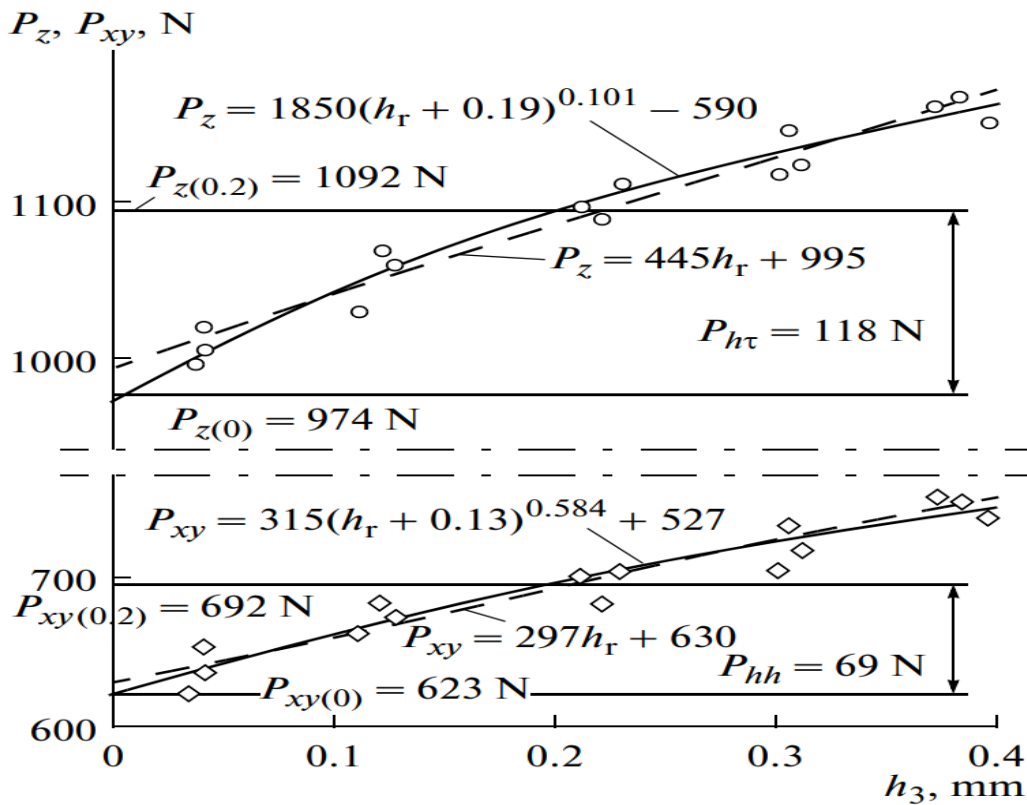


Figure 7: P_z and P_{xy} vs. Wear Area Width h [15]

The extrapolation method is not a precise method to determine the plowing forces. When extrapolating the cutting forces into zero feed, the force obtained is the plowing force but at ideal sharpness. Ideal sharpness doesn't exist; therefore, the plowing force received by the extrapolation method is imprecise.

Consequently, cutting forces follow a bilinear fashion to be determined by understanding the physics happening behind the cutting process. Various parameters affect the cutting process. One of the major parameters is the cutting-edge radius which increases the parasitic forces. When the cutting-edge radius is minimal (i.e., Ideal Sharpness), plowing forces are negligible to cutting forces. As the cutting-edge wears, the radius increases becoming round thus not of a constant value. If the cutting-edge radius becomes larger than the uncut chip thickness t , the plowing forces increase drastically leading for it to take up a large portion of the cutting forces; this state of cutting is inefficient from an energy perspective.

Eggleston et al. [16] conducted 2D orthogonal tests with varying both the rake angle and speed as test parameters. Analyzing this data, it is noticed that while the tangential force varies linearly versus feed, this is not the case with thrust where the shape is very nonlinear. Such behavior is eluded to in recent work by Roth and Ismail [17] where a bi-linear fit was utilized to model the experimentally measured forces versus feed. For very small feeds, the forces were much lower than would be predicted have they extrapolated back to zero feed from relatively large feeds. Using orthogonal tests conducted on AL2024-T4 by Eggleston, vertical and horizontal edge forces generated by the deviation of the tool from sharp ideal sharp tool geometry are estimated using: (1) Extrapolation to zero feed axis of linearly fitted data and (2) Extrapolation to zero feed axis of a bilinear fitted data [16]. So, edge forces obtained using linear extrapolation and bilinear extrapolation to zero feed are generated for Brass and Aluminum 2024-T4. Several fitting models are used: a linear, fourth-order, exponential, and a power fits and are compared:

In the case of both forces, the speed was found to increase the edge forces for practically all values of rake angle and for the same velocities, the edge force decreases as the rake angle increase. For modeling the edge forces, a similar form to that proposed by Hamade et al [18] and Stephenson [19] was employed for modeling cutting force in general. A bilinear extrapolation to zero feed for estimating edge forces is applied. Analyzing the variation of estimated normal and horizontal edge force as a function of tool rake angle, a linear dependency is clearly identified. Nevertheless, expected edge forces for the same material (brass) and equal cutting rake angles estimated using bilinear extrapolation are lower than edge forces estimated using bilinear extrapolation.

Rech, J. et al. [20] studied the Influence of cutting-edge radius on the wear resistance of PM-HSS milling inserts. The paper analyzed the performance of PM-HSS inserts with various cutting-edge radii in face milling in an annealed case-hardening steel experimentally. The behavior of coated PM-HSS milling inserts was revealed to depend strongly on the surface pre-treatment before coating. The main factors inducing the wear resistance was found to be the modifications of the cutting-edge radius and the modifications of the surface texture. Honed tools with a cutting-edge radius of 10 micrometers performed best in dry milling. The cutting tool life affectedly increased by a factor of 4–5 compared to a standard ground tool. The small cutting-edge radius averts the PM-HSS tool from chipping off the substrate and from fatigue fracture of the coating. Furthermore, based on FE modeling, an optimum cutting edge radius of 14 micrometers was revealed to exist, permitting a minimization of the equivalent stress inside the coating, delaying the crack initiation, and improving the wear resistance of the tool [20].

Iwata, K. et al. [21] attempted to construct modeling of orthogonal cutting process by using the rigid-plastic finite element method (FEM) as an analytical tool. The paper discussed the effect of tool geometry on the mode of deformation. For an edge radius of $r/t=0.1$, the results simulated were compared to an edge radius of $r/t=0.5$. As shown in Figure 8, as the radius increases, the deformation region extends deeper into the material, and the resulted strain also becomes larger. Also, with increasing radius, both cutting and thrust forces increase while the curl radius of chip decreases. The thickness of the chip is found to be independent of the radius of the tool edge [21].

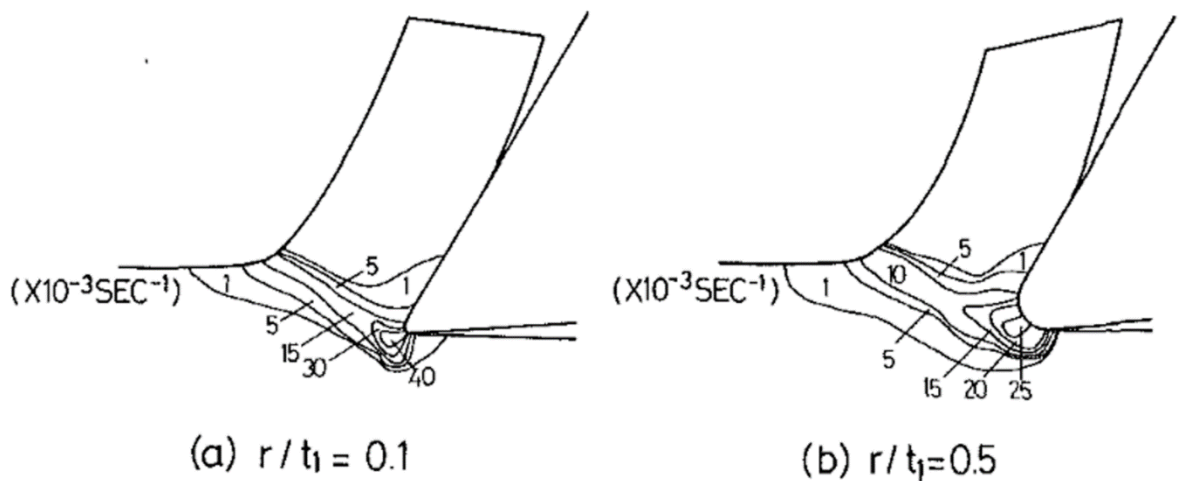


Figure 8: Effect of radius of tool edge on mode of deformation in cutting ($\alpha = 30$ deg, $t_1 = 50 \mu\text{m}$, $\mu = 0.5$, $mF = 0.5$, $v = 1 \mu\text{m/sec}$) [21].

Tansel, I.N. et al. [22] proposed two different encoding methods to assess wear during the machining of soft materials such as aluminum. Estimation of the tool condition is precise when the feed and thrust cutting forces are measured at identical cutting conditions. It was noticed that during the machining of aluminum or any soft

material, cutting forces variations increased continuously. Meaning that the cutting edges progressively lost their effectiveness. The results also indicated that tool condition is easier to be estimated when machining soft materials, while it was harder when machining hard materials [22].

Waldorf, D. J. [23] proposed a simplified 2D slip line field for deformation so that the 3D forces caused by chamfered or rounded edges are predicted knowing the size of the hone, chamfer, and the material shear stress. Tangential, longitudinal, and radial forces were collected, and the chips were collected to determine the shear angle. It was noticed that the forces increased upon increasing the edge radius. The results in Figure 9 displays that the tangential force increased slightly while on the other hand, the radial/longitudinal increased dramatically [23].

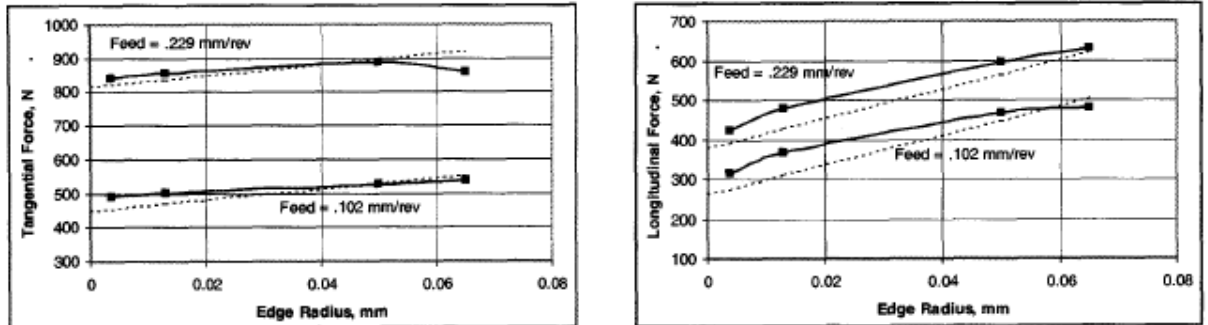


Figure 9: Effect of Cutting Edge Radius on Tangential and Longitudinal forces respectively

Another research was done by Waldorf, D.J. et al. [24] which focused on two models of material flow. The first is based on the assumption of a material separation existing between the tool and the work piece, while the second model suggests the existence of a stable build-up of work piece material adhering to the edge and creating a

larger practical clearance face for the tool, leading to diverting material at its outer extreme or edge. Both models are depicted in Figure 10 and Figure 11.

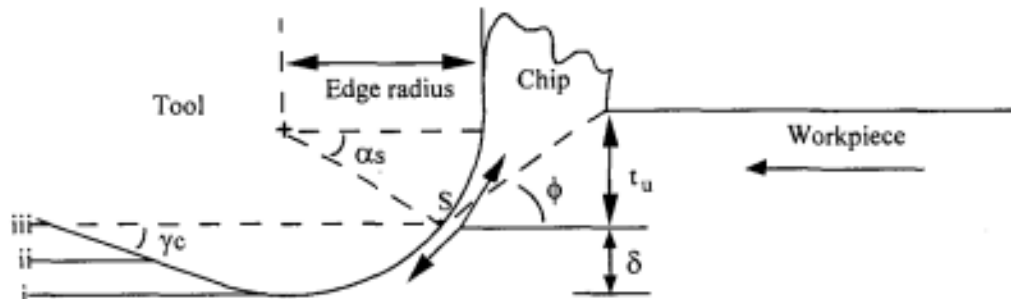


Figure 10: Cutting with material separation point on edge with 3 recovery scenarios [24]

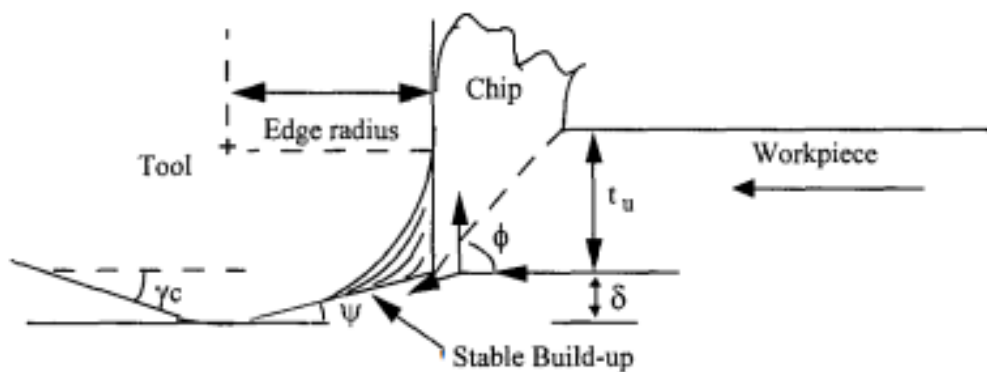


Figure 11: Cutting with a stable build-up on edge [24]

As a result, the plowing components were seen to accommodate 60 to 70 percent of the thrust force and 25 to 40 percent of the cutting force having the feed rate approaching the value of the edge radius under the blunt indenter model. It was also noticed in all cases, that at a cutting-edge radius of 0.3969 mm, the plowing components are about half of those observed for the 0.7938 mm edge radius. From Figure 12 and Figure 13 it was found out that predictions don't drift far from experimental results as

the average relative deviation of the observed values from the model predictions was calculated to 16.20 percent [24].

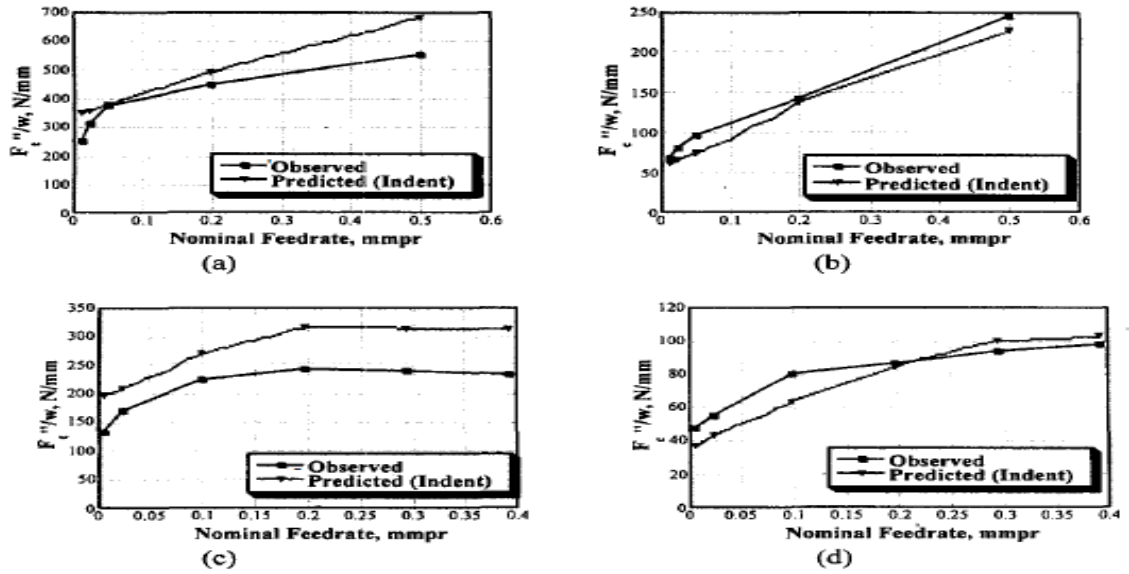


Figure 12: Observed and predicted plowing forces using cylinder indenter model for (a) $r = 0.7938$ mm thrust direction (b) $r = .7938$ mm cutting direction (c) $r = .3969$ mm thrust $r = .7938$ mm cutting direction (c) $r = .3969$ mm thrust direction and (d) $r = .396$ [24]

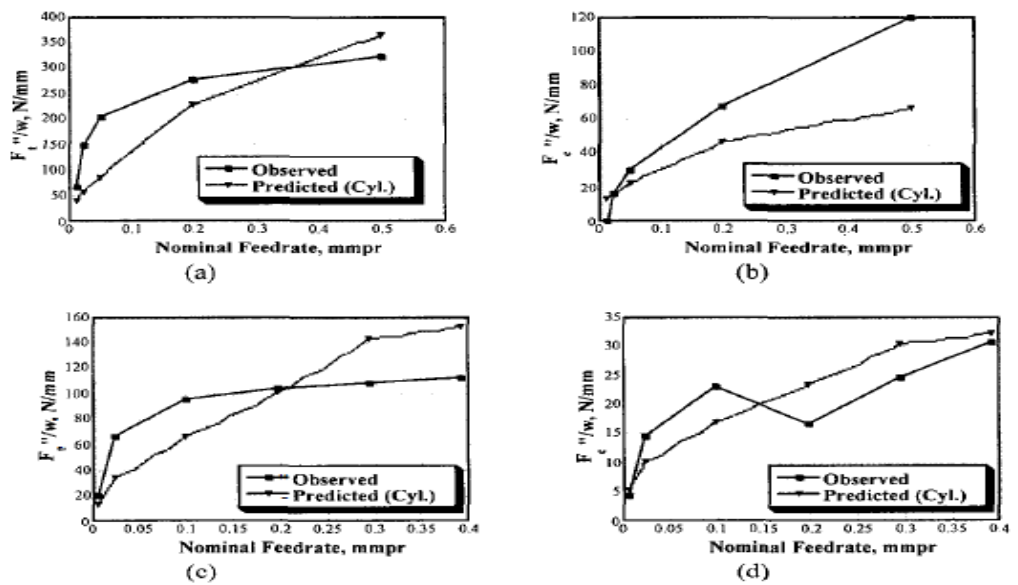


Figure 13: Observed and predicted plowing forces using blunt indenter model for (a) $r_c = 0.7938$ mm thrust direction (b) $r_c = 0.7938$ mm cutting direction (c) $r_c = 0.3969$ mm thrust $r_c = 0.7938$ mm cutting direction (d) $r_c = 0.3969$ mm thrust direction and (d) $r_c = 0.3969$ mm cutting direction [24]

In this research experimental measurements of parasitic forces will be done on the HAAS SL 20 CNC at minimal feeds less than the cutting-edge radius. Since the feeds are less than the CER, such experiments would allow to measure directly the parasitic forces at different cutting speeds and feeds, studying the effects of various parameters on the cutting process in 2D orthogonal cutting. An analytical model would also be developed that relates the parasitic forces to different settings involving cutting edge radius, feed, cutting speed, and operating temperature. At the end of the research, a model characterizing parasitic forces would be created defining 2D orthogonal, taking into consideration all the parameters affecting the process from feeds, cutting speeds, rake angle, temperature, and cutting-edge radius.

CHAPTER II

METHODOLOGY

A. Experimental

1. Tool Setup and Force Measurements

The experiments were performed on the HAAS SL 20 CNC machine found. The CNC lathe machine possesses a maximum spindle speed of 4000 RPM with a maximum power of 14.9 kW. Geometrically, the machine has a chuck size of 210 mm and a bar capacity of 64 mm possessing up to 12 tool stations. As for the axis motors, the maximum thrust force in the X direction is 18238 N, while it reaches a value of 22686 N in the Y direction. For the fixture, firstly, a tool holder was designed to accompany all the tools available. A steel block of dimensions 82x50x50 mm was first cut. Then a groove of depth 20 mm and thickness 28 mm was milled across the block from the front side and the left side. The tool holder would be firmly mounted on a Kistler 3-Component (Fx, Fy, Fz) Dynamometer (Type 9254). At the back side of the dynamometer, a rod is attached to connect the dynamometer to the tool station of the CNC. The rod at the back would prove to be a very important asset preventing vibrations and therefore allowing for a smoother, more accurate experiments.

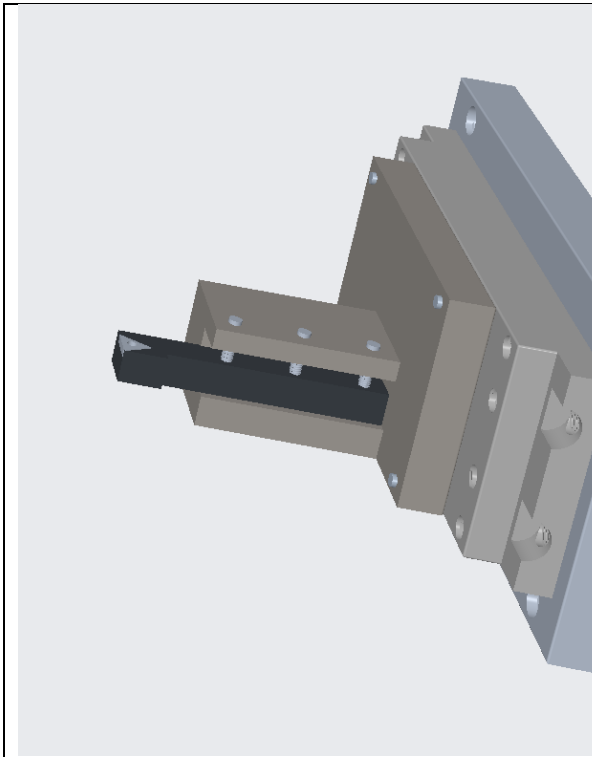


Figure 14: Setup design on CREO

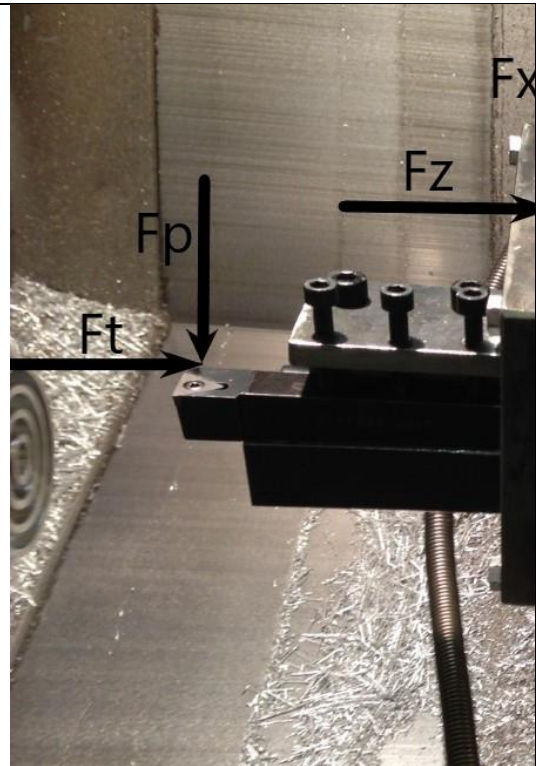


Figure 15: The final design manufactured and used in the experiments

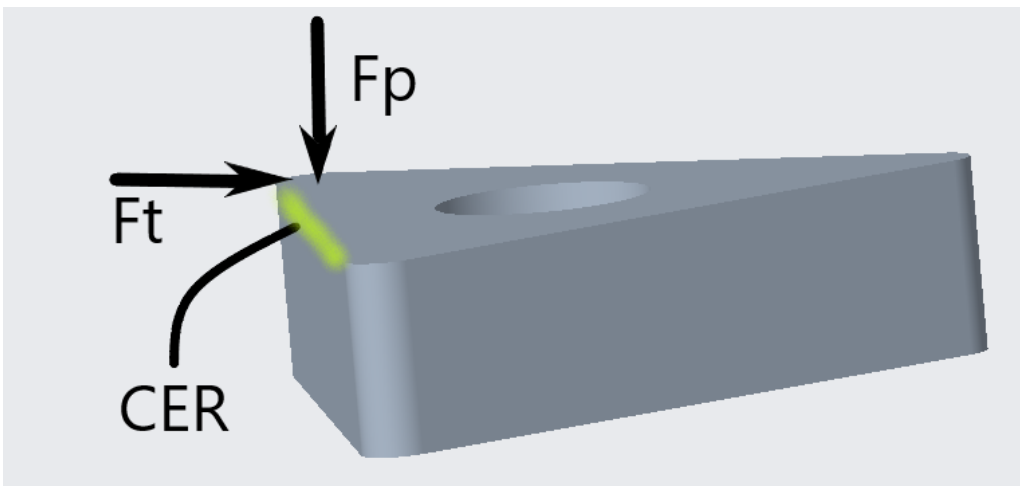


Figure 16: Forces on the Cutting-Edge Radius

The Kistler 5070 charge amplifier acquires and amplifies the signal emanating from the dynamometer, which is then collected by a custom Kistler software. The

amplifier possesses a typical error percentage of just 0.3 % with a maximum of 1 %.

The system would start taking measurements 5 seconds before cutting and would stop 5 seconds after the tool completely disengages from the work piece. The sampling rate is to be input at 1000 Hz. The data would then be saved and exported into an excel sheet to have the plowing force calculated.

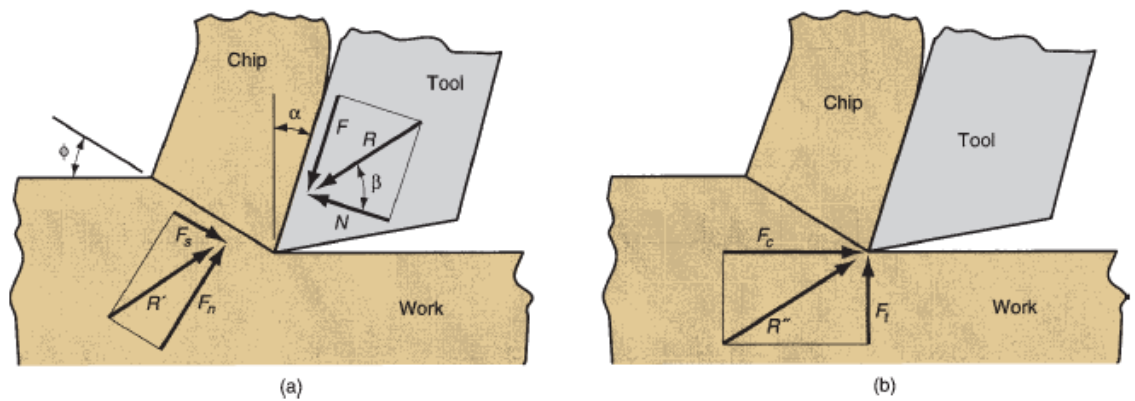


Figure 17: Forces in metal cutting: (a) forces acting on the chip in orthogonal cutting, and (b) forces acting on the tool that can be measured

As described in Figure 17 the forces acting on the chip are then calculated using the Equation (2-8):

$$F = F_c \sin \alpha + F_t \cos \alpha \quad (2)$$

$$N = F_c \cos \alpha + F_t \sin \alpha \quad (3)$$

$$F_s = F_c \cos \phi + F_t \sin \phi \quad (4)$$

$$F_n = F_c \sin \phi + F_t \cos \phi \quad (5)$$

However, since rake angle=0,

$$F = Ft \quad (6)$$

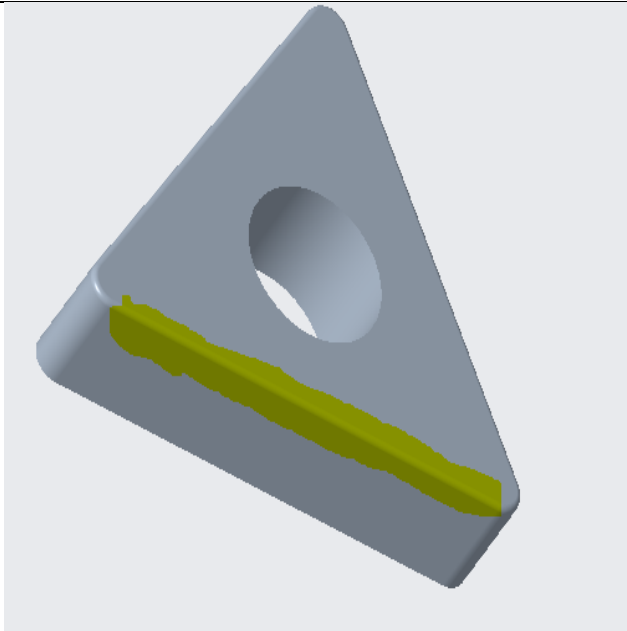

$$N = Fc \quad (7)$$

$$\mu = F/N = Ft/Fc \quad (8)$$

F and N were measured and then substituted into Equation (8) where the coefficient of friction was obtained.

2. Tool scanning and verification

It is then required to measure the cutting-edge radius using the optical profiler, to identify its effect on cutting and thrust forces. The order of magnitude is 20 to 30 micrometers. The tool was scanned initially to find the cutting-edge radius which was measured to be 5 micrometers as shown in Figure 19.

	
<p>Figure 18: Portion of the tool scanned under the microscope. (The Cutting-Edge Radius)</p>	<p>Figure 19: Cutting Edge Radius scanned under the microscope</p>

3. Temperature Measurements

Afterward, the temperature will also be taken by FLIR C2 Spot thermal Camera. Measuring temperature during cutting helps in understanding the thermal behavior that the tool insert is experiencing.



Figure 20: Thermal Camera

4. Process Parameters

Cutting parameters significantly affect the experiments being done; thus, a proper variety of parameters is critical. The data obtained from the literature were utilized to develop the test matrix displayed in

Table 2. The cutting time would be fixed to be 1 second for all tests. An additional 1 second of rubbing is added to the end of each cut; zero feed cutting. The work piece would be made from five concentric tubes shown in Figure 21.

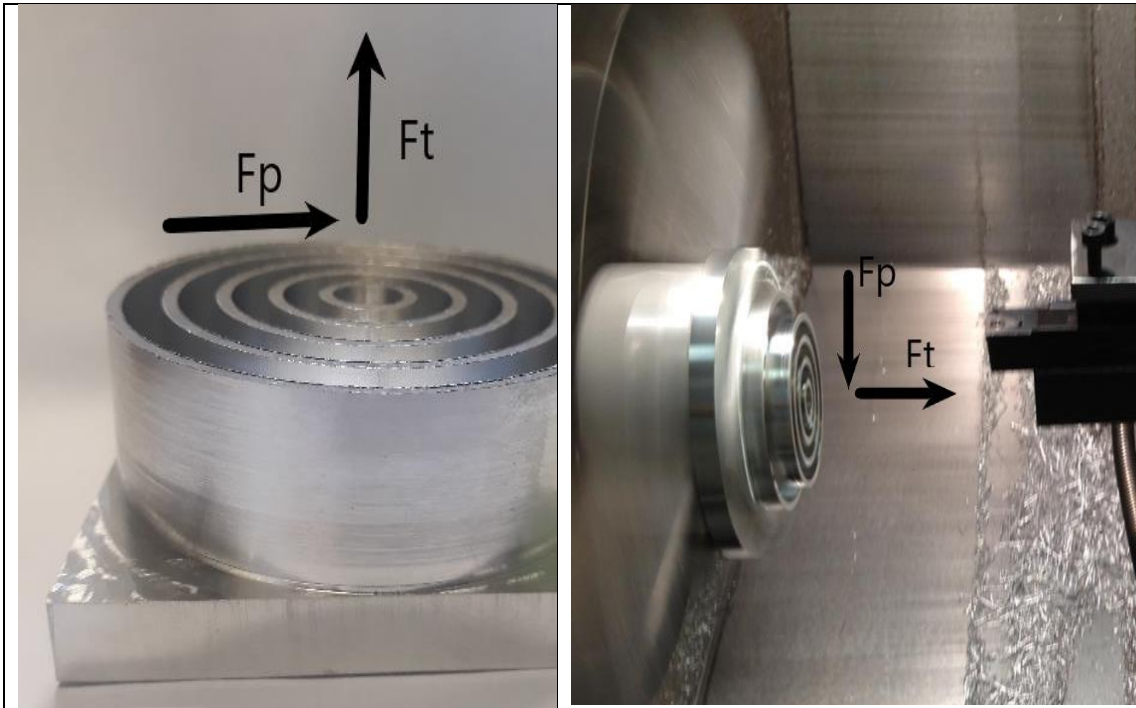


Figure 21 (a) AZ31 Workpiece

(b) AZ31 Workpiece mounted on the CNC

a. Cutting Speeds

Fixing the spindle rotational speed at 720 RPM, the following range of cutting speed would be covered shown in Table 1

Table 1: Cutting Speeds

		Average tube diameter (mm)	resulting cutting speed m/min
at 720 Rpm	1- tube 1	68	153.8
	2-tube 2	54	122.1
	3-tube 3	40	90.5
	4-tube 4	26	58.8
	5-tube 5	12	27.1

b. Test Matrix

As for the feed, it was decided to start with a value of 0.0025 mm/rev and then keep doubling until a value of 0.025 mm/rev. Cutting at higher feeds would be needless since parasitic forces are minimal at such ranges. Hence, a low range is preferred in this research to determine the parasitic forces.

Table 2: Experimental test matrix covering all feeds and RPMs.

			Spindle RPM				
			720	720	720	720	720
			cutting speed m/min				
			27	60	90	120	150
			A	B	C	D	E
Feed mm/ rev	0.0005	1	X	X	x	x	x
	0.001	2	X	X	x	x	x
	0.0015	3	X	X	x	x	x
	0.002	4	X	X	x	x	x
	0.0025	5	X	X	x	x	x
	0.003	6	X	X	x	x	x
	0.0035	7	X	X	x	x	x
	0.004	8	X	X	x	x	x
	0.0045	9	X	X	x	x	x
	0.005	10	X	X	x	x	x
	0.006	11	X	X	x	x	x
	0.007	12	X	X	x	x	x
	0.008	13	X	X	x	x	x
	0.009	14	X	X	x	x	x
	0.01	15	X	X	x	x	x

For each cutting speed a fresh cutting edge was used to perform the tests at that speed. As for the tests order, tests were done in order starting from 0.0005 mm/rev reaching 0.01 mm/rev. The test order is represented in

Table 3.

Table 3: Experimental test matrix covering all feeds and RPMs.

			Spindle RPM				
			720	720	720	720	720
			cutting speed m/min				
			27	60	90	120	150
			A	B	C	D	E
Feed mm/ rev	0.0005	1	1 st	1 st	1 st	1 st	1 st
	0.001	2	2 nd	2 nd	2 nd	2 nd	2 nd
	0.0015	3	3 rd	3 rd	3 rd	3 rd	3 rd
	0.002	4	4 th	4 th	4 th	4 th	4 th
	0.0025	5	5 th	5 th	5 th	5 th	5 th
	0.003	6	6 th	6 th	6 th	6 th	6 th
	0.0035	7	7 th	7 th	7 th	7 th	7 th
	0.004	8	8 th	8 th	8 th	8 th	8 th
	0.0045	9	9 th	9 th	9 th	9 th	9 th
	0.005	10	10 th	10 th	10 th	10 th	10 th
	0.006	11	11 th	11 th	11 th	11 th	11 th
	0.007	12	12 th	12 th	12 th	12 th	12 th
	0.008	13	13 th	13 th	13 th	13 th	13 th
	0.009	14	14 th	14 th	14 th	14 th	14 th
	0.01	15	15 th	15 th	15 th	15 th	15 th

Table 4: Machining time meter

			Spindle RPM				
			720	720	720	720	720
			cutting speed m/min				
			27	60	90	120	150
			A	B	C	D	E
Feed mm/ rev	0.0005	1	5 sec	5 sec	5 sec	5 sec	5 sec
	0.001	2	10 sec	10 sec	10 sec	10 sec	10 sec
	0.0015	3	15 sec	15 sec	15 sec	15 sec	15 sec
	0.002	4	20 sec	20 sec	20 sec	20 sec	20 sec
	0.0025	5	25 sec	25 sec	25 sec	25 sec	25 sec
	0.003	6	30 sec	30 sec	30 sec	30 sec	30 sec
	0.0035	7	35 sec	35 sec	35 sec	35 sec	35 sec
	0.004	8	40 sec	40 sec	40 sec	40 sec	40 sec
	0.0045	9	45 sec	45 sec	45 sec	45 sec	45 sec
	0.005	10	50 sec	50 sec	50 sec	50 sec	50 sec
	0.006	11	55 sec	55 sec	55 sec	55 sec	55 sec
	0.007	12	60 sec	60 sec	60 sec	60 sec	60 sec
	0.008	13	65 sec	65 sec	65 sec	65 sec	65 sec
	0.009	14	70 sec	70 sec	70 sec	70 sec	70 sec
	0.01	15	75 sec	75 sec	75 sec	75 sec	75 sec

B. Analytical solutions (using Matlab)

1. Cutting regions & Force Diagram:

A new force diagram is developed for this research shown in Figure 22. The cutting process is represented by 3 regions: Region 1: Rubbing, Region 2: Plowing, and Region 3: Cutting.

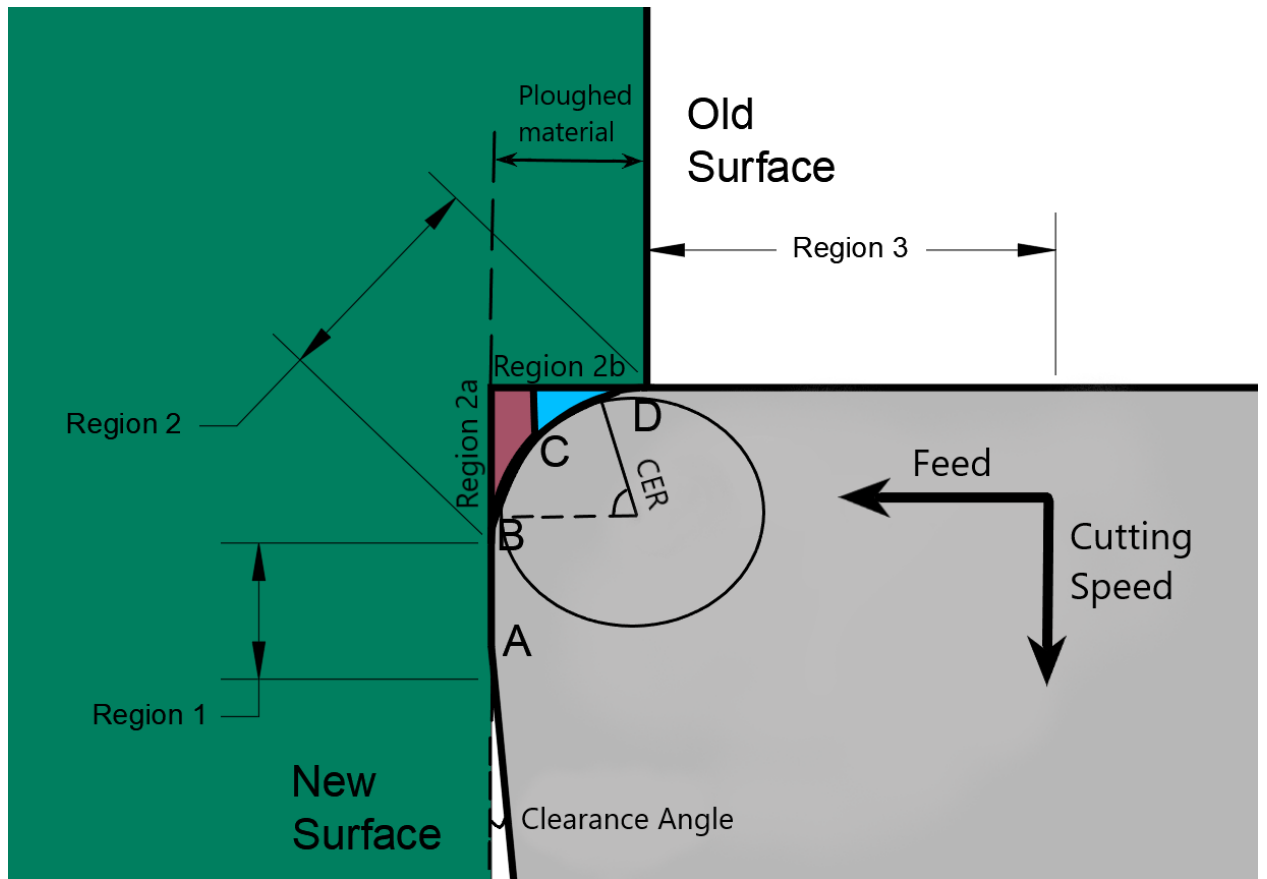


Figure 22: Cutting Regions

2. *Region 1: Rubbing Phase*

Starting with very small feed values (approximately 0), only friction forces are acting on the tool. The process happening in this case is purely rubbing as shown in Figure 23.

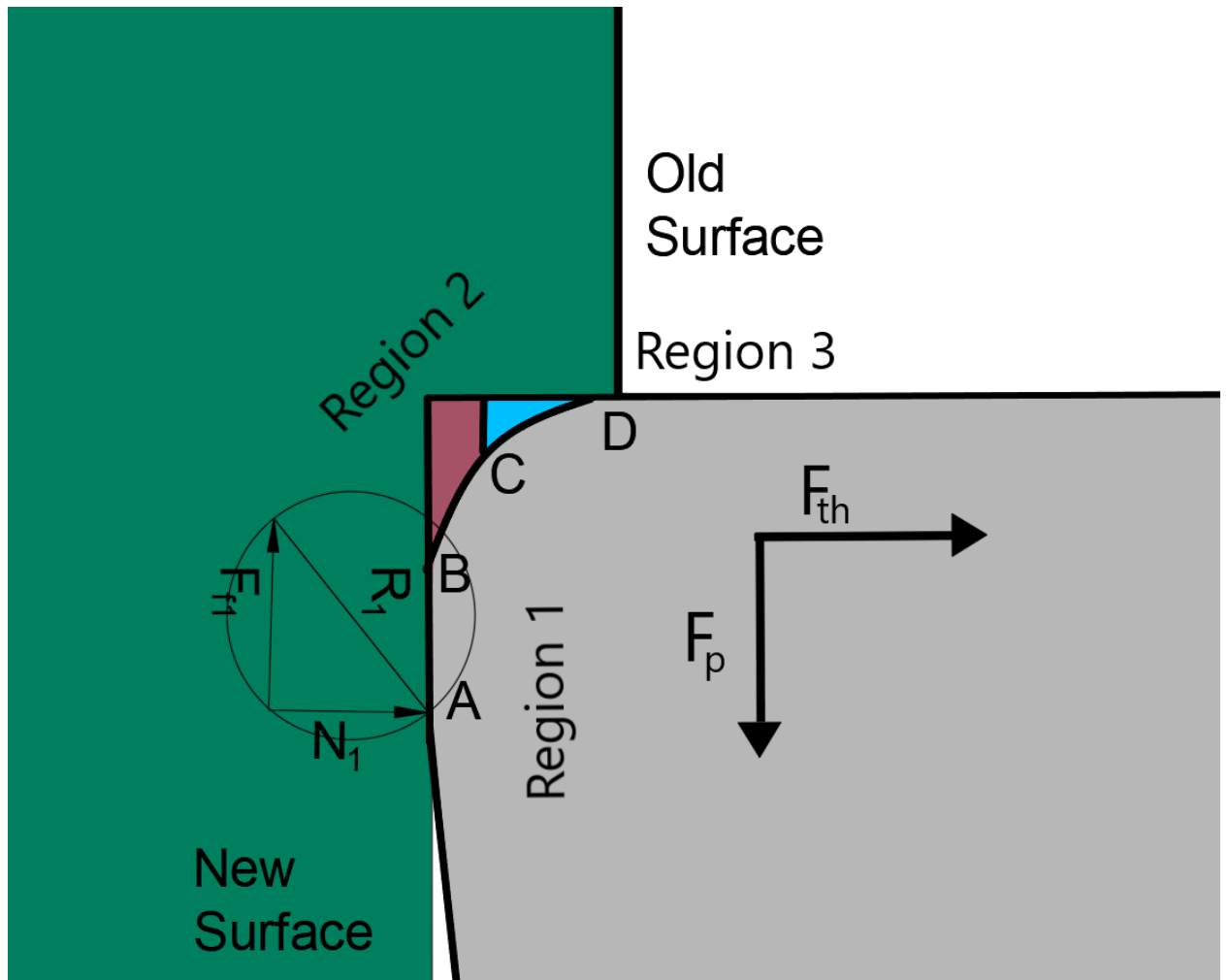


Figure 23: Forces acting in Region 1. (Phase 1)

The total forces acting in this region is R_1 , composed of the friction force component and normal force component

$$\text{Total Forces} = R_1 = F_{f1} + N_1 \quad (9)$$

Where,

$$F_{f1} = \mu \times \text{Length of contact area in Region 1} \quad (10)$$

To calculate the friction forces, several friction models are proposed:

- Constant Shear Friction Coefficient

$$\mu = 0.3$$

- Temperature dependent friction Coefficient

To calculate the friction forces, friction model proposed by [25] is followed:

$$\mu = 1 - ae^{\frac{b}{T+c}} \quad (11)$$

3. Region 2: Plowing Phase

As the feed increases, another force is added to the process which is the plowing force. When the feed becomes larger than the cutting-edge radius, plowing forces start acting on the tool leading for it to take up a large portion of the cutting forces. Various parameters affect the plowing forces some of which are the cutting speed, feed, and the cutting-edge radius of the tool. As the tool wears, the cutting-edge radius increases and upon reaching a value larger than the feed, the plowing forces increase drastically. The force diagram is shown in Figure 24:

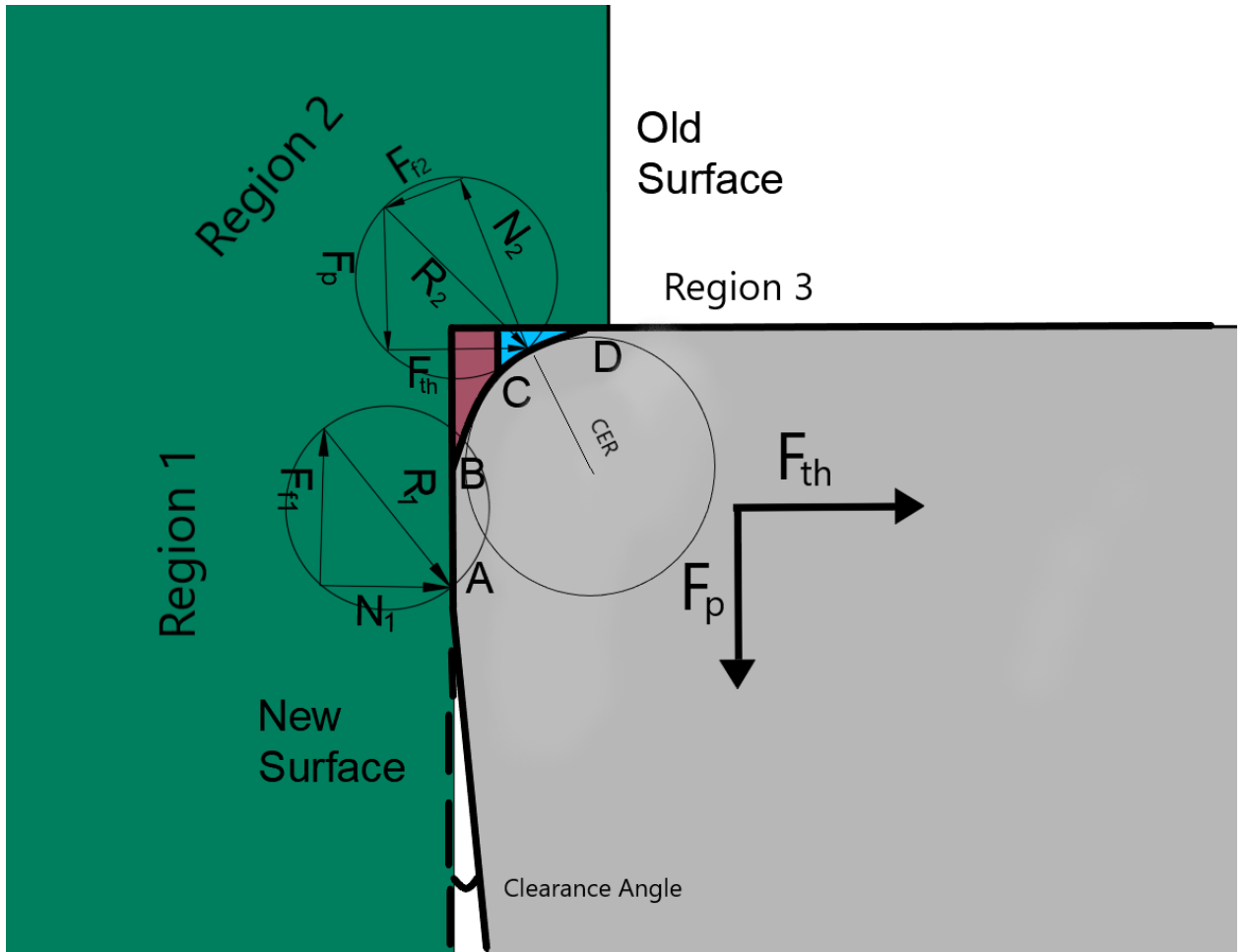


Figure 24: Forces acting in Region 1 and Region 2. (Phase 2)

Region 1 & 2 are engaged in this state, so the total forces acting on the tool are calculated by:

$$R_1 = F_{f1} + N_1 \quad (9)$$

$$R_2 = F_{f2} + N_2 + F_p + F_t \quad (12)$$

$$F_x = F_{f1} + F_p - F_{f2} \quad (13)$$

$$F_z = N_1 + F_t - F_{f2} \quad (14)$$

$$Total\ Forces = R_1 + R_2 = F_{f1} + N_1 + F_{f2} + N_2 + F_p + F_t \quad (15)$$

As in region 1, the friction force F_{f2} acting in region 2 depends on the length of the contact area between the tool and the workpiece. It depends on how engaged the tool into the work piece is.

$$F_{f2} = \mu \times Length\ of\ Contact\ Area\ in\ Region\ 2 \quad (16)$$

The cutting edge of the tool will be assumed to be a quadrant of a circle. So, the contact area between the tool and the work piece is an arc. To calculate the length of contact, the length of an arc is to be calculated.

Where,

$$Length\ of\ Arc\ l_2 = (2 \times \pi \times CER) \left(\frac{\theta}{360} \right) \quad (17)$$

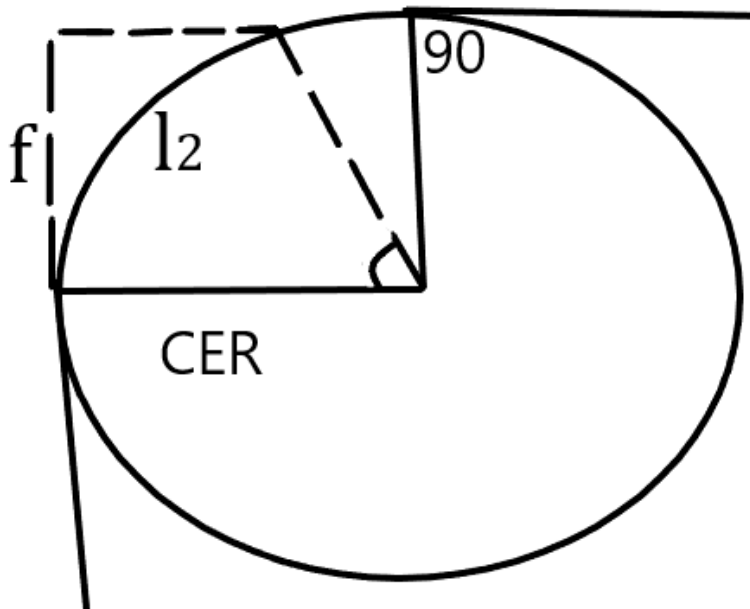


Figure 25: Calculation of angle theta

Since the cutting edge is a quadrant, θ ranges from 0 to 90

Therefore,

$$F_{f2} = \int_0^{90} \mu (2 \times \pi \times CER) \left(\frac{\theta}{360} \right) d\theta \quad (18)$$

Integrating from 0 to 90

$$F_{f2} = \mu (2 \times \pi \times CER) \left(\frac{\theta^2}{720} \right) \quad (19)$$

Projecting F_{f2} on x & z:

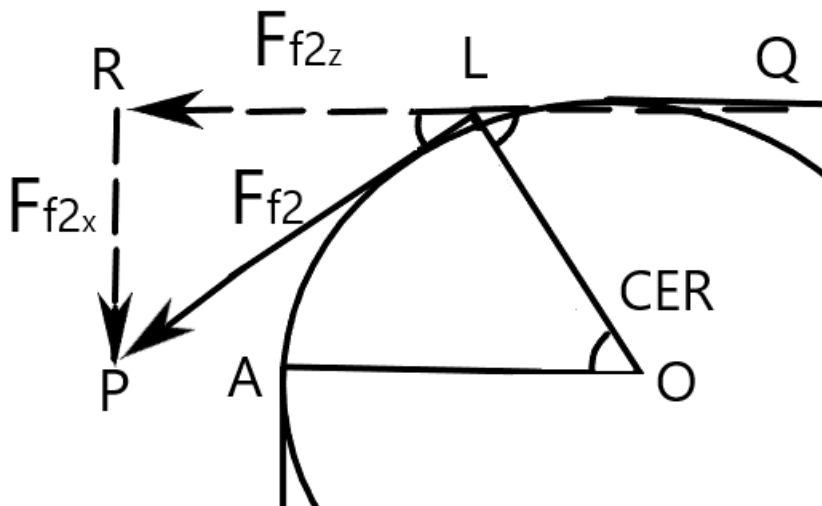


Figure 26: Projection of Friction force 2 on x and z

$$\widehat{AOL} = \widehat{OLQ} \quad (\text{Alternate Angles})$$

But,

$$\widehat{QLO} + \widehat{OLP} + \widehat{PLR} = 180$$

$$\widehat{OLP} = 90 \quad (F_{f2} \text{ is tangent to the arc})$$

Therefore,

$$\widehat{PLR} = 90 - \widehat{OLQ} = 90 - \widehat{AOL}$$

$$\widehat{PLR} = 90 - \theta$$

$$F_{f2x} = F_{f2} \sin (90 - \theta) \quad (20)$$

$$F_{f2z} = F_{f2} \cos (90 - \theta) \quad (21)$$

Projecting N_2 on x & z:

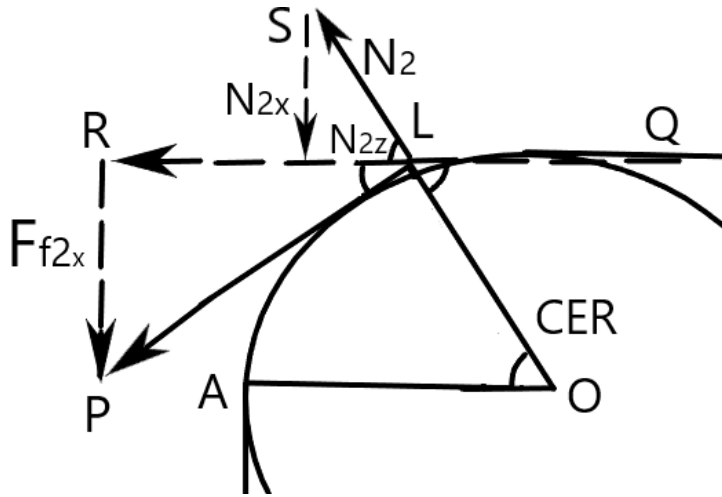


Figure 27: Projection of Normal 2 on x and z

$$\widehat{RLS} = \widehat{AOL} \text{ (Corresponding Angles)}$$

$$\widehat{RLS} = \theta$$

$$N_{2x} = N_2 \sin (\theta) \quad (22)$$

$$N_{2z} = N_2 \cos (\theta) \quad (23)$$

The indentation force F_{2i} calculated by using the model proposed by Waldorf [24] by:

$$F_{2i}(x) = F_{2i}(0) \times \sqrt{\left(1 - \frac{x}{a}\right)^2}$$

(24)

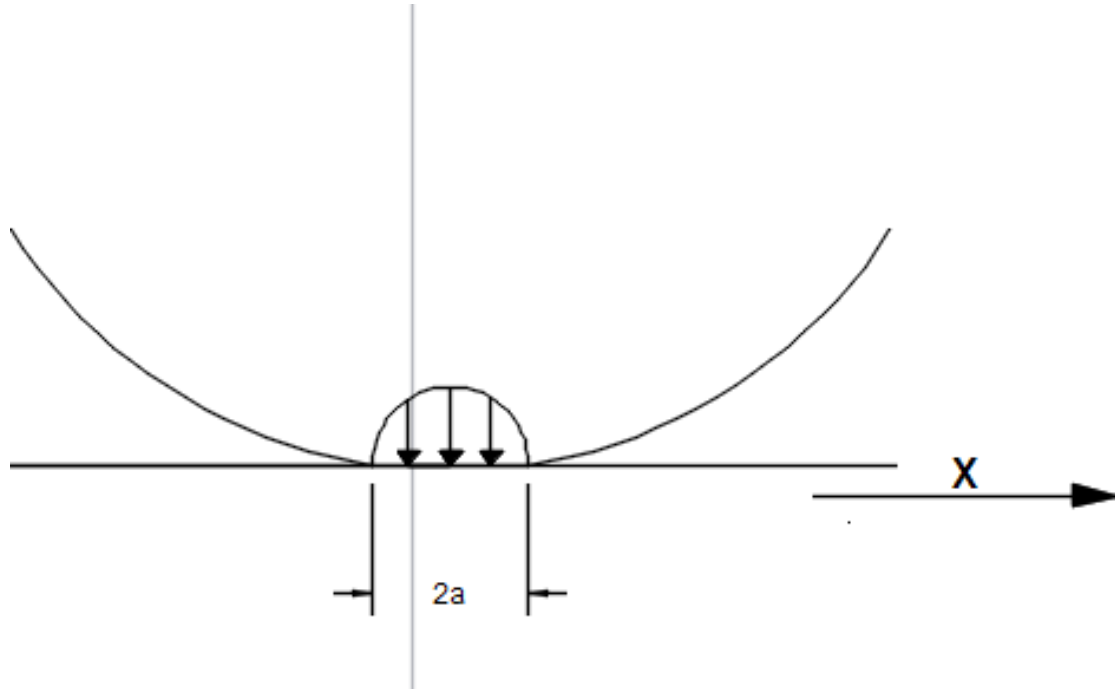


Figure 28: Half space model [24]

Where $F_{2i}(0)$ is the maximum pressure in the center of contact ($x=0$), and $F_{2i}(x)$ goes to zero at the ends of contact ($x \pm a$). $F_{2i}(0)$ is related to the total load F_i by:

$$F_{2i}(0) = \left(\frac{2F_i}{\pi a l}\right) \quad (25)$$

The total is related to the half-space material properties and the cutting-edge radius r by:

$$a_{yield} = \frac{2(1-\nu^2)CER}{0.43E} \cdot k \quad (26)$$

$$\delta_{yield} = 4.75 \frac{a^2_{yield}}{2xCER} \quad (27)$$

$$P_{yield} = \frac{\pi a_{yield}^2 E}{4(1-\nu^2) \cdot CER} \cdot w \quad (28)$$

$$P = \frac{\delta}{\delta_{yield}} \cdot P_{yield} \quad (29)$$

Only half of the cylinder is assumed to be in contact, so the thrust direction force due to plowing F_t , is equal to one half of P [24].

Therefore,

$$F_t = 0.5P \quad (30)$$

A tangential force component Q arises due to friction from the sliding edge. The friction contact along the interface is assumed to be adhesive in nature with the shear stress proportional to the flow stress by a friction factor m . It is assumed that for the small values of θ found in the experiments, the contact area is approximately parallel to the work piece surface. The cutting direction force due to ploughing F_p is given by

$$F_p = (m \cdot k) \cdot CER \cdot \cos^{-1} \left(1 - \frac{\delta}{CER} \right) \cdot w \quad (31)$$

Substituting Equations (10) (19) and (28) in Equation (13):

$$F_x = \overbrace{\mu \times l_1}^{F_{f1}} + \overbrace{(k) \times CER \times \cos^{-1} \left(1 - \frac{\delta}{CER} \right) \times w}^{F_p} - \underbrace{(0.1k) \times CER \times \cos^{-1} \left(1 - \frac{\delta}{CER} \right) \times w \sin(\theta)}_{N_{2x}} + \underbrace{\mu(2 \times \pi \times CER) \left(\frac{\theta^2}{720} \right) \sin(90 - \theta)}_{F_{2x}}$$

(32)

$$F_z = \overbrace{P_{yield}}^{N_1} + \overbrace{\frac{5\pi(1-\nu^2) \cdot CER \cdot k^2}{0.43 \times E} \cdot w}^{F_t} + \overbrace{N_2 \cos(\theta)}^{N_{2z}} + \overbrace{F_{f2} \sin(\theta)}^{F_{2z}}$$

(33)

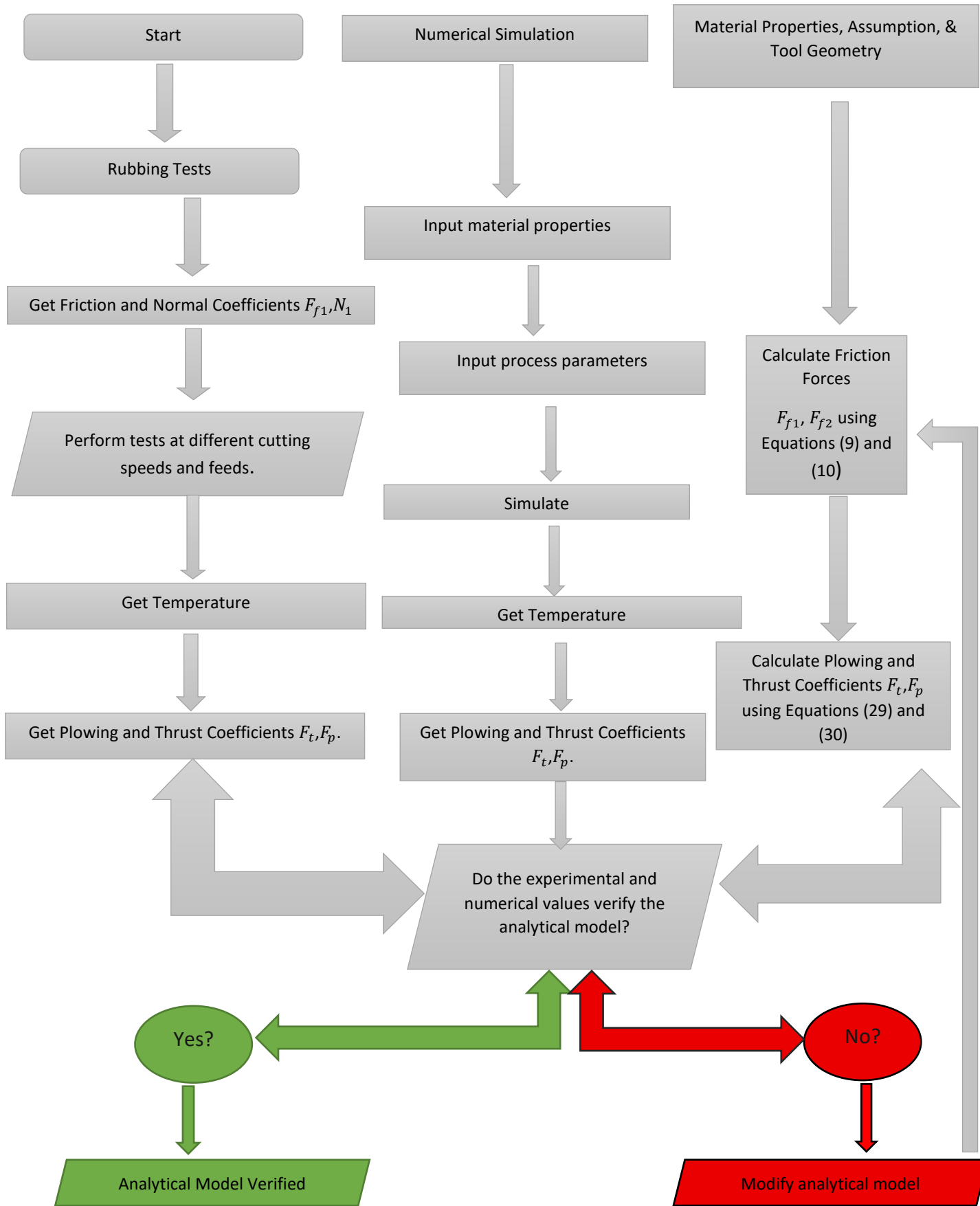
4. Cutting Edge Radius and Tool wear:

In the above analytical solution for the plowing and the friction forces, the equations for each is written in terms of the cutting-edge radius and the contact length respectively. However, it is well known that tool inserts wear with increasing machined length and both CER wear and flank wear are observed in most cutting processes. Hence, the CER and the contact length are not constant and are variables with varying speed and feed.

To try and predict the flank wear happening to the tool the equation proposed by followed:

$$\text{CER} = a_1 f^2 + b_1 V^2 \quad (34)$$

$$\text{VB} = a_2 f^2 + b_2 V^2 \quad (35)$$



C. Numerical Modeling (FEM)

Numerical Modeling is one of the main methods used to study machining processes. Finite element modeling (FEM) is widely used to simulate metal cutting processes when attempting to obtain different parameters such as forces, stresses, strains, temperature, and damage done to the tool. Finite Element Modeling through DEFORM will be used in this research to verify the experimental data obtained.

1. Pre-Simulation

a. Modeling of Shear Behavior:

The model describing the shear behavior of AZ31B has been determined as a function of the plastic strain, the strain rate and the temperature:

$$\bar{\epsilon} = A[\sinh \alpha \bar{\sigma}]^n \exp \left[-\frac{\Delta H}{RT_{abs}} \right]$$

Where,

Table 5: Parameters for AZ31B

Constant (A)	Constant (α)	Activation energy ΔH	Stress Component (n)	Gas constant R
27.5	0.052	130000	1.8	8.31447

b. Tool Geometry:

Table 6: Tool Geometry

	Tool 1
ISO Name	<i>TCMW16 T308</i>
Inscribed Circle Diameter	9.525 mm
Cutting Edge Length	16.5 mm
Rake Angle	0
Clearance Angle	7
EPSR	60
Insert Thickness	3.97 mm
Corner Radius	0.8 Mm

c. Parameters:

Simulations will be done at different speeds and feed to mirror the experimental work done. All the cells shown in the test matrix in

Table 2 are to be replicated.

The friction coefficient will be modeled as a function of temperature. The data obtained from the experimental work would be utilized to input a temperature dependent friction function into DEFORM.

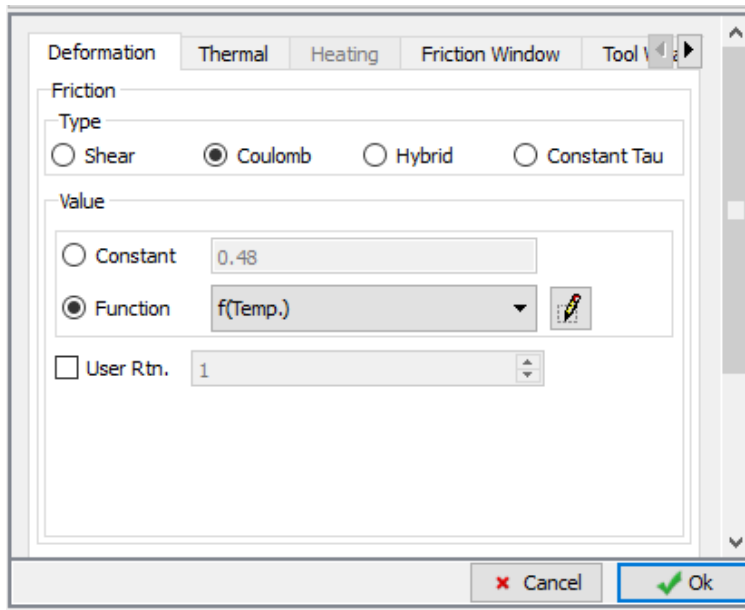
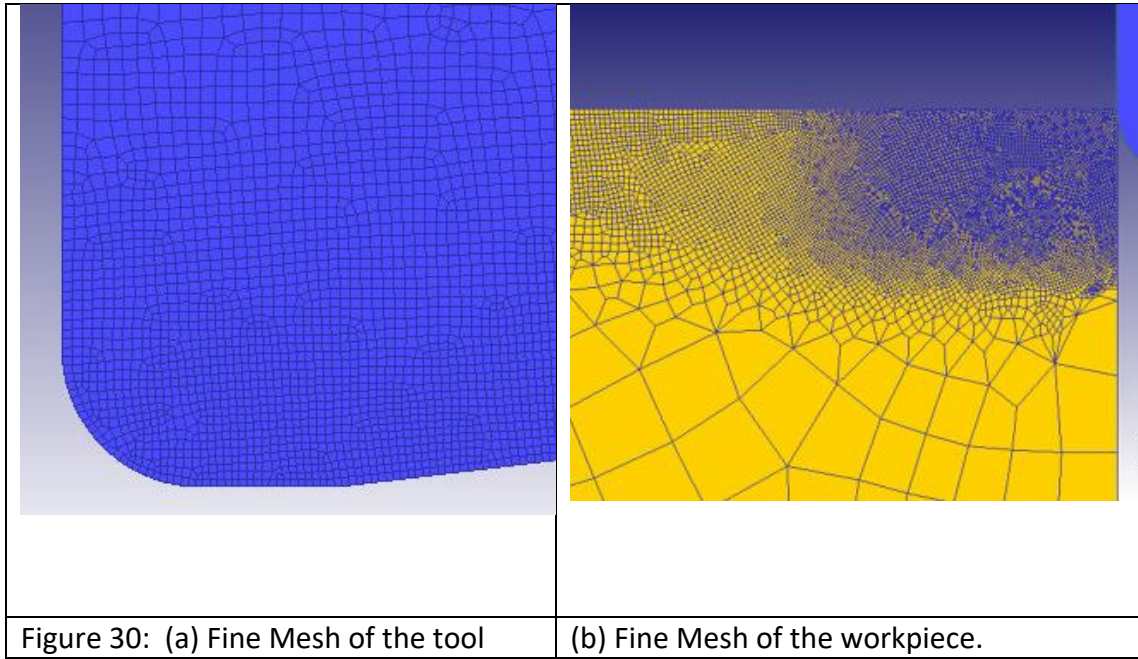


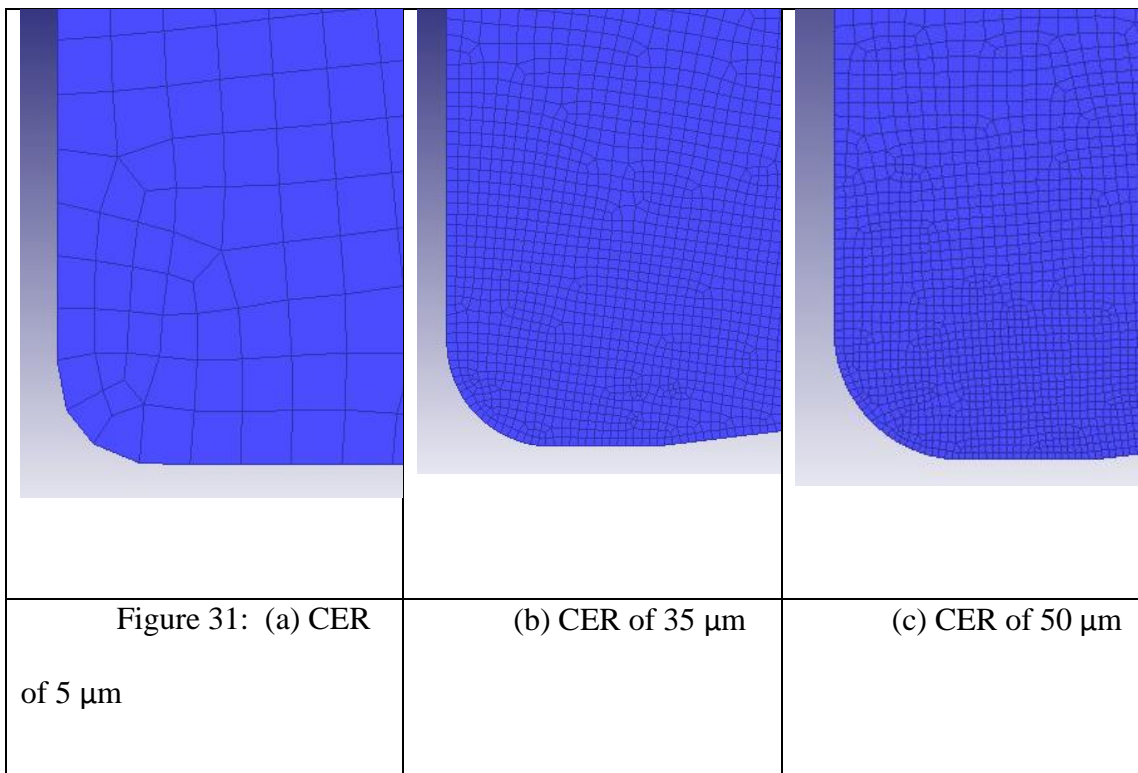
Figure 29: Deform Friction Coefficient Input

d. Mesh size

The mesh size in Deform was inserted to the smallest value thus a fine mesh was followed. The number of elements per uncut chip thickness was inserted to be the maximum value of 40. For example, if the feed is to be 0.005 mm/rev, the mesh size is $0.005/40=0.0008$.



e. Cutting Edge Radius



The tool is modeled on DEFORM by setting the cutting-edge radius and the flank wear. After each run, the CER is increased to correct for wear. Such correction will allow for better accuracy with respect to the experimental and the analytical values.

2. Post Simulation

a. Forces

The forces F_c and F_t are plotted vs. time. From Equation (2), F and N could be calculated and compared to the forces obtained from the experimental work:

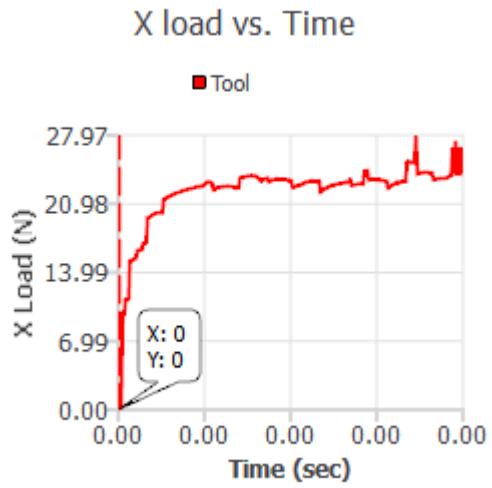
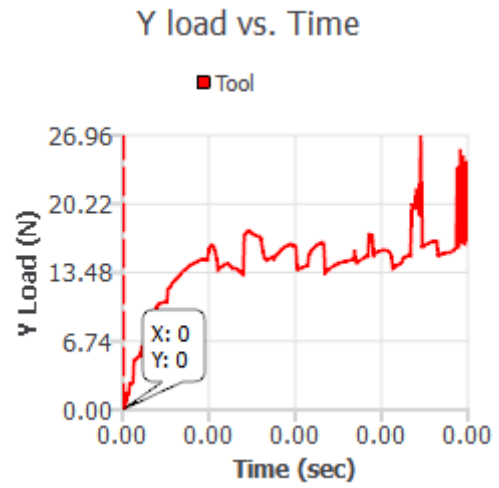


Figure 32: (a) Xload vs. Time



(b) Yload vs. Time

b. Stresses and Strains

Stresses and Strains can also be determined at the end of the run:

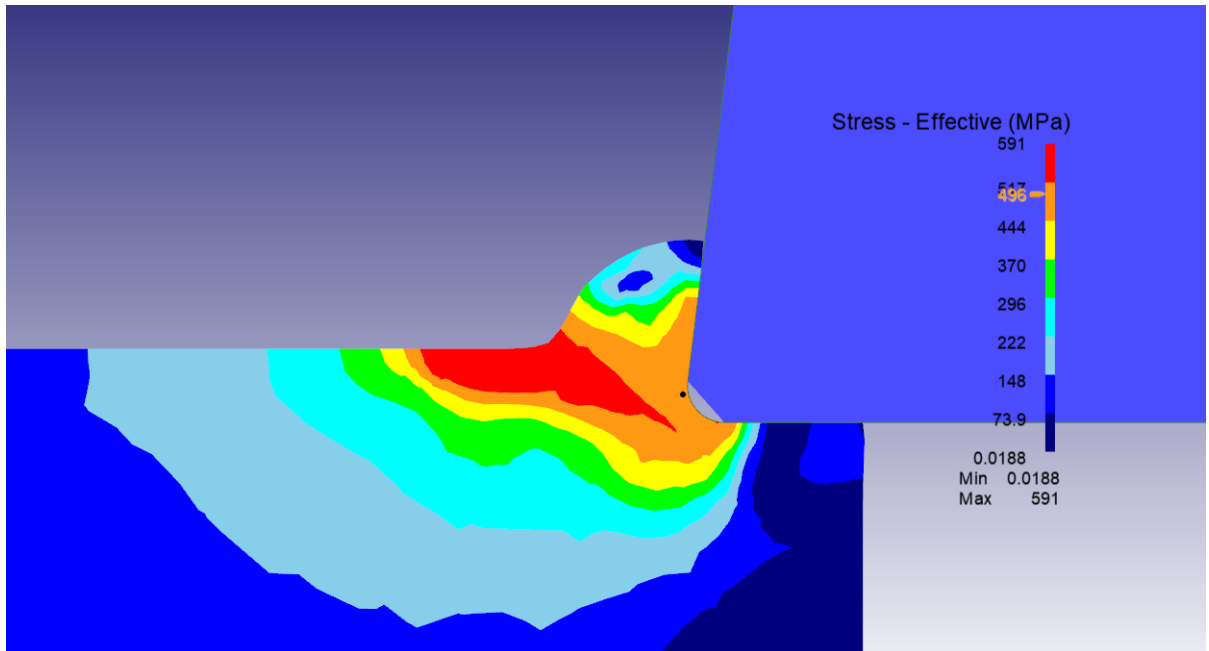


Figure 33: Effective Stresses

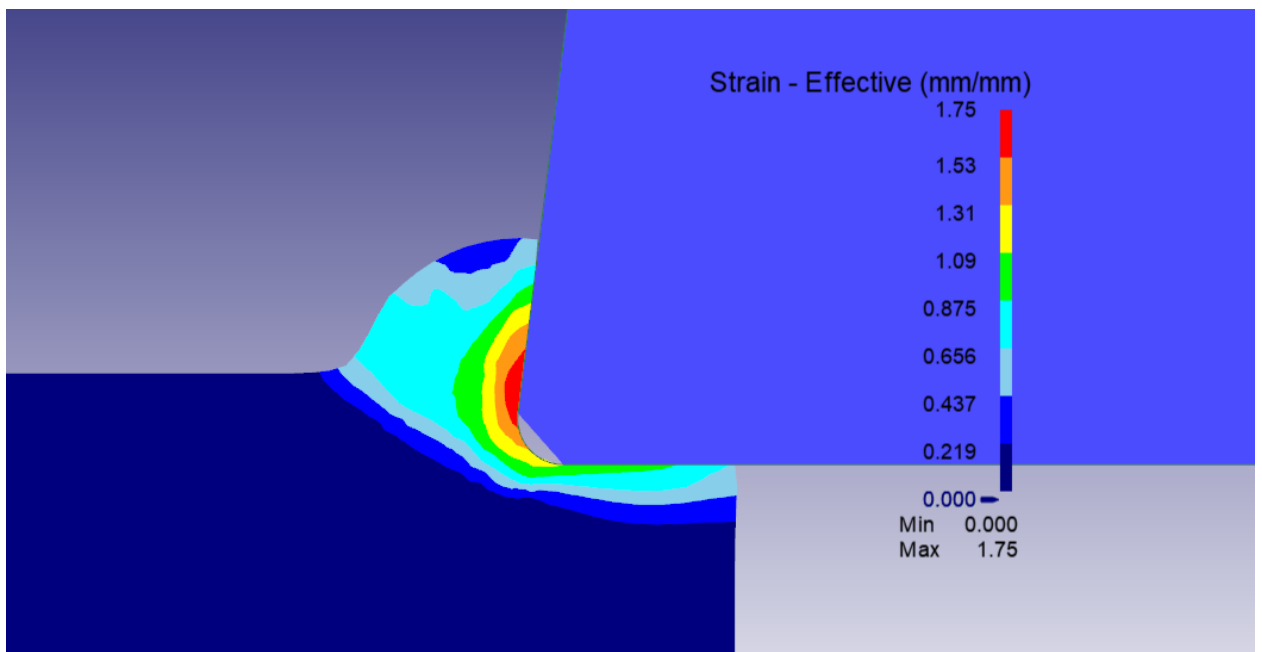


Figure 34: Effective Strain

CHAPTER III

RESULTS

A. Experimental

1. Influence of Cutting Speed on Frictional forces

Rubbing runs were done at all speeds to obtain the friction forces acting in Region 1. To achieve rubbing, first cutting at a minimal feed of 0.0005 mm/rev was done for 3 seconds to accomplish contact between the tool and work piece after which a dwelling time of 3 seconds was done to get the rubbing forces. A sample of the raw data obtained is shown in Figure 35; the average of the last 3 seconds is calculated to get the friction forces. The calculated frictional and normal forces are listed in Table 7

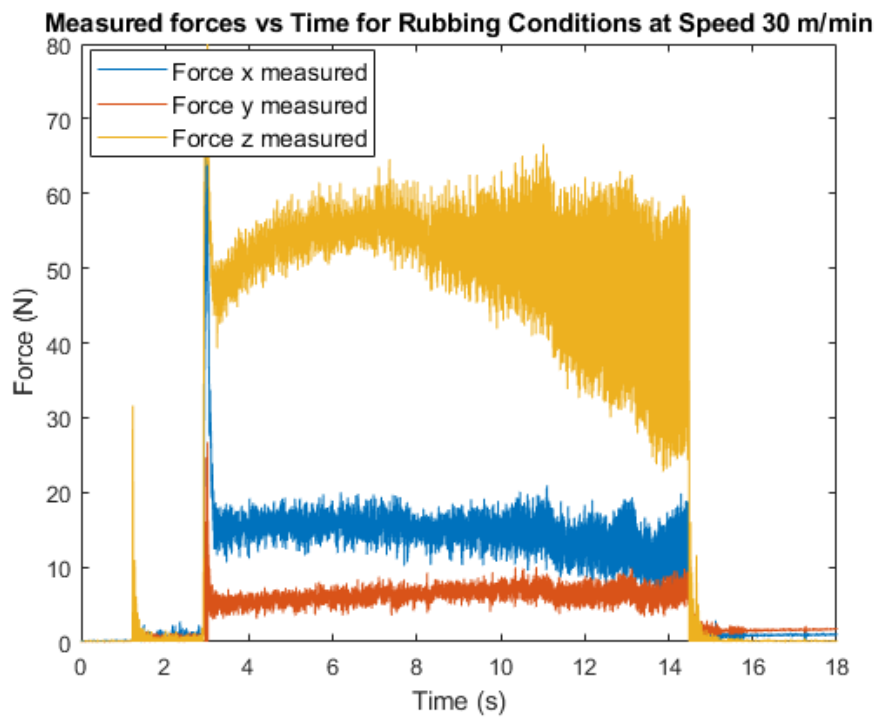


Figure 35: Forces vs. time at Cutting speed 30 m/min

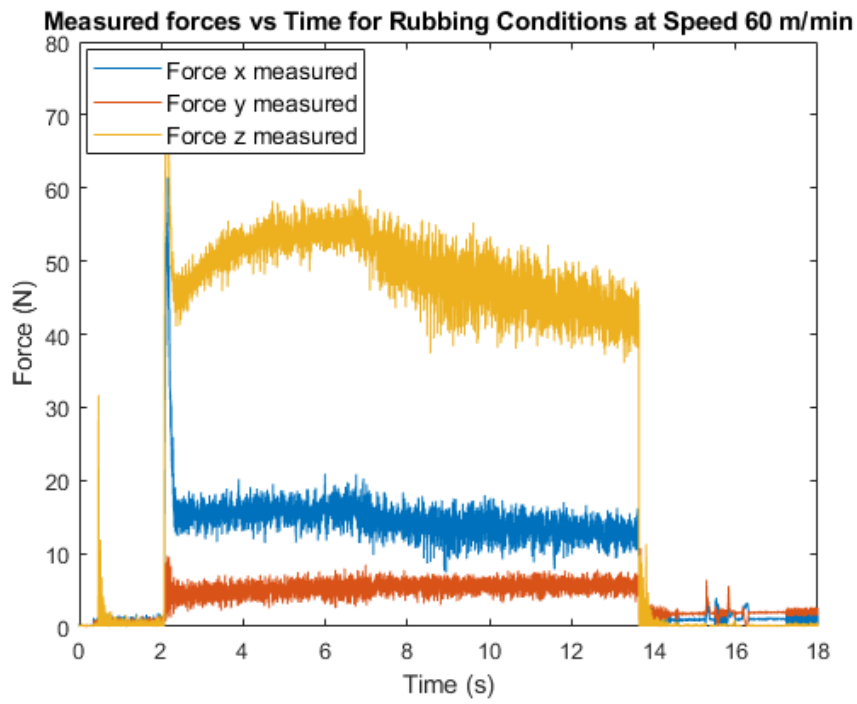


Figure 36: Forces vs. time at Cutting speed 60 m/min

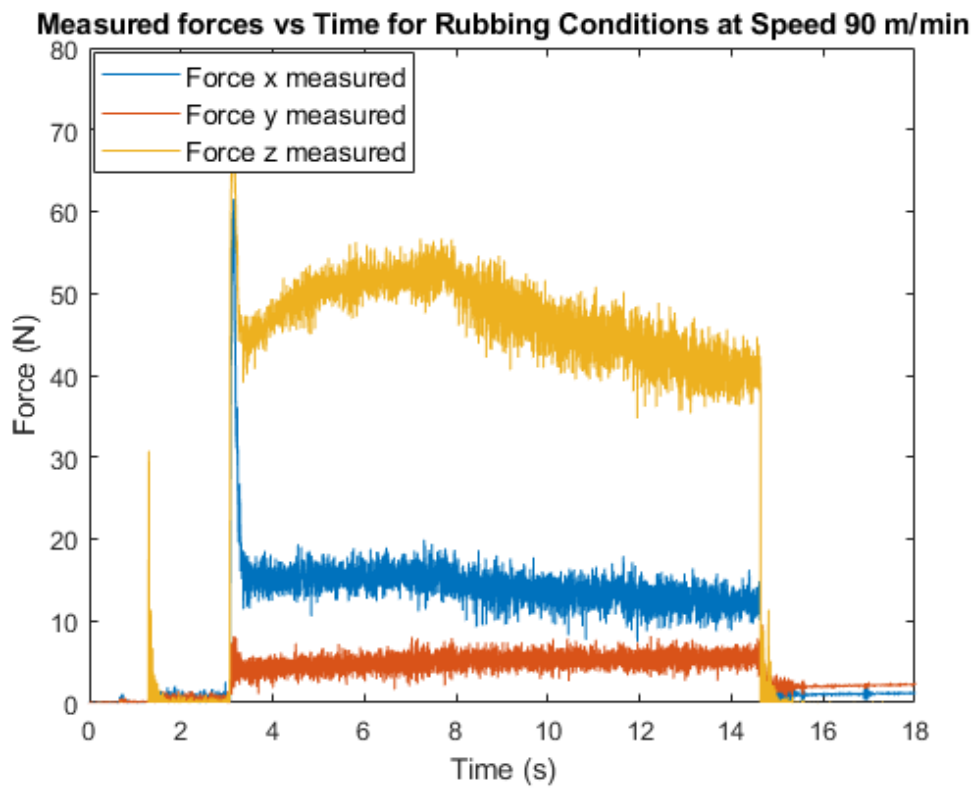


Figure 37: Forces vs. time at Cutting speed 90 m/min

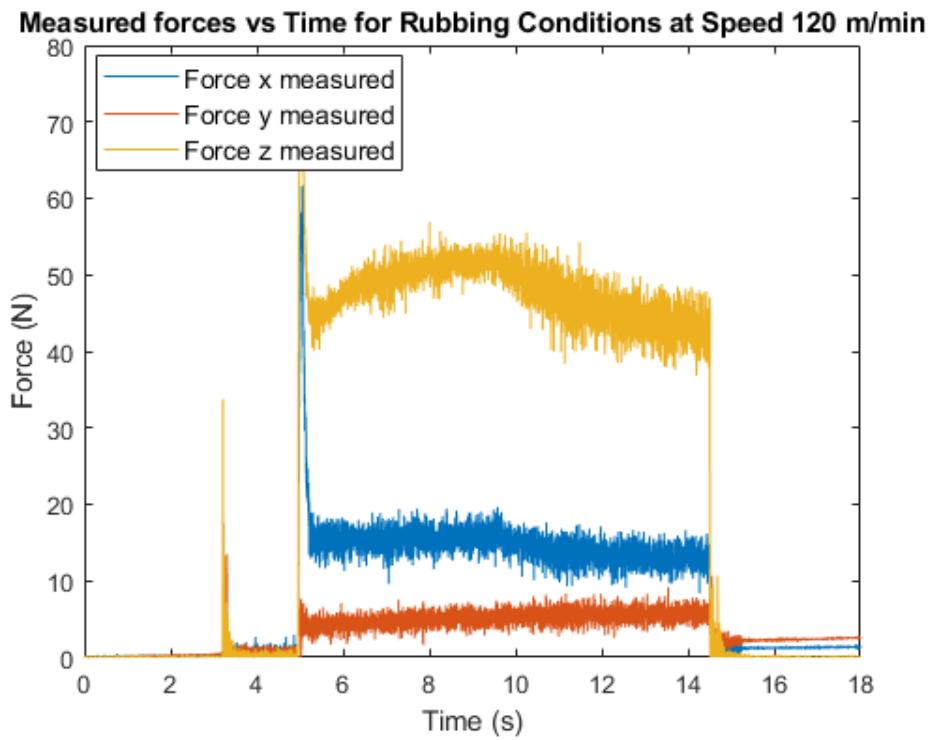


Figure 38: Forces vs. time at Cutting speed 120 m/min

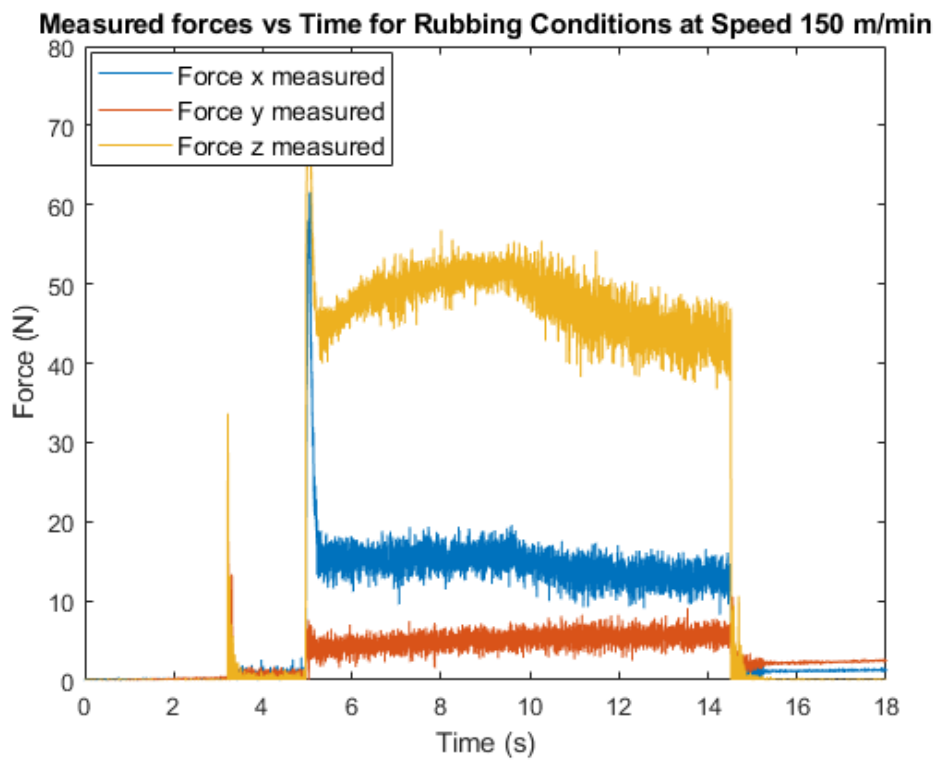


Figure 39: Forces vs. time at Cutting speed 150 m/min

Table 7: Forces acting in Region 1

	Spindle RPM				
	720	720	720	720	720
	cutting speed m/min				
	27	60	90	120	150
	A	B	C	D	E
Normal Force in Region 1	46.23	45.31	44.83	44.46	39.9
Friction Force in Region 1	13.5	13.46	13.44	13.31	13

For different cutting speeds, Figure 40 represents the trend frictional forces follow with increasing cutting speed. It is well known that the coefficient of friction tends to decrease with increasing velocity, thus having low frictional forces at high cutting speeds.

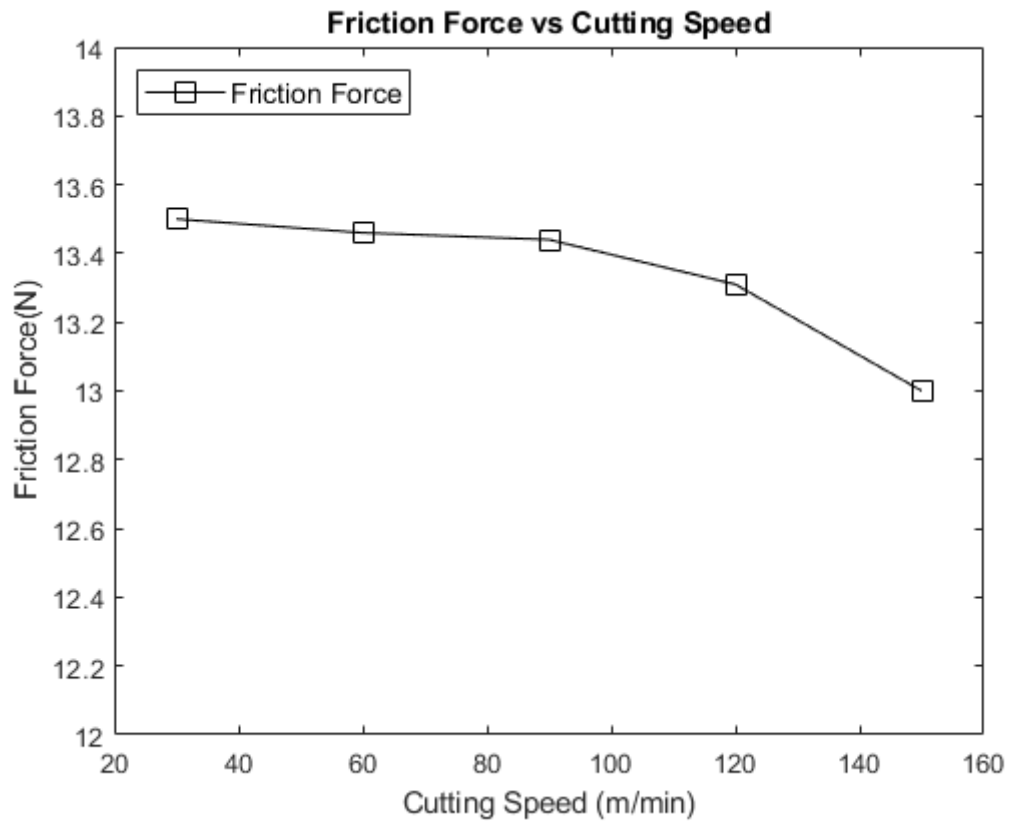


Figure 40: Frictional Forces vs. Cutting Speed

Figure 40: Frictional Forces vs. Cutting Speed characterizes how the friction forces at Region 1 are affected by the increase in the cutting speed. Going down from a cutting speed of 30 m/min to 120 m/min, a linear decrease of the friction force is seen from a value of 13.5 N/mm to a value of 13.31 N/mm. Increasing the speed up to 150 m/min, the friction force drops tremendously into a value of 13 N/mm. Such drop could be tracked back to thermal softening affecting the tool at high speeds.

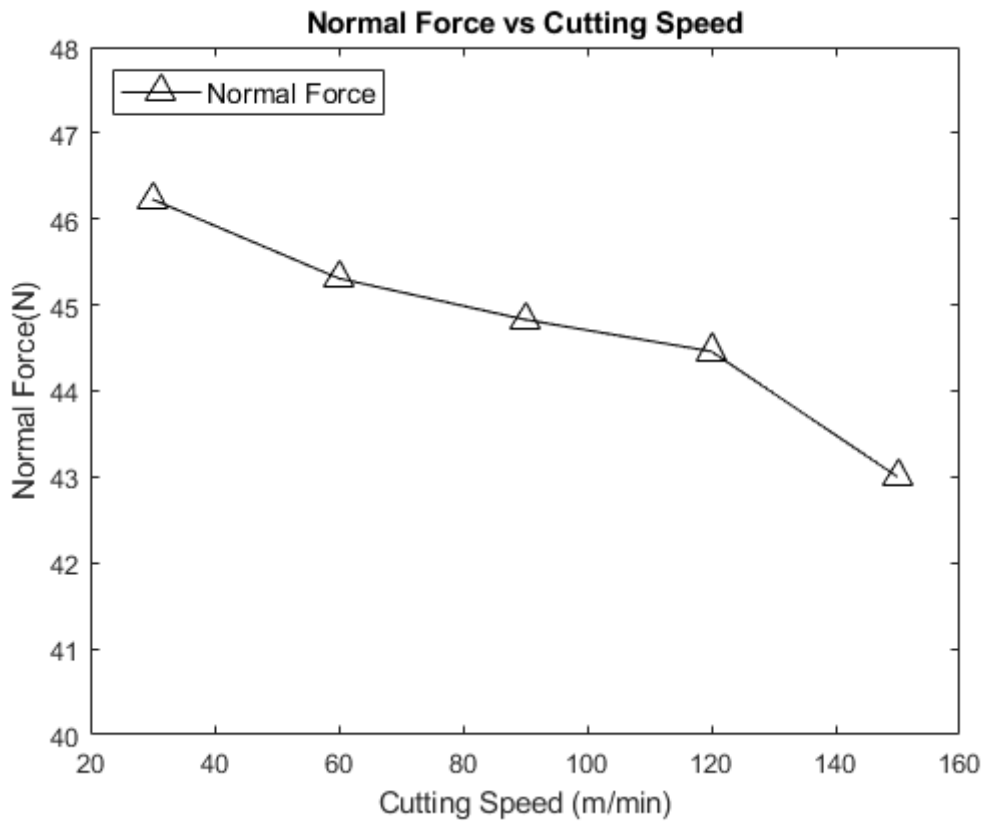


Figure 41: Normal Forces vs. Cutting Speed

2. Influence of uncut chip thickness on plowing forces.

Furthermore, Tests were done at feeds ranging from 0.0005 mm/rev to 0.01 mm/rev. A sample of the raw data obtained is shown in *Figure 42*. Force X is the plowing force, Force Y is the radial force, and Force Z is the Thrust force. To acquire the cutting and the thrust forces, the average value of each force is calculated at steady state. Afterward, the values are divided by the width of the chip (2 mm) to obtain the plowing and the thrust coefficients.

Thrust Coefficient

$$= \frac{\text{Raw Thrust Force}}{w} \quad (36)$$

Plowing Coefficient

$$= \frac{\text{Raw Plowing Force}}{w} \quad (37)$$

Rubbing Coefficient

$$= \frac{\text{Raw Rubbing Force}}{w} \quad (38)$$

The values of the plowing and the thrust coefficients are represented in Table 8 and Table 9 respectively.

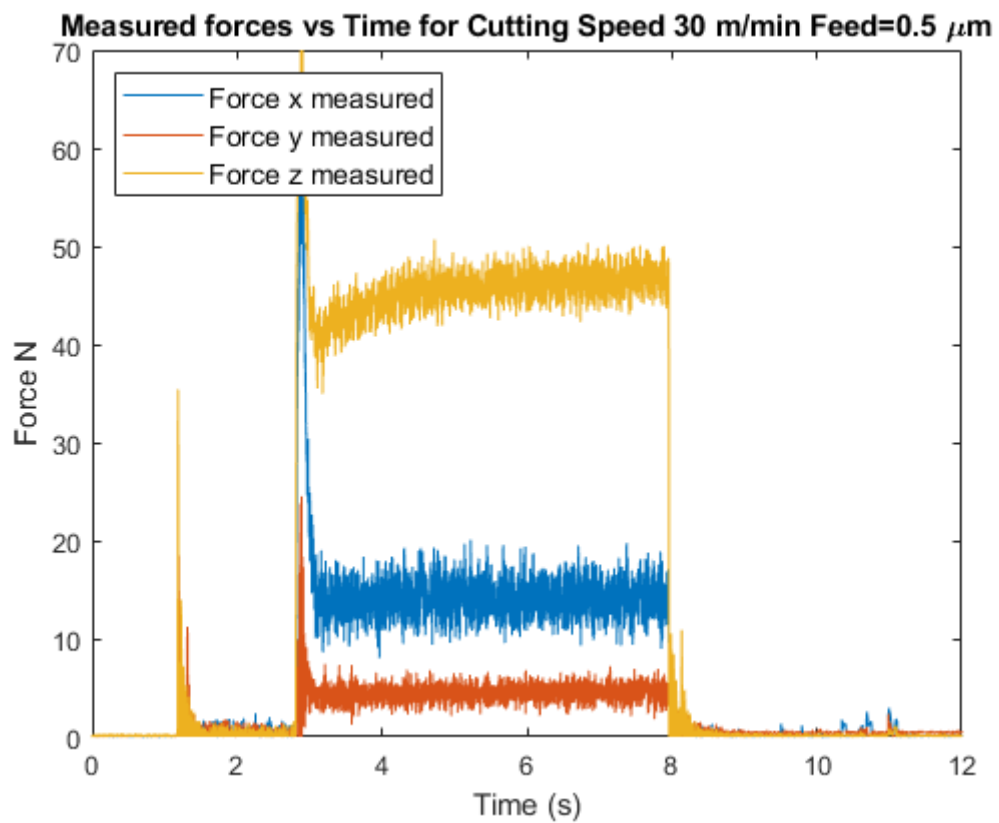


Figure 42: Typical cutting forces (RPM = 720, Cutting speed= 30 m/min, feed = 0.0005 mm/rev OR Feed rate of mm/min = N. F = 720 * 0.0005 mm/rev = 0.36 mm/min).

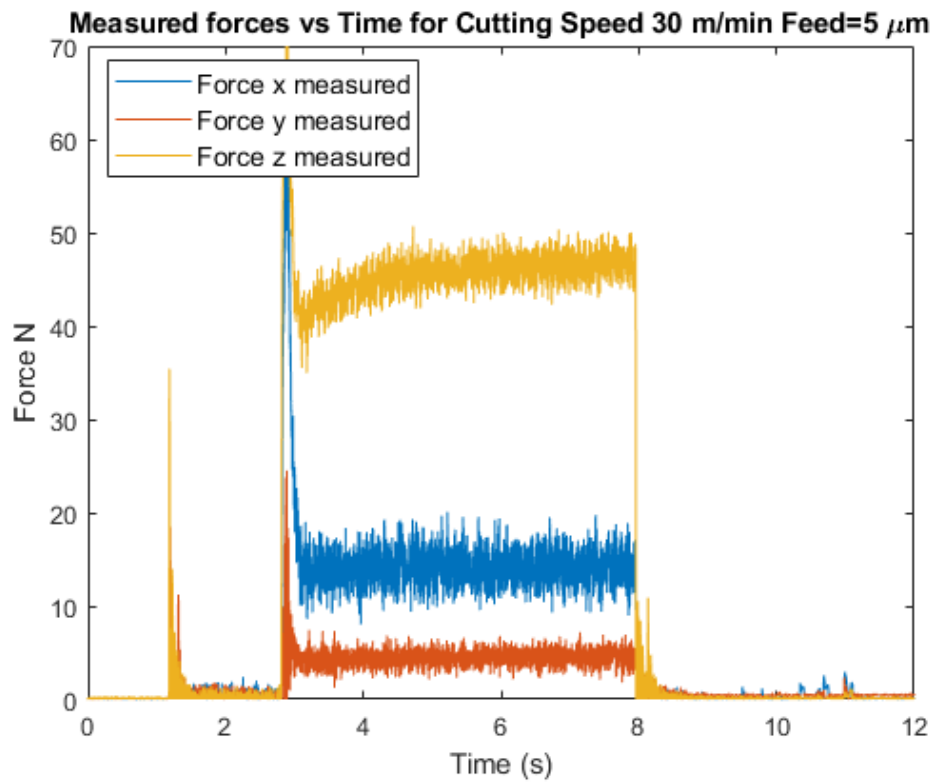


Figure 43: Typical cutting forces (RPM = 720, Cutting speed= 30 m/min, feed = 0.005 mm/rev OR Feed rate of mm/min = N. F = 720 * 0.005 mm/rev = 3.6 mm/min).

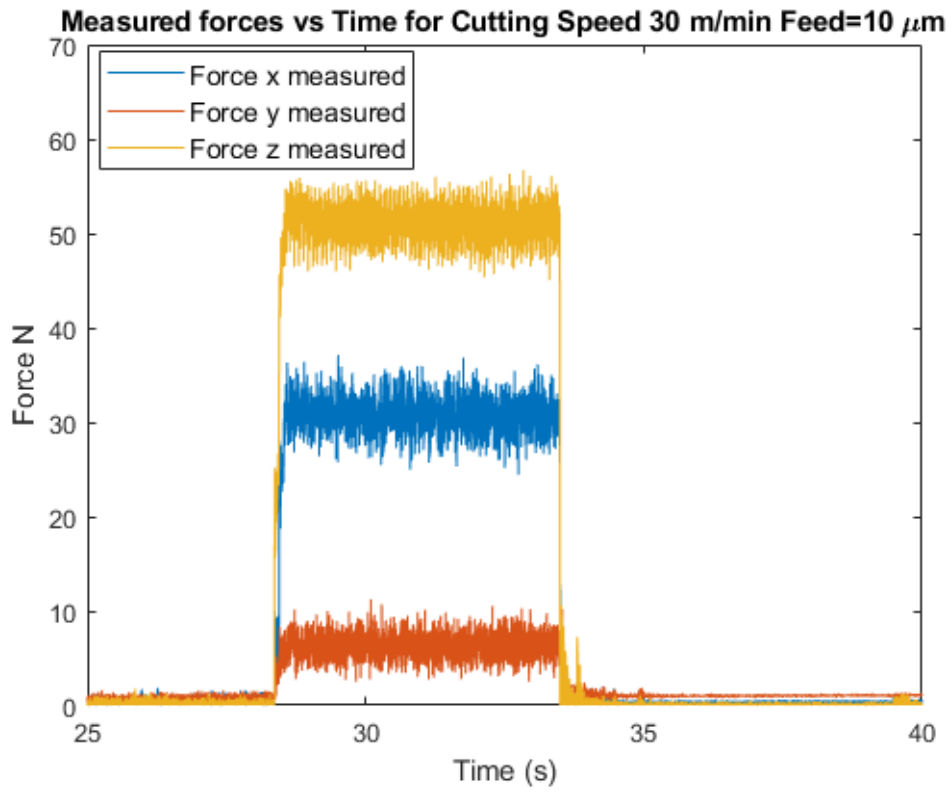


Figure 44: Typical cutting forces (RPM = 720, Cutting speed= 30 m/min, feed = 0.01 mm/rev OR Feed rate of mm/min = N. F = 720 * 0.01 mm/rev = 7.2 mm/min).

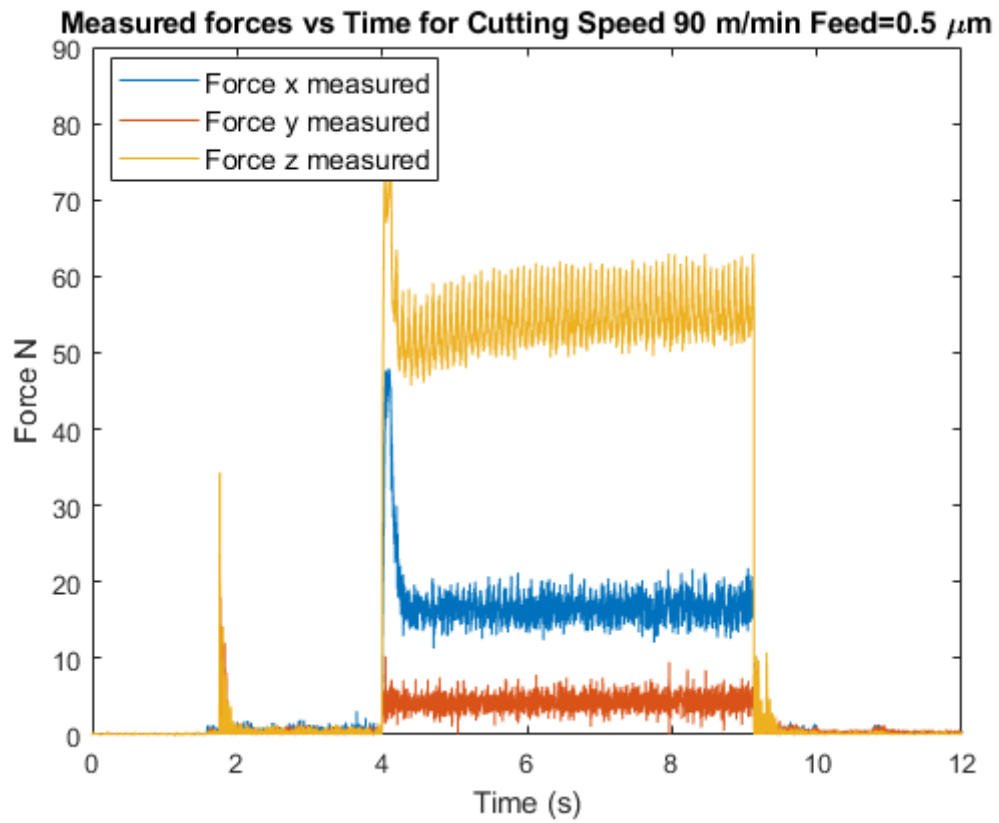


Figure 45: Typical cutting forces (RPM = 720, Cutting speed= 90 m/min, feed = 0.0005 mm/rev OR Feed rate of mm/min = $N \cdot F = 720 \cdot 0.0005 \text{ mm/rev} = 0.36 \text{ mm/min}$).

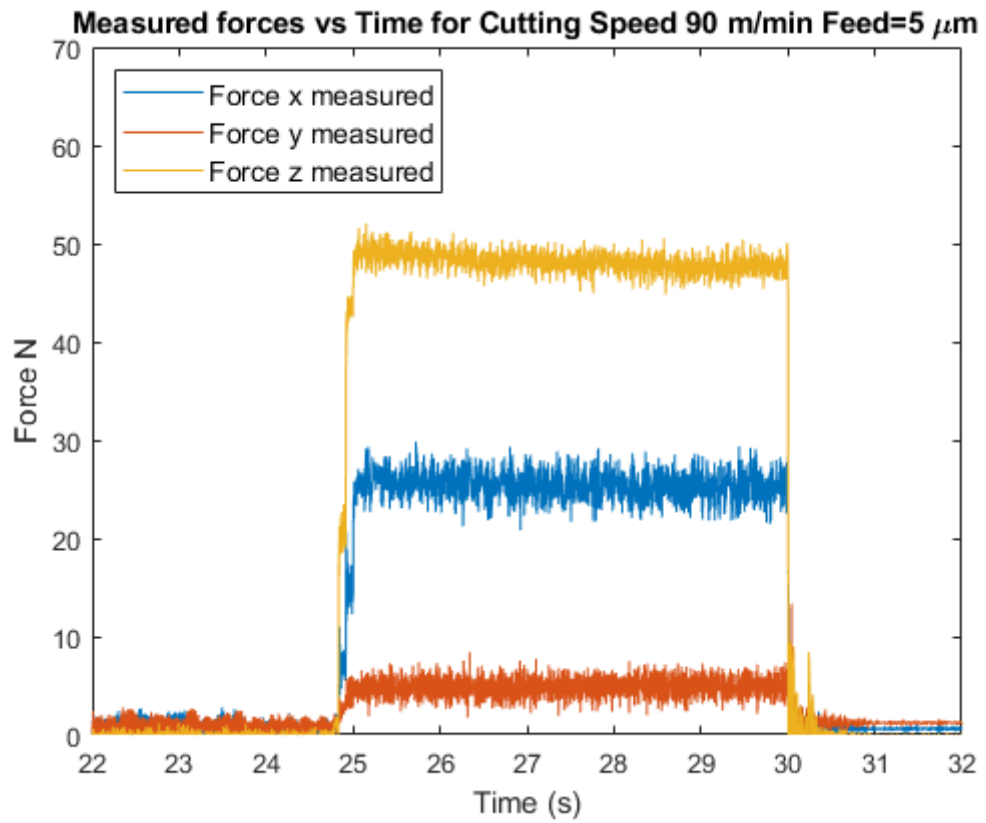


Figure 46: Typical cutting forces (RPM = 720, Cutting speed= 90 m/min, feed = 0.005 mm/rev OR Feed rate of mm/min = N. $F = 720 * 0.005 \text{ mm/rev} = 3.6 \text{ mm/min}$).

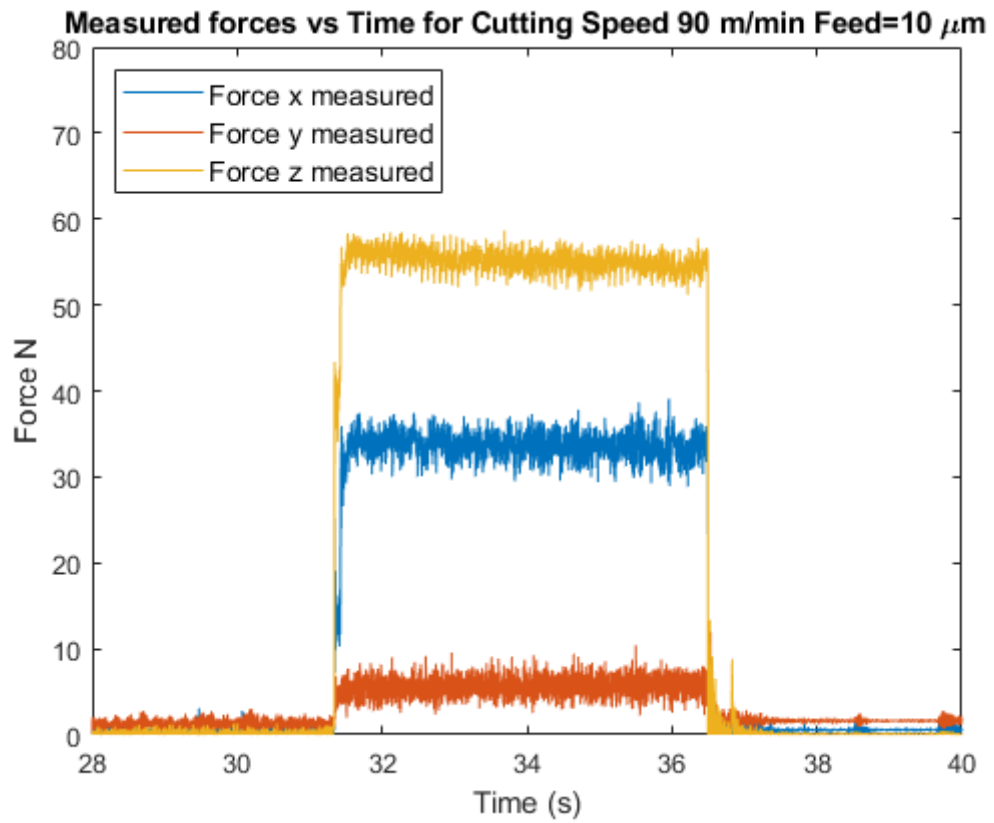


Figure 47: Typical cutting forces (RPM = 720, Cutting speed= 90 m/min, feed = 0.01 mm/rev OR Feed rate of mm/min = $N \cdot F = 720 \cdot 0.01 \text{ mm/rev} = 7.2 \text{ mm/min}$).

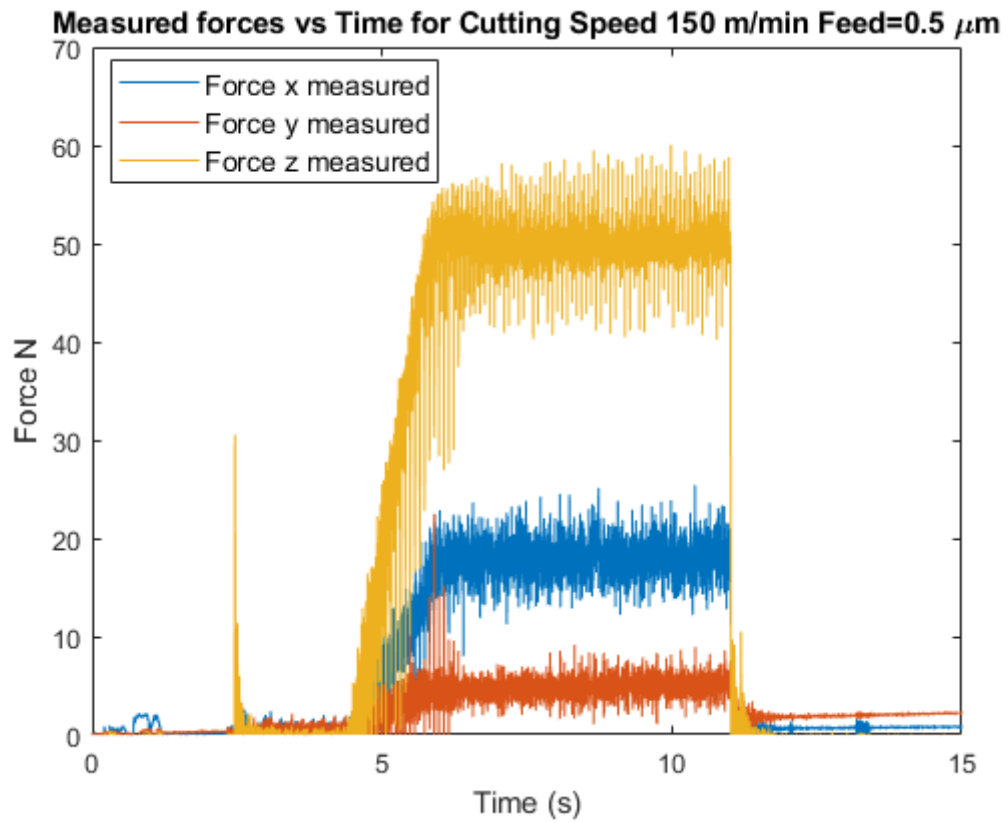


Figure 48: Typical cutting forces (RPM = 720, Cutting speed= 150 m/min, feed = 0.0005 mm/rev OR Feed rate of mm/min = $N \cdot F = 720 * 0.0005 \text{ mm/rev} = 0.36 \text{ mm/min}$).

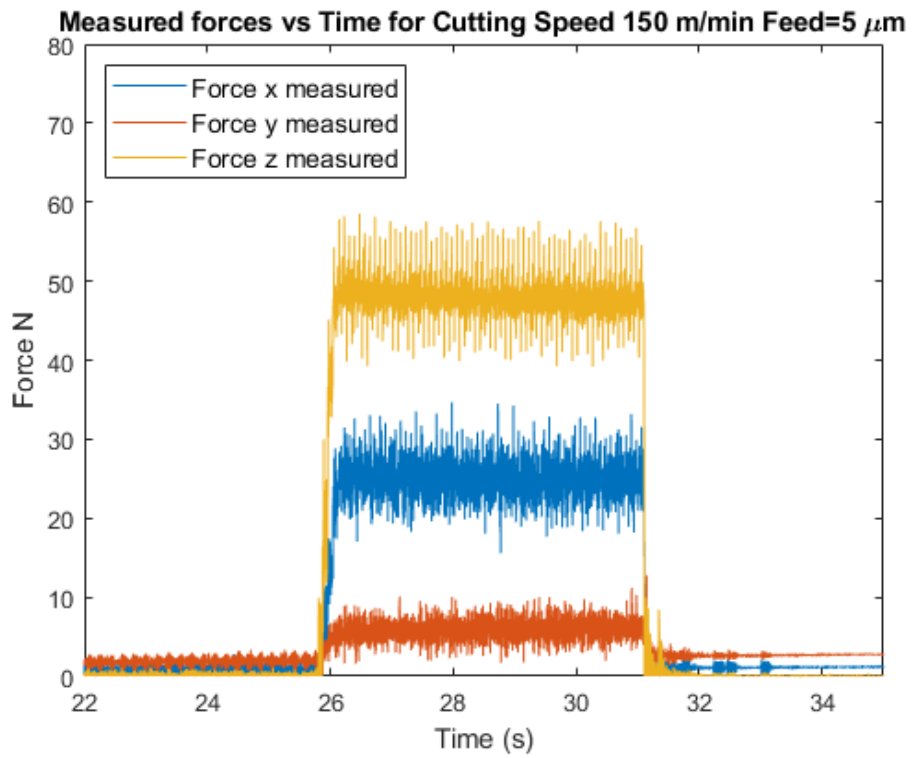


Figure 49: Typical cutting forces (RPM = 720, Cutting speed= 150 m/min, feed = 0.005 mm/rev OR Feed rate of mm/min = N. F = 720 * 0.005 mm/rev = 3.6 mm/min).

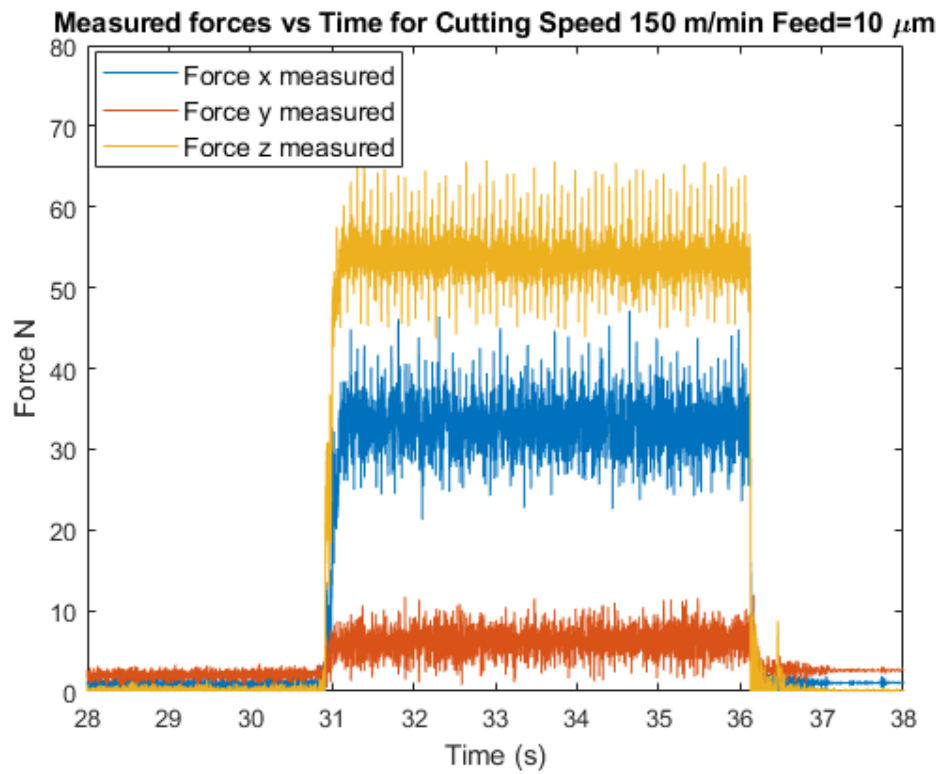


Figure 50: Typical cutting forces (RPM = 720, Cutting speed= 150 m/min, feed = 0.01 mm/rev OR Feed rate of mm/min = N. F = 720 * 0.01mm/rev = 7.2 mm/min).

Table 8: Plowing Coefficient at different feeds and RPMs.

			Spindle RPM				
			720	720	720	720	720
			cutting speed m/min				
			27	60	90	120	150
			A	B	C	D	E
	Rubbing	1	6.572	6.59	7	6.655	5.79
Feed mm/ rev	0.0005	2	7.65	8.395	7.77	7.485	6.95
	0.001	3	8.4	9.005	8.695	8.42	8.965
	0.0015	4	9.347	9.78	9.7625	9	10
	0.002	5	9.9	10.725	10.5	9.9	10.5
	0.0025	6	10.6525	11.5915	10.916	10.565	10.95
	0.003	7	11	12	11.4	10.815	11.8
	0.0035	8	11.5385	12.2	12	11.07	11.85
	0.004	9	11.8055	12.229	12.13	11.2	11.675
	0.0045	10	11.885	12.42	12.355	11.5	11.855
	0.005	11	12.2155	12.5365	12.615	12.02	12.4055
	0.006	12	13.021	13.44	13.4435	12.5	13.2165
	0.007	13	13.7775	14.357	14.2445	13.605	13.96
	0.008	14	14.6755	15.227	15.41	14.66	14.965
	0.009	15	15.435	15.9155	16.095	15.105	15.684
	0.01	16	16	16.698	16.855	16.1	16.375

Table 9: Thrust Coefficient at different feeds and RPMs.

			Spindle RPM				
			720	720	720	720	720
			cutting speed m/min				
			27	60	90	120	150
			A	B	C	D	E
	Rubbing	1	23.115	22.655	21.2	22.3	19.95
Feed mm/ rev	0.0005	2	23.3	24.852	27.508	23.3935	20.375
	0.001	3	23.5	25.75	27.94	24.098	25.125
	0.0015	4	24.23	26.16	28.32	24.798	26.03
	0.002	5	24.39	26.205	27.265	23.775	25.2215
	0.0025	6	24.503	26.2865	26.735	23.5	24.44
	0.003	7	24.1	25.565	26.09	22.7945	24.3
	0.0035	8	24	24.9465	25.235	21.81	23.4495
	0.004	9	23.9	24	24.695	21.61	23.6945
	0.0045	10	23.5	24.375	23.9795	22.04	23.7945
	0.005	11	23.9	24.5	24.175	22.302	23.991
	0.006	12	24.3	24.85	25.08	22.84	24.533
	0.007	13	24.9	25.445	25.5885	23.2945	25.08
	0.008	14	25.21	26.22	26.523	24.2945	25.79
	0.009	15	25.62	26.745	26.99	24.475	26.25
	0.01	16	26	27.375	27.555	25.532	26.755

To study the values more evidently, a correction was done by separating the plowing and the thrust forces from the rubbing forces. Such approach tips to a better and a clearer understanding of the behavior each force are following. The rubbing coefficients are subtracted from the plowing and the thrust coefficients to get the corrected values.

Corrected Thrust Coefficient

$$= \text{Raw Thrust Coefficient} - \text{Rubbing Coefficient}$$

Corrected Plowing Coefficient

$$= \text{Raw Plowing Coefficient} - \text{Rubbing Coefficient}$$

Represented in Table 10 and Table 11, are the updated corrected values for the plowing and thrust coefficient.

Table 10: Corrected Plowing Coefficients for all feeds and speeds

			Spindle RPM				
			720	720	720	720	720
			cutting speed m/min				
			27	60	90	120	150
			A	B	C	D	E
	Rubbing	1	0	0	0	0	0
Feed mm/ rev	0.0005	2	1.078	1.805	0.77	0.83	1.16
	0.001	3	1.828	2.415	1.695	1.765	3.175
	0.0015	4	2.775	3.19	2.7625	2.345	4.21
	0.002	5	3.328	4.135	3.5	3.245	4.71
	0.0025	6	4.0805	5.0015	3.916	3.91	5.16
	0.003	7	4.428	5.41	4.4	4.16	6.01
	0.0035	8	4.9665	5.61	5	4.415	6.06
	0.004	9	5.2335	5.639	5.13	4.545	5.885
	0.0045	10	5.313	5.83	5.355	4.845	6.065
	0.005	11	5.6435	5.9465	5.615	5.365	6.6155
	0.006	12	6.449	6.85	6.4435	5.845	7.4265
	0.007	13	7.2055	7.767	7.2445	6.95	8.17
	0.008	14	8.1035	8.637	8.41	8.005	9.175
	0.009	15	8.863	9.3255	9.095	8.45	9.894
	0.01	16	9.428	10.108	9.855	9.445	10.585

Table 11: Corrected Thrust Coefficient at different feeds and speeds.

			Spindle RPM				
			720	720	720	720	720
			cutting speed m/min				
			27	60	90	120	150
			A	B	C	D	E
	Rubbing	1	0	0	0	0	0
Feed mm/ rev	0.0005	2	0.185	2.197	6.308	1.0935	0.425
	0.001	3	0.385	3.095	6.74	1.798	5.175
	0.0015	4	1.115	3.505	7.12	2.498	6.08
	0.002	5	1.275	3.55	6.065	1.475	5.2715
	0.0025	6	1.388	3.6315	5.535	1.2	4.49
	0.003	7	0.985	2.91	4.89	0.4945	4.35
	0.0035	8	0.885	2.2915	4.035	-0.49	3.4995
	0.004	9	0.785	1.345	3.495	-0.69	3.7445
	0.0045	10	0.385	1.72	2.7795	-0.26	3.8445
	0.005	11	0.785	1.845	2.975	0.002	4.041
	0.006	12	1.185	2.195	3.88	0.54	4.583
	0.007	13	1.785	2.79	4.3885	0.9945	5.13
	0.008	14	2.095	3.565	5.323	1.9945	5.84
	0.009	15	2.505	4.09	5.79	2.175	6.3
	0.01	16	2.885	4.72	6.355	3.232	6.805

The corrected coefficients are plotted vs. uncut chip thickness for different cutting speeds. Figure 51-Figure 55) show the trend each coefficient is ensuing. The plowing coefficient follows an increasing trend with increasing uncut chip thickness.

When going from a feed of 0.0005 mm/rev to a feed of 0.005 mm/rev, the plowing forces increase with a nonlinear fashion (bilinear). However, going over 0.005 mm/rev, the plowing force remain increasing but with a linear fashion.

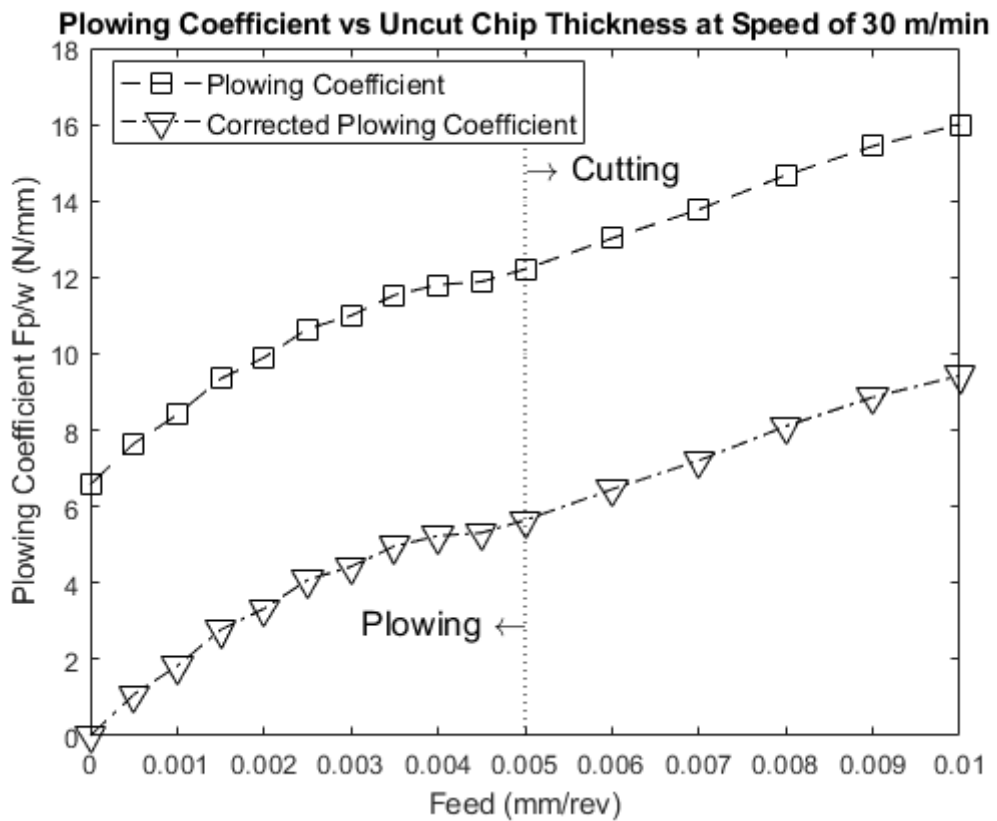


Figure 51: Plowing Coefficient vs. Uncut Chip Thickness at Speed 30 m/min

At 0.0005 mm/rev, the plowing force was measured to be 7.65 N/mm, increasing the feed to 0.005 mm /rev, the plowing force increases to 12.2155 N/mm. The increasing trend between the two points in nonlinear bilinear. Reaching a feed of

0.01 mm/rev, the measured force was valued at 16 N/mm. The increasing trend between the two points is noticed be linear.

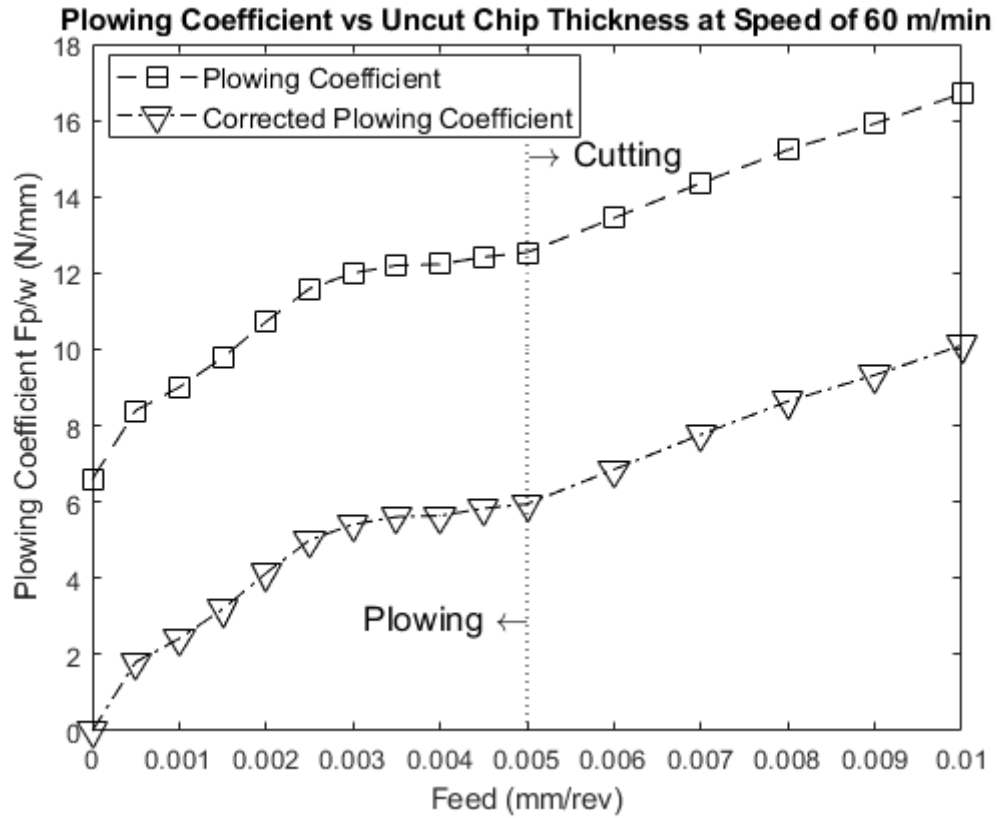


Figure 52: Plowing Coefficient vs. Uncut Chip Thickness at Speed 60 m/min

With a feed of 0.0005 mm/rev, the plowing force measured was 8.395 N/mm, when the feed was increased to 0.005 mm/rev the force increased to 12.536 N/mm. Lastly at 0.001 the force measured was 16.698 N/mm. The forces measured at 60 m/min is seen to be larger than the forces at 30 m/min contradicting the theoretical notion.

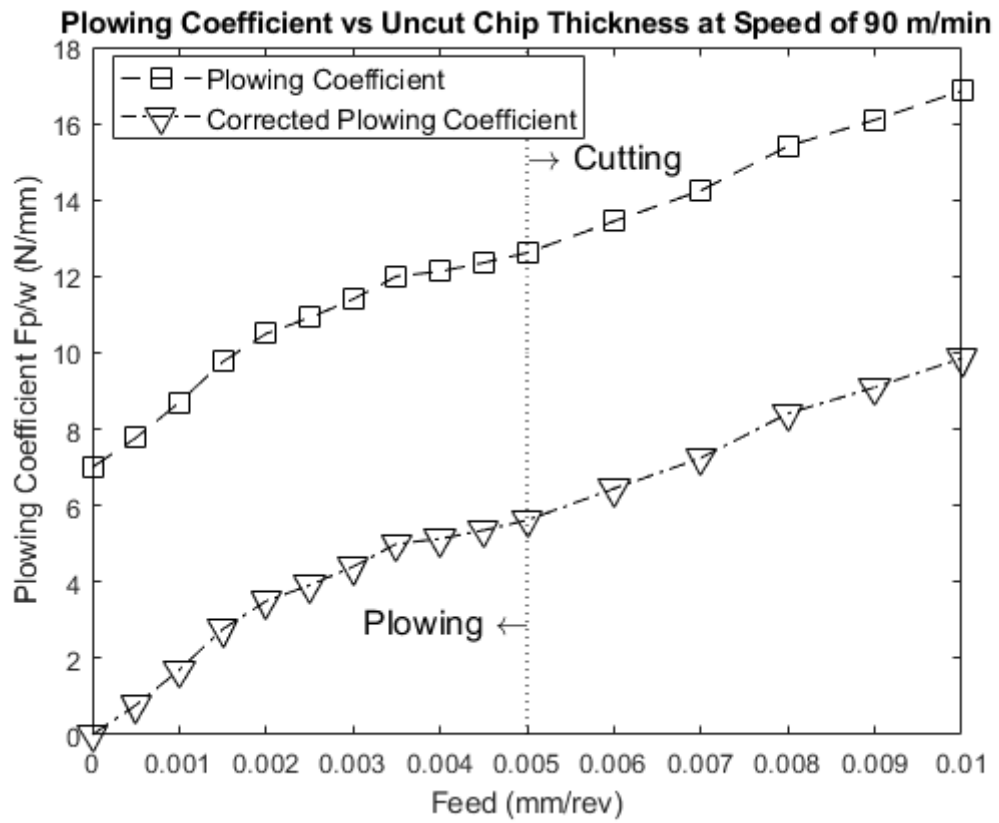


Figure 53: Plowing Coefficient vs. Uncut Chip Thickness at Speed 90 m/min

At 0.0005 mm/rev, the plowing force was measured to be 7.77 N/mm, increasing the feed to 0.005 mm /rev, the plowing force increases to 12.615 N/mm. Reaching a feed of 0.01 mm/rev, the measured force was valued at 16.855 N/mm. As expected, the value of the forces increased decreased going from 60 m/min to 90 m/min.

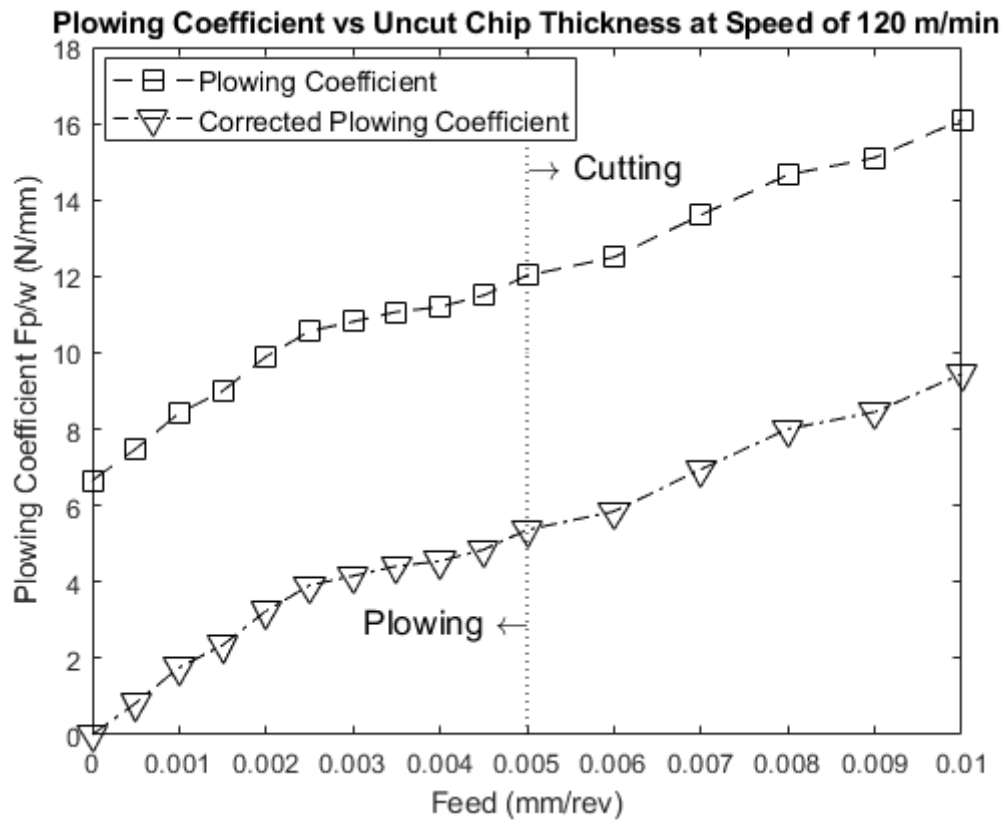


Figure 54: Plowing Coefficient vs. Uncut Chip Thickness at Speed 120 m/min

With a feed of 0.0005 mm/rev, the plowing force measured was 7.485 N/mm, when the feed was increased to 0.005 mm/rev the force increased to 12.02 N/mm. Lastly at 0.001 the force measured was 16.11 N/mm.

The forces further decreased as the cutting speed increased from 90 m/min to 120 m/min.

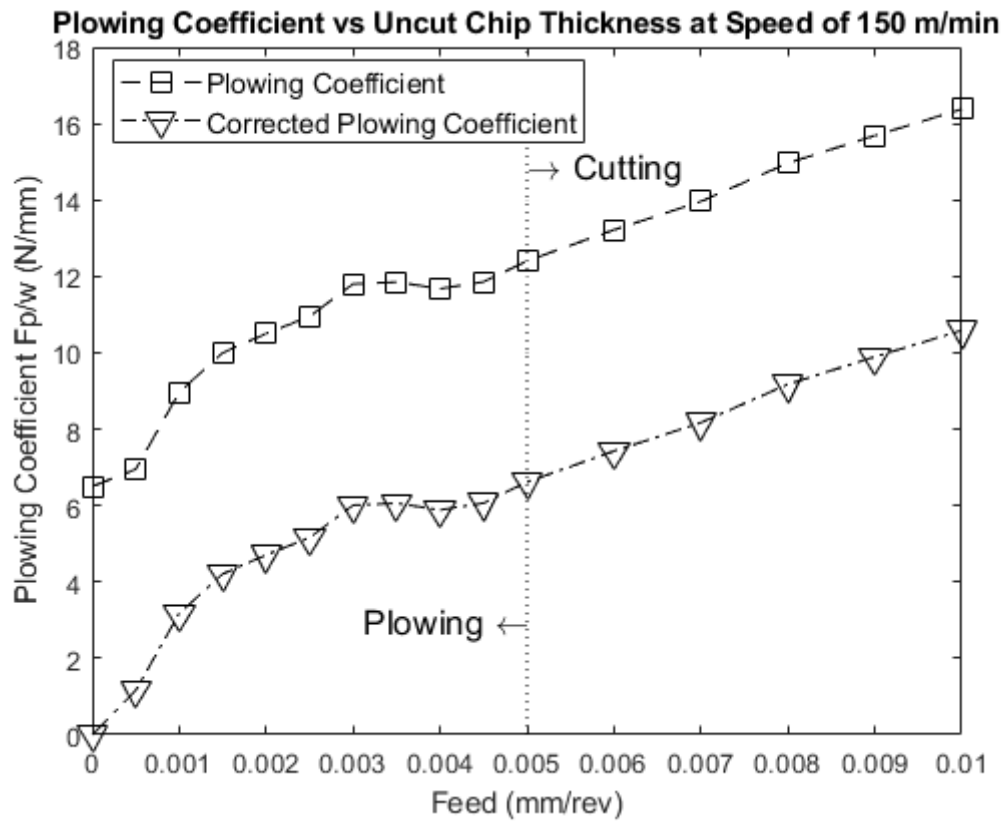


Figure 55: Plowing Coefficient vs. Uncut Chip Thickness at Speed 150 m/min

At 0.0005 mm/rev, the plowing force was measured to be 6.95 N/mm, increasing the feed to 0.005 mm /rev, the plowing force increases to 12.4 N/mm. However, reaching a feed of 0.01 mm/rev, the measured force was valued at 16.375.

Lastly, the increase in speed to 150 m/min decreased the values measured from those measured at a speed of 120 m/min

From Figure 51-Figure 55) ,the plowing forces are seen to be following an increasing behavior with increasing speed throughout all the experiments. However, such fashion differs between two intervals. At the first interval of feeds (0.0005mm/rev-0.005 mm/rev), the plowing forces follow a bilinear fashion. At the second interval (0.005 mm/rev – 0.01 mm/rev), the plowing forces follow a linear fashion. To support such observation, force values were taken at feeds of 0.0005, 0.005, and 0.01 mm/rev.

Afterwards, the average values were calculated to inspect the linearity of the trends. The average value of the force between 0.0005 mm/rev and 0.005 mm/rev was obtained to be much less than the actual value obtained at 0.0025 mm/rev. However, at the second interval (0.005 mm/rev – 0.01 mm/rev), the average value of the two points was obtained to be very close to the actual value at 0.007 mm/rev. Such results support the non-linearity of the first interval and the linearity of the second interval.

On the other hand, the thrust coefficient follows a different trend. Three different intervals could be noticed in Figure 56-Figure 60). The first interval at very low feeds (0 mm-0.002 mm), the second interval ranging between 0.002- 0.005 mm, and lastly the third interval is the cutting interval ranging between 0.005 mm and 0.01 mm. At the first interval, the thrust coefficient increases with increasing feed. Going into the second interval, the thrust coefficient decreases with growing feed. Such a decrease could be drawn back to the negative affect the friction force acting on the cutting-edge radius would have on the process. Lastly, going over to the cutting

interval, the thrust coefficient goes back into following a linear behavior increasing with increasing feed.

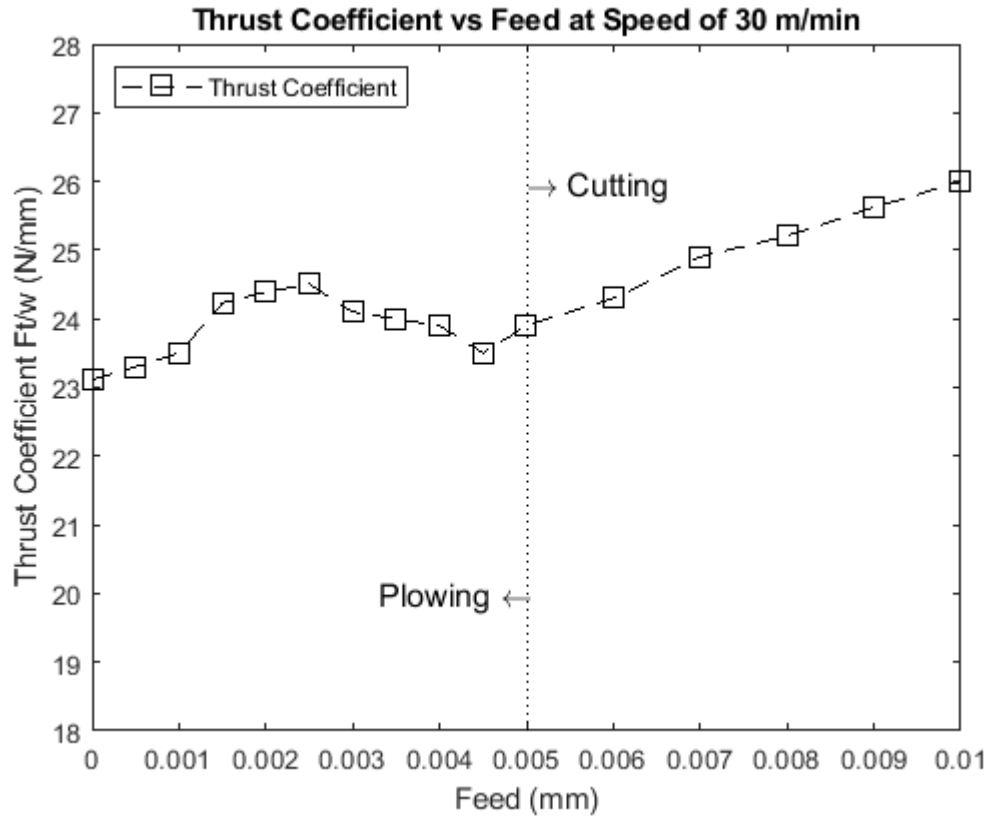


Figure 56: Thrust Coefficient vs. Uncut Chip Thickness at Speed 30 m/min

At 0.0005 mm/rev, the thrust force was measured to be 23.3 N/mm, increasing the feed to 0.0015 mm /rev, the thrust force increases to 24.504 N/mm. However, passing this feed, the thrust forces starts decreasing until reaching a value of 23.5 N/mm at a feed of 0.0045 mm/rev. The forces then increase linearly until reaching a value of 26 N/mm at the largest feed of 0.01 mm/rev.

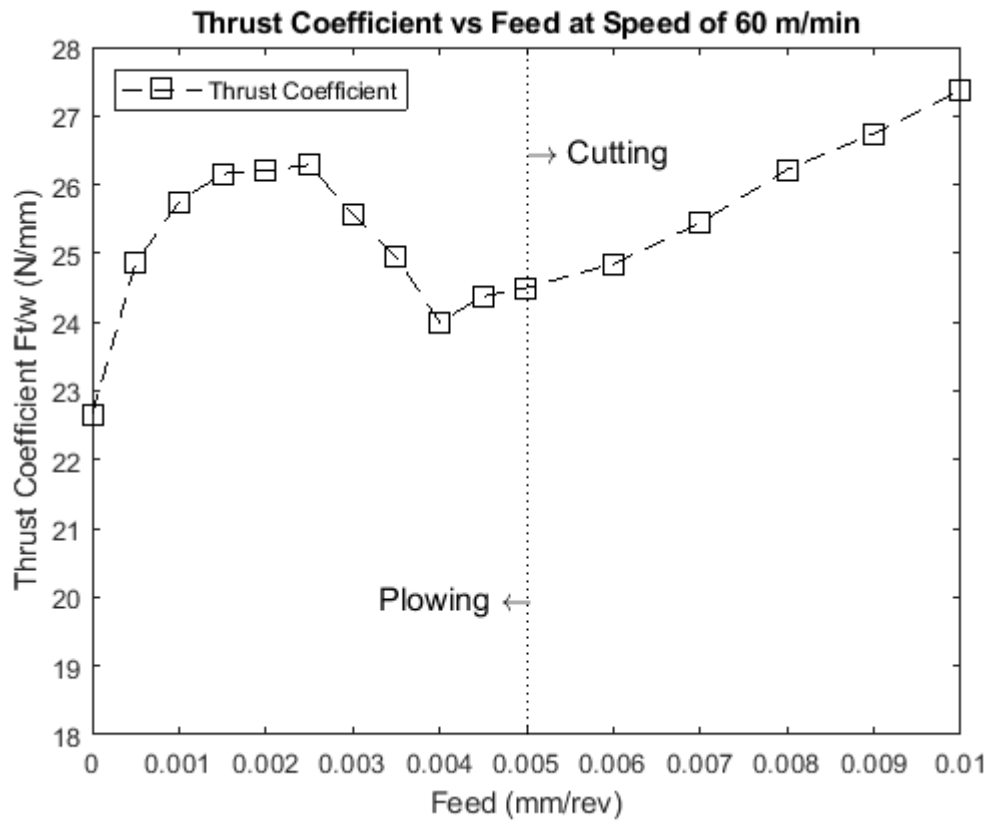


Figure 57: Thrust Coefficient vs. Uncut Chip Thickness at Speed 60 m/min

With a feed of 0.0005 mm/rev, the thrust force measured was 24.852 N/mm, when the feed was increased to 0.002 mm/rev the force increased to 26.205 N/mm. Afterwards, the forces starts decreasing to a value of 24 N/mm at a feed of 0.004 mm/rev, before increasing to 27.375 N/mm at 0.001 mm/rev.

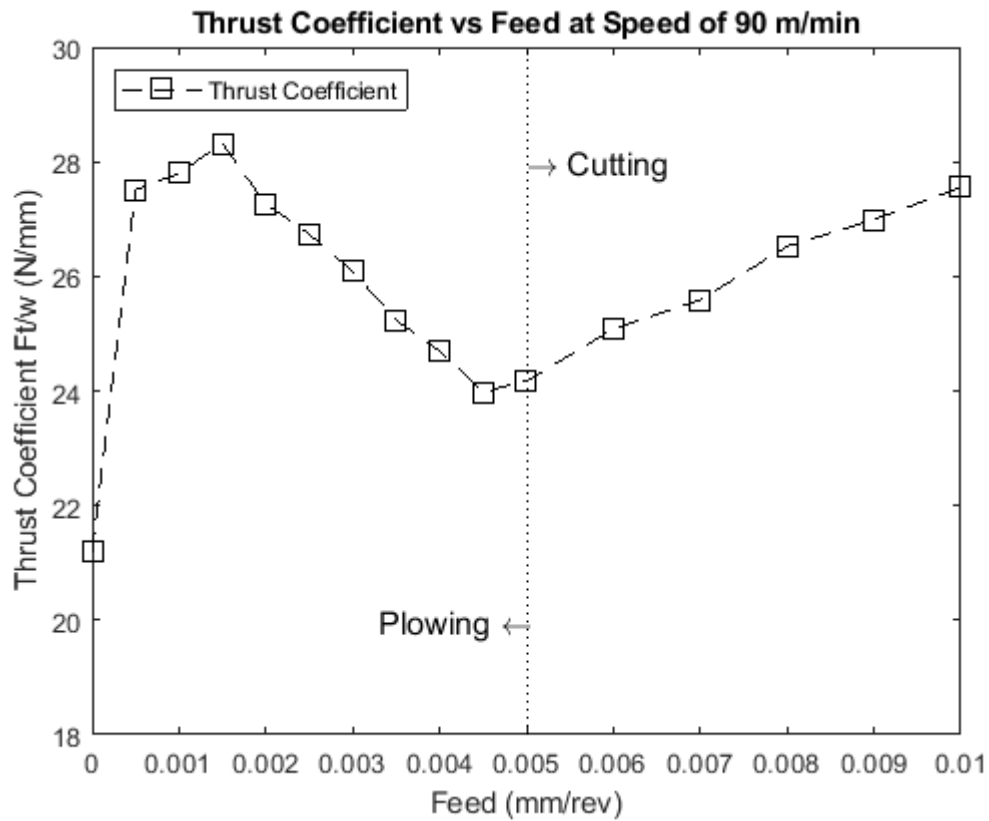


Figure 58: Thrust Coefficient vs. Uncut Chip Thickness at Speed 90 m/min

At 0.0005 mm/rev, the thrust force was measured to be 27.508 N/mm, increasing the feed to 0.0015 mm /rev, the thrust force increases to 28.32 N/mm. However, passing this feed, the thrust forces starts decreasing until reaching a value of 23.9795 N/mm at a feed of 0.0045 mm/rev. The forces then increase linearly until reaching a value of 27.555 N/mm.

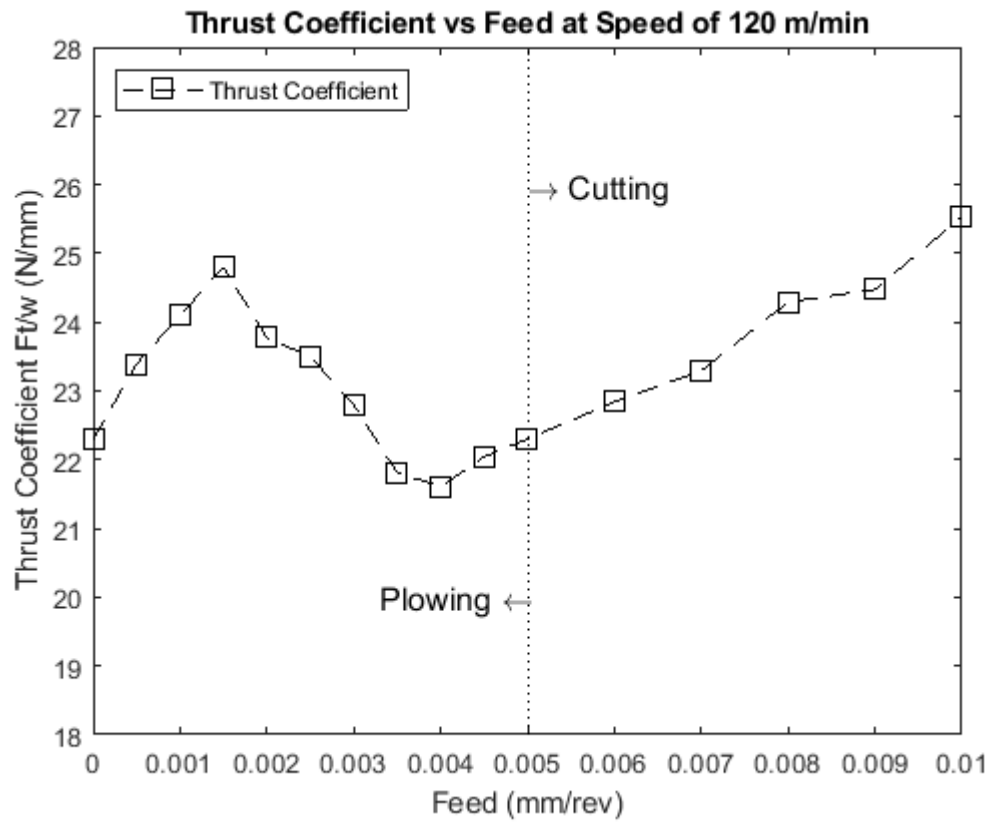


Figure 59: Thrust Coefficient vs. Uncut Chip Thickness at Speed 120 m/min

With a feed of 0.0005 mm/rev, the thrust force measured was 23.3935 N/mm, when the feed was increased to 0.0015 mm/rev the force increased to 23.775 N/mm. Afterwards, the forces starts decreasing to a value of 21.61 N/mm at a feed of 0.004 mm/rev, before increasing to 25.532 N/mm at 0.001 mm/rev.

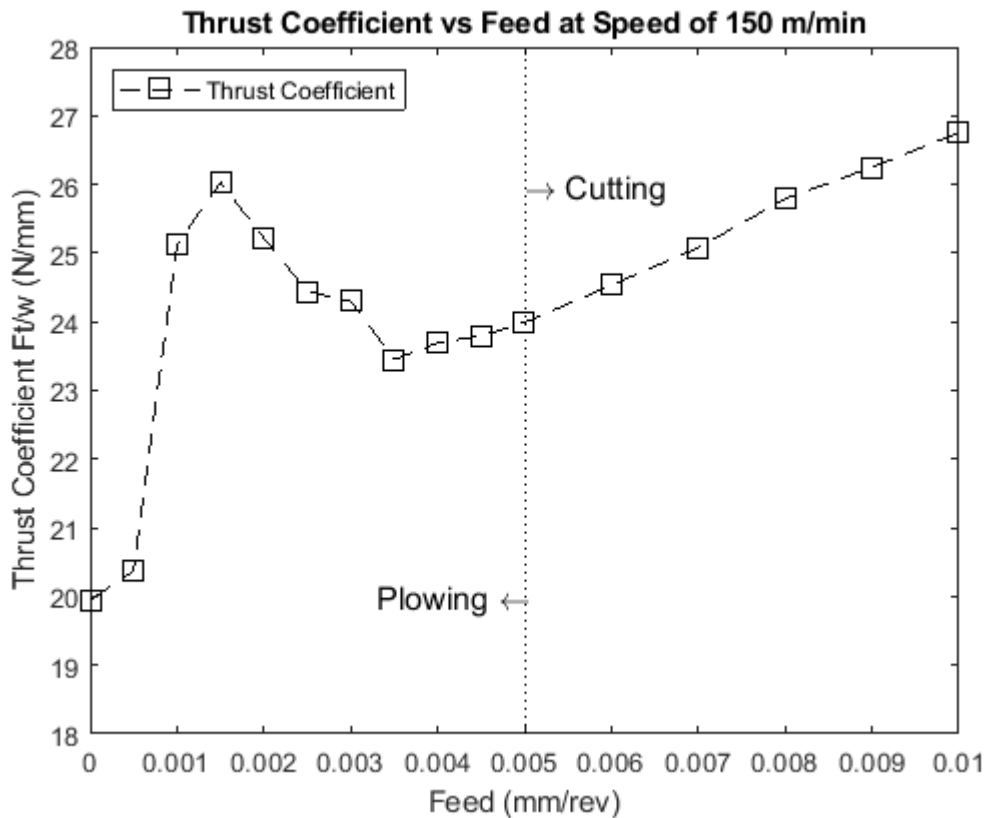


Figure 60: Thrust Coefficient vs. Uncut Chip Thickness at Speed 150 m/min

At 0.0005 mm/rev, the thrust force was measured to be 20.375 N/mm, increasing the feed to 0.0015 mm /rev, the thrust force increases to 26.04 N/mm. However, passing this feed, the thrust forces starts decreasing until reaching a value of 23.4495 N/mm at a feed of 0.0035 mm/rev. The forces then increase linearly until reaching a value of 26.755 N/mm.

3. Influence of cutting speed on plowing forces.

The plowing coefficient is also plotted vs. Uncut Chip Thickness for each cutting speed in an attempt to observe how the speed affects the forces. For each speed, a fresh new cutting edge was used thus tool wear is disregarded when shifting from a

cutting speed to another. Figure 61 represents how the plowing coefficient graph shifts as the cutting speed changes.

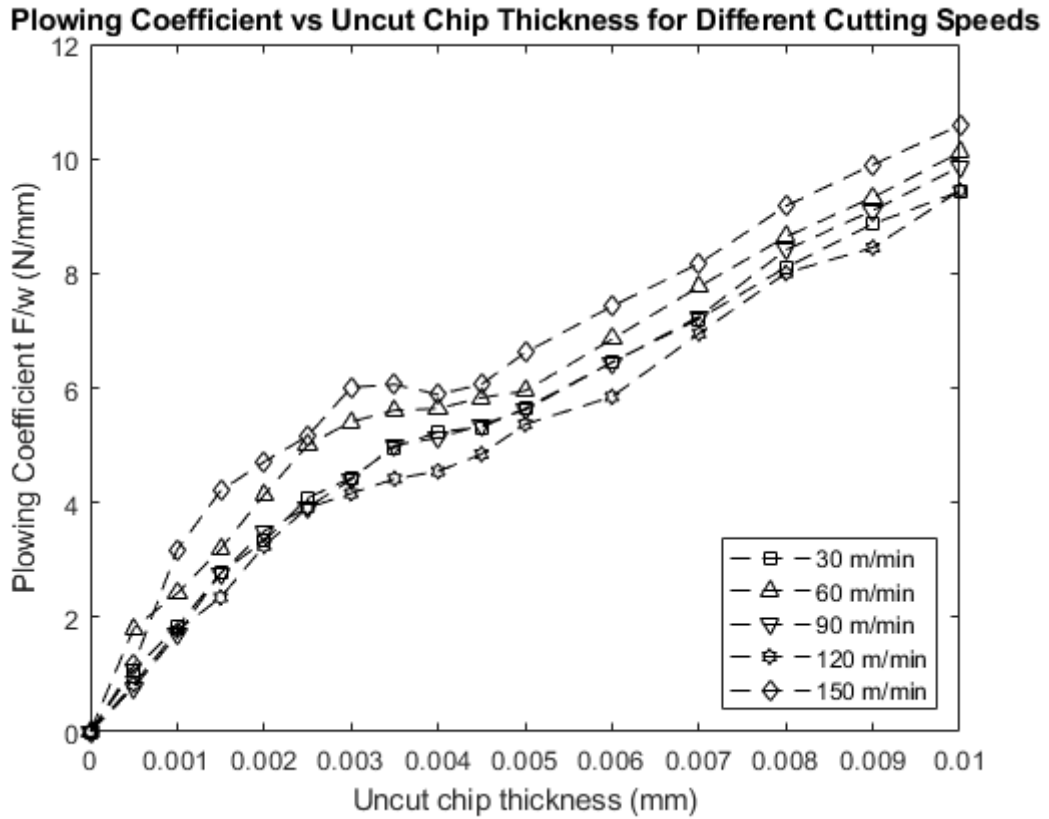


Figure 61: Plowing Coefficient vs. Uncut Chip Thickness at different Cutting Speeds.

Theoretically, it is believed that the plowing coefficients would decrease with increasing speed. Such behavior could be seen in Figure 61 at cutting speeds of 60 m/min, 90 m/min, and 120 m/min. As the speed increases from 60 to 90 to 120 m/min, the graph of each cutting speed shifts downward with increasing speed, thus lower plowing coefficients. However, the trend changes upon going from speed 30 m/min to 60 m/min. Instead of shifting downward, the graph moves upward. The same behavior is observed upon going from 120 m/min to 150 m/min as the figure shifts upward too.

For each speed, a fresh new cutting edge radius was used, thus tool wear is not a reason for irregular shifts. The absence of interdependency between the two could be drawn back to the effect of thermal softening, as stated by [10]

4. Temperature Measurements:

Temperature measurements were taken using FLIR TG165 Spot thermal Camera. The average temperature at the tip of the tool was calculated using FLIR tool specified software as shown in Figure 62 and Figure 63. The values obtained are shown in Table 12.

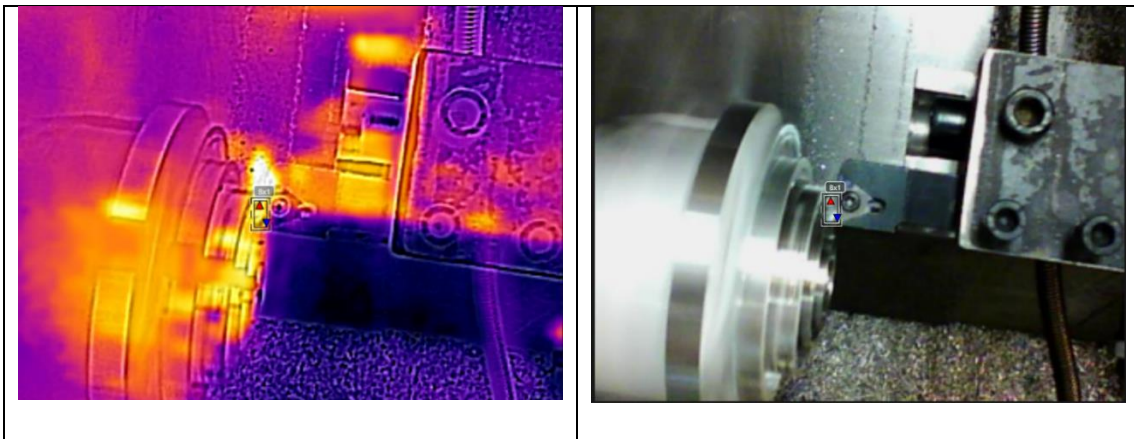


Figure 62: Thermal Photos of experiments at Speed 90 m/min and feed 0.005 mm

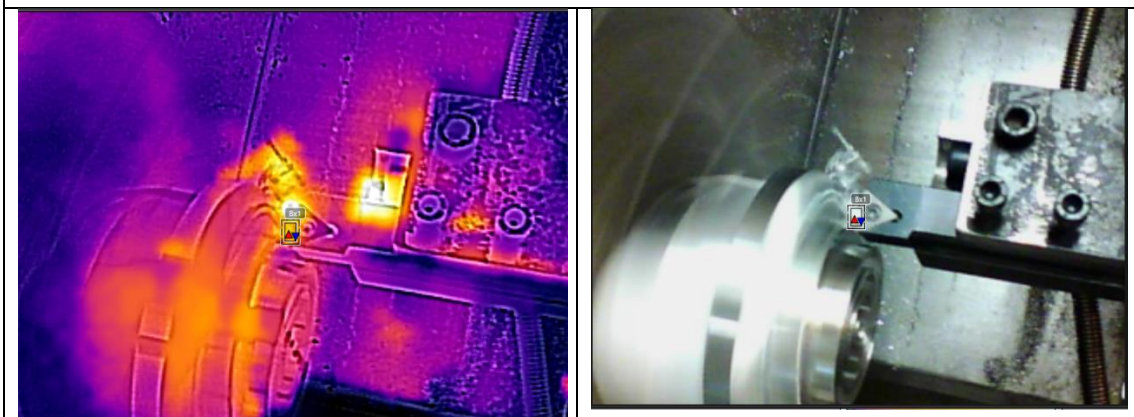


Figure 63: Thermal Photos of experiments at Speed 150 m/min and feed 0.005 mm.

Table 12: Temperature Measurements

			Spindle RPM				
			720	720	720	720	720
			cutting speed m/min				
			27	60	90	120	150
			A	B	C	D	E
	Rubbing	1	27.7	27	26	25.4	24.6
Feed mm/ rev	0.0005	2	28.1	27.9	26.4	26	25.2
	0.001	3	29	28	27	26.4	27.2
	0.0015	4	28.1	28.2	27.7	27.1	28.4
	0.002	5	28.8	28.4	28.1	29.2	28.6
	0.0025	6	30	28.8	28.2	25.8	28.8
	0.003	7	30.3	29.3	28.7	26.1	30.2
	0.0035	8	30.7	29.3	29.8	26.9	31.3
	0.004	9	32	29.4	30.4	27.1	31.9
	0.0045	10	32.2	31.3	30.7	26.5	32
	0.005	11	32.7	31.5	30.9	27	32.3
	0.006	12	33	32.6	31.8	28	32.9
	0.007	13	33.3	33.7	30.9	28.8	33.1
	0.008	14	33.8	32	30.3	29.6	33.4
	0.009	15	34	34.1	33.7	30	33.7
	0.01	16	34.4	34.4	34	31.8	32.6

For each cutting speed, temperature measurements are plotted vs. uncut chip thickness, as shown in Figure 64(Figure 68), the temperature increases as the uncut chip

increases. However, the difference in temperature between the maximum and the minimum feed is minimal. The value of feeds being worked on is minimal (0.0005 mm-0.01 mm), so a massive difference in temperature is improbable.

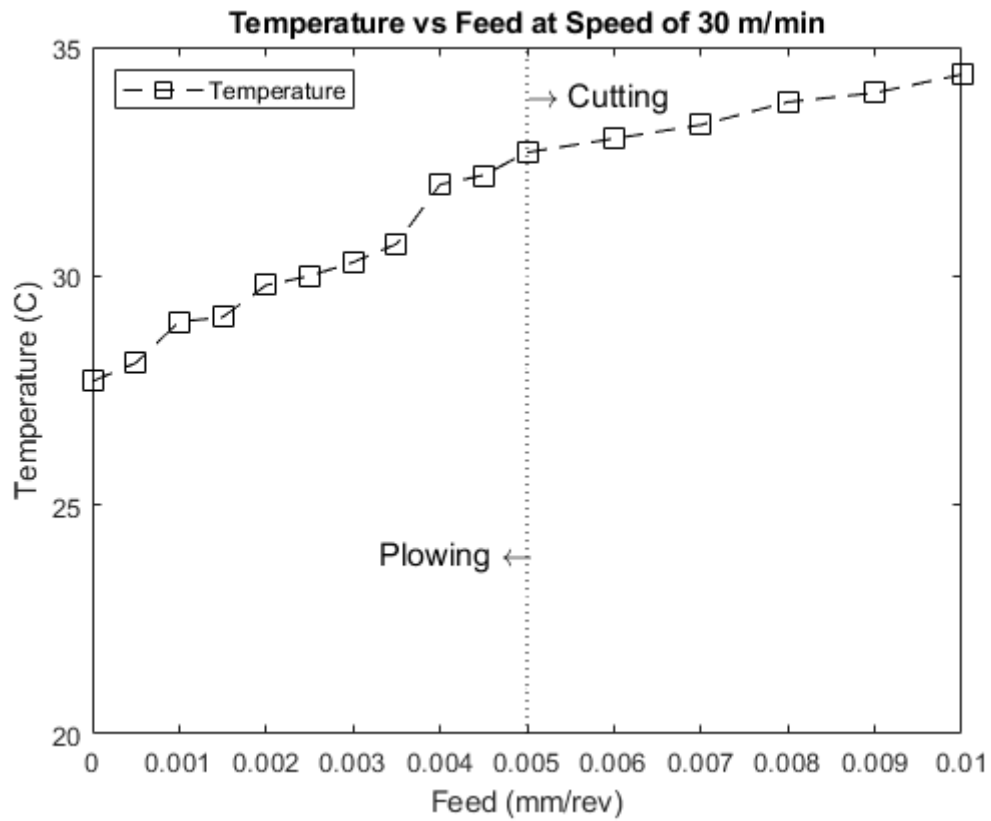


Figure 64: Temperature vs. Uncut Chip Thickness at Speed 30 m/min

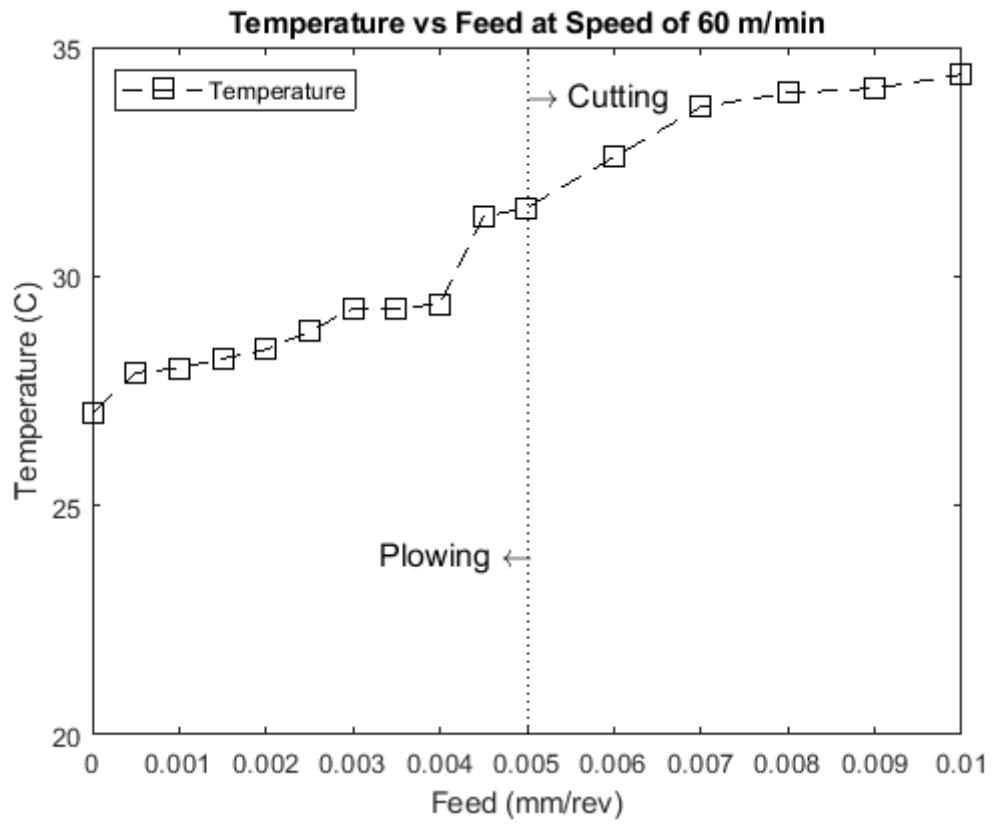


Figure 65: Temperature vs. Uncut Chip Thickness at Speed 60 m/min

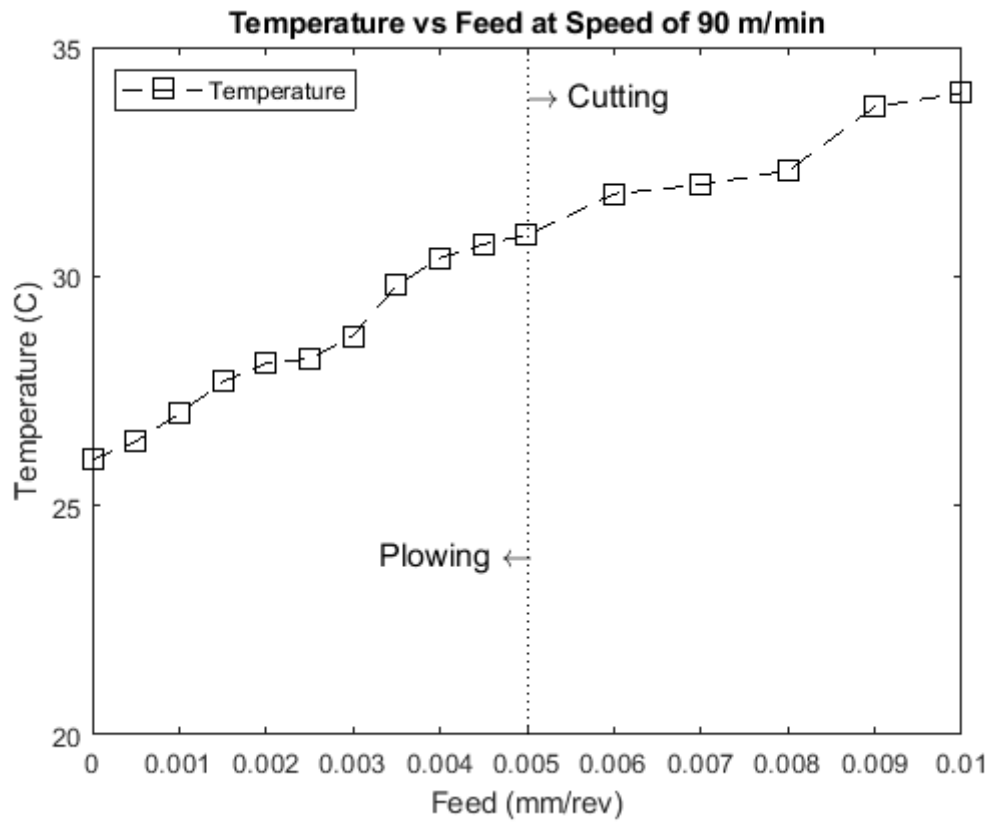


Figure 66: Temperature vs. Uncut Chip Thickness at Speed 90 m/min

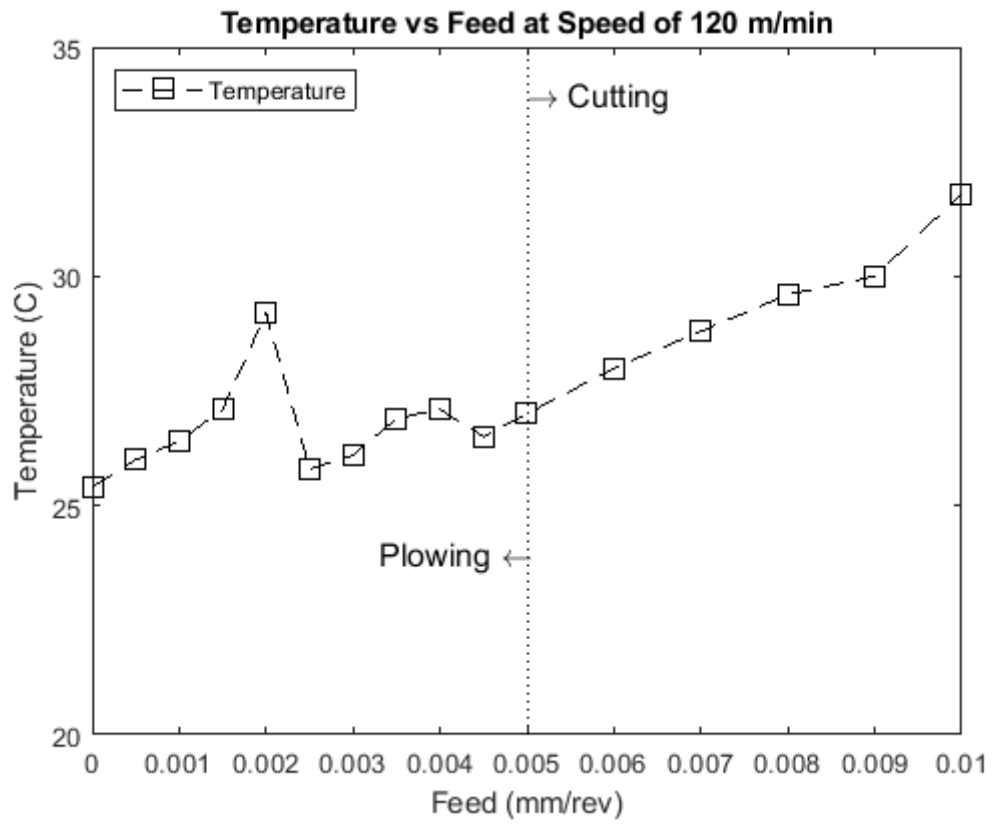


Figure 67: Temperature vs. Uncut Chip Thickness at Speed 120 m/min

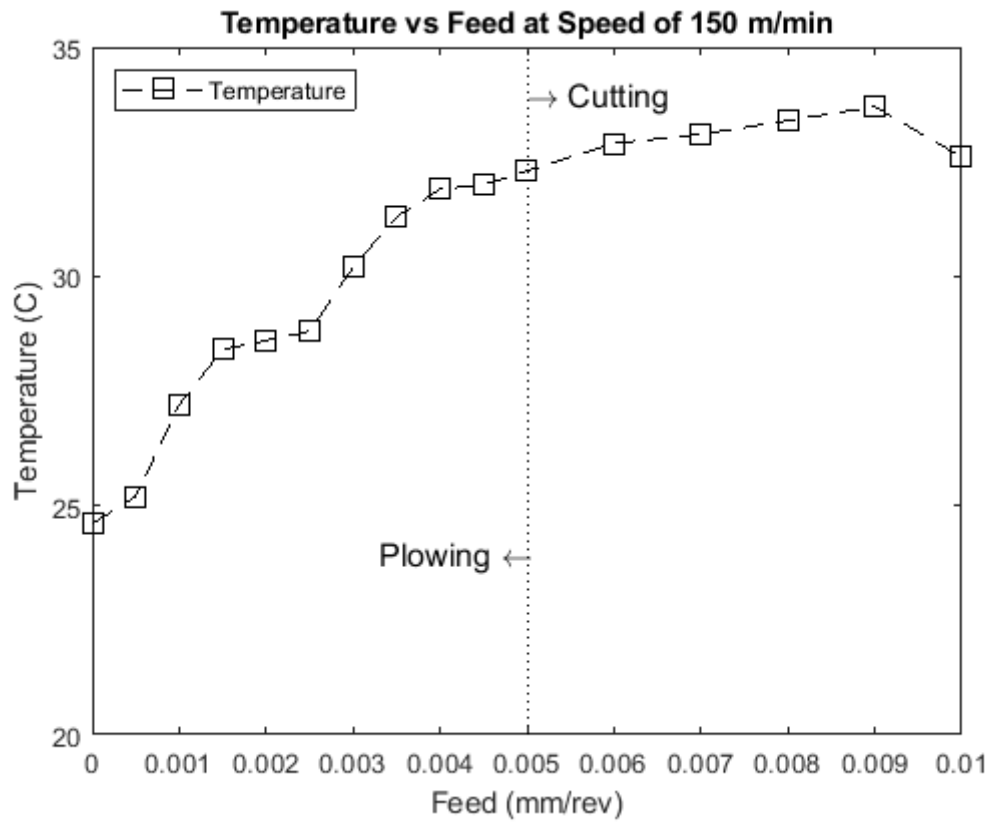


Figure 68: Temperature vs. Uncut Chip Thickness at Speed 150 m/min

5. Tool Scanning:

After completing the rubbing tests, the flank side of the tool was scanned under the microscope to measure the length of contact between the tool and work piece upon rubbing. It is assumed that the length of contact is the flank wear that affected the tool is due to friction.

Figure 69 represents the flank wear shown under the microscope. The length of contact between the tool and the work piece is measured to be ranging between 42 μm and 50 μm

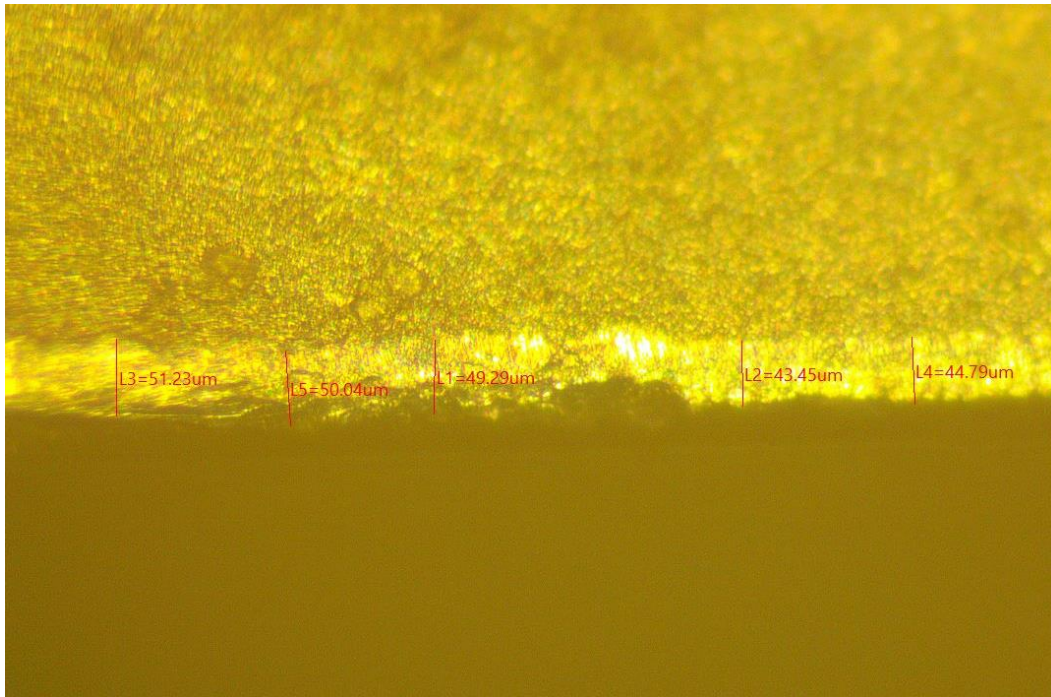


Figure 69: Length of contact

B. Analytical

To compare between experimental and analytical values, Equations (13) and (14) are to be obtained and compared with their experimental counterparts F_x and F_z . Each factor in the equations is to be determined by the analytical equations set above.

1. Region 1.

First, the total forces acting in this region is R_1 , composed of the friction force component F_{f1} and normal force component N_1 . See Figure 23.

$$\text{Total Forces} = R_1 = F_{f1} + N_1 \quad (9)$$

Using Equation (10) to get F_{f1} ,

$$F_{f1} = \mu \times \text{Length of contact area in Region 1 } l_1 \quad (10)$$

Where *Length of contact area in Region 1* $l_1 = 50 \mu\text{m}$ measured in Figure 69.

To calculate the friction forces, several friction models are proposed:

1. Constant Shear Friction Coefficient

$$\mu = 0.3$$

$$F_{f1} = 0.8 \times \frac{50}{2} = 7.5 \text{ N}$$

2. Temperature dependent friction Coefficient

To calculate the friction forces, friction model proposed by [25] is followed:

$$\mu = 1 - ae^{\frac{b}{T+c}} \quad (11)$$

The temperature data obtained from the experiments is plugged in into MATLAB along the experimental values of μ . Using the function Isqcurvefit, the constants a, b, and c were tabulated to be:

$$a=7.4954 \times 10^{-5}$$

$$b=1865.1$$

$$c=329.5205$$

Therefore,

$$\mu = 1 - 7.4954 \times 10^{-5} e^{\frac{1865.1}{T+329.5205}}$$

2. *Region 2.*

To obtain the forces in region 2, first the friction force acting in the region is calculated by equation (15):

$$F_{f2} = \int_0^{\theta} \mu (2 \times \pi \times CER) \left(\frac{\theta}{360} \right) d\theta$$

The predicted plowing and thrust coefficients are computed using Equations (27) and (28) using MATLAB for all uncut chip thickness using the material properties listed in Table 13:

Table 13: AZ31B Material Properties

Modulus of Elasticity E	44 MPa
Poisson's Ratio	0.35
Shear Yield Stress	226 MPa

Equations (13) and (14) are used to sum the values from Equations (27) and (28) with the values attained from Equations (10) and (19) to obtain F_x and F_z respectively. Two cases are simulated using Matlab. First, a constant cutting-edge radius is plugged in the equations and then, variable CER is plugged in using Equation (32). The comparison between the experimental and analytical values is shown in Figure 70- Figure 82):

a. Constant Cutting-Edge Radius

First, the cutting-edge radius of the tool is assumed to be constant meaning that tool wear is assumed to be minimal or nonexistent. The predicted forces are shown below in Figure 70.

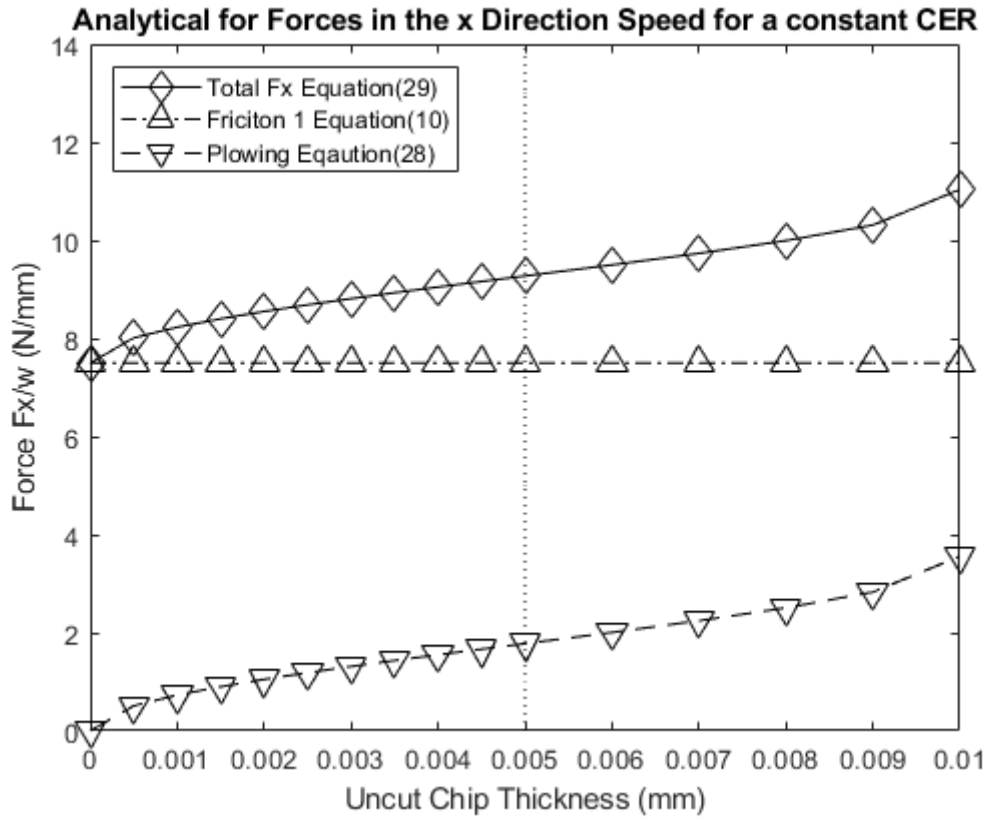


Figure 70: Analytical Values

Analytical vs Experimental Values for Forces in the x Direction Speed 30 m/min

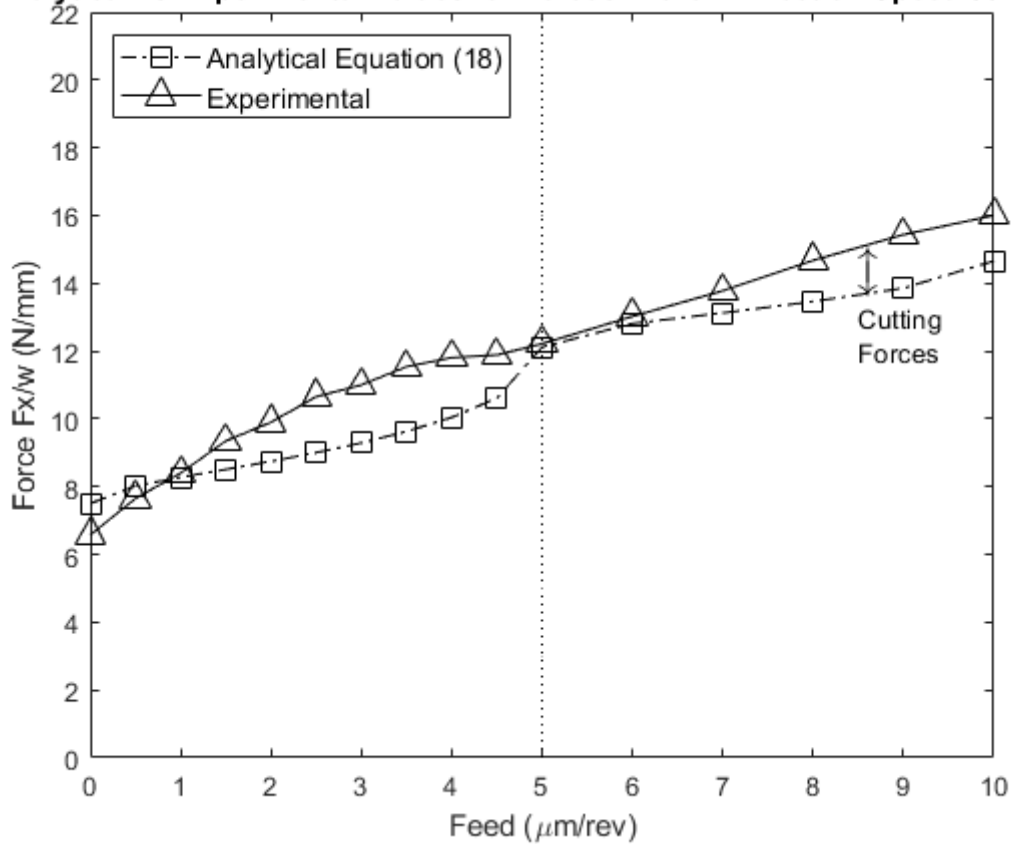


Figure 71: Analytical vs. Experimental Corrected Values for Speed 30 m/min.

With a cutting speed of 30 m/min, the analytical model is seen to be predicting the plowing forces with a great accuracy. The difference between the experimental and the analytical values was calculated to be 6.93 % between feeds of 0 and 0.005 mm/rev. However, when the feed is above 0.005 mm/rev, the difference increases to a value of 12.2 %. Such increase in the value of the difference could be drawn back to the admission of the cutting forces into the process. Such forces are not depicted in the analytical model utilized and thus the increase in the difference is justified.

Analytical vs Experimental Values for Forces in the x Direction Speed 60 m/min

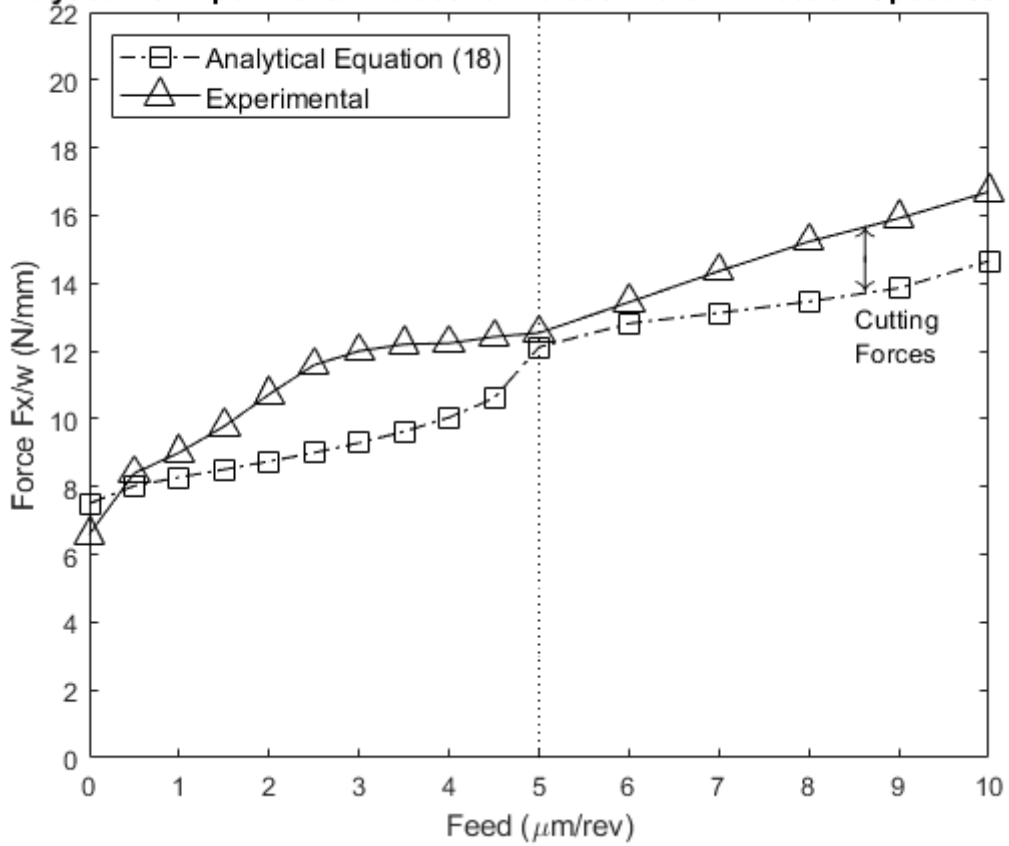


Figure 72: Analytical vs. Experimental Values for Speed 60 m/min

Increasing the cutting speed to 60 m/min, the analytical model is seen to be predicting the plowing forces with an excellent accuracy of 11.37 % between feeds of 0 and 0.005 mm/rev. Furthermore, when the feed increases above 0.005 mm/rev, the difference increases to a value of 17.84 %.

Analytical vs Experimental Values for Forces in the x Direction Speed 90 m/min

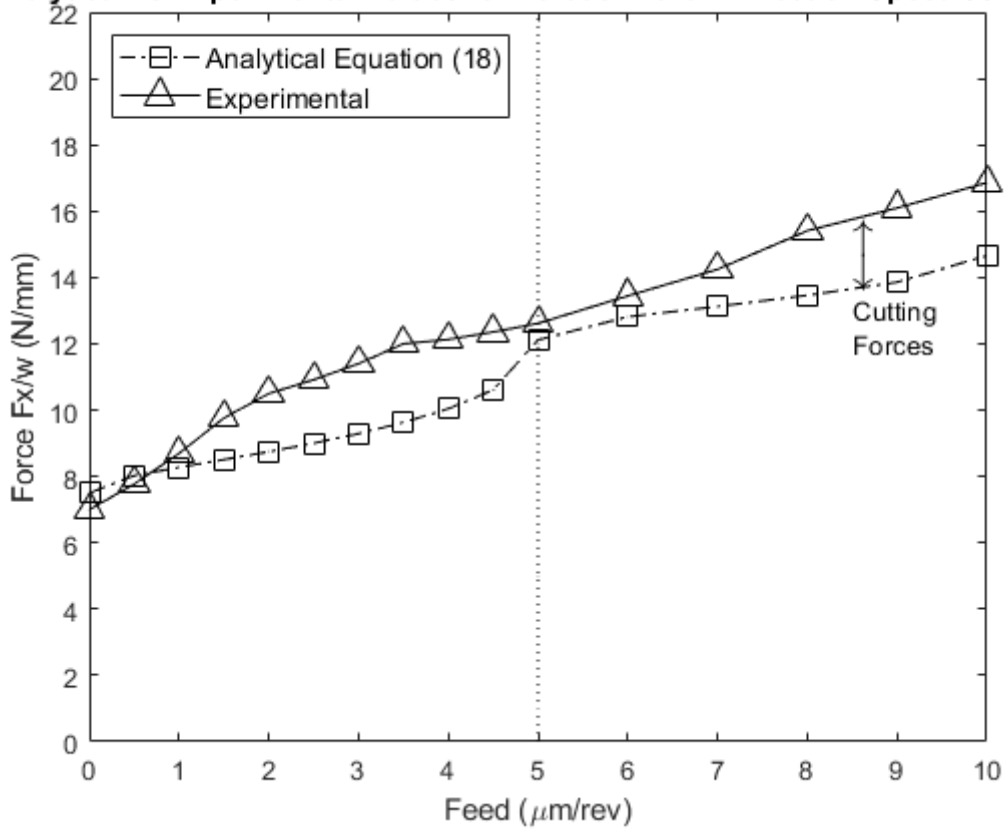


Figure 73: Analytical vs. Experimental Values for Speed 90 m/min.

Increasing the cutting speed to 90 m/min, the analytical model is seen to be predicting the plowing forces with a good accuracy. The difference calculated decreased to a value of 10.45 % between feeds of 0 and 0.005 mm/rev. As in the cases before, the difference increases to a value of 16.18 % the feed increases above 0.005 mm/rev.

Analytical vs Experimental Values for Forces in the x Direction Speed 120 m/min

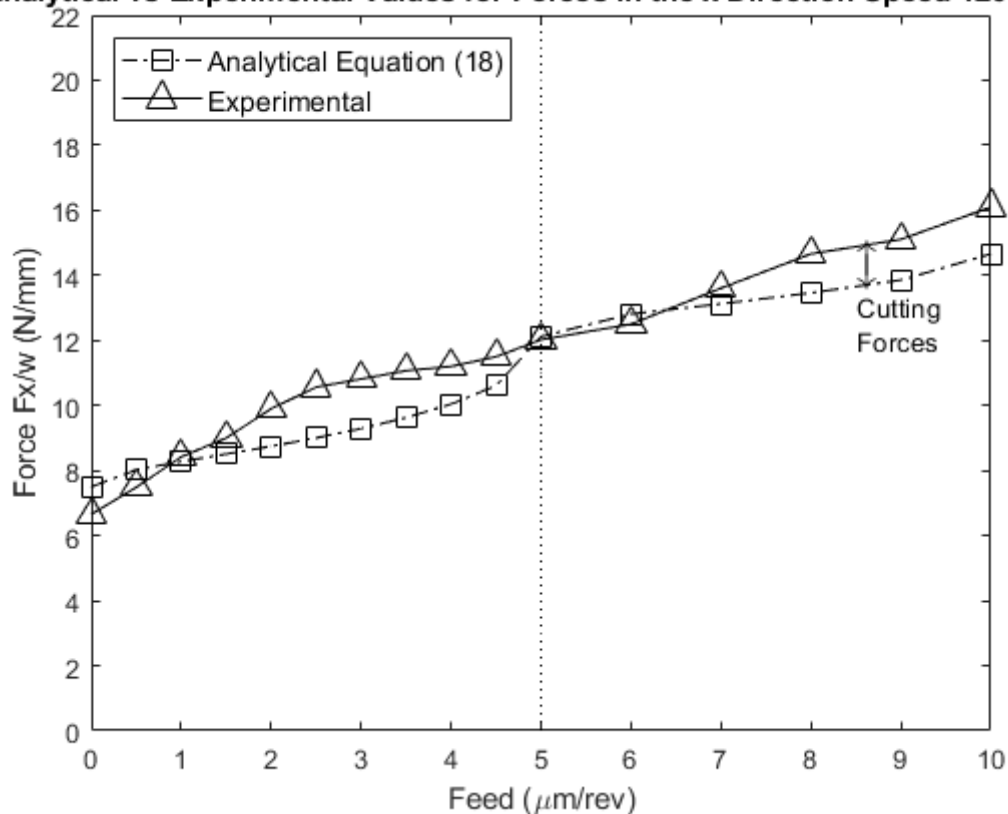


Figure 74: Analytical vs. Experimental Values for Speed 120 m/min

At a cutting speed of 120 m/min, the analytical model is still perceived to be predicting the plowing forces with an excellent accuracy. The difference calculated decreased to a value of just 5.28 % between feeds of 0 and 0.005 mm/rev. At higher feeds, the difference surprisingly decreases to 8.39 %.

Analytical vs Experimental Values for Forces in the x Direction Speed 150 m/min

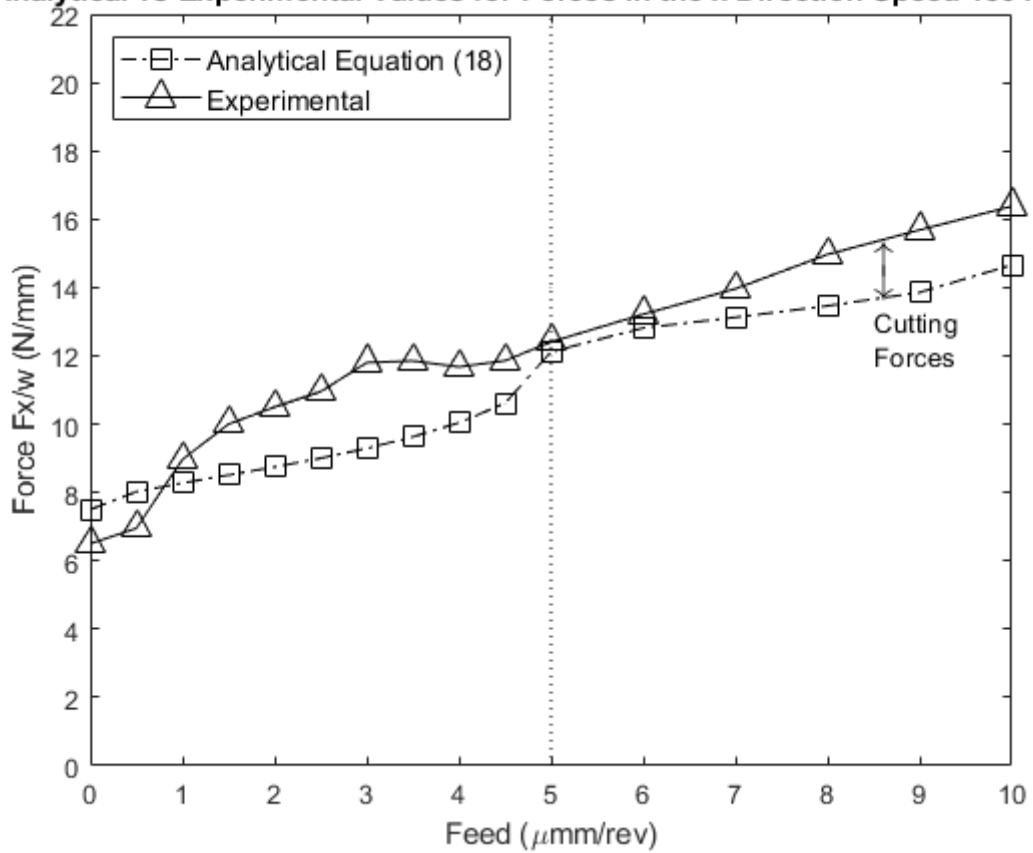


Figure 75: Analytical vs. Experimental Values for Speed 150 m/min

Increasing the cutting speed to 150 m/min, the analytical model is seen to be predicting the plowing forces with a good accuracy. The difference calculated decreased to a value of 10.3 % between feeds of 0 and 0.005 mm/rev. As in the cases before, the difference increases to a value of 16.2 % the feed increases above 0.005 mm/rev.

b. Variable Cutting Edge Radius

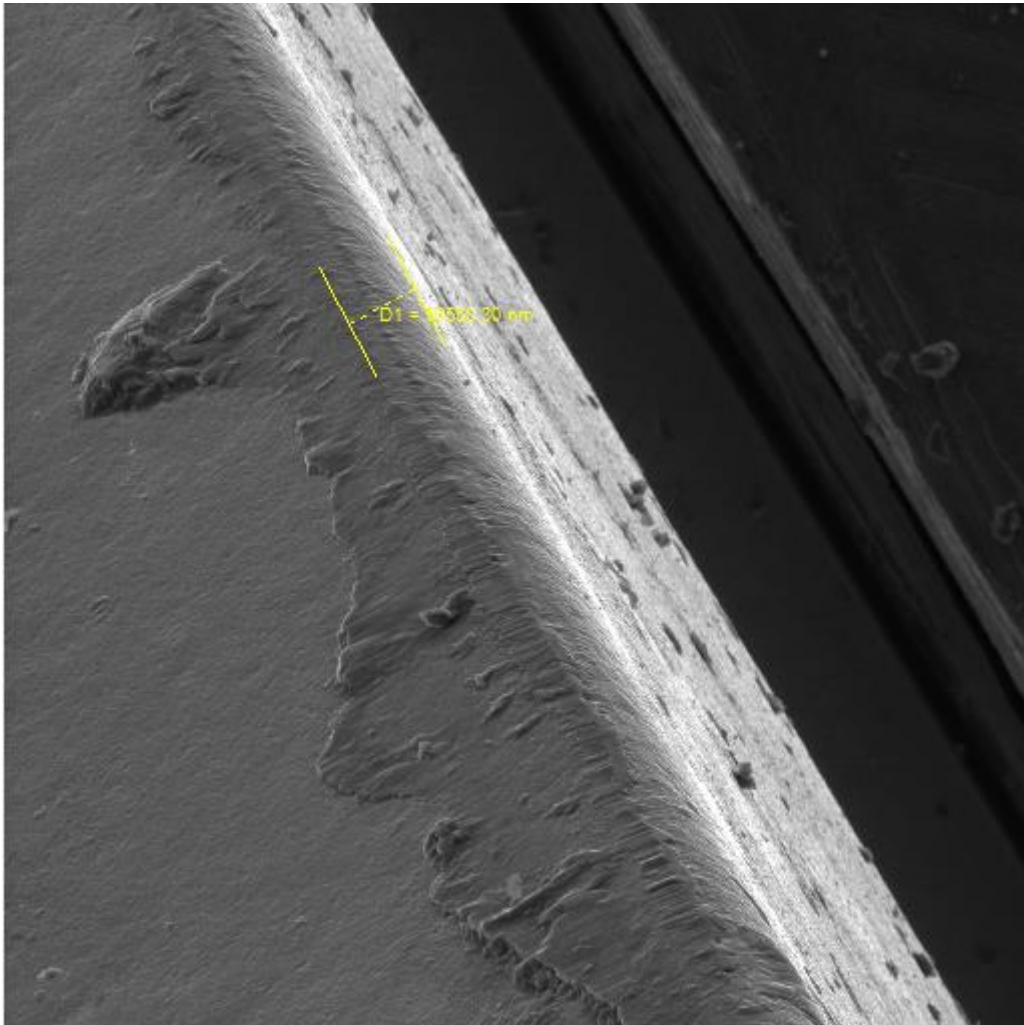


Figure 76: Damaged Cutting-Edge Radius

In this case, the cutting-edge radius is taken to be variable varying with feed and speed. So, tool wear is taken into consideration and the analytical values are wear corrected. As seen in Figure 76, the cutting-edge radius increased from 5 micrometers to 50. Equations (33-37) were used and plugged in Matlab. The analytical data are shown in Figure 78-Figure 82):

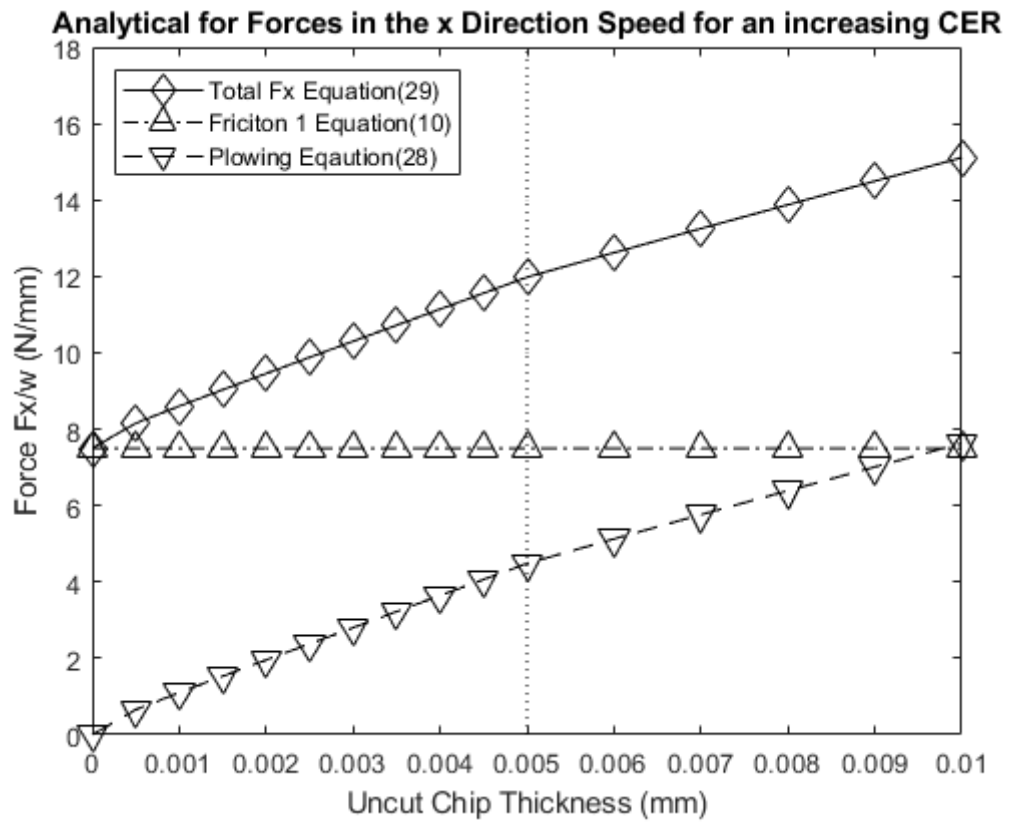


Figure 77: Analytical Values

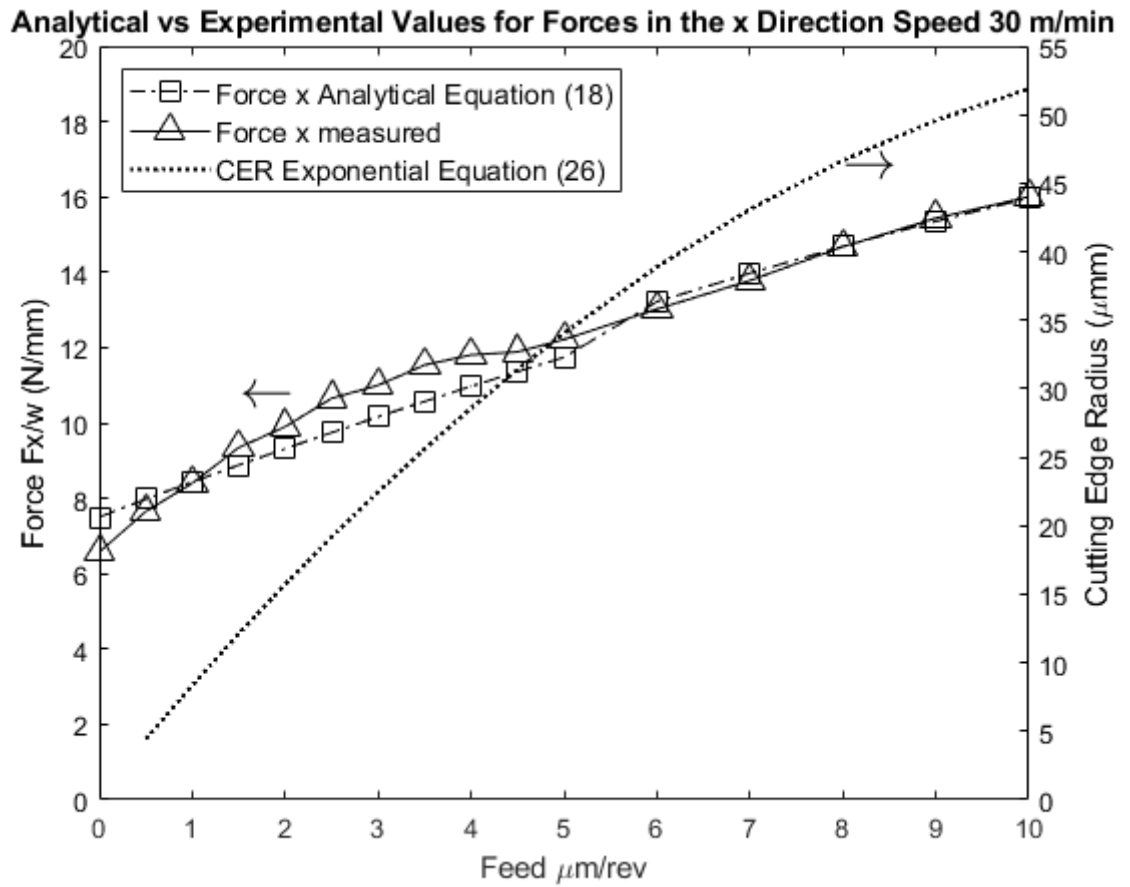


Figure 78: Analytical vs. Experimental values in the x direction for a variable CER at Speed 30 m/min.

With a cutting speed of 30 m/min, the analytical model is seen to be predicting the plowing forces with a very high accuracy. The difference between the experimental and the analytical values was calculated to be 1.84 %.

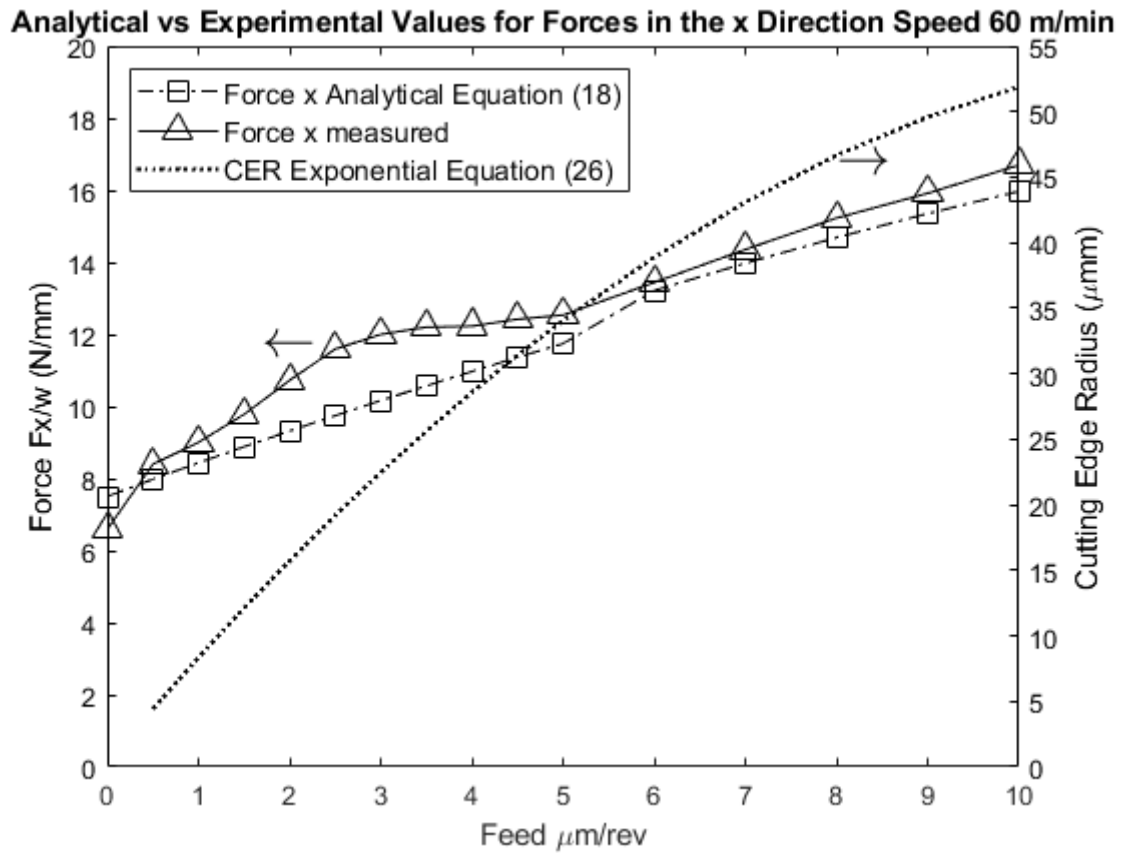


Figure 79: Analytical vs. Experimental values in the x direction for a variable CER at Speed 60 m/min.

Increasing the cutting speed to 60 m/min, the analytical model is seen to be predicting the plowing forces with a relatively good accuracy. The difference increased to larger but still a good value of 6.755 %.

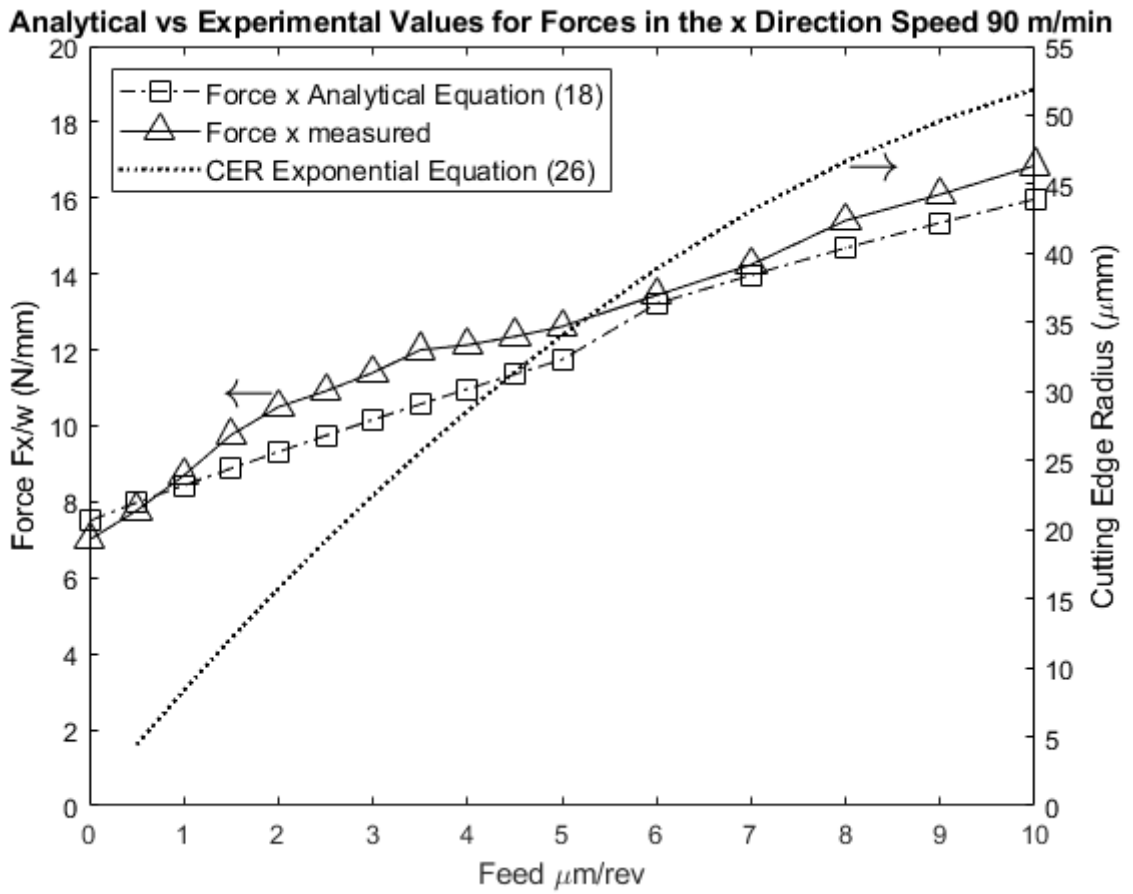


Figure 80: Analytical vs. Experimental values in the x direction for a variable CER at Speed 90 m/min.

Increasing the cutting speed to 90 m/min, the analytical model is seen to be predicting the plowing forces with a good accuracy. The difference calculated decreased to a value of 5.07 %.

Analytical vs Experimental Values for Forces in the x Direction Speed 120 m/min

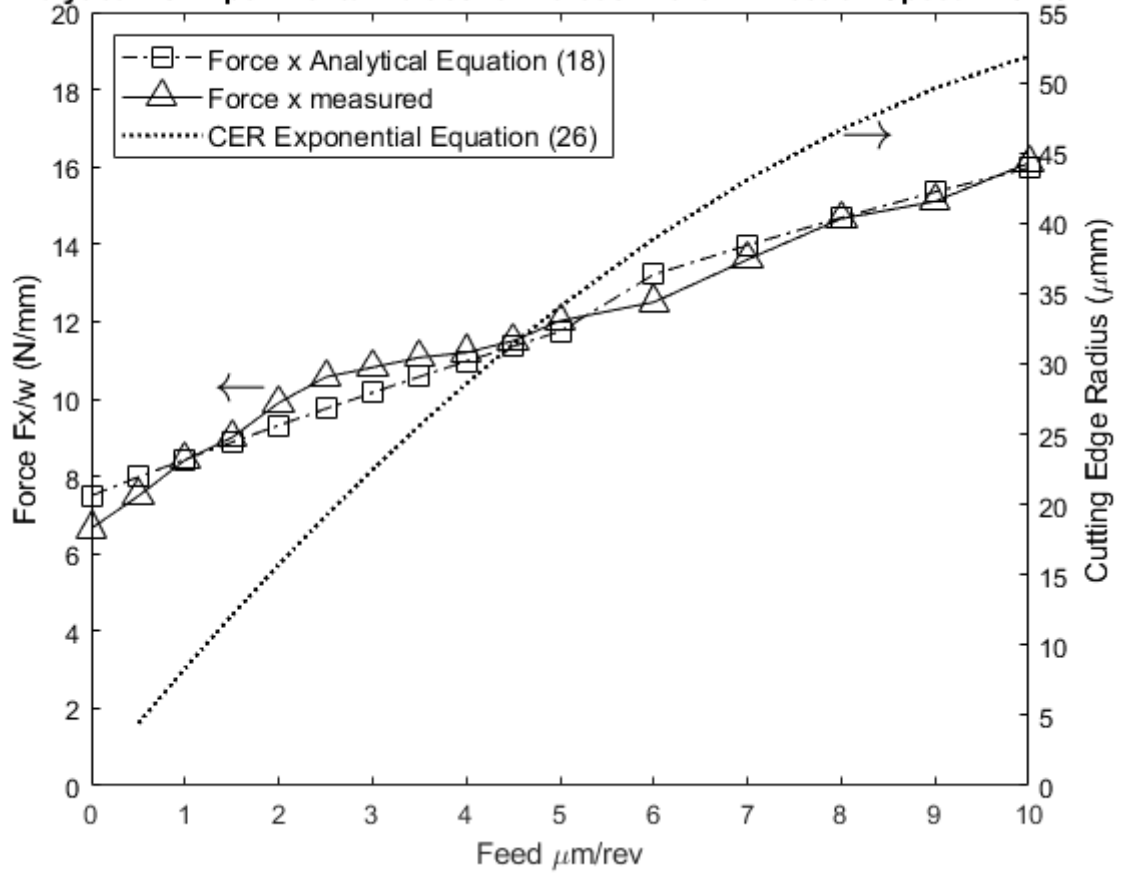


Figure 81: Analytical vs. Experimental values in the x direction for a variable CER at Speed 120 m/min.

At a cutting speed of 120 m/min, the analytical model predicted the force values with a minimal percentage difference of 0.131 %.

Analytical vs Experimental Values for Forces in the x Direction Speed 150 m/min

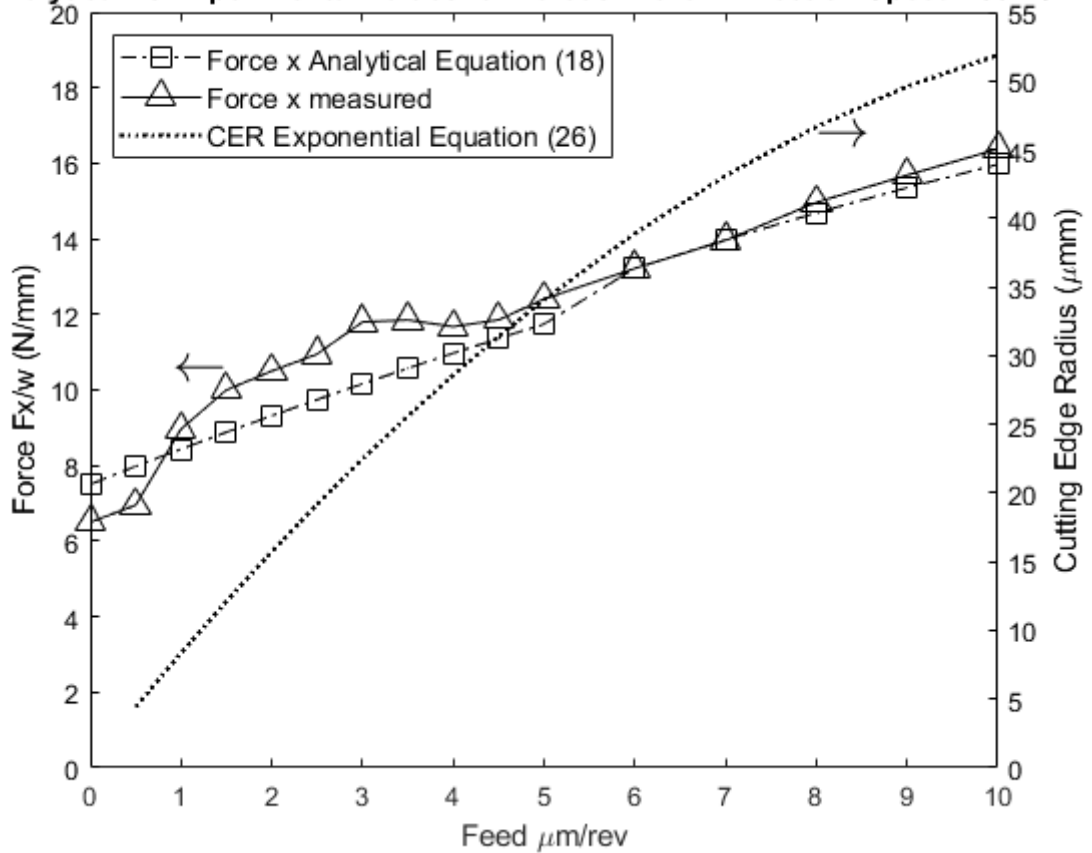


Figure 82: Analytical vs. Experimental values in the x direction for a variable CER at Speed 150 m/min.

Increasing the cutting speed to 150 m/min, the analytical model is seen to be predicting the plowing forces with a good accuracy. The difference calculated increased to a value of 3.84 %.

From, the analytical model has predicted the value relatively well with respect to the experimental values. The average percentage of difference between the plowing analytical predictions and the experimental values is approximated to be 8.5075 % percent for a constant cutting-edge radius, whereas the difference dropped to a mere 3.095 % for a variable cutting edge radius using the equations correcting for wear. As

one may expect, the increase in difference in the interval of 0.005 mm-0.01 mm is drawn back to the admission of the cutting forces into the process. Since the cutting forces are not portrayed in the analytical model utilized in this research, the experimental values are increasing without the analytical model compensating for that increase in its prediction. Thus, the experimental values shift away from the analytical values and so the difference increases drastically.

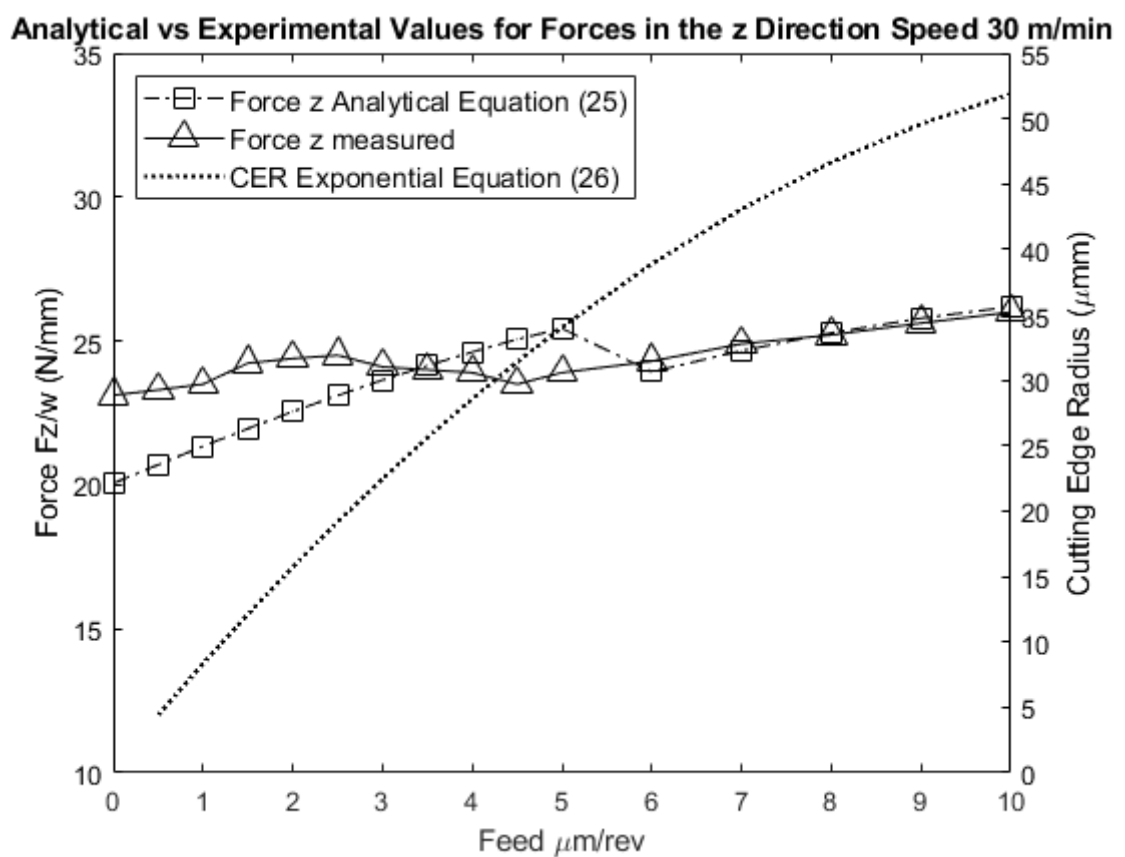


Figure 83: Analytical vs. Experimental values in the z direction for a variable CER at Speed 30 m/min.

Analytical vs Experimental Values for Forces in the z Direction Speed 60 m/min

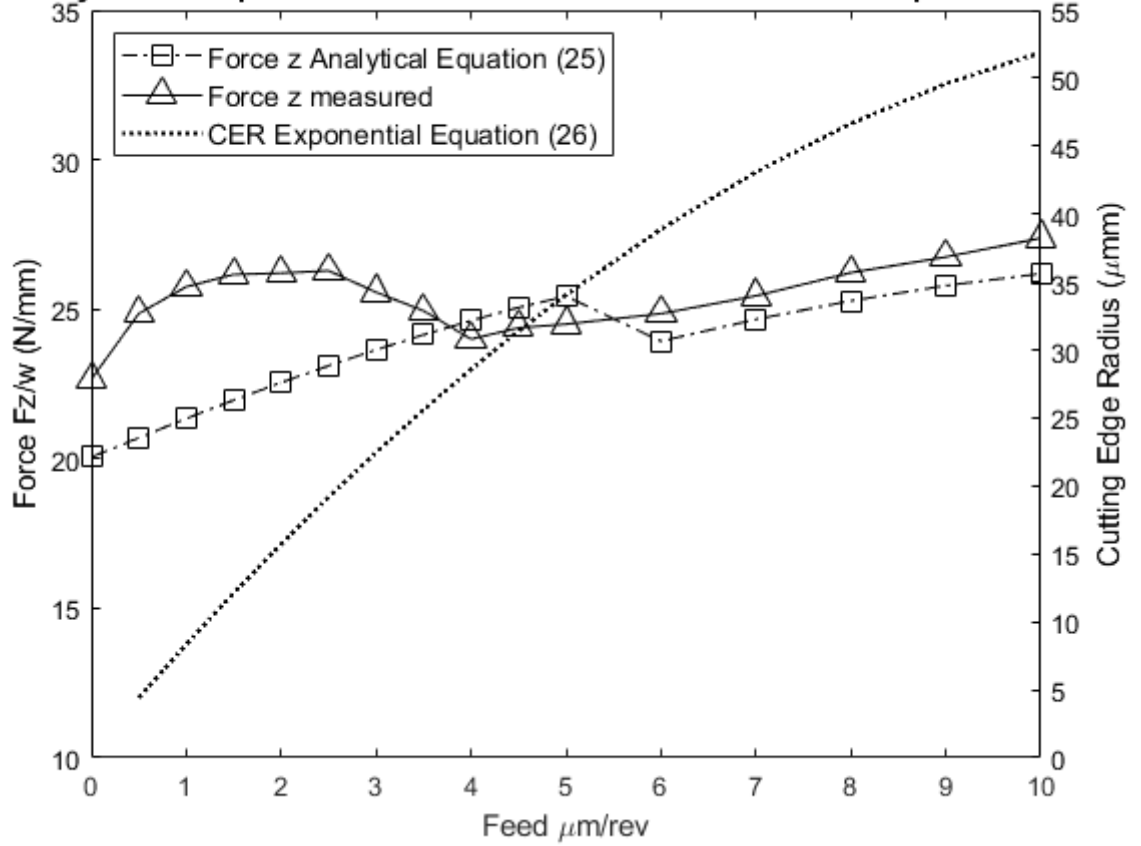


Figure 84: Analytical vs. Experimental values in the z direction for a variable CER at Speed 60 m/min.

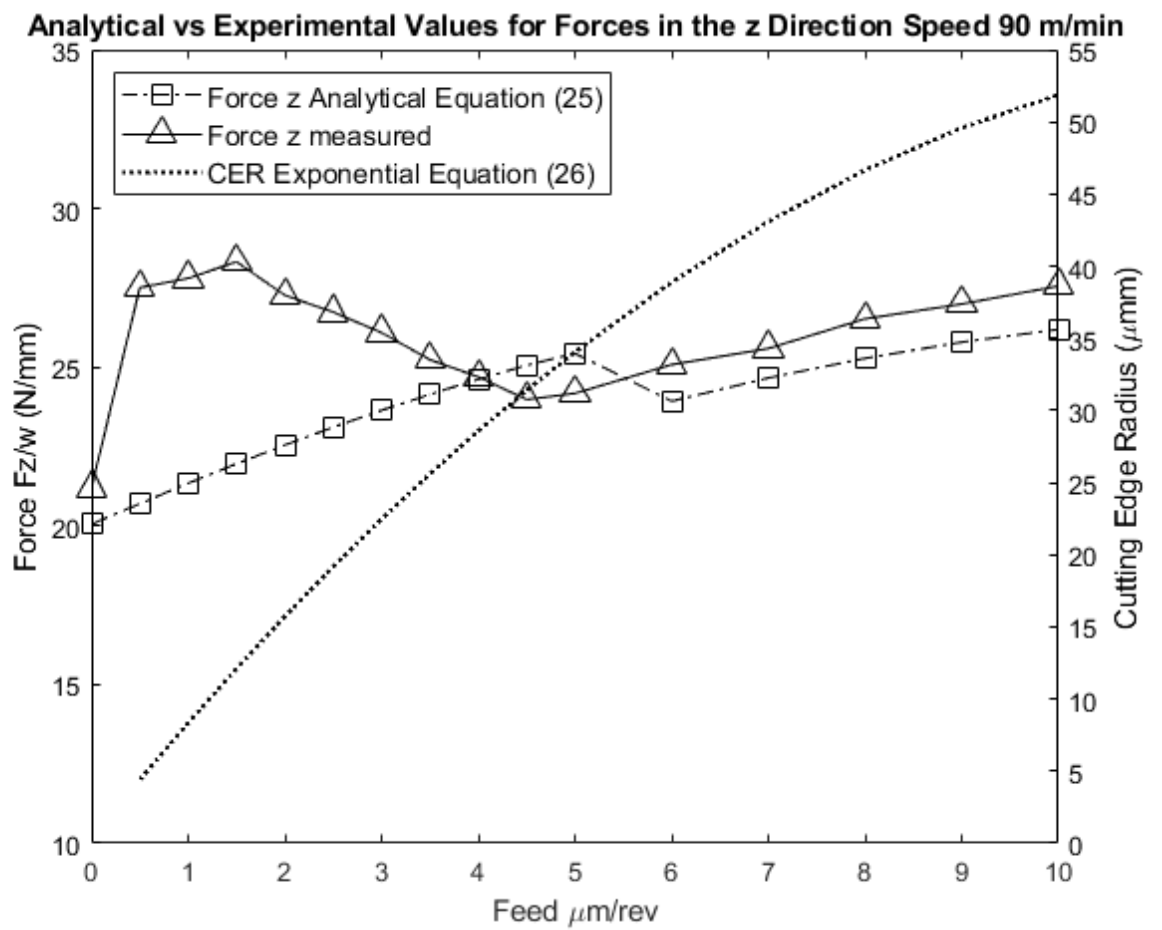


Figure 85: Analytical vs. Experimental values in the z direction for a variable CER at Speed 90 m/min.

Analytical vs Experimental Values for Forces in the z Direction Speed 120 m/min

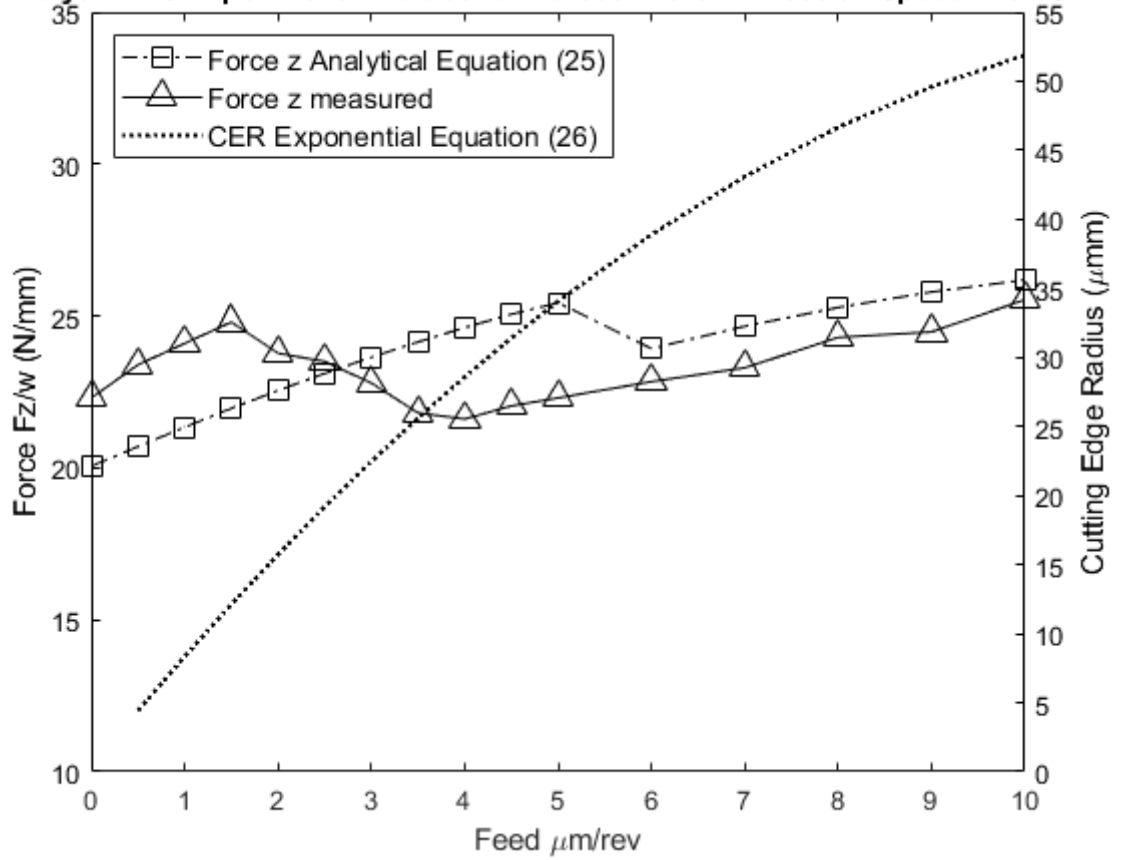


Figure 86: Analytical vs. Experimental values in the z direction for a variable CER at Speed 120 m/min.

Analytical vs Experimental Values for Forces in the z Direction Speed 150 m/min

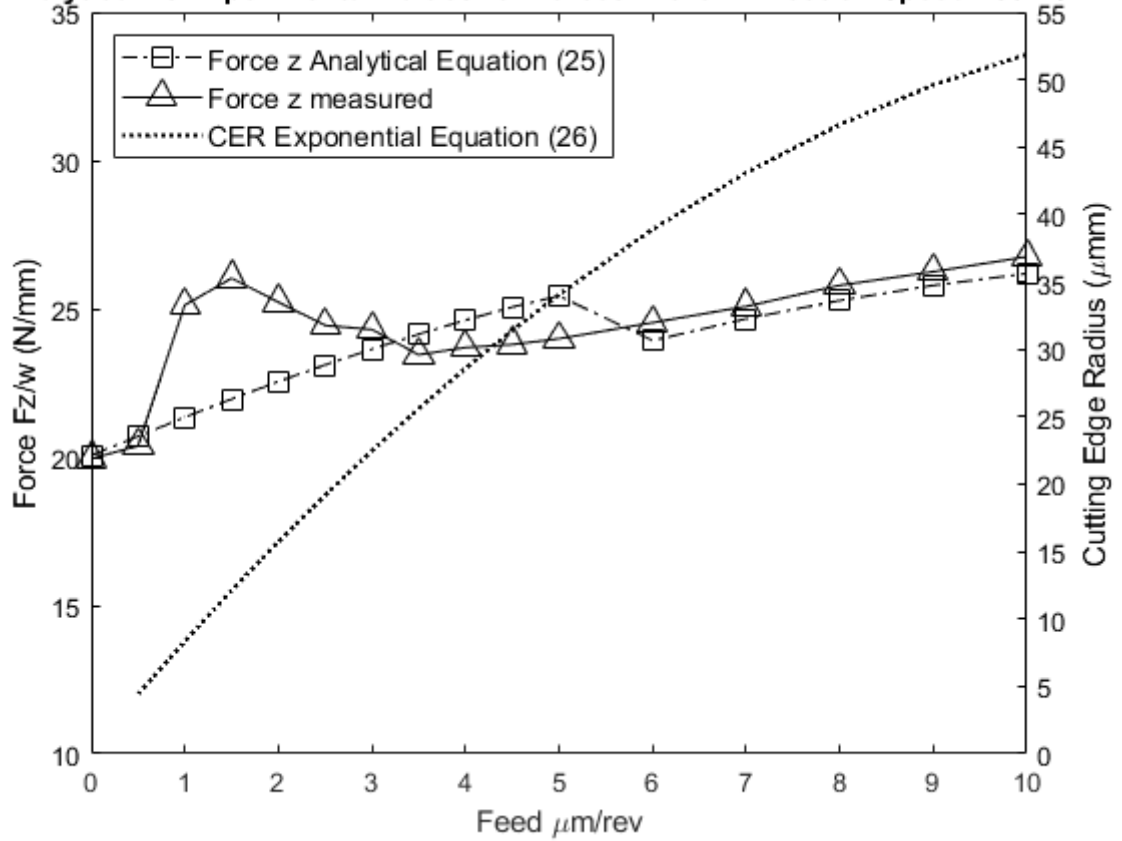


Figure 87: Analytical vs. Experimental values in the z direction for a variable CER at Speed 150 m/min.

The analytical model of this research predicted the forces in the z direction with a good accuracy. The model successfully predicted the anomaly in the trend (the bump seen in all the figures of force z) that was witnessed in the experimental values, although at a later stage.

C. Numerical

Simulations of the process were done on Deform for all speeds and feeds reported in

Table 2. Correction for wear was applied by varying the cutting-edge radius with increasing feed.

1. Stagnation Point

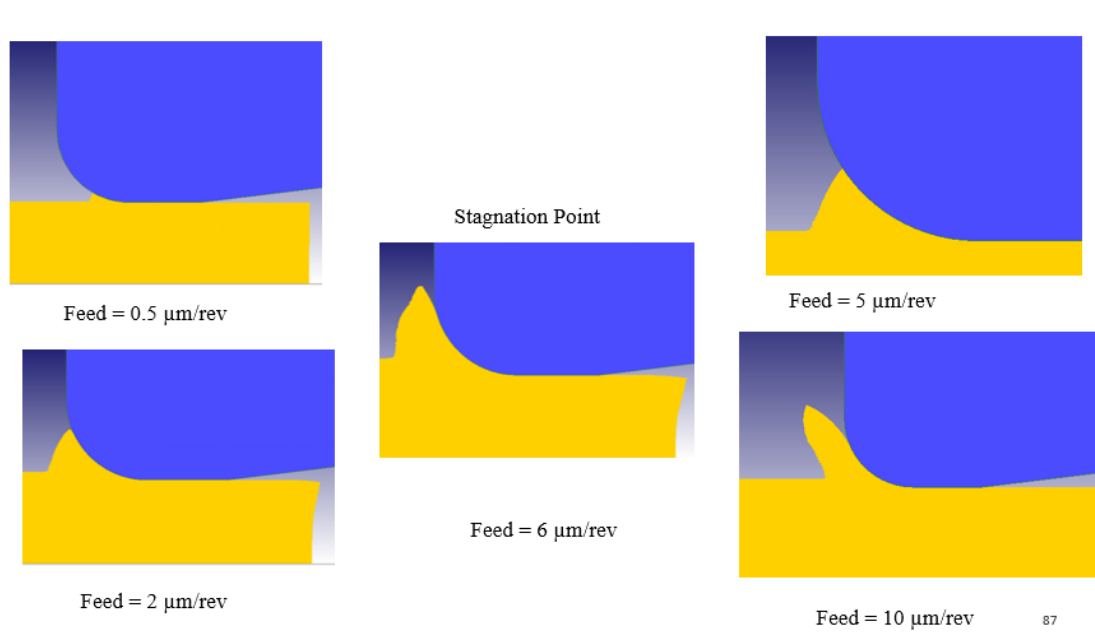


Figure 88: Stagnation Point

The stagnation point is the point along the arc of the cutting-edge radius at which a chip would flow out along the rake face of the tool. From the runs done through DEFORM, between 0.5 μm and 5 μm the material was compressed and deformed under tool and no chip was formed. However, reaching a feed of 6 μm, a chip was formed flowing upwards along the rake face of the tool.

2. Forces

Table 14: Force z Numerical values obtained by DEFORM for all speeds and feeds.

			Spindle RPM				
			720	720	720	720	720
			cutting speed m/min				
			27	60	90	120	150
			A	B	C	D	E
	Rubbing	1	6	5.5	5	4.5	4.3
Feed mm/ rev	0.0005	2	6.405	6	5.3775	4.755	4.53
	0.001	3	6.905	6.5	5.8775	5.255	5.03
	0.0015	4	7.405	7	6.3775	5.755	5.53
	0.002	5	8.41	8.005	7.3825	6.76	6.535
	0.0025	6	8.805	8.4	7.7775	7.155	6.93
	0.003	7	9.22	8.815	8.4075	8	7.775
	0.0035	8	9.405	9	8.75	8.5	8.275
	0.004	9	9.805	9.4	9.2	9	8.775
	0.0045	10	10.105	9.7	9.45	9.2	8.975
	0.005	11	11.125	10.72	10.0975	9.475	9.25
	0.006	12	11.685	11.28	10.6575	10.035	9.81
	0.007	13	12.295	11.89	11.2675	10.645	10.42
	0.008	14	12.905	12.5	11.8775	11.255	11.03
	0.009	15	13.33	12.925	12.3025	11.68	11.455
	0.01	16	13.755	13.35	13.0975	12.845	12.62

Table 15: Force z Numerical values obtained by DEFORM for all speeds and feeds.

			Spindle RPM				
			720	720	720	720	720
			cutting speed m/min				
			27	60	90	120	150
			A	B	C	D	E
	Rubbing	1	13.53	13.2	12.8	12.3	12.4
Feed mm/ rev	0.0005	2	13.745	13.36	12.98	12.6	12.51
	0.001	3	15.385	15	14.62	14.24	14.15
	0.0015	4	16.385	16	15.62	15.24	15.15
	0.002	5	17.66	17.275	16.895	16.515	16.425
	0.0025	6	18.225	17.84	17.46	17.08	16.99
	0.003	7	18.79	18.405	18.03	17.655	17.565
	0.0035	8	18.985	18.6	18.55	18.5	18.41
	0.004	9	19.385	19	18.82	18.64	18.55
	0.0045	10	19.885	19.5	19.12	18.74	18.65
	0.005	11	20.83	20.445	20.065	19.685	19.595
	0.006	12	21.42	21.035	20.655	20.275	20.185
	0.007	13	22.045	21.66	21.28	20.9	20.81
	0.008	14	22.67	22.285	21.905	21.525	21.435
	0.009	15	23.3525	22.9675	22.5875	22.2075	22.1175
	0.01	16	24.035	23.65	23.575	23.5	23.41

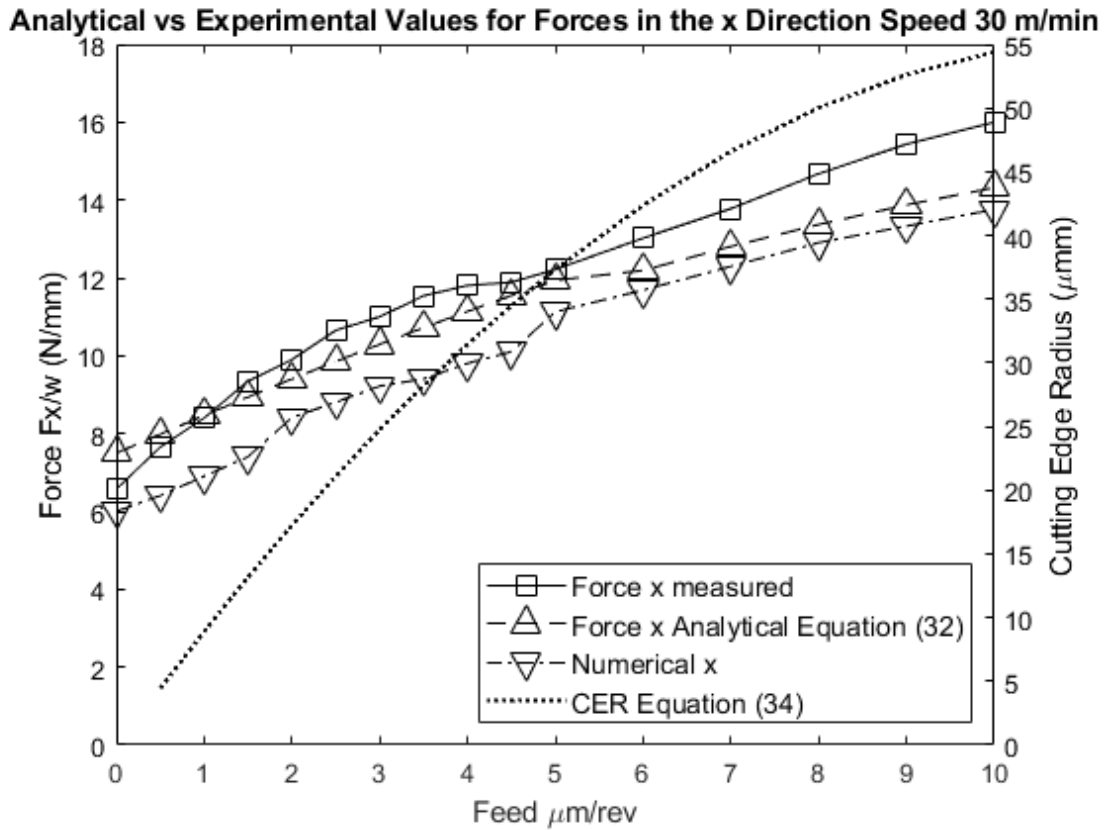


Figure 89: Numerical vs. Analytical vs. Experimental values for different feeds at Speed of 30 m/min for Forces in the x direction

At a speed of 30 m/min, the percentage difference between the simulations and the analytical model is 10.501%. While the simulation predicted the experimental values with an accuracy of 14.5 %.

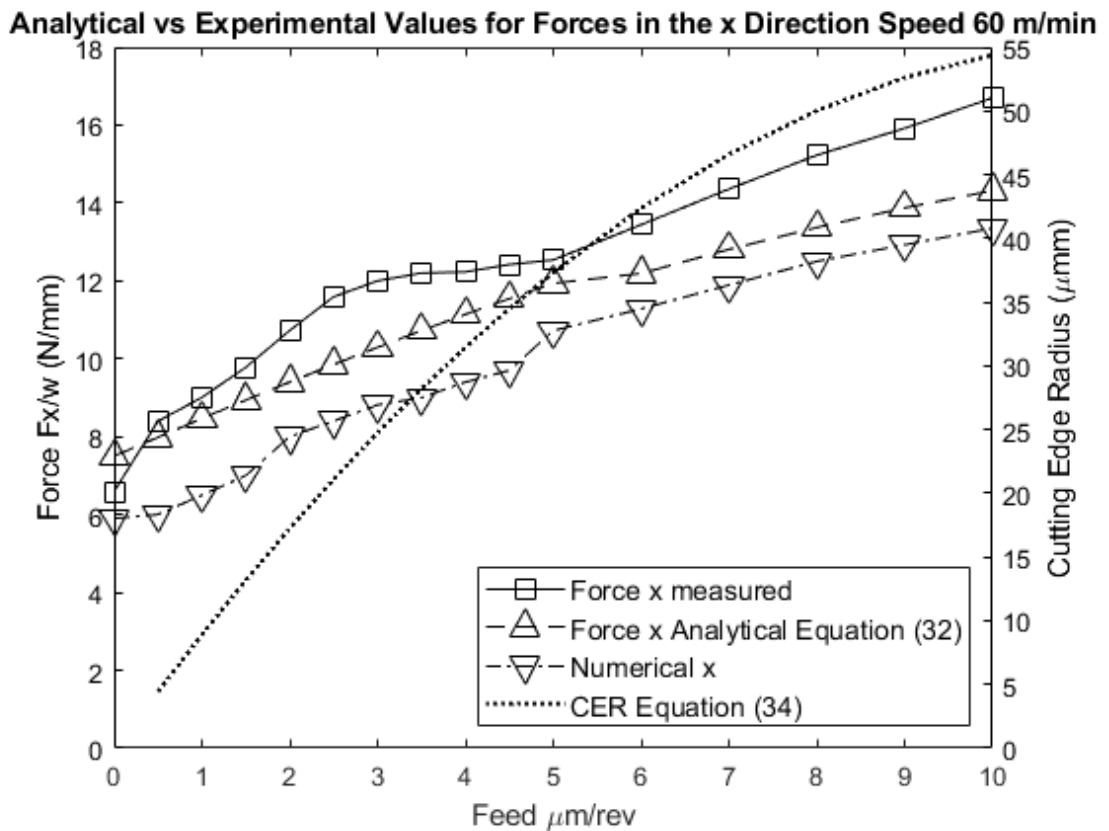


Figure 90: Numerical vs. Analytical vs. Experimental values for different feeds at Speed of 60 m/min for Forces in the x direction

At a speed of 60 m/min, the percentage difference between the simulations and the analytical model is 14.11%. While the simulation predicted the experimental values with an accuracy of 21.908 %.

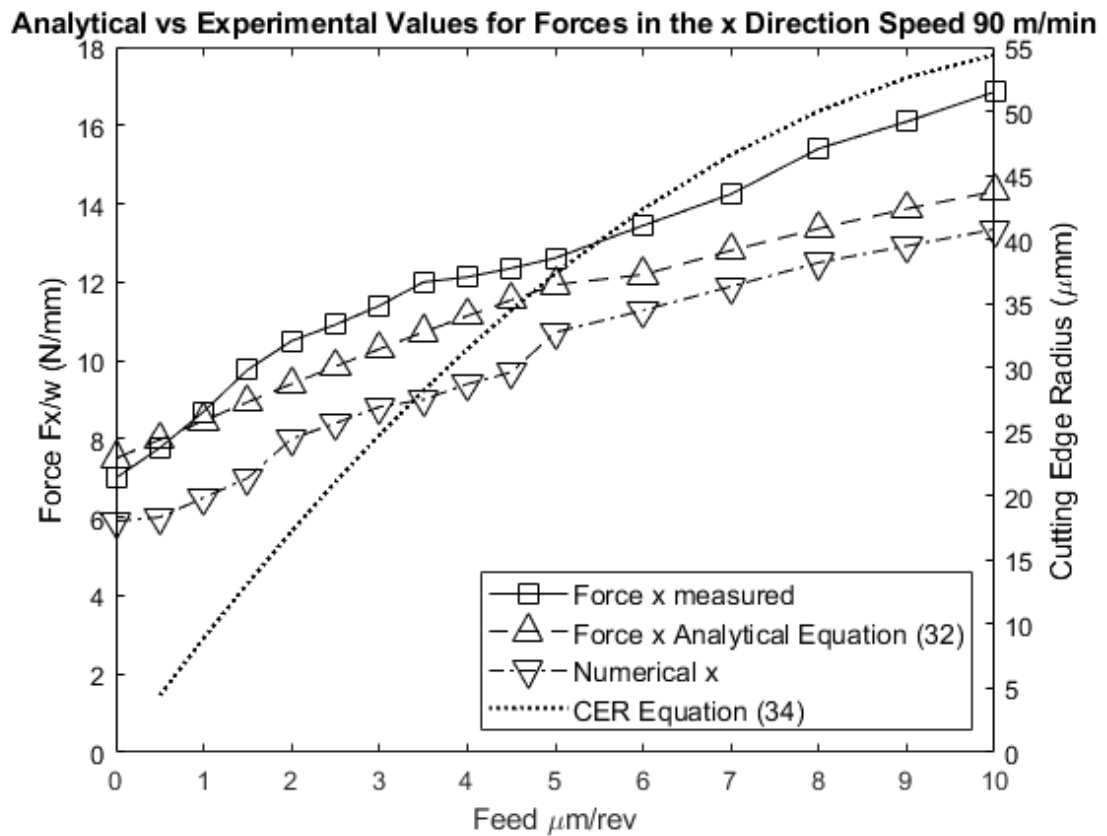


Figure 91: Numerical vs. Analytical vs. Experimental values for different feeds at Speed of 90 m/min for Forces in the x direction.

At a speed of 90 m/min, the percentage difference between the simulations and the analytical model is 16.37%. While the simulation predicted the experimental values with an accuracy of 23.08 %.

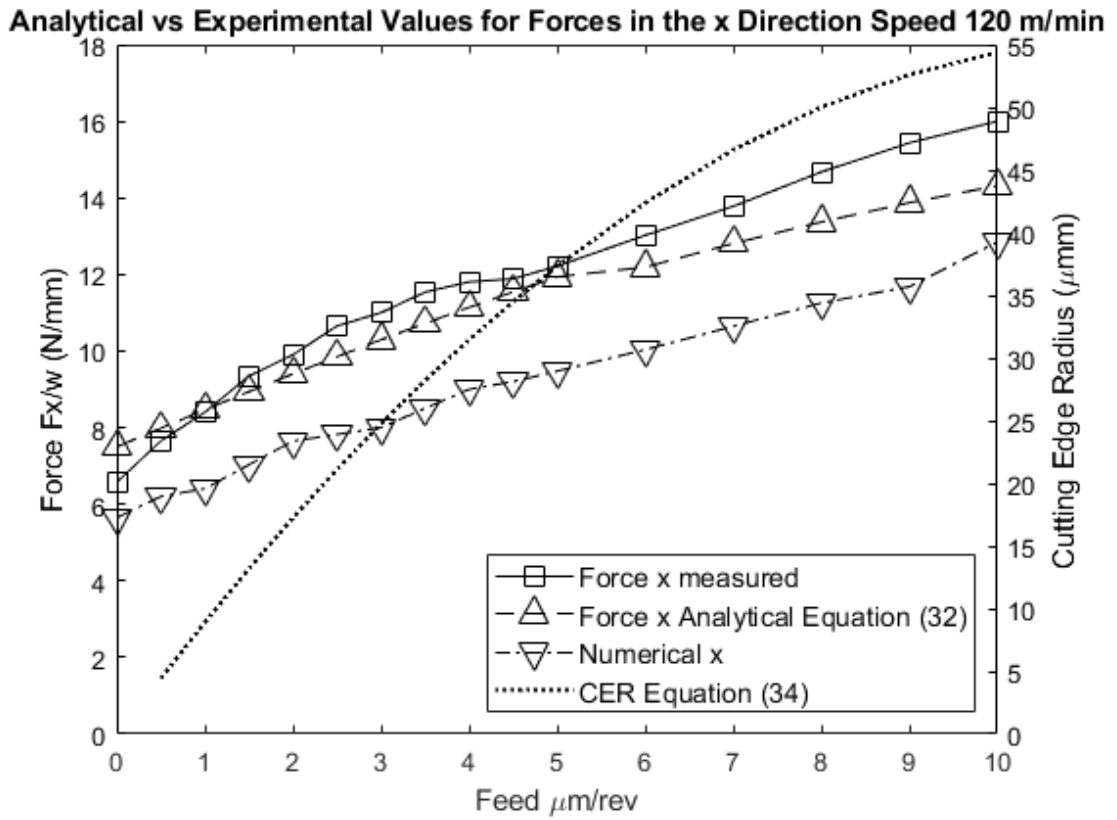


Figure 92: Numerical vs. Analytical vs. Experimental values for different feeds at Speed of 120 m/min for Forces in the x direction

At a speed of 120 m/min, the percentage difference between the simulations and the analytical model is 19.35 %. While the simulation predicted the experimental values with an accuracy of 21.52 %.

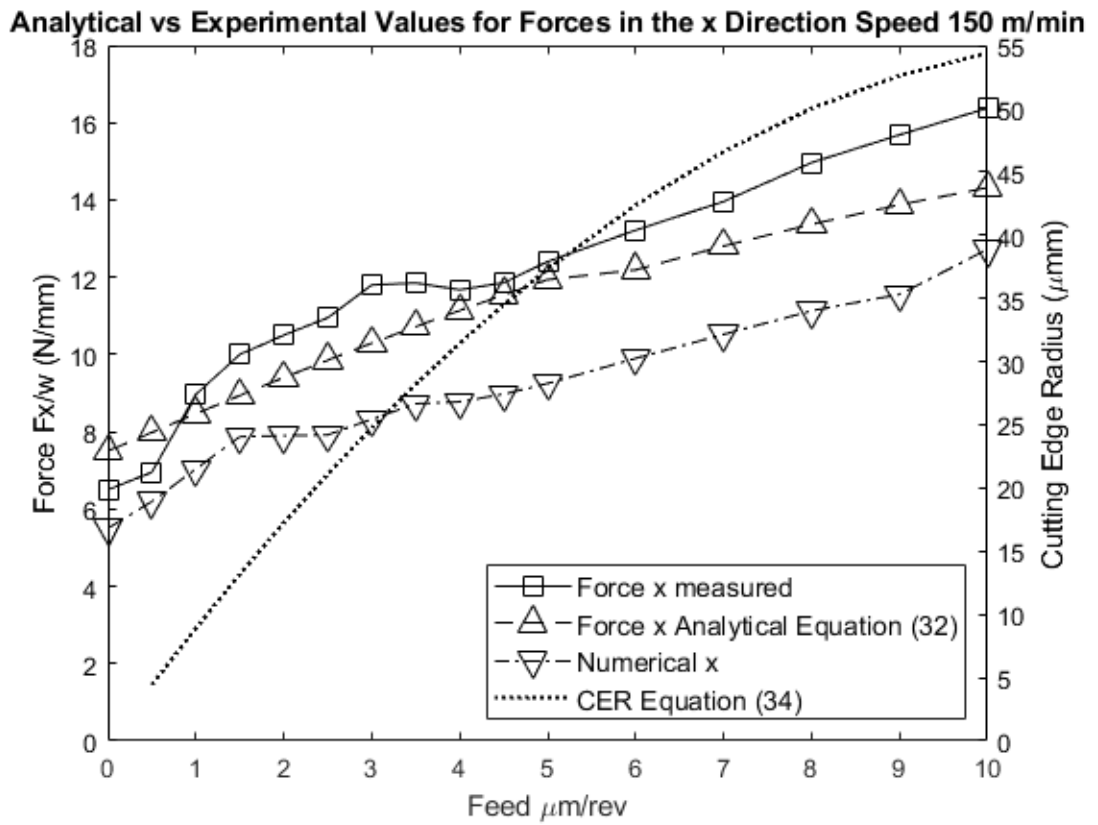


Figure 93: Numerical vs. Analytical vs. Experimental values for different feeds at Speed of 150 m/min for Forces in the x direction

At a speed of 150 m/min, the percentage difference between the simulations and the analytical model is 18.54%. While the simulation predicted the experimental values with an accuracy of 23.49 %.

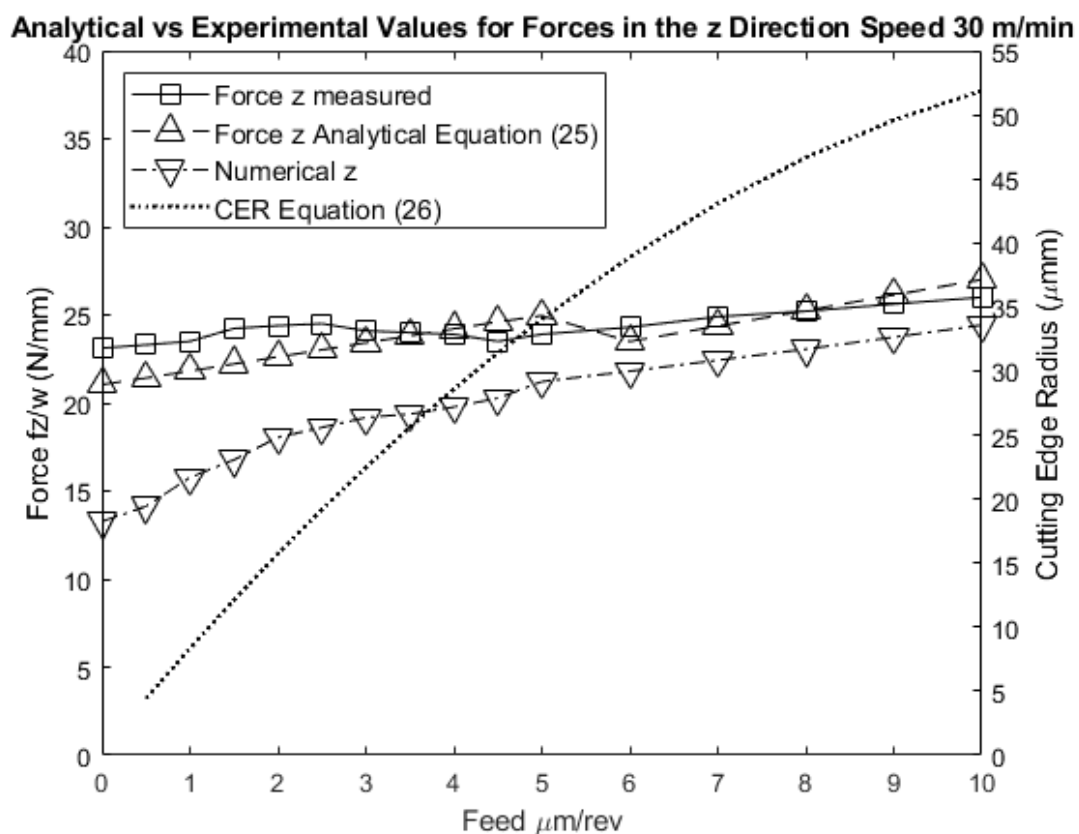


Figure 94: Numerical vs. Analytical vs. Experimental values for different feeds at Speed of 30 m/min for Forces in the z direction

At a speed of 30 m/min, the percentage difference between the simulations and the analytical model is 18 %. The percentage difference increased when predicting the z forces than when predicting the x forces.

Analytical vs Experimental Values for Forces in the z Direction Speed 60 m/min

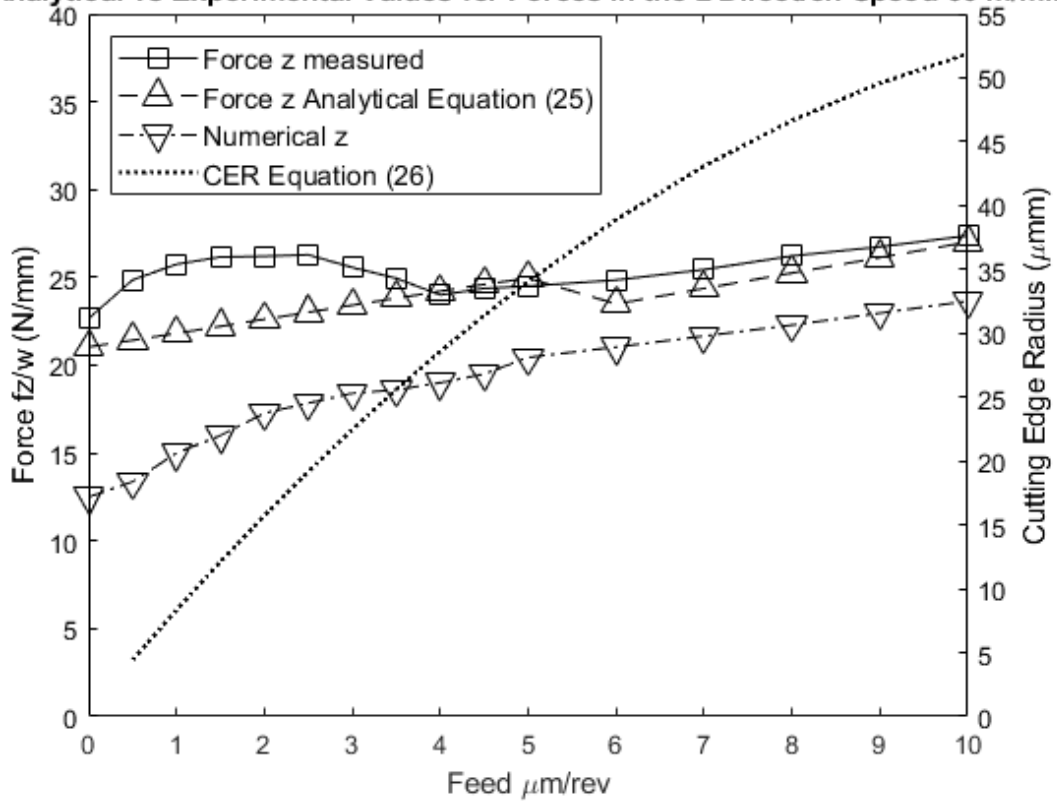


Figure 95: Numerical vs. Analytical vs. Experimental values for different feeds at Speed of 60 m/min for Forces in the z direction

At a speed of 60 m/min, the percentage difference between the simulations and the analytical model is 20.84 %.

Analytical vs Experimental Values for Forces in the z Direction Speed 90 m/min

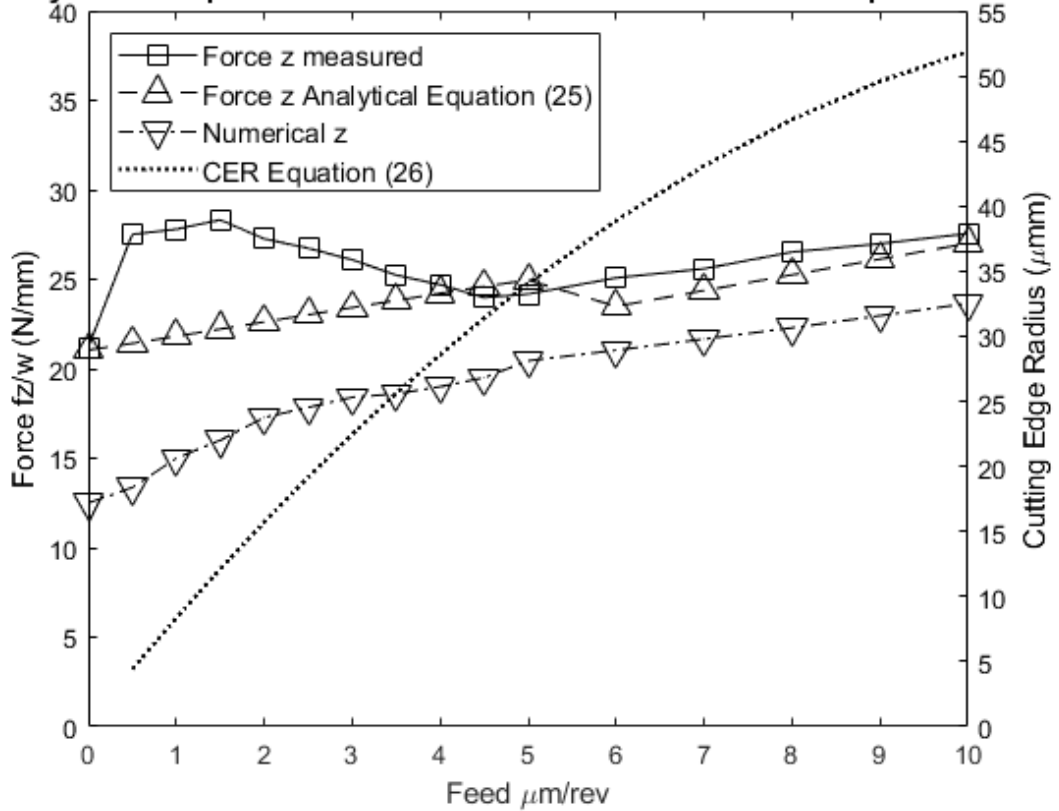


Figure 96: Numerical vs. Analytical vs. Experimental values for different feeds at Speed of 90 m/min for Forces in the z direction

At a speed of 90 m/min, the percentage difference between the simulations and the analytical model is 21 %.

Analytical vs Experimental Values for Forces in the z Direction Speed 120 m/min

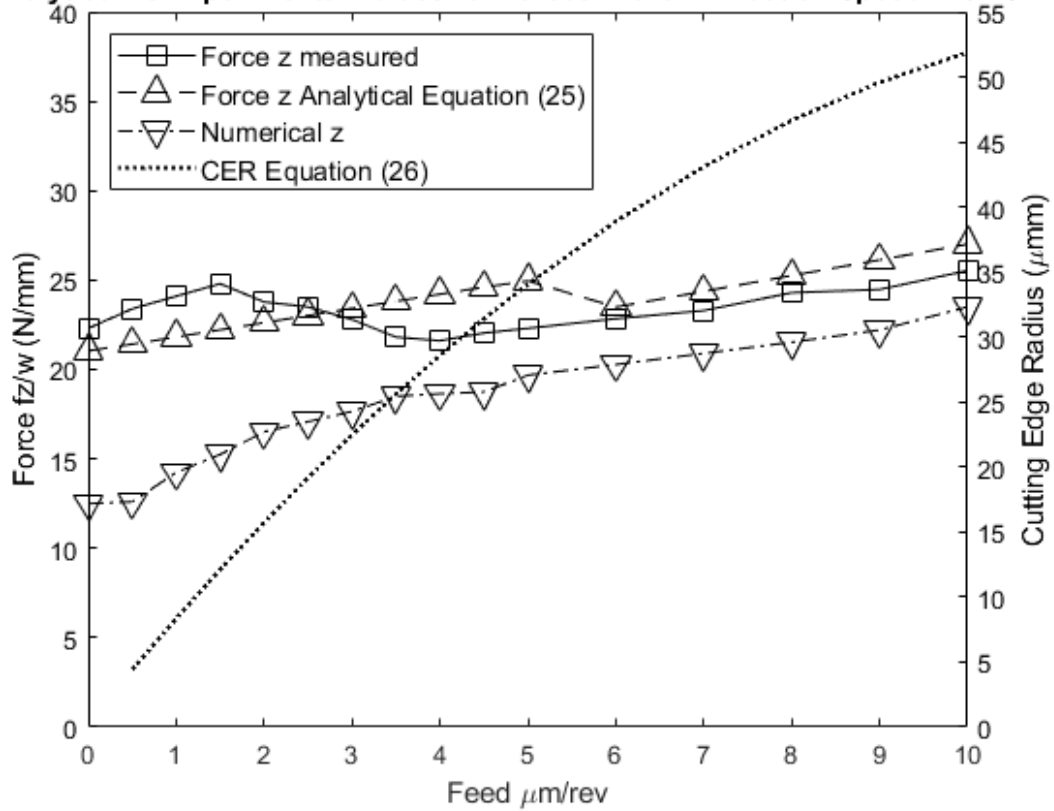


Figure 97: Numerical vs. Analytical vs. Experimental values for different feeds at Speed of 120 m/min for Forces in the z direction

At a speed of 120 m/min, the percentage difference between the simulations and the analytical model is 24.14 %.

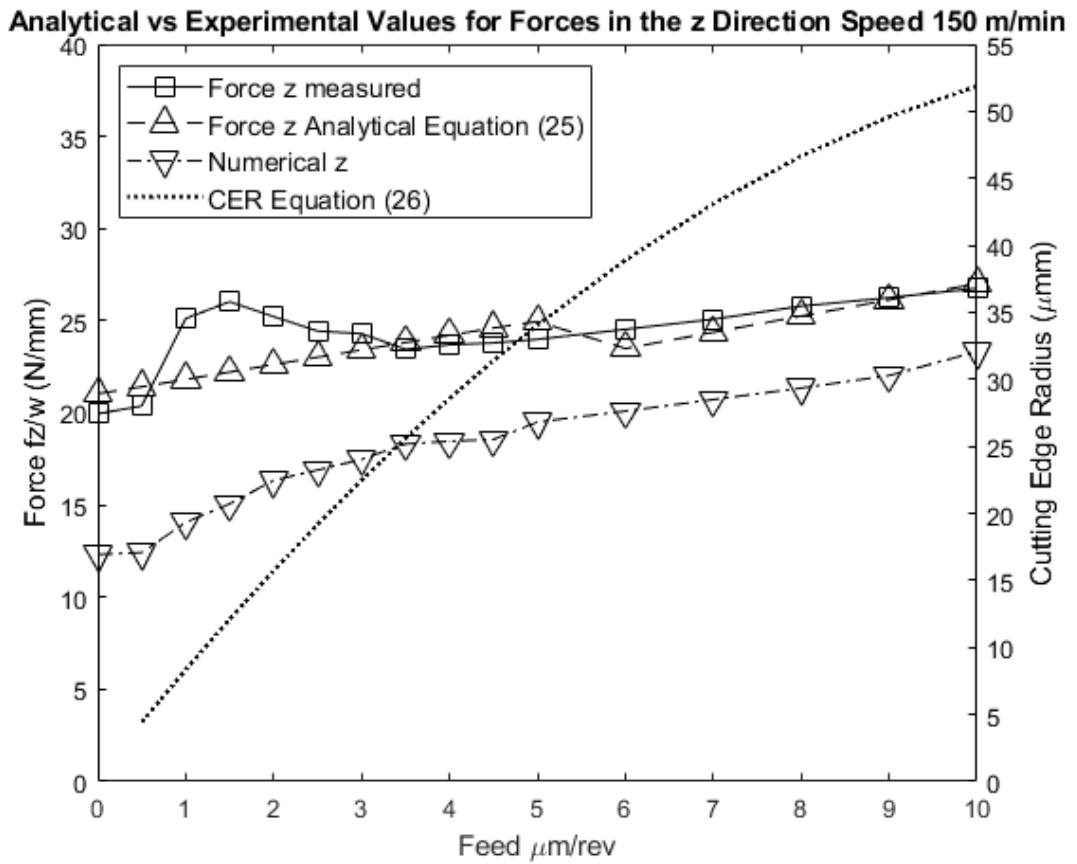


Figure 98: Numerical vs. Analytical vs. Experimental values for different feeds at Speed of 150 m/min for Forces in the z direction

At a speed of 150 m/min, the percentage difference between the simulations and the analytical model is 25.14 %.

3. Temperature

Temperature values were taken from deform for all speeds and feeds, and then were compared with the values obtained from the thermal camera.

The values from the simulation are much higher than those of the thermal camera. The reason behind that is that the thermal camera measures the temperature at the surface, while from deform the temperature is obtained at the tool-chip interface. When getting the temperature at the surface from deform, the values coincide with those of the thermal camera.

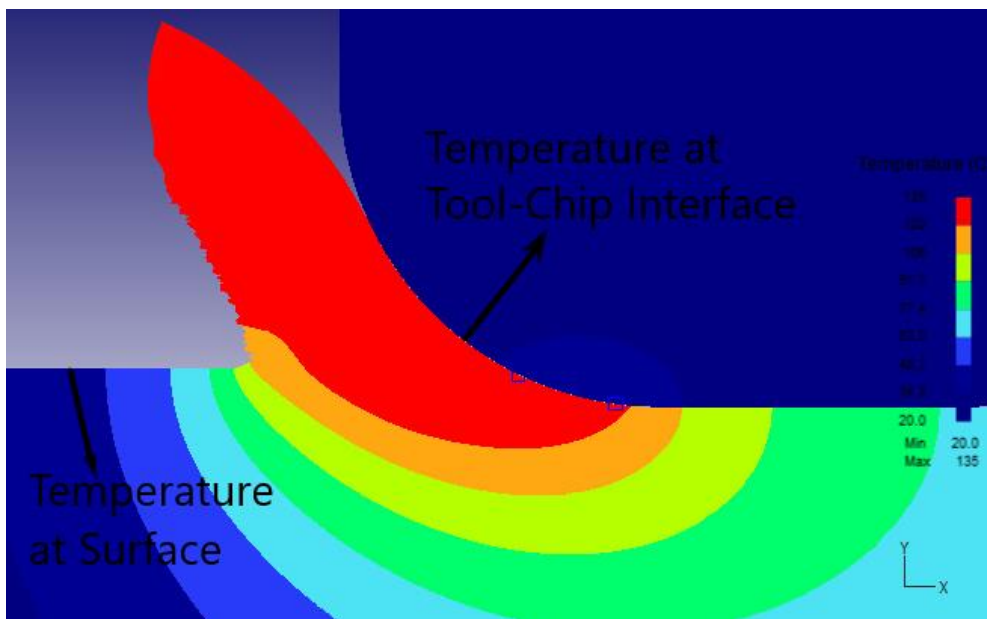


Figure 99: Temperature distribution from deform

Temperature values are plotted vs. feed for different cutting speeds in Figure 100. From Figure 100, the temperature is noticed to be increasing with increasing cutting speed, and also increasing with increasing feed. As the feed increases, the contact area between the tool and the workpiece increases, thus more forces are introduced into the process and thus the temperature will increase.

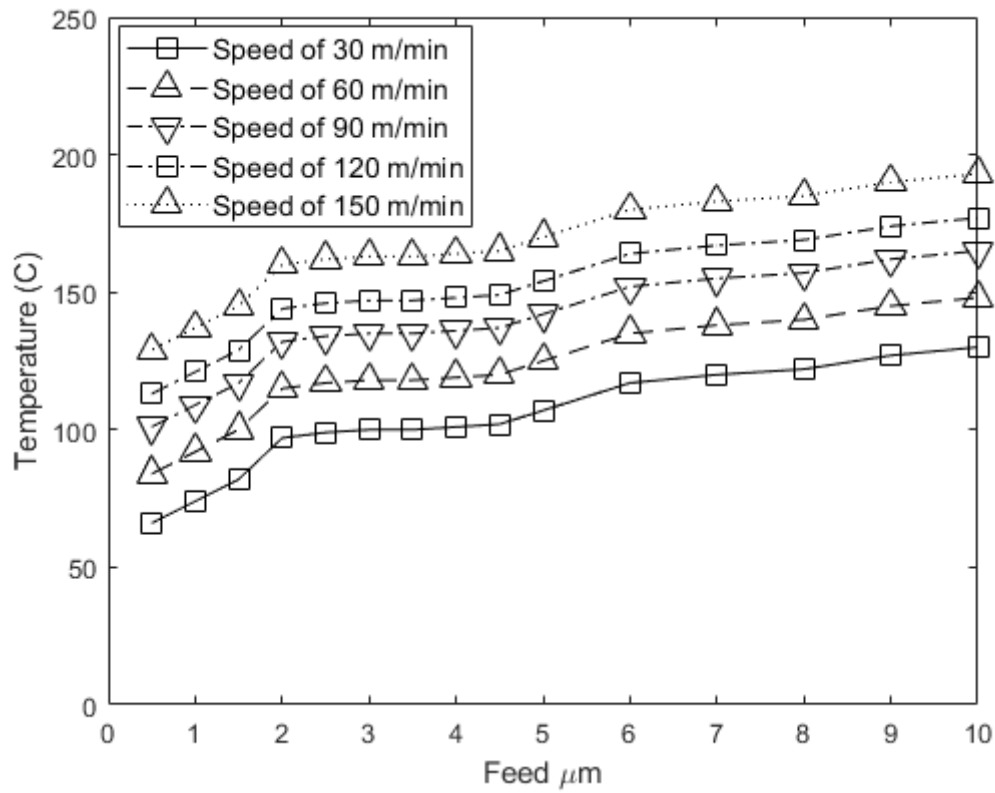


Figure 100: Temperature vs. Feed for different cutting speeds.

The values are then inserted into Matlab to generate the temperature dependent friction coefficient function shown in Equation (11). Equation (11) proposed by [25] relates the friction coefficient to the temperature of the tool-chip interface as follows:

$$a=7.4954 \times 10^{-5}$$

$$b=1865.1$$

$$c=329.5205$$

Therefore,

$$\mu = 1 - 7.4954 \times 10^{-5} e^{\frac{1865.1}{T+329.5205}} \quad (11)$$

The temperature dependent friction coefficient is then substituted in Equations (11) and (16) instead of a constant friction coefficient. The new analytical values are plotted vs. Experimental in Figure 101 (Figure 105).

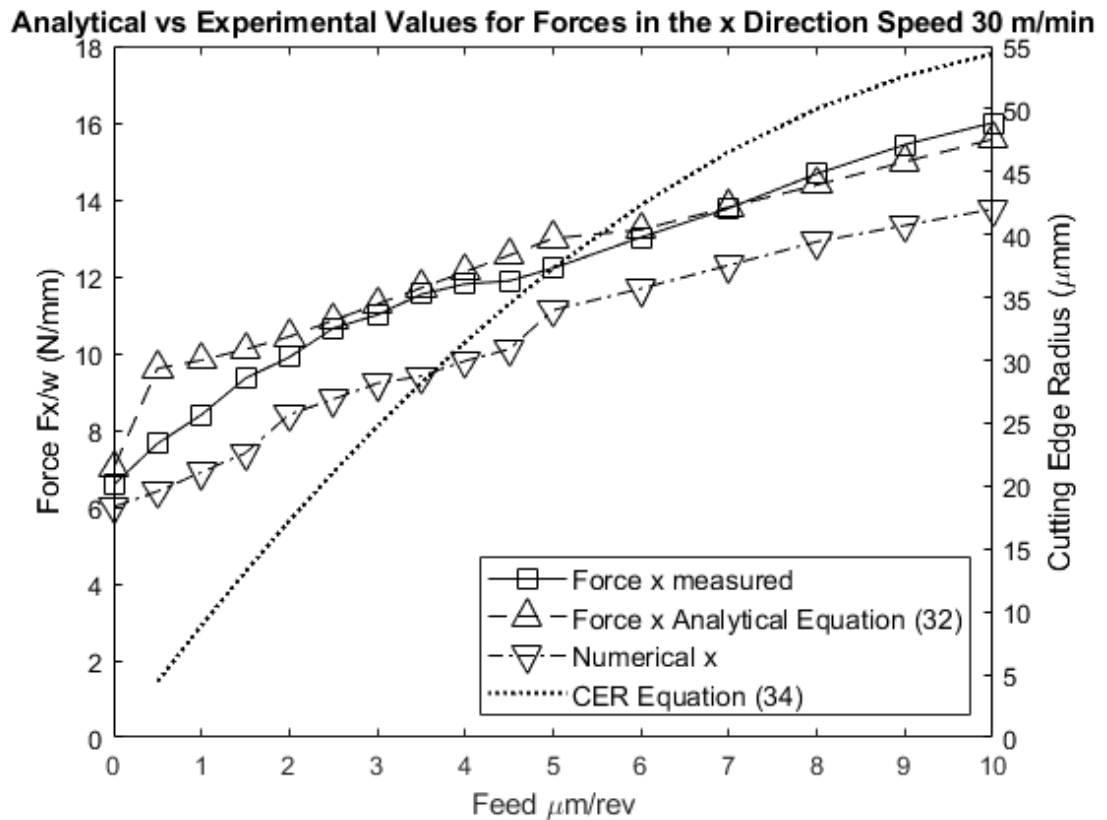


Figure 101: Analytical vs. Experimental for Speed of 30 m/min

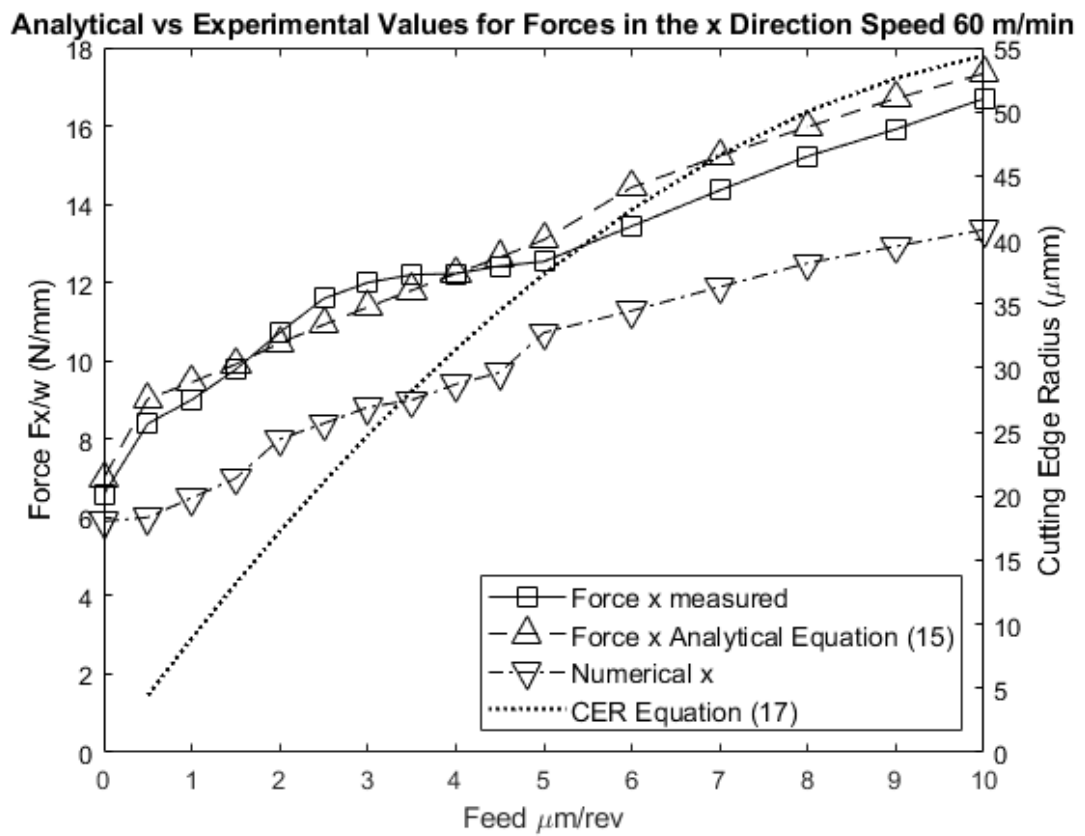


Figure 102: Analytical vs. Experimental for Speed of 60 m/min

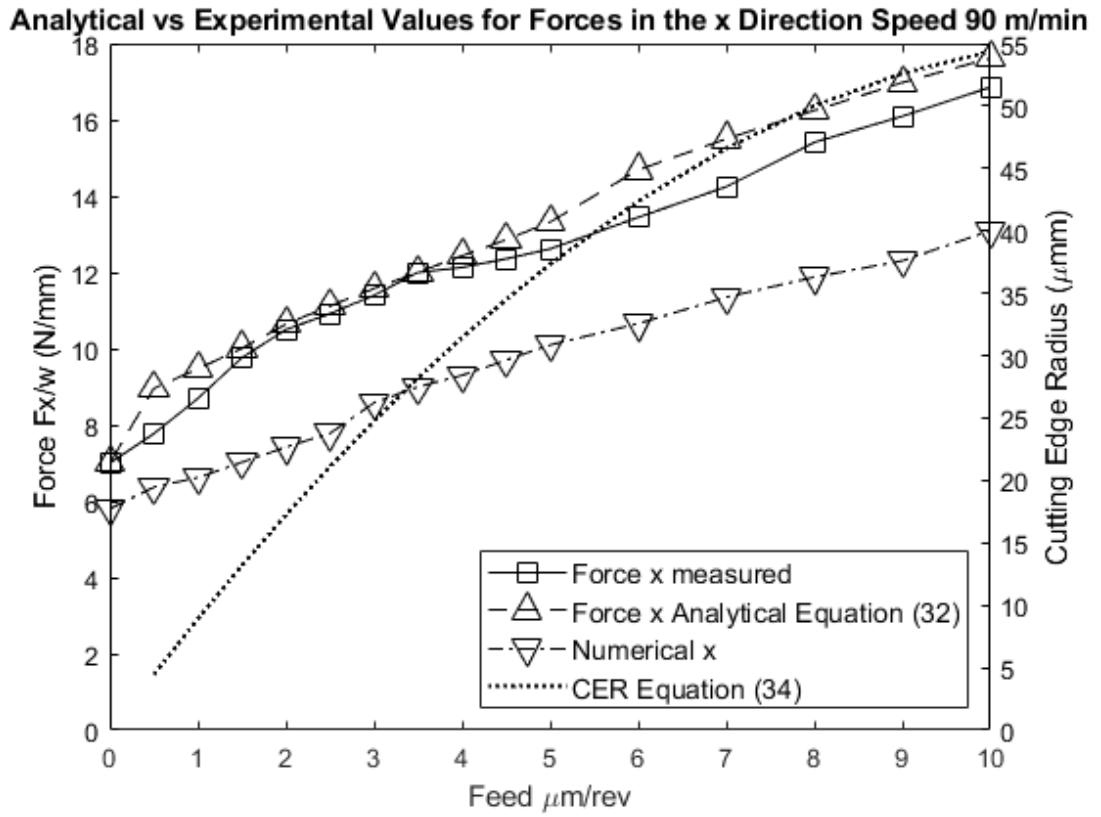


Figure 103: Analytical vs. Experimental for Speed of 90 m/min

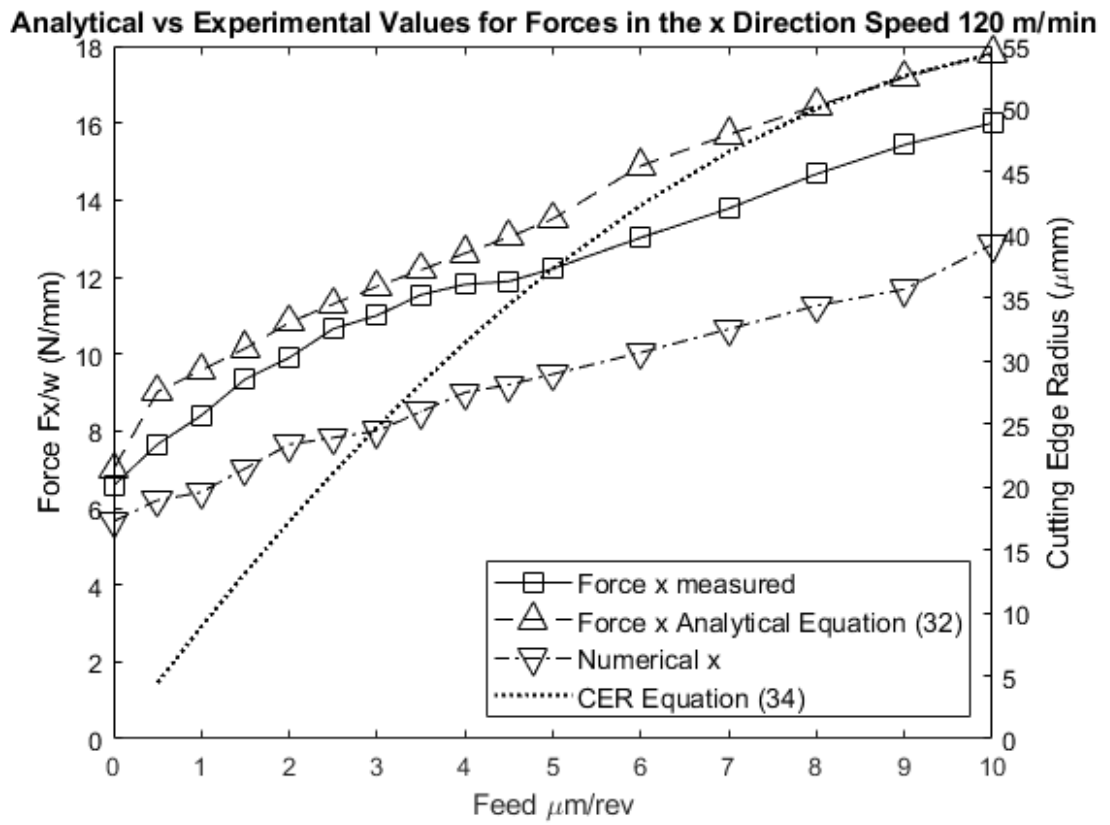


Figure 104: Analytical vs. Experimental for Speed of 120 m/min

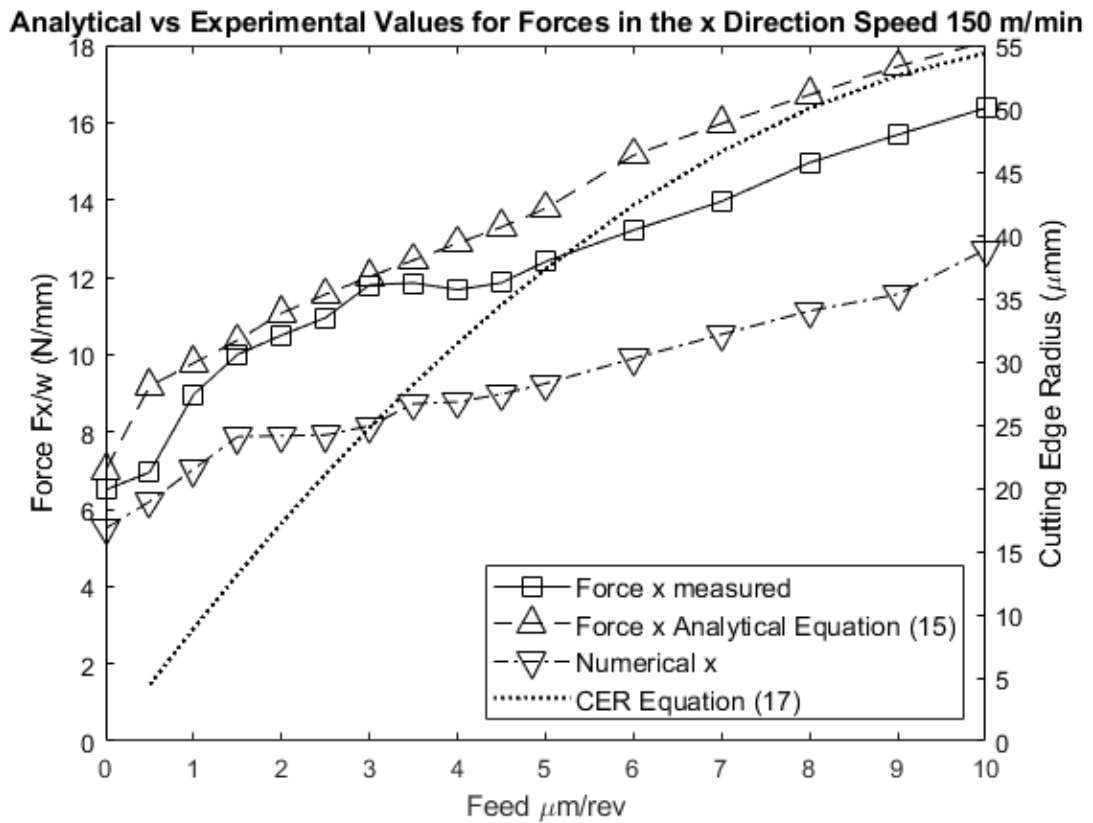


Figure 105: Analytical vs. Experimental for Speed of 150 m/min

From Figure 101(Figure 105), the analytical values are seen to be predicting the experimental values with much higher accuracy than when substituting a constant friction coefficient. The accuracy of the model calculated to be 99.97 % when comparing with Experimental values.

The temperature dependent friction coefficient from Equation (11) takes into consideration the effect of cutting speed and adds it to the analytical model; thus, for every cutting speed a unique solution is generated, whereas with a constant friction coefficient, a single solution was generated for different cutting speeds. So, the analytical model now predicts the forces of the process taking into consideration all the parameters affecting it from feed, to speed and temperature.

CHAPTER IV

DISCUSSION

Comparing the work done in this research to other work, research done by Hamade, R F. [27] presenting a novel actuator design for vibration-induced micromachining (BUEVA). The bi-directional ultrasonic elliptical vibration actuator (BUEVA) possesses a combination of features that renders it suitable for machining a wide range of materials over a variety of cutting parameters. Experimental work was done, and direct measurements of cutting and thrust forces were performed. The analytical model introduced by Arcona [28] was utilized to predict the cutting and thrust forces. Represented in Figure 106 are the experimental and the theoretical data obtained.

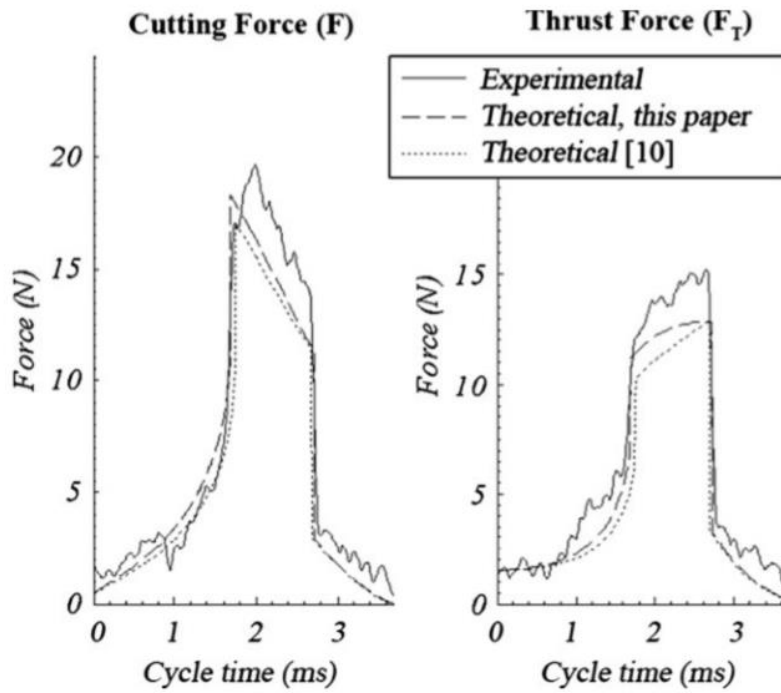


Figure 106: Experimental versus theoretical force components for Al2024 cutting tests [27]

Comparing the data obtained by [27] to the data from this research, the cutting forces are found to be very close and non-different. A value of 20 N was obtained by [27] compared to values ranging between 12 N and 24 N in this research. However, the thrust force is where the difference appears. Thrust forces were measured by [27] to be around 15 N, whereas, in this research the thrust forces were measured to be 40 N.

$$F_c = \frac{HA_c}{3} \left(\frac{\cot \varphi}{\sqrt{3}} + 1 \right) + \mu_f A_f \times \left(0.62H \sqrt{\frac{43H}{E}} \right)$$

$$F_t = \mu \left[\frac{HA_c}{3} \left(\frac{\cot \varphi}{\sqrt{3}} + 1 \right) \right] + A_f \times \left(0.62H \sqrt{\frac{43H}{E}} \right)$$

Another research by Hamade R.F. [29] was done to extract cutting force coefficients from drilling experiments. Figure 107 represents the plowing and the thrust

coefficients extracted from the drilling experiments. Comparing the coefficients obtained by [29] to the coefficients extracted by this research, the plowing coefficients agree.

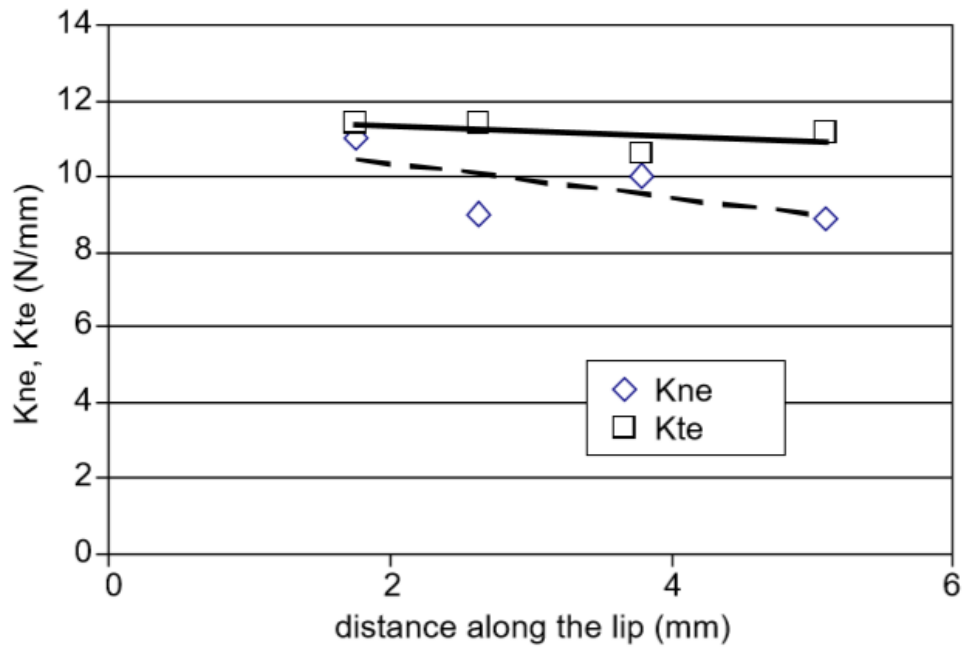


Figure 107: K_{ne} and K_{te} for the cutting edge only shown plotted along the length of the lip. Values correspond to cutting speed of 50 m/min [29]

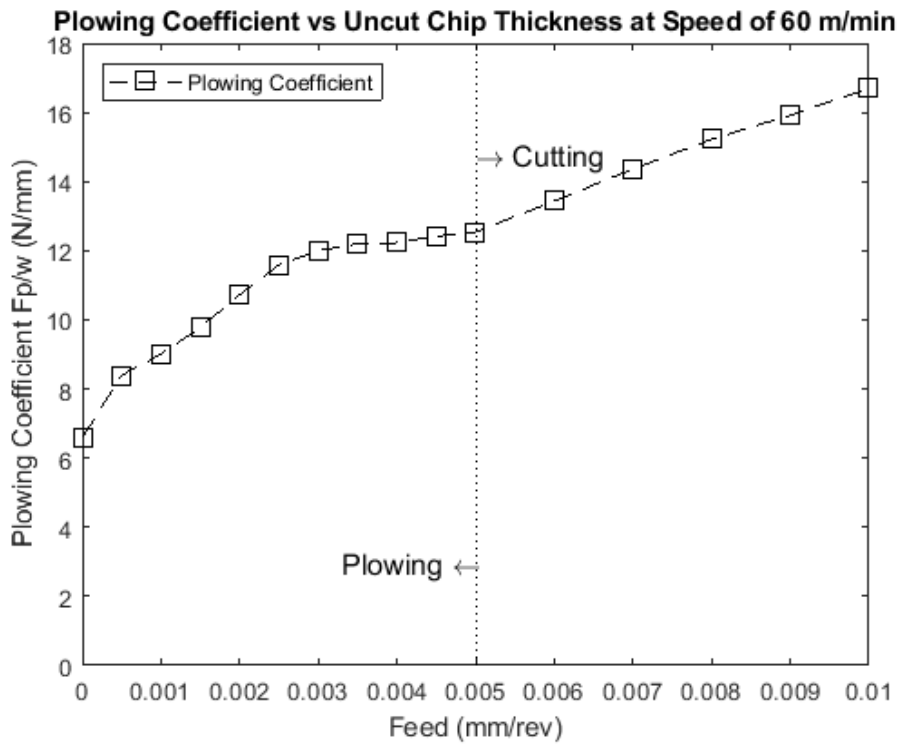


Figure 108: Plowing Coefficient at Cutting Speed of 60 m/min.

Examining Figure 107 and Figure 108, the plowing coefficients overlap ranging between 8 N/mm and 12 N/mm in both pieces of research. The trend differs, however. The plowing coefficients in the drilling experiments decrease as the distance along the lip increases. Whereas in orthogonal cutting, the plowing coefficient increases as the feed increases. The disagreement is also found when comparing the thrust coefficients. The thrust coefficients obtained in this research are twice the values extracted from the drilling experiments.

The work done by Roth and Ismail [17] on the 5-axis milling machine yielded a radial coefficient of 5.778 N/mm and a thrust coefficient of 13.863 N/mm.

Additionally, values obtained from [10] are represented in Figure 109. The plowing forces measured by [10] concur with the forces measured by our experiments for high cutting speeds and low cutting-edge radius.

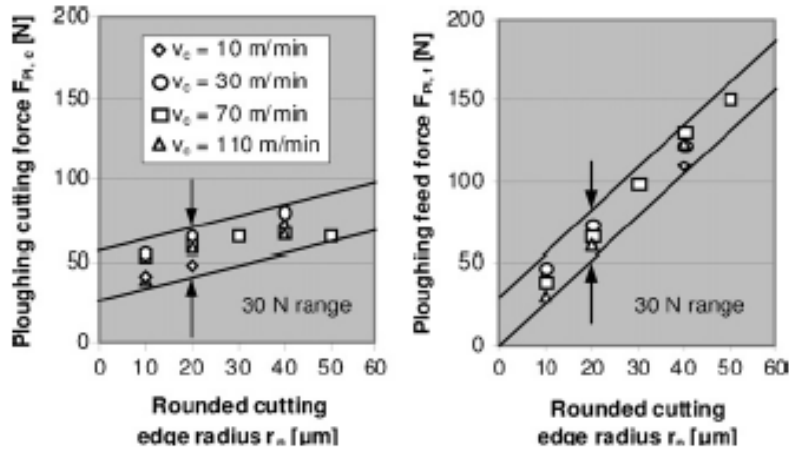


Figure 109: Influence of cutting edge radius on plowing force in turning Ti–6Al–4V at different cutting speeds, forces are standardized to a cutting width of $b = 1\text{mm}$ [10].

Comparing the results with some micro assisted machining values results from [38] are shown in Figure 110. At the interval of (0-0.005 mm), the values are seen to be varying between 2 and 1 N. The equations used by [38] are:

$$F_c = \frac{F_s}{\cos\theta} \cos(\gamma - \alpha)$$

$$F_t = \frac{F_s}{\cos\theta} \sin(\gamma - \alpha)$$

Where,

$$F_s \text{ is the shear force} = k_{AB} \times l_s \times w$$

And k_{AB} is the average material flow stress in the shear plane is given by the Johnson-Cook model

The equations used by [38] doesn't account for friction; for that reason, the values from [38] are compared to the corrected plowing coefficients obtained, the values agree. Friction forces were not regarded by [38] since in Vibration Assisted Machining friction forces are minimal. So, plowing forces are corrected by subtracting the friction forces in order to have a straight comparison with [38].

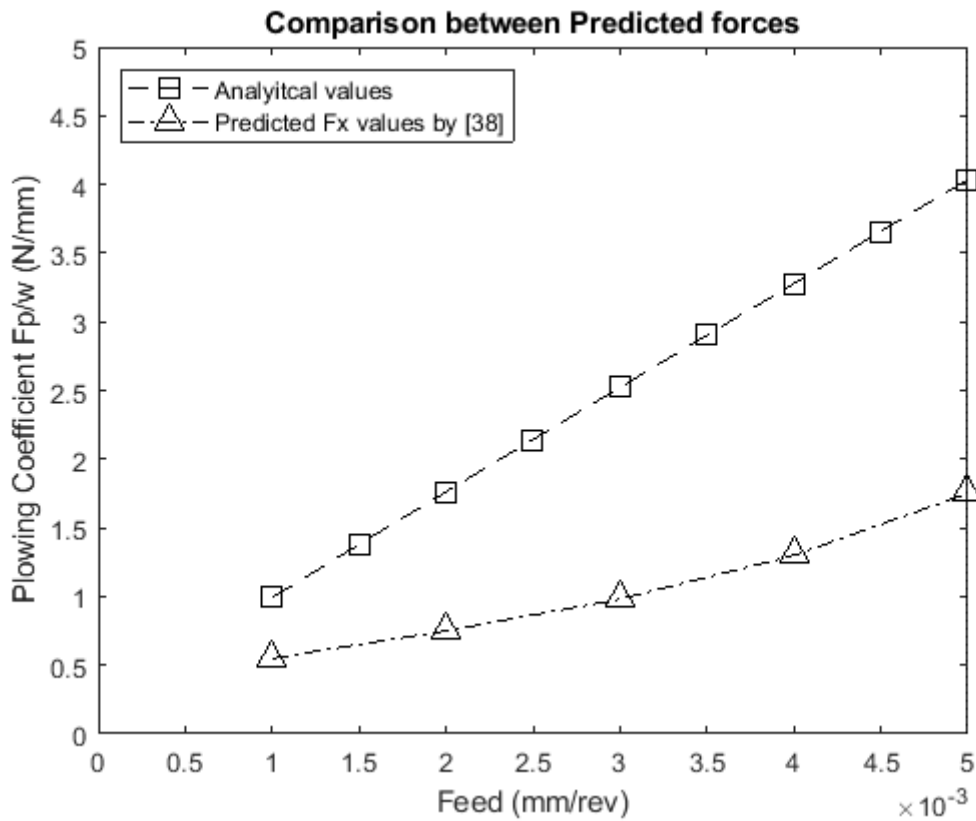


Figure 110: Comparison between the analytical model of this research and the predicted values of [38].

Chang et al. [39] compared conventional grinding and laser-assisted grinding. Laser cutting is concluded to be requiring less force than conventional grinding. A Laser is known to decrease material strength, which makes it easier for the material to

be removed, therefore requiring less force. The values obtained from [39] agree with values obtained by ours.

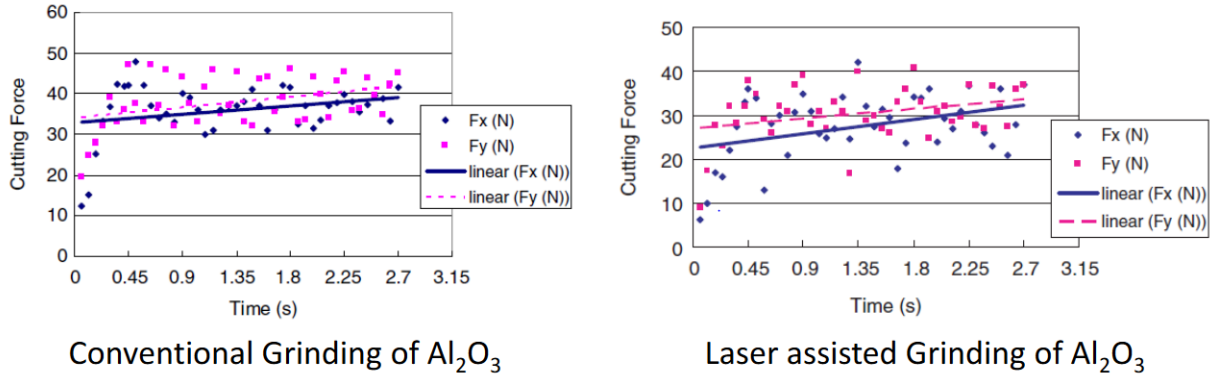


Figure 111: Conventional Grinding vs. Laser-assisted Grinding [39]

Lastly, the plowing coefficients extracted from this research follow a nonlinear bilinear fashion at low feeds (less than CER) agreeing with research done by Eggleston [16], Roth and Ismail [17], Hamade et al. [18] and Stephenson D.A. [19]. It is also to be stated that the extrapolation method would be proved to be not accurate since the method relies on the linear behavior of plowing forces, which was deemed to be nonlinear through this research.

CHAPTER V

CONCLUSION

At the end of this research, a model characterizing parasitic forces was created defining 2D orthogonal, taking into consideration all the parameters affecting the process from feeds, cutting speeds, rake angle, temperature, and cutting-edge radius. Such model successfully reduces uncertainties in machining, allowing for a better and clearer understanding of the machining process.

The plowing forces are found to be affected greatly by the feed, increasing with increasing feed. As for cutting speed, there hasn't been an interdependency with the plowing forces. However, the cutting speed was found to affect the friction forces acting on the tool. A relation of the friction coefficient was created, relating the coefficient with temperature and cutting speed.

BIBLIOGRAPHY

- [1] Piljek, P. (2014). MICROMACHINING- REVIEW OF LITERATURE FROM 1980 TO 2010. *Interdisciplinary Description of Complex Systems* 12(1).
- [2] Dornfeld, D., Min. S. and Takeuchi, Y. (2006). Recent Advances in Mechanical Micromachining. *CIRP Annals- Manufacturing Technology* 55(2), 745-768.
- [3] Cheng, K., Hou, D. (2013). *Micro-Cutting: Fundamentals and Applications 1st ed.* Chichester: John Wiley & Sons Inc.,.
- [4] Chae, J.; Park, S.S. and Freiheit. T. (2006). Investigation of Micro-Cutting Operations. *International Journal of Machine Tools & Manufacture* 46(3-4), 313-332.
- [5] Sun, X. a. (2010). Micro-/Nano-Machining through Mechanical Cutting. *Micro-Manufacturing Engineering and Technology.*, 24-38.
- [6] Woon, K. a. (2010). Extrusion-like Chip Formation Mechanism and its Role in Suppressing Void Nucleation. *CIRP Annals-Manufacturing Technology* 59(1), 129-132.
- [7] Ducobu, F., Riviere-Lophevre, E., & Filippi, E. Chip Formation in Micro-cutting. *In 9th National Congress on Theoretical and Applied Mechanics, Brussels, 2012*
- [8] Gietzelt, T., & Eichhorn, L. (2012). Mechanical Machining by Drilling, Milling and Slotting. *Micromachining Techniques for Fabrication of Micro and Nano Structures.*, 159-182.
- [9] Albricht, P (1960). New Developments in the Theory of the Metal Cutting Process. *ASME*, 348-357.
- [10] Wyen, C.-F. a. (2010). "Influence of cutting edge radius on cutting forces in machining titanium.". *CIRP Annals-Manufacturing Technology* 59.1, 93-96.
- [11] R. Stevenson. (1998). The Measurement of Parasitic Forces in Orthogonal Cutting. *Int. J. Mach. Tools Manufact. Vol. 38, Nos 1-2*, 113-130.
- [12] Guo, Y. B. (2004). The determination of ploughing force and its influence on material properties in metal cutting. 148.3. *Journal of materials processing technology* , 368-375.
- [13] Bailey, J. A. (1975). "Friction in metal machining—mechanical aspects.". *Wear* 31.2, 243-275.
- [14] Popov, A. a. (2015). Effect of uncut chip thickness on the ploughing force in orthogonal cutting. *The International Journal of Advanced Manufacturing Technology* 76.9-12, 1937-1945.
- [15] Lipatov, A. A. (2010). Determining the Cutting Forces at the Rear Tool Surface. *RUSSIAN ENGINEERING RESEARCH Vol. 30 No. 11*, 1158-1160.

- [16] Eggleston D.M., Herzog, R., & Thomsen E.G., (1959). Observations On The Angle Relationships In Metal Cutting, American Society of Mechanical Engineers Transactions. *Journal of Engineering for Industry* 81, 263-279.
- [17] Roth, D., Ismail, F., and Bedi, S., *Mechanistic modeling of 5-axis milling using an adaptive and local depth buffer*, *Computer-Aided Design* 39(4):302-312; 2007
- [18] R.F. Hamade, C.Y. Seif, and F. Ismail, Using drilling experiments to extract specific cutting force coefficients, *International Journal of Machine Tools and Manufacture* 46(3):387-396, 2006
- [19] D.A. Stephenson and P. Bandyopahyay, Process-Independent Force Characterization for Metal-Cutting Simulation, *Transactions of the ASME, Journal of Engineering Materials and Technology*, 119 (1997) 86-94
- [20] Rech, J. (2005). Influence of cutting edge radius on the wear resistance. *Wear* 259, 1168–1176.
- [21] Iwata, K. (1984). Process Modeling of Orthogonal Cutting by the Rigid-Plastic Finite Element Method. *ASME Journal Vol 106*, 132-138.
- [22] Tansel, I. (2000). Tool wear estimation in micro-machining. Part I: tool usage–cutting force
- [23] Waldorf, D. J. (2006). A simplified model for ploughing forces in turning. *Journal of manufacturing processes* 8.2, 76-82.
- [24] Waldorf, D. J. (1999). An Evaluation of Ploughing Models for Orthogonal Machining. *Journal of Manufacturing Science and Engineering Vol 121*, 550-558.
- [25] Grueebler, R. (2009). Temperature dependent friction modeling for sheet metal forming. *International Journal of Material Forming*.
- [26] Hamade, R. (2010). Compact core drilling in basalt rock using PCD inserts: Wear characteristics and cutting forces. *Journal of Materials Processing Technology*, 1326-1339.
- [27] Hamade, R. F. (2012). BUEVA: a bi-directional ultrasonic elliptical vibration actuator for micromachining. *Int J Adv Manuf Technol* , 991-1001.
- [28] Arcona, C. (1996). *Tool Force, Chip Formation and Surface Finish in Diamond Turning. Dissertation*. Raleigh, NC: North Carolina State University, Mechanical and Aerospace Engineering Department.
- [29] Hamade, R. (2006). Extracting cutting forces coefficients from drilling experiments. *International Journal of Machine Tools & Manufacture*, 387-396.
- [30] Durul, U., & Tuğrul, Ö. (2012). METHODOLOGY TO DETERMINE FRICTION IN ORTHOGONAL CUTTING WITH APPLICATION TO MACHINING TITANIUM AND NICKEL BASED ALLOYS. *2012 ASME International Conference on Manufacturing Science and Engineering*, (pp. 4-8). West Lafayette, IN .

- [31] Smith, J. (1953). Stress Due to Tangential and Normal Loads on an Elastic Solid with Application to Some Contact Stress Problems. *ASME Journal of Applied Mechanics*, 157-166.
- [32] Dumas, G. and Baronet, C.N. (1971). Elastoelastic Indentation of a Half-space by an Infinitely Long Rigid Cylinder. *Int. J. Mech. Sci Vol.13*, 519-530.
- [33] Rubenstein, C. (1990). The edge force components in oblique cutting.30.1. *International Journal of Machine Tools and Manufacture* , 141-149.
- [34] G. Johnson, W. Cook, 1983, Proceedings 7th international symposium on ballistics, 541-547
- [35] M. Avedesian, H. Baker, 1999, Magnesium and Magnesium alloys, ASM specialty handbook, ASM Int.,Materials Park, OH.
- [36] Hasenpouth, Dan. Tensile high strain rate behavior of AZ31B magnesium alloy sheet. MS thesis. University of Waterloo, 2010.
- [37] Kurukuri, Srihari, et al. "Rate sensitivity and tension–compression asymmetry in AZ31B magnesium alloy sheet." *Philosophical Transactions of the Royal Society A: Mathematical, Physical and Engineering Sciences* 372.2015 (2014): 20130216
- [38] Feng, Y.; Hsu, F.; Lu, Y.; Lin, Y.; Lin, C.; Lin, C.; Lu, Y.; Liang, S.Y. Force Prediction in Ultrasonic Vibration-Assisted Milling. Preprints 2019, 2019060190 (doi: 10.20944/preprints201906.0190.v1).
- [39] Chang, Chih-Wei, and Chun-PaoKuo. "An investigation of laser-assisted machining of Al₂O₃ ceramics planing." *International Journal of Machine Tools and Manufacture* 47, no. 3-4 (2007): 452-461

APPENDIX

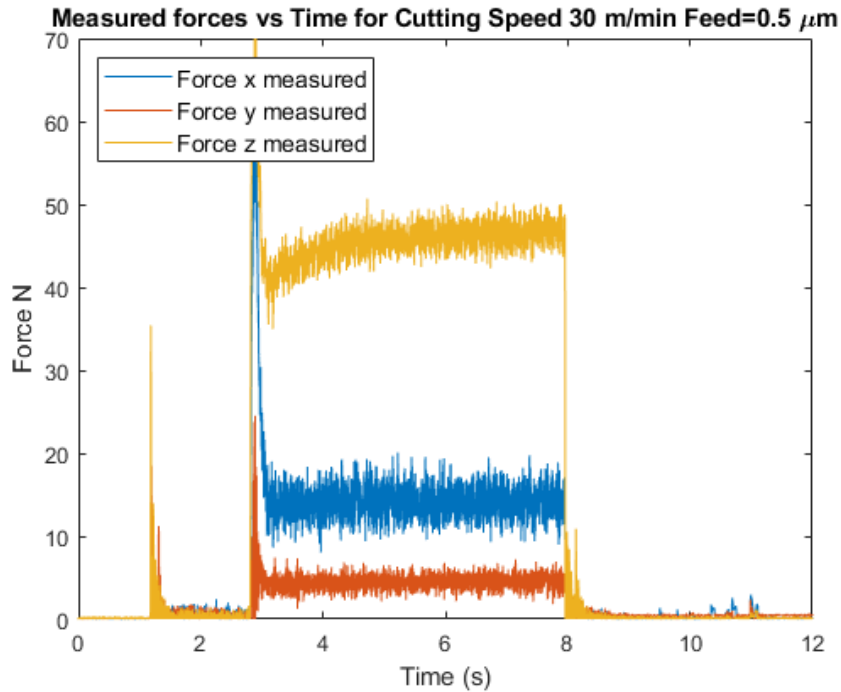


Figure 112: Typical cutting forces (RPM = 720, Cutting speed= 30 m/min, feed = 0.0005 mm/rev OR Feed rate of mm/min = N. $F = 720 * 0.0005 \text{ mm/rev} = 0.36 \text{ mm/min}$).

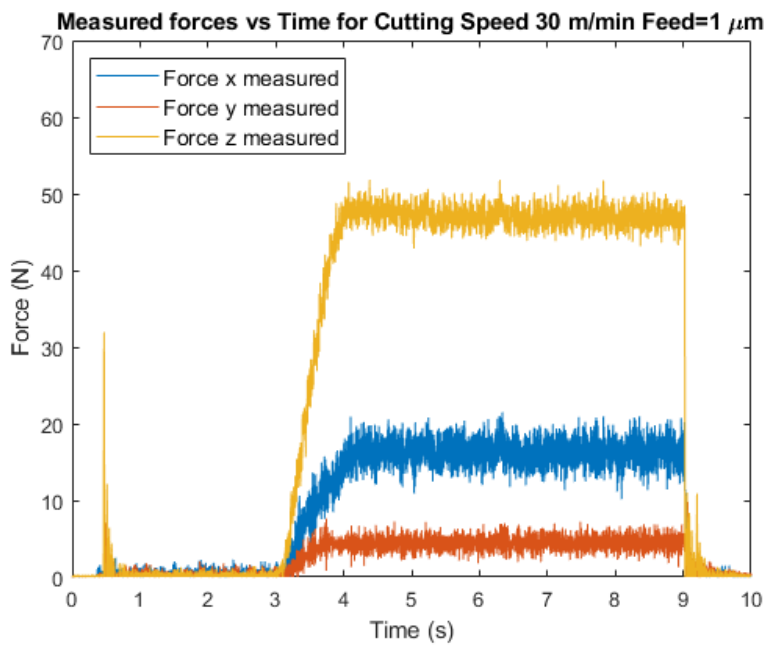


Figure 113: Typical cutting forces (RPM = 720, Cutting speed= 30 m/min, feed = 0.001mm/rev OR Feed rate of mm/min = N. $F = 720 * 0.001 \text{ mm/rev} = 0.72 \text{ mm/min}$).

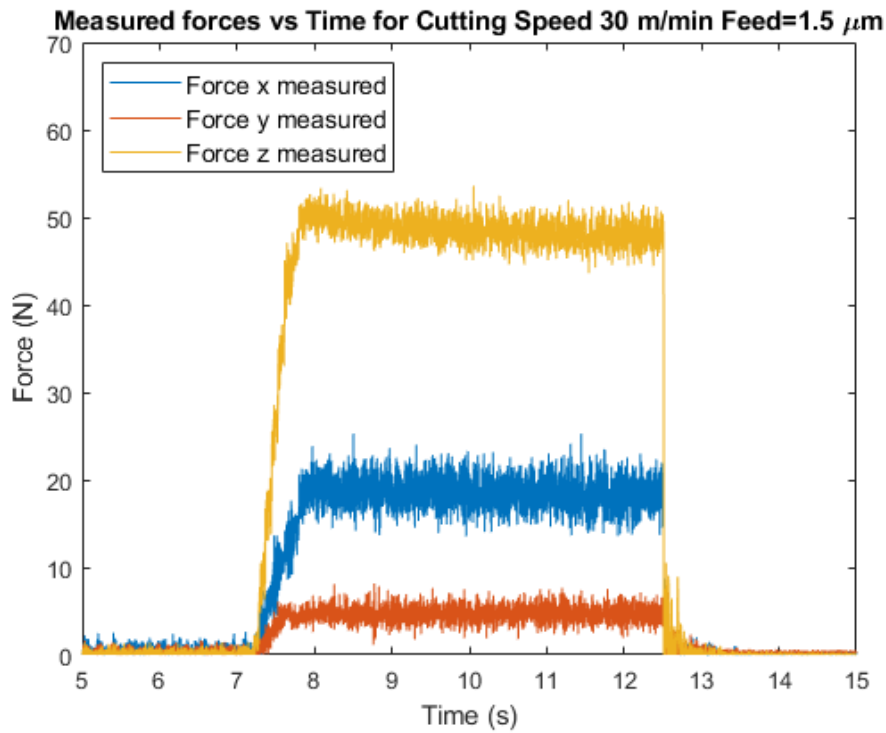


Figure 114: Typical cutting forces (RPM = 720, Cutting speed= 30 m/min, feed = 0.0015 mm/rev OR Feed rate of mm/min = $N.F = 720 * 0.0015 \text{ mm/rev} = 1.08 \text{ mm/min}$).

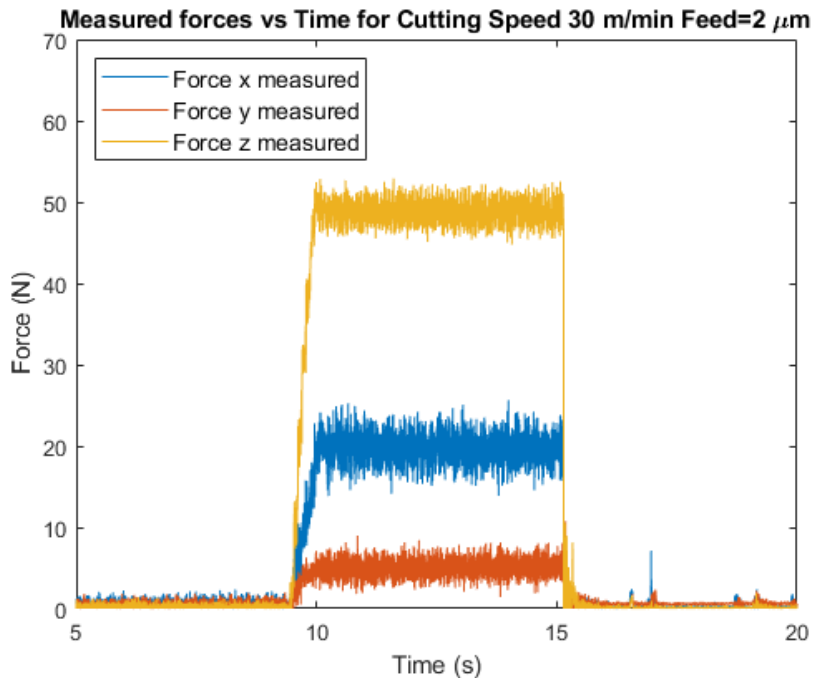


Figure 115: Typical cutting forces (RPM = 720, Cutting speed= 30 m/min, feed = 0.002 mm/rev OR Feed rate of mm/min = $N.F = 720 * 0.002 \text{ mm/rev} = 1.44 \text{ mm/min}$).

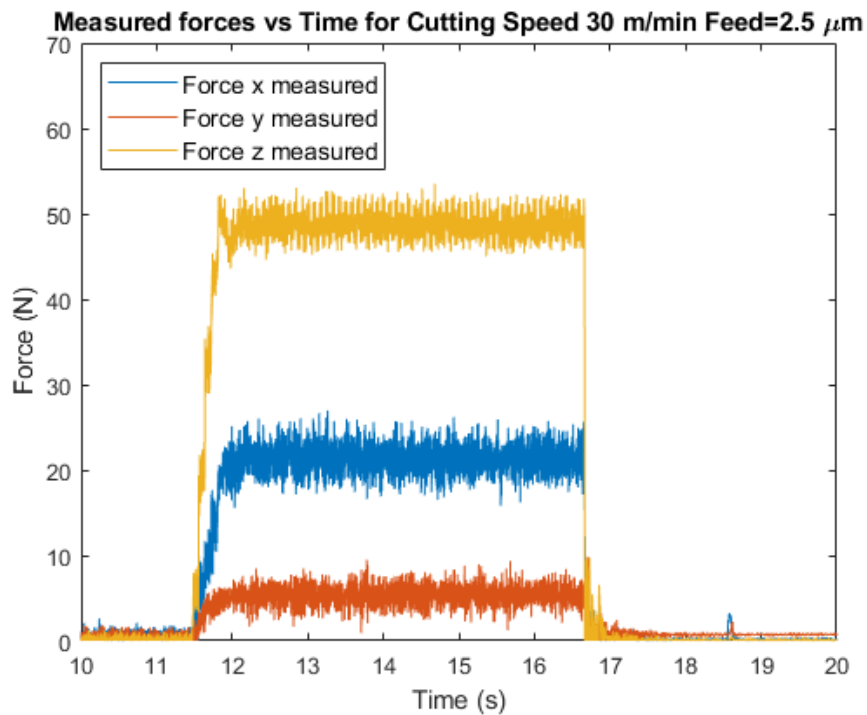


Figure 116: Typical cutting forces (RPM = 720, Cutting speed= 30 m/min, feed = 0.0025 mm/rev OR Feed rate of mm/min = N. $F = 720 * 0.0025 \text{ mm/rev} = 1.8 \text{ mm/min}$).

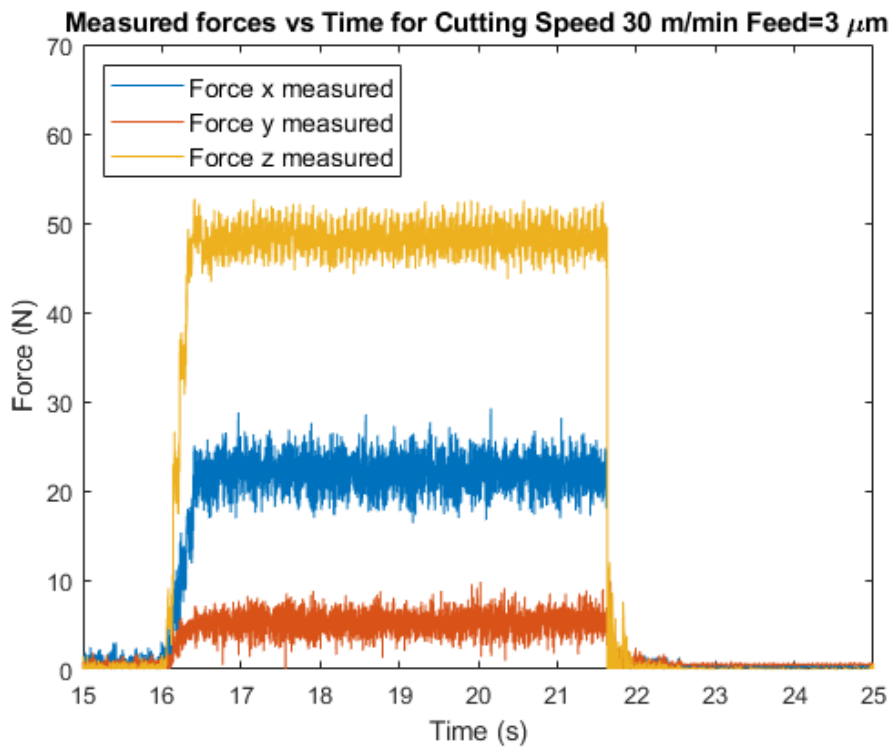


Figure 117: Typical cutting forces (RPM = 720, Cutting speed= 30 m/min, feed = 0.003 mm/rev OR Feed rate of mm/min = N. $F = 720 * 0.003 \text{ mm/rev} = 2.16 \text{ mm/min}$).

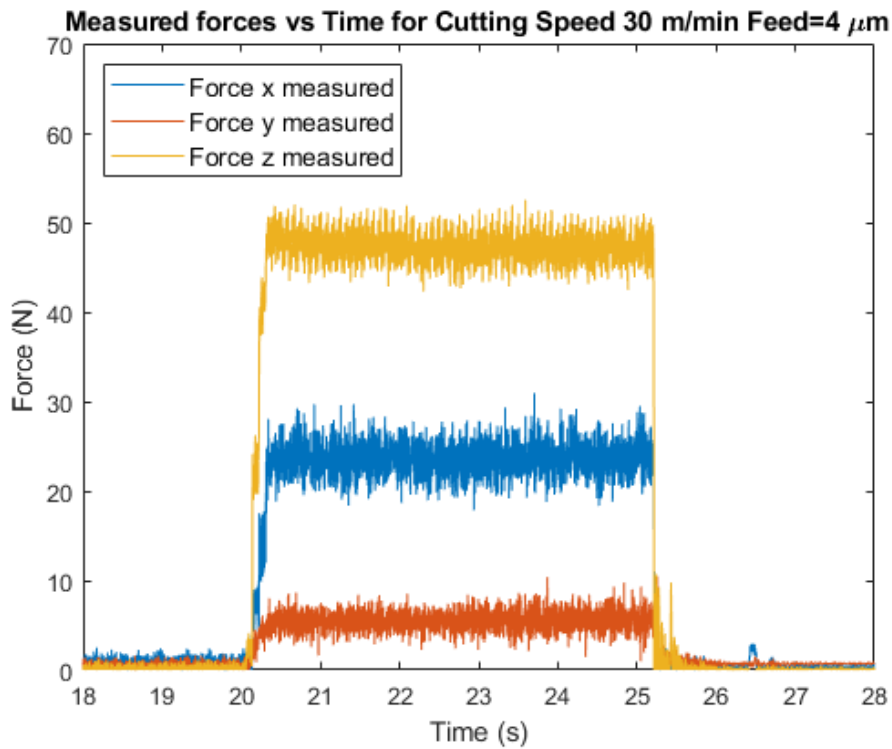


Figure 118: Typical cutting forces (RPM = 720, Cutting speed= 30 m/min, feed = 0.0035 mm/rev OR Feed rate of mm/min = N. $F = 720 * 0.0035 \text{ mm/rev} = 2.52 \text{ mm/min}$).

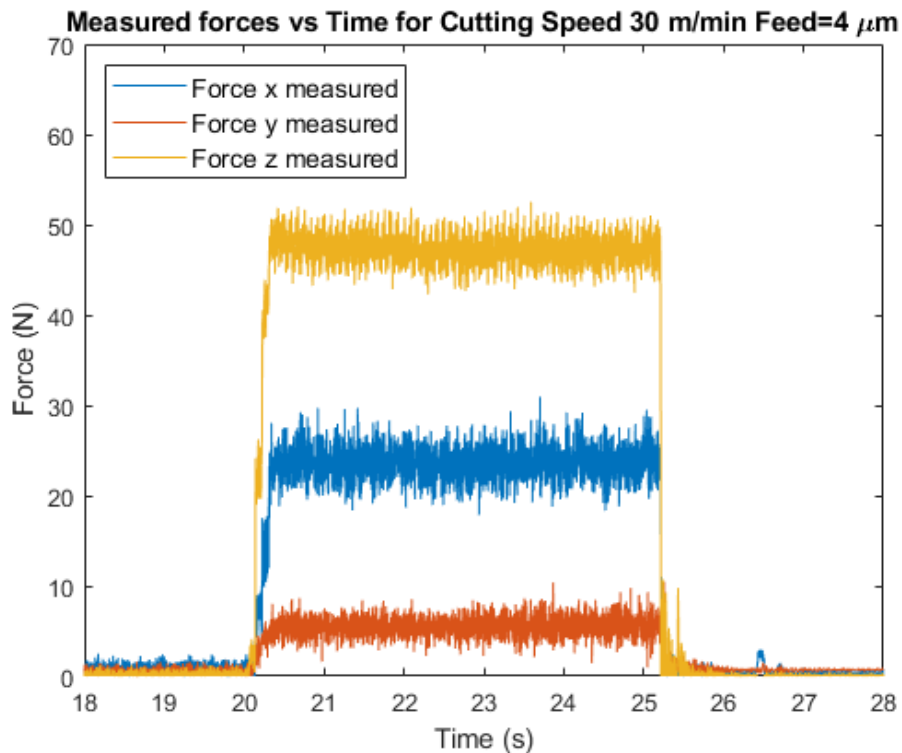


Figure 119: Typical cutting forces (RPM = 720, Cutting speed= 30 m/min, feed = 0.004 mm/rev OR Feed rate of mm/min = N. $F = 720 * 0.004 \text{ mm/rev} = 2.88 \text{ mm/min}$).

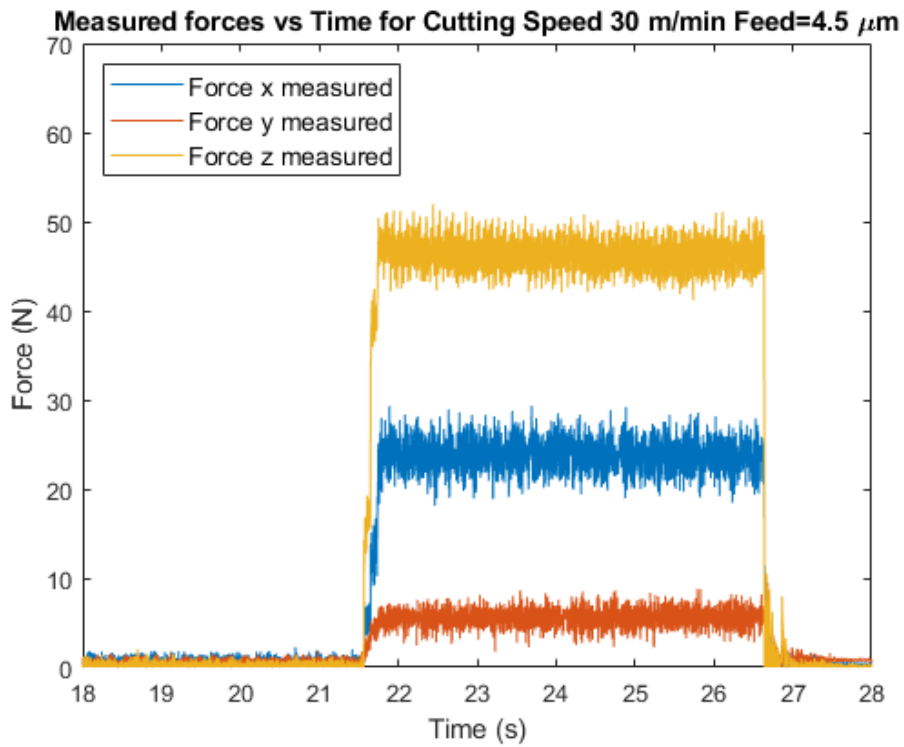


Figure 120: Typical cutting forces (RPM = 720, Cutting speed= 30 m/min, feed = 0.0045 mm/rev OR Feed rate of mm/min = N. $F = 720 * 0.0045 \text{ mm/rev} = 3.24 \text{ mm/min}$).

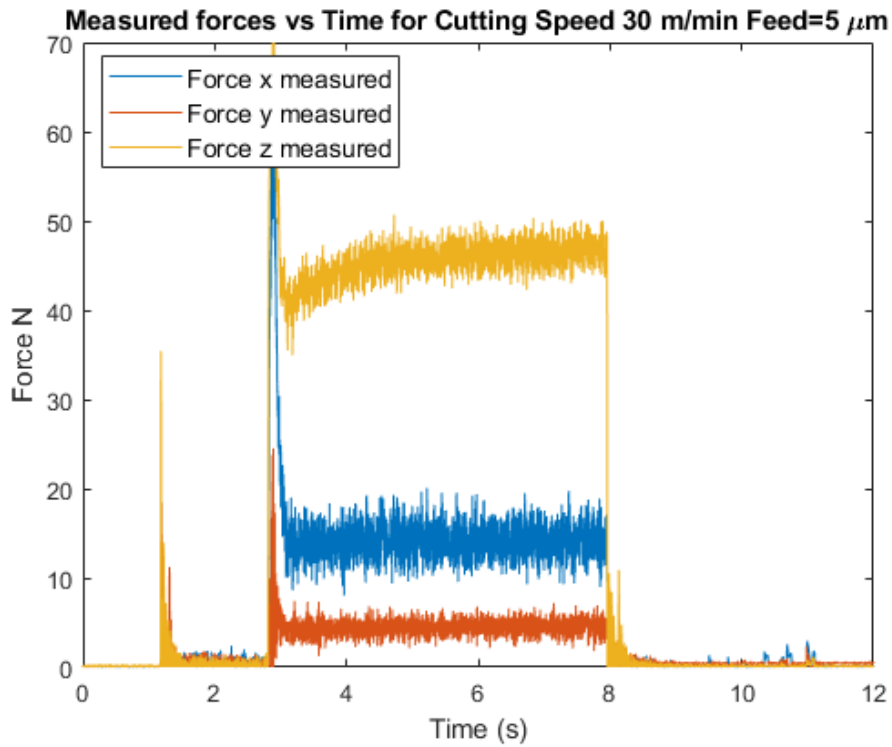


Figure 121: Typical cutting forces (RPM = 720, Cutting speed= 30 m/min, feed = 0.005 mm/rev OR Feed rate of mm/min = N. $F = 720 * 0.005 \text{ mm/rev} = 3.6 \text{ mm/min}$).

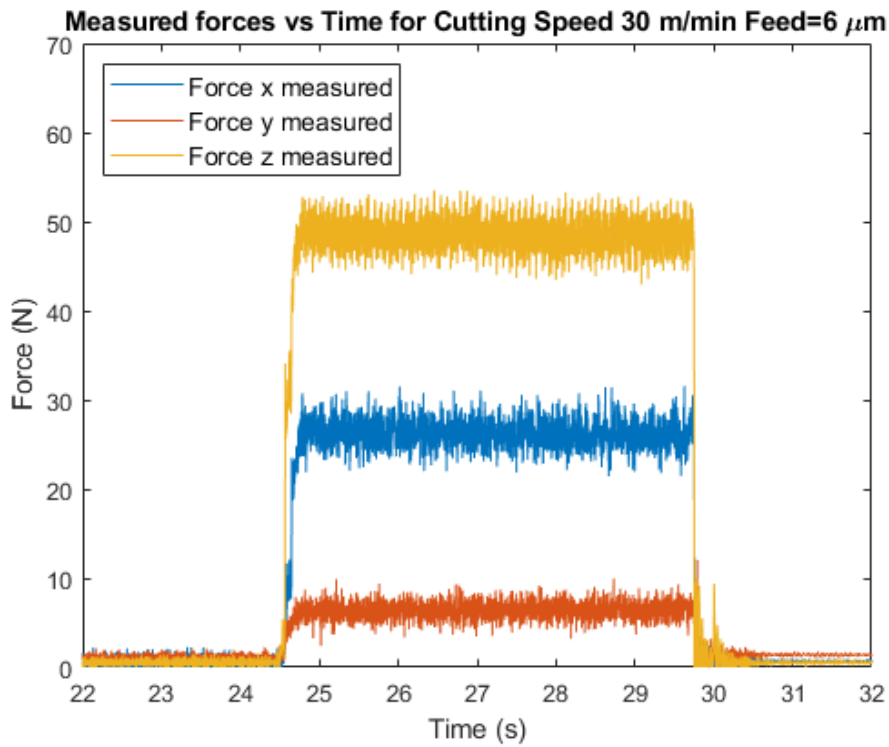


Figure 122: Typical cutting forces (RPM = 720, Cutting speed= 30 m/min, feed = 0.006 mm/rev OR Feed rate of mm/min = N. $F = 720 * 0.006 \text{ mm/rev} = 4.32 \text{ mm/min}$).

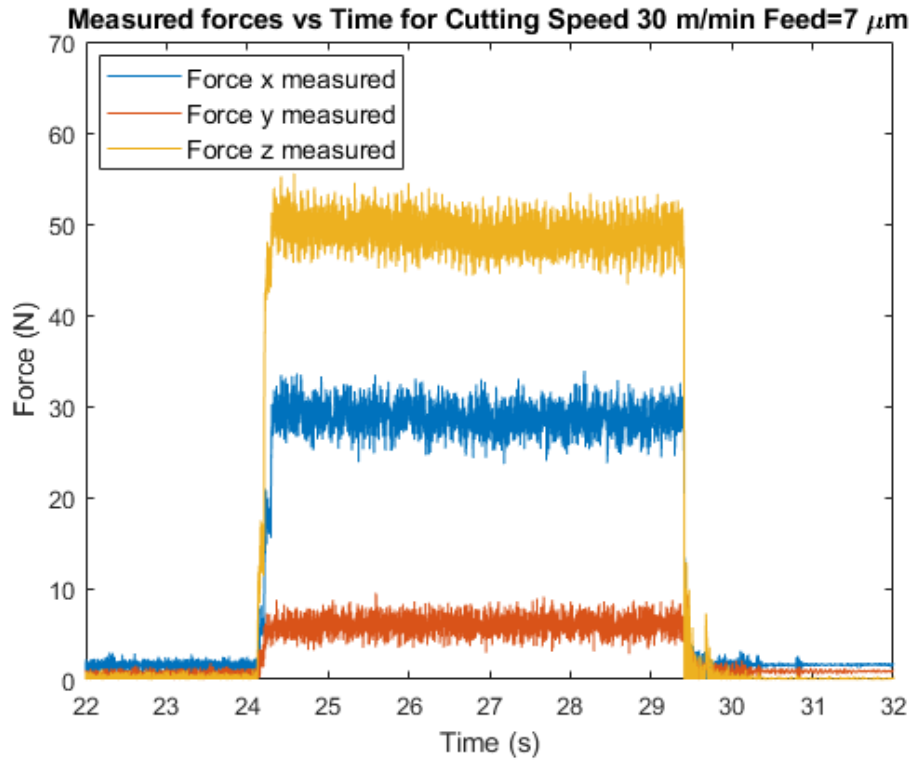


Figure 123: Typical cutting forces (RPM = 720, Cutting speed= 30 m/min, feed = 0.007 mm/rev OR Feed rate of mm/min = N. $F = 720 * 0.007 \text{ mm/rev} = 5.04 \text{ mm/min}$).

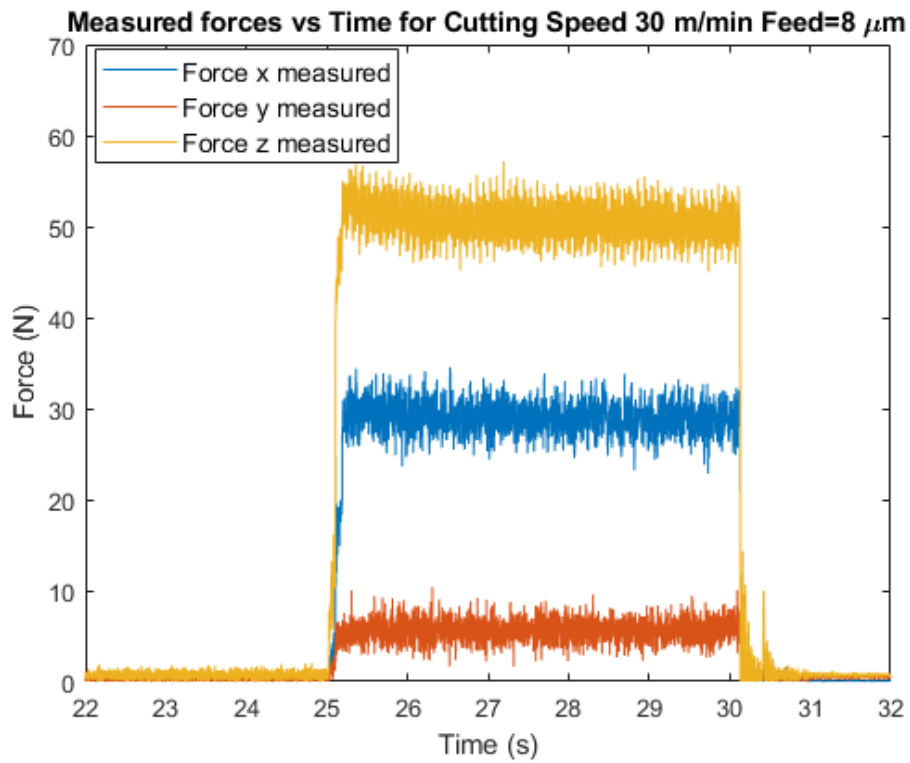


Figure 124: Typical cutting forces (RPM = 720, Cutting speed= 30 m/min, feed = 0.008 mm/rev OR Feed rate of mm/min = $N \cdot F = 720 * 0.008 \text{ mm/rev} = 5.76 \text{ mm/min}$).

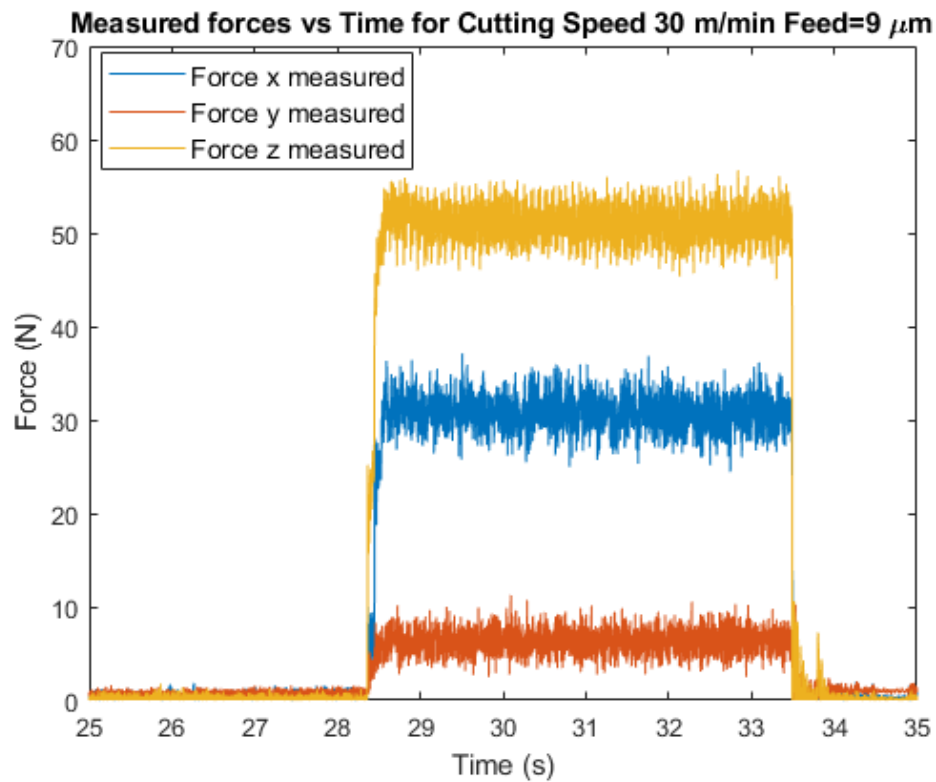


Figure 125: Typical cutting forces (RPM = 720, Cutting speed= 30 m/min, feed = 0.009 mm/rev OR Feed rate of mm/min = $N \cdot F = 720 * 0.009 \text{ mm/rev} = 6.48 \text{ mm/min}$).

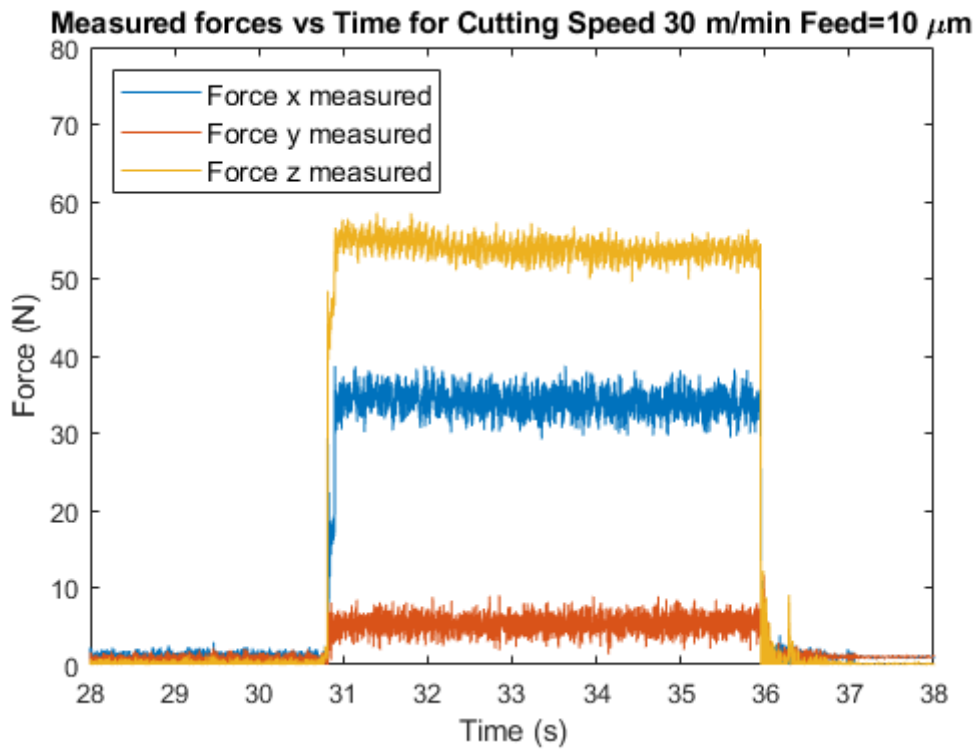


Figure 126: Typical cutting forces (RPM = 720, Cutting speed= 30 m/min, feed = 0.01 mm/rev OR Feed rate of mm/min = N. $F = 720 * 0.01 \text{ mm/rev} = 7.2 \text{ mm/min}$).

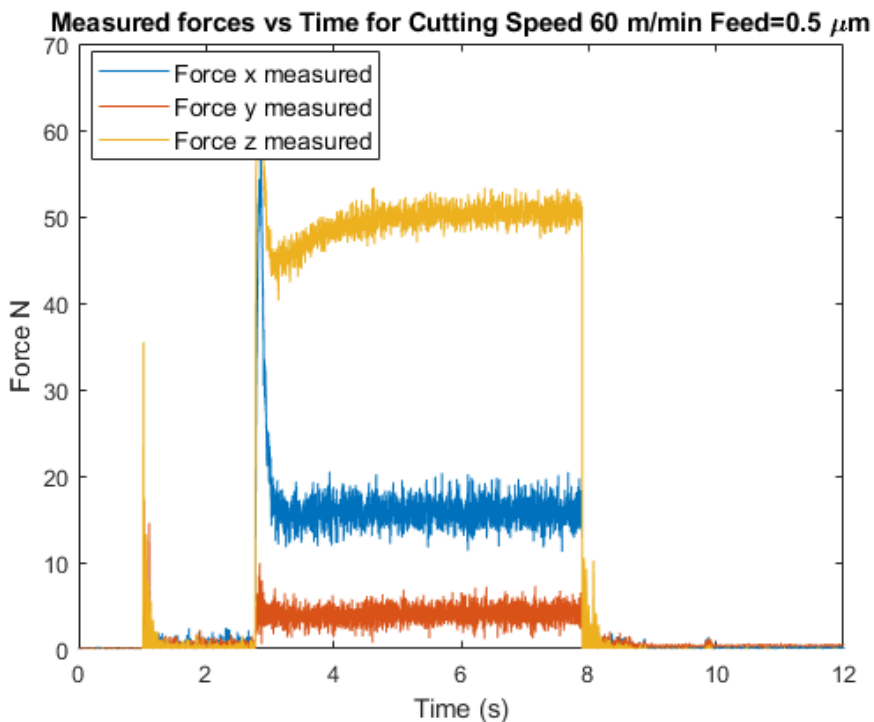


Figure 127: Typical cutting forces (RPM = 720, Cutting speed= 60 m/min, feed = 0.0005 mm/rev OR Feed rate of mm/min = N. $F = 720 * 0.0005 \text{ mm/rev} = 0.36 \text{ mm/min}$).

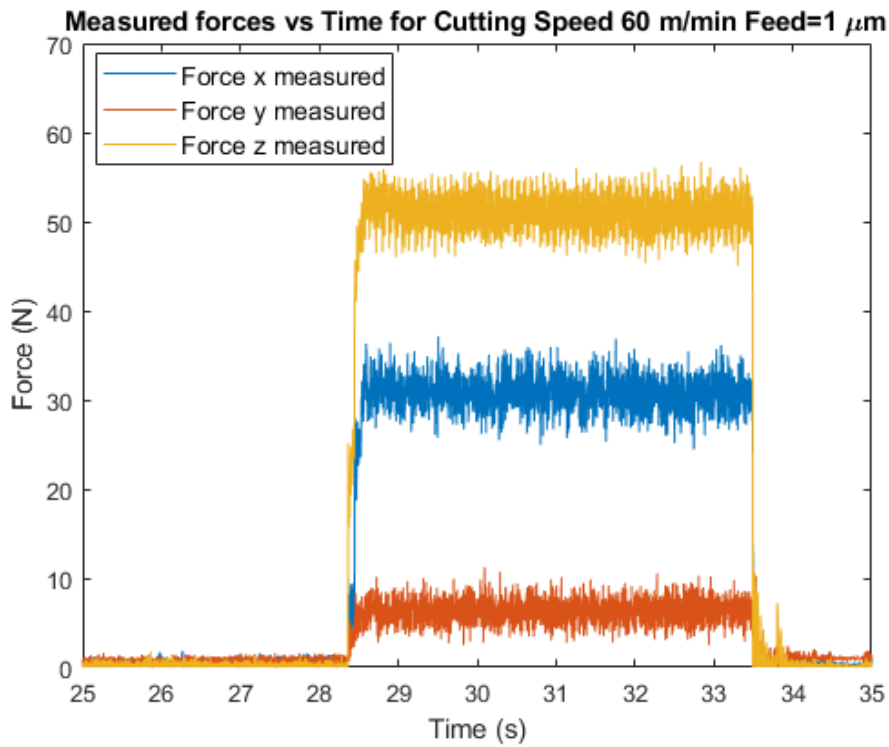


Figure 128: Typical cutting forces (RPM = 720, Cutting speed= 60 m/min, feed = 0.001 mm/rev OR Feed rate of mm/min = $N \cdot F = 720 * 0.001 \text{ mm/rev} = 0.72 \text{ mm/min}$).

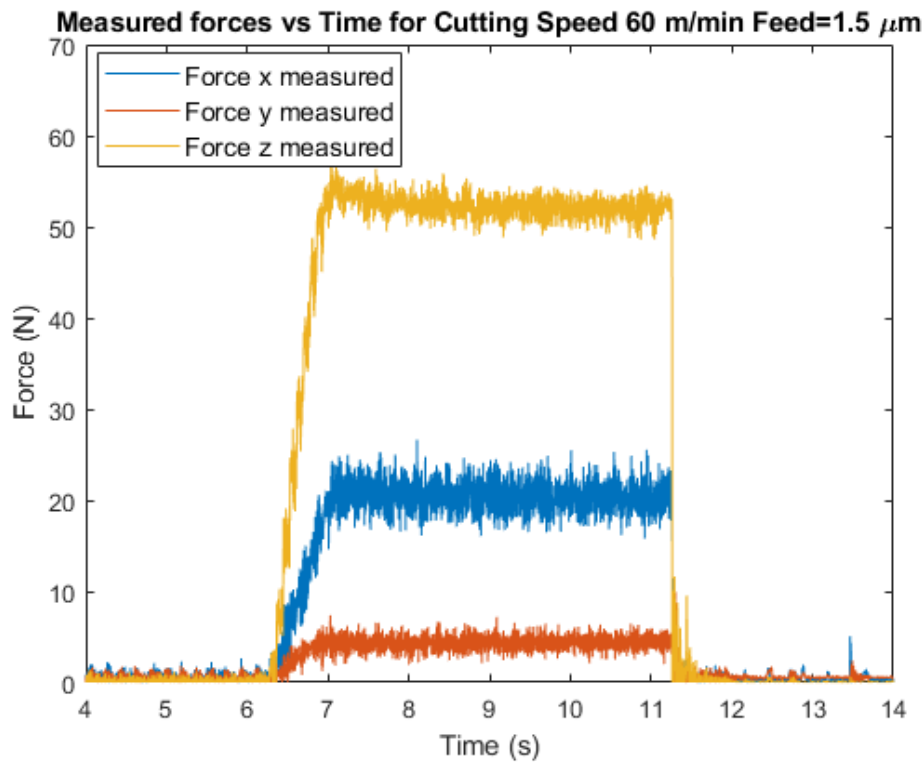


Figure 129: Typical cutting forces (RPM = 720, Cutting speed= 60 m/min, feed = 0.0015 mm/rev OR Feed rate of mm/min = $N \cdot F = 720 * 0.0015 \text{ mm/rev} = 1.08 \text{ mm/min}$).

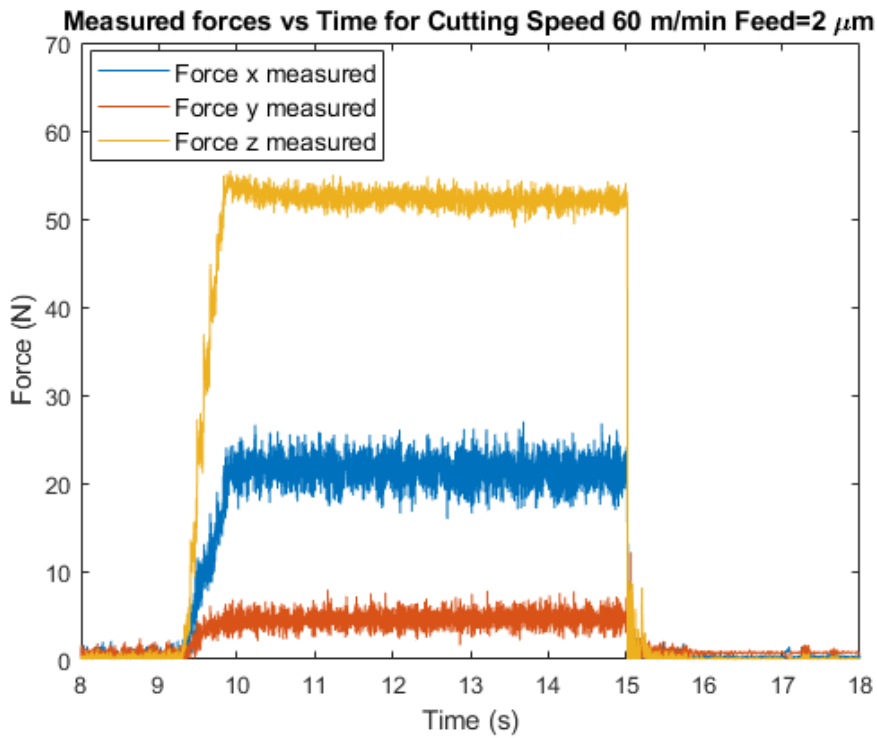


Figure 130: Typical cutting forces (RPM = 720, Cutting speed= 60 m/min, feed = 0.002 mm/rev OR Feed rate of mm/min = $N.F = 720 * 0.002 \text{ mm/rev} = 1.44 \text{ mm/min}$).

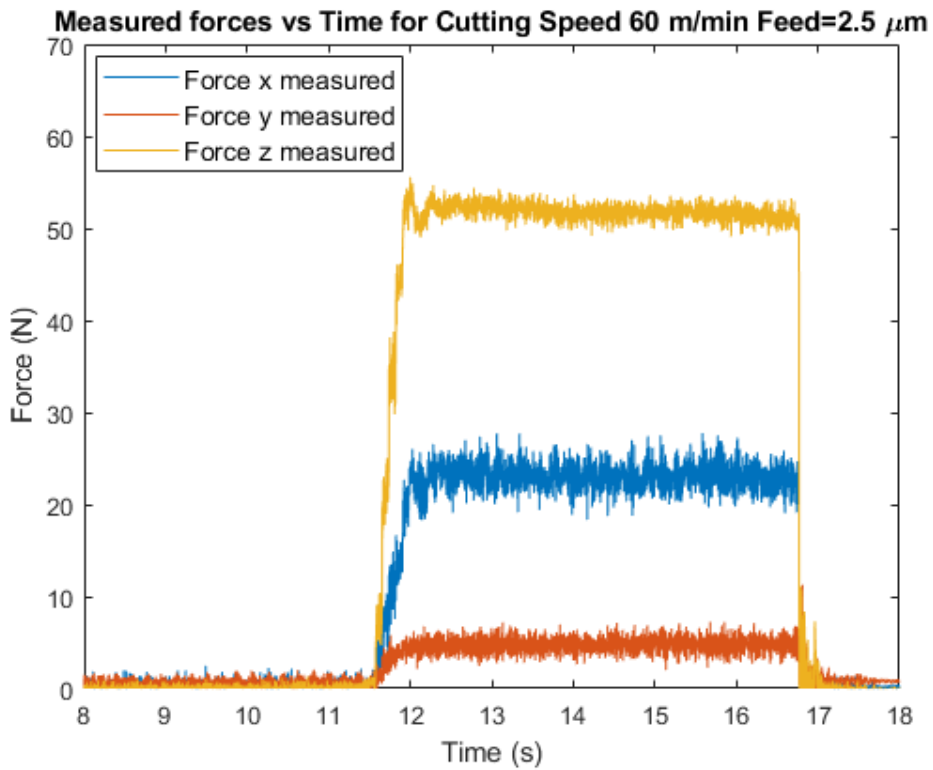


Figure 131: Typical cutting forces (RPM = 720, Cutting speed= 60 m/min, feed = 0.0025 mm/rev OR Feed rate of mm/min = $N.F = 720 * 0.0025 \text{ mm/rev} = 1.8 \text{ mm/min}$).

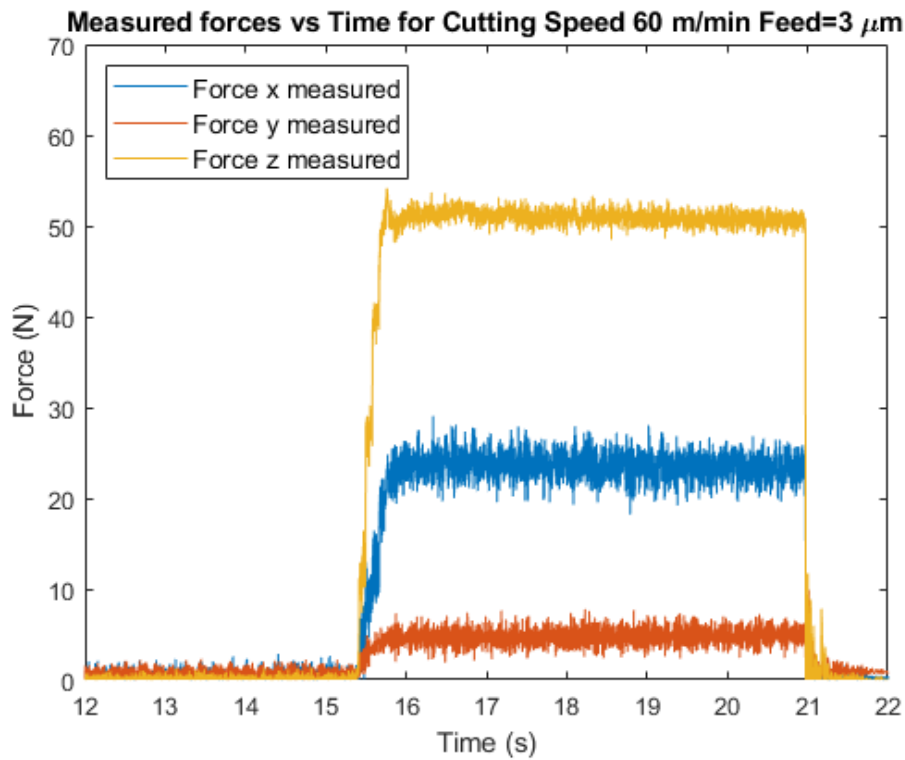


Figure 132: Typical cutting forces (RPM = 720, Cutting speed= 60 m/min, feed = 0.003 mm/rev OR Feed rate of mm/min = N. F = 720 * 0.003 mm/rev = 2.16 mm/min).

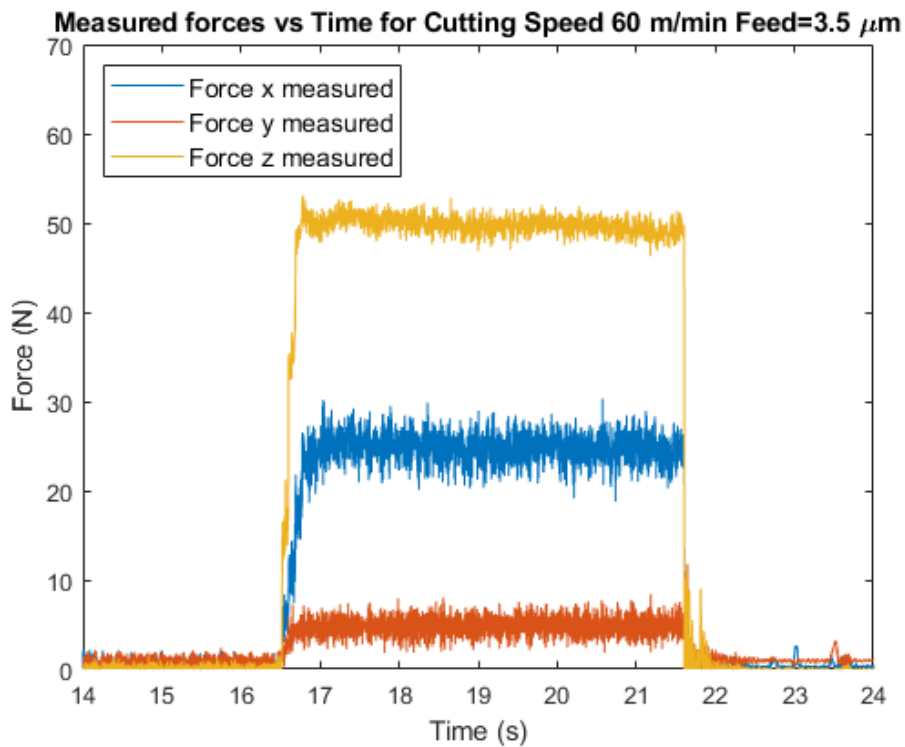


Figure 133: Typical cutting forces (RPM = 720, Cutting speed= 60 m/min, feed = 0.0035 mm/rev OR Feed rate of mm/min = N. F = 720 * 0.0035 mm/rev = 2.52 mm/min).

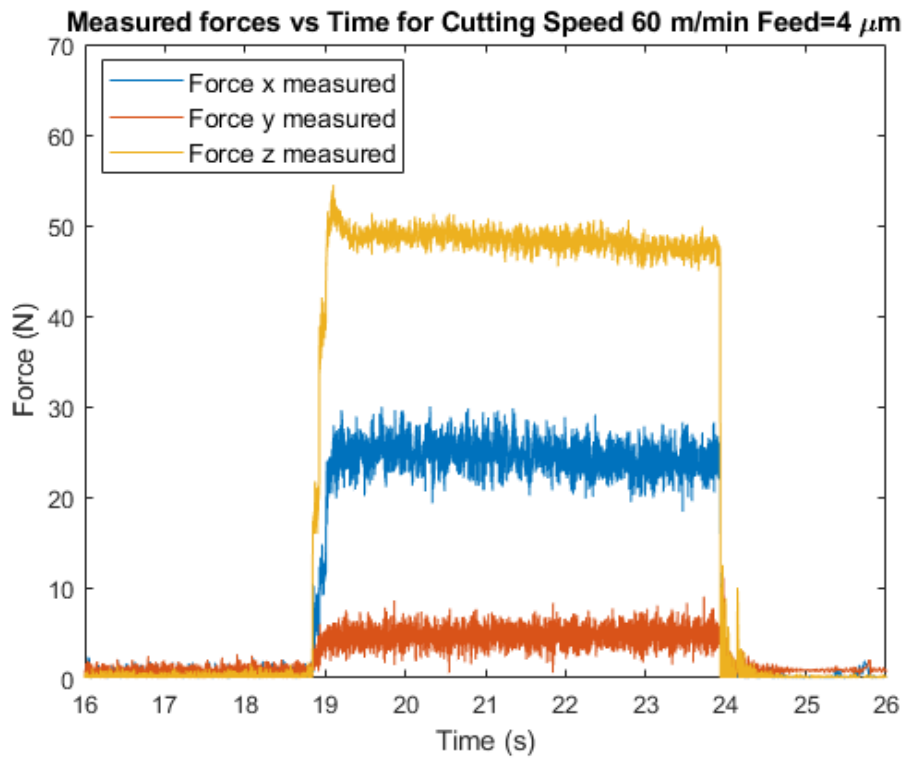


Figure 134: Typical cutting forces (RPM = 720, Cutting speed= 60 m/min, feed = 0.004 mm/rev OR Feed rate of mm/min = N. F = 720 * 0.004 mm/rev = 2.88 mm/min).

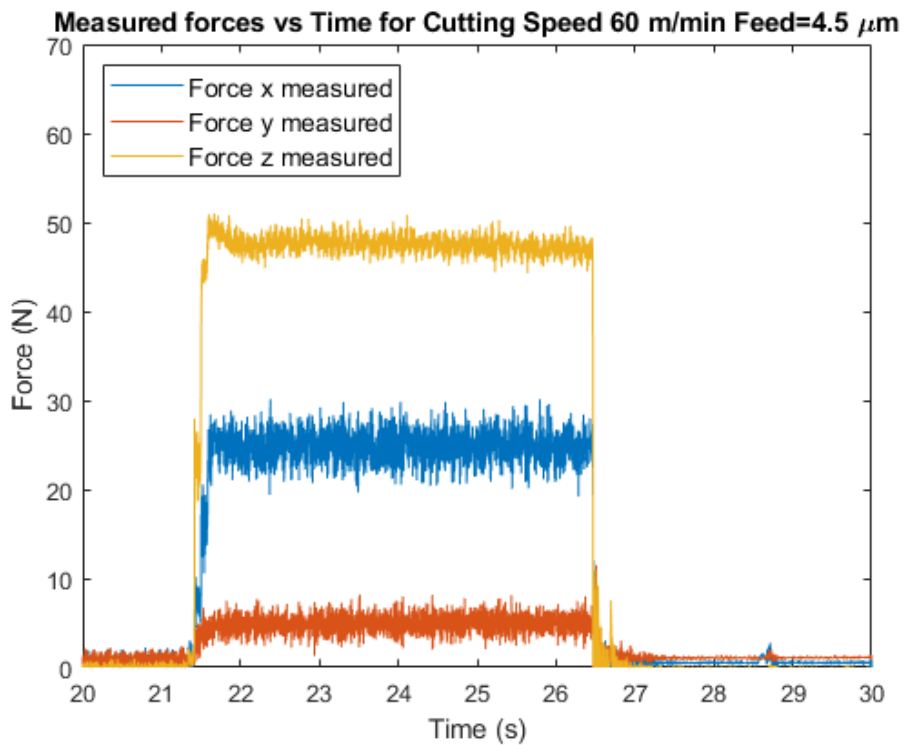


Figure 135: Typical cutting forces (RPM = 720, Cutting speed= 60 m/min, feed = 0.0045 mm/rev OR Feed rate of mm/min = N. F = 720 * 0.0045 mm/rev = 3.24 mm/min).

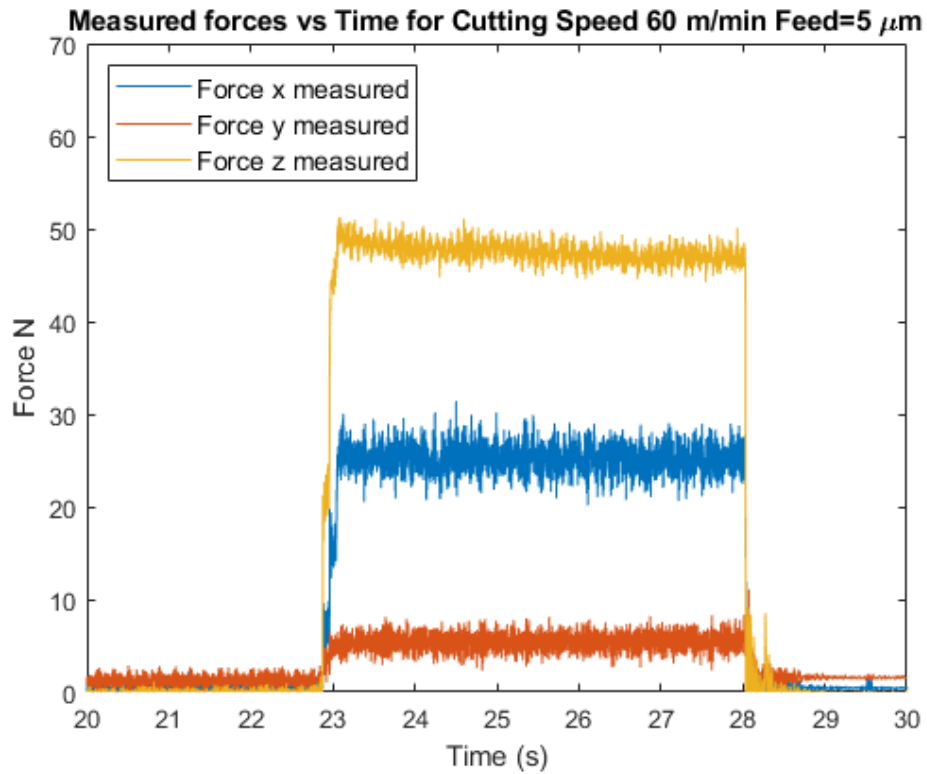


Figure 136: Typical cutting forces (RPM = 720, Cutting speed= 60 m/min, feed = 0.005 mm/rev OR Feed rate of mm/min = $N \cdot F = 720 * 0.005 \text{ mm/rev} = 3.6 \text{ mm/min}$).

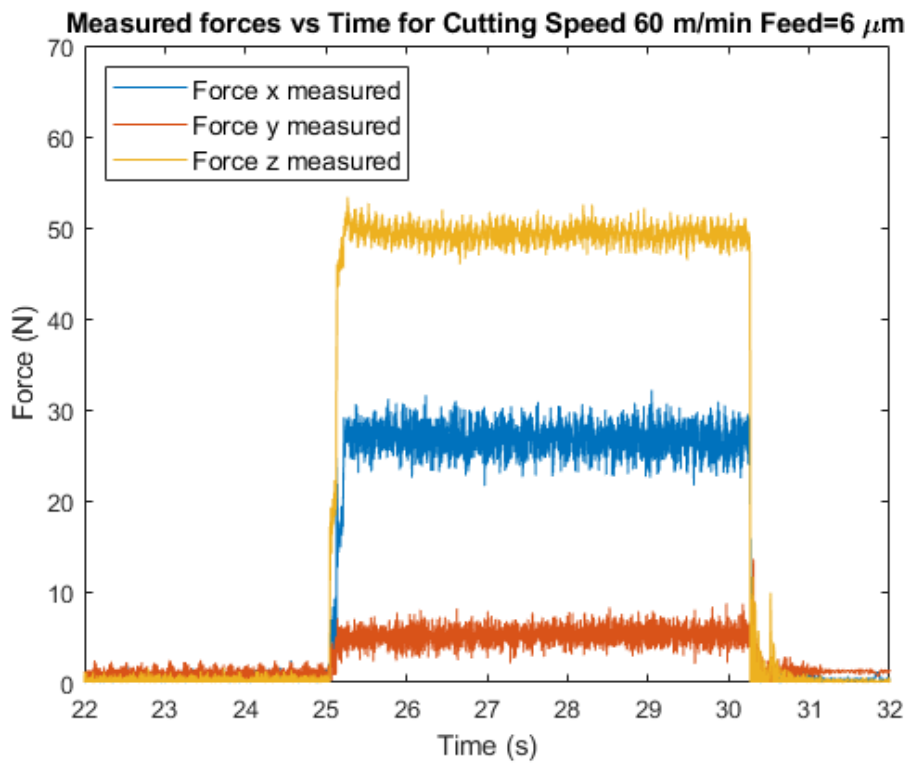


Figure 137: Typical cutting forces (RPM = 720, Cutting speed= 60 m/min, feed = 0.006 mm/rev OR Feed rate of mm/min = $N \cdot F = 720 * 0.006 \text{ mm/rev} = 4.32 \text{ mm/min}$).

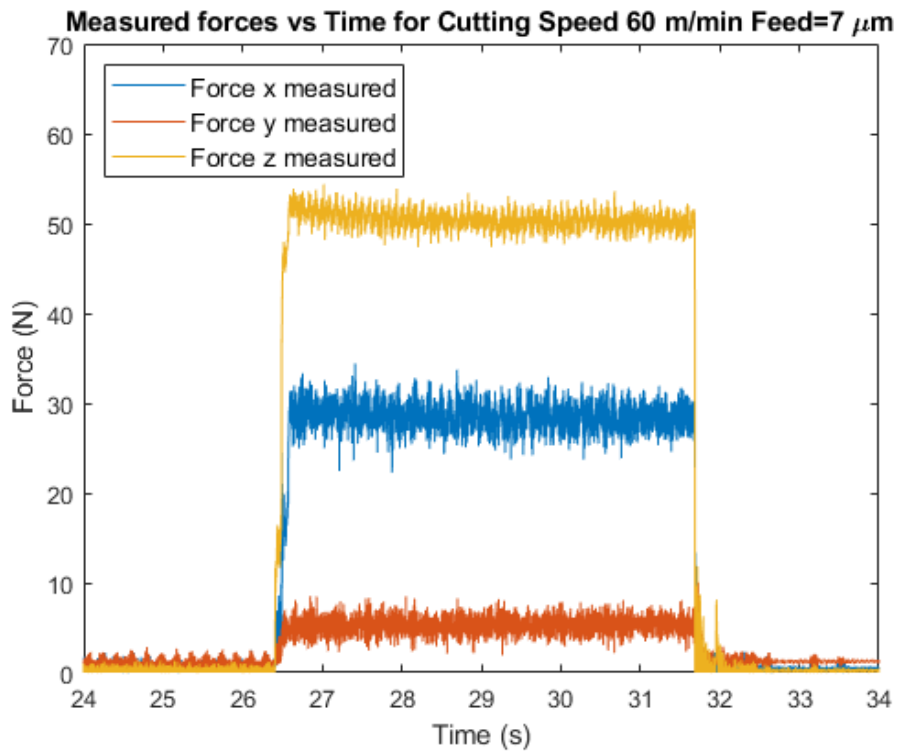


Figure 138: Typical cutting forces (RPM = 720, Cutting speed= 60 m/min, feed = 0.007 mm/rev OR Feed rate of mm/min = N. F = 720 * 0.007 mm/rev = 5.04 mm/min).

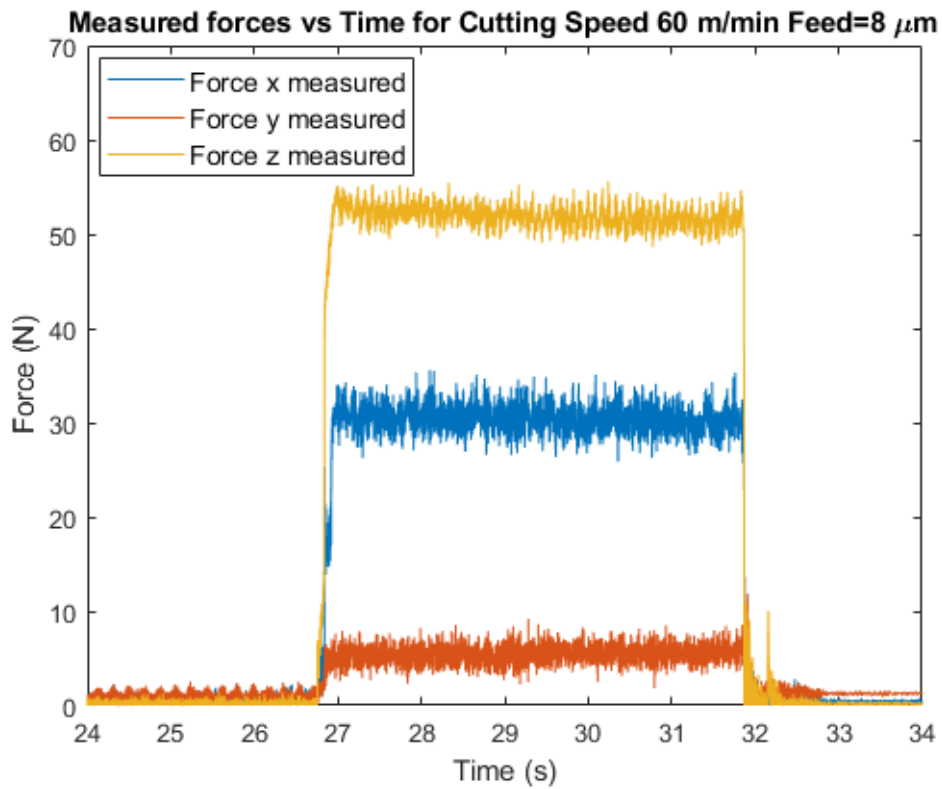


Figure 139: Typical cutting forces (RPM = 720, Cutting speed= 60 m/min, feed = 0.008 mm/rev OR Feed rate of mm/min = N. F = 720 * 0.008 mm/rev = 5.76 mm/min).

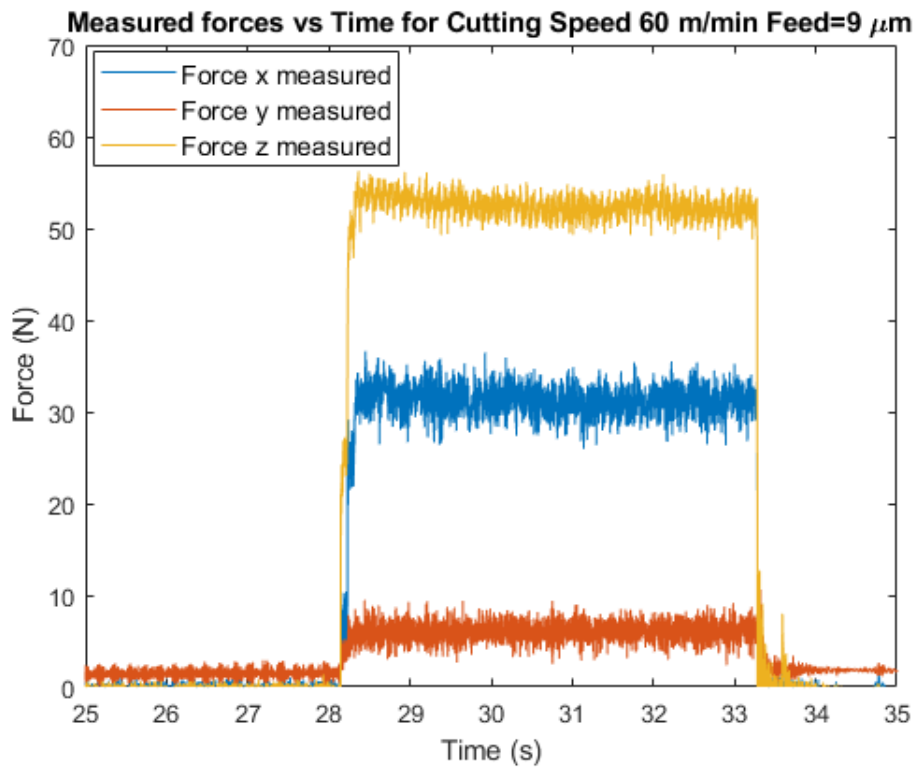


Figure 140: Typical cutting forces (RPM = 720, Cutting speed= 60 m/min, feed = 0.009 mm/rev OR Feed rate of mm/min = $N \cdot F = 720 * 0.009 \text{ mm/rev} = 6.48 \text{ mm/min}$).

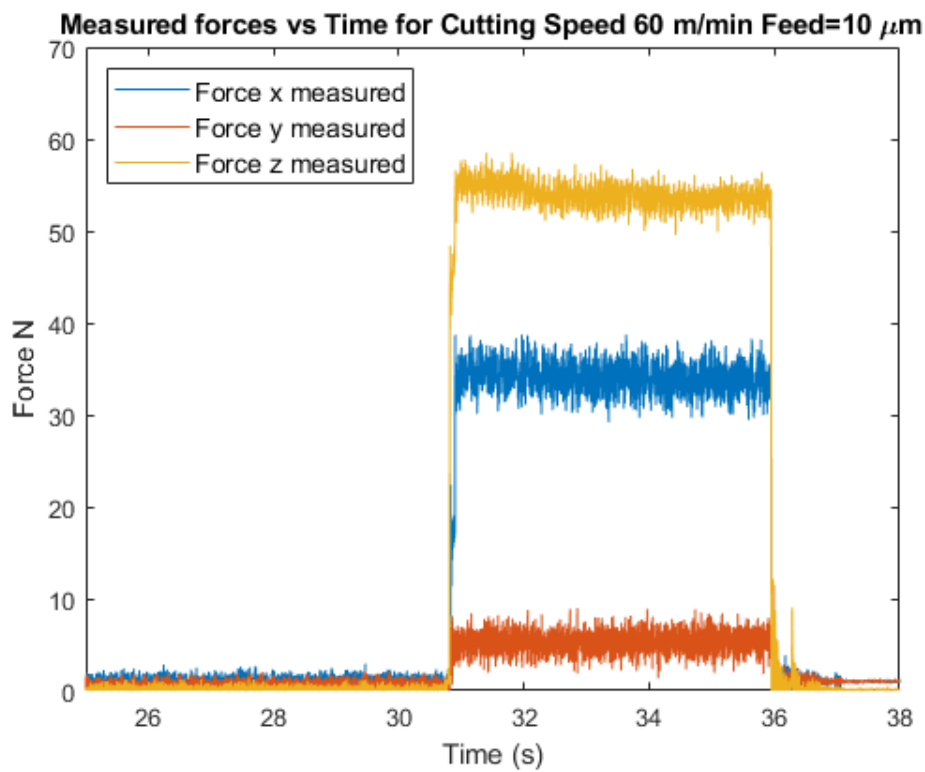


Figure 141: Typical cutting forces (RPM = 720, Cutting speed= 60 m/min, feed = 0.01 mm/rev OR Feed rate of mm/min = $N \cdot F = 720 * 0.01 \text{ mm/rev} = 7.2 \text{ mm/min}$).

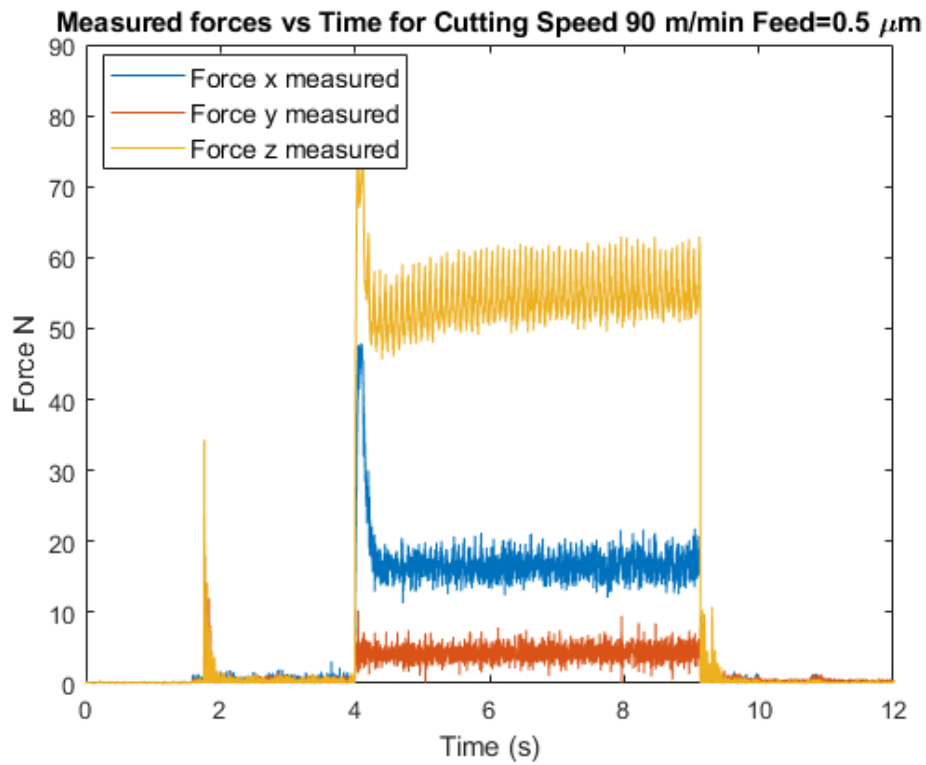


Figure 142: Typical cutting forces (RPM = 720, Cutting speed= 90 m/min, feed = 0.0005 mm/rev OR Feed rate of mm/min = N. $F = 720 * 0.0005 \text{ mm/rev} = 0.36 \text{ mm/min}$).

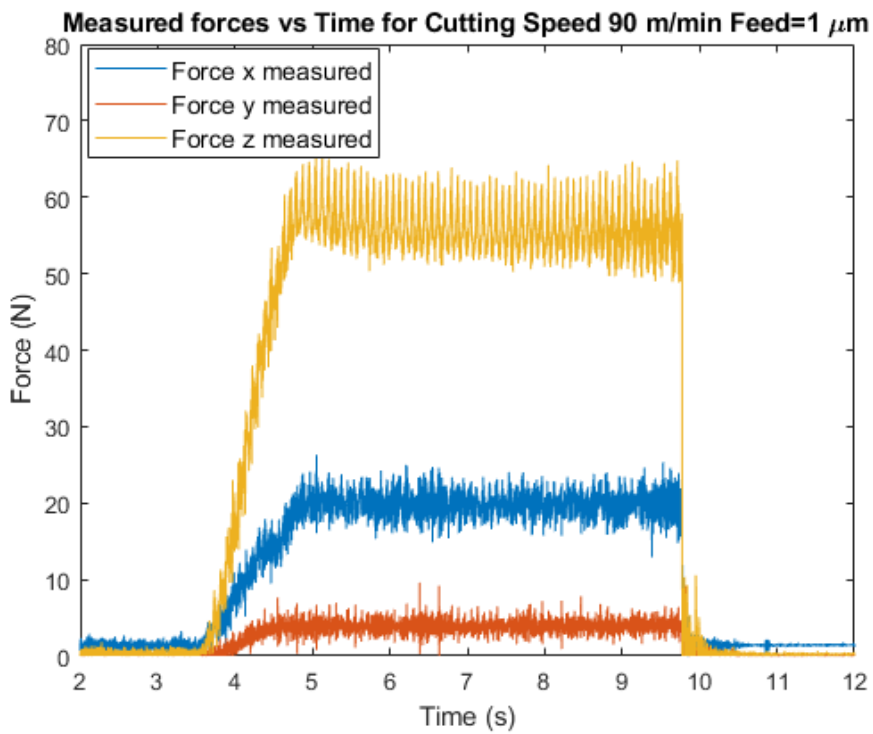


Figure 143: Typical cutting forces (RPM = 720, Cutting speed= 90 m/min, feed = 0.001 mm/rev OR Feed rate of mm/min = N. $F = 720 * 0.001 \text{ mm/rev} = 0.72 \text{ mm/min}$).

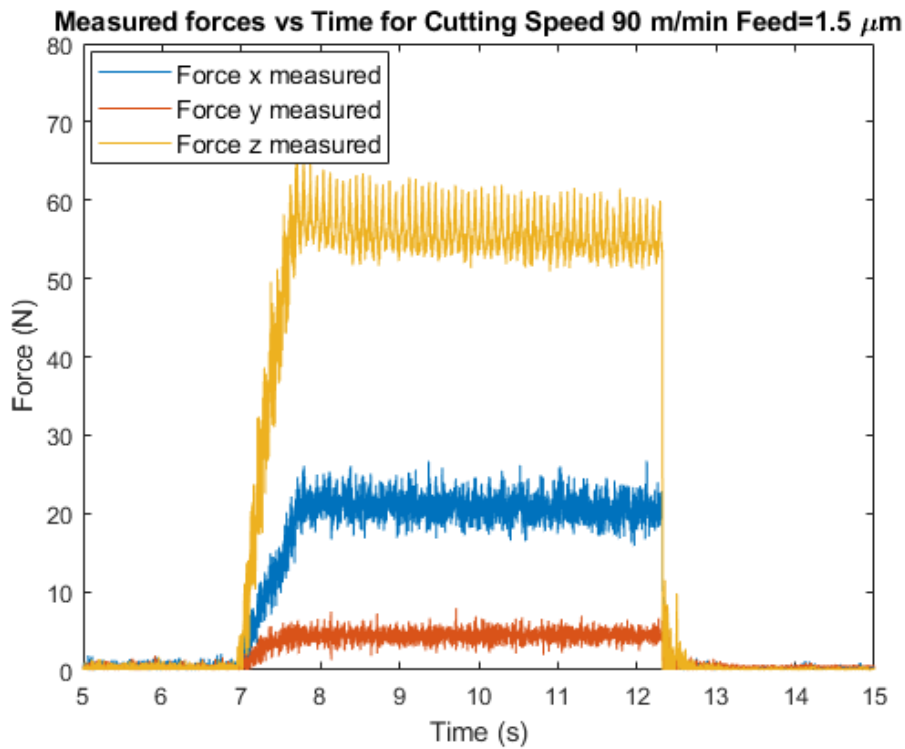


Figure 144: Typical cutting forces (RPM = 720, Cutting speed= 90 m/min, feed = 0.0015 mm/rev OR Feed rate of mm/min = N. $F = 720 * 0.0015 \text{ mm/rev} = 1.08 \text{ mm/min}$).

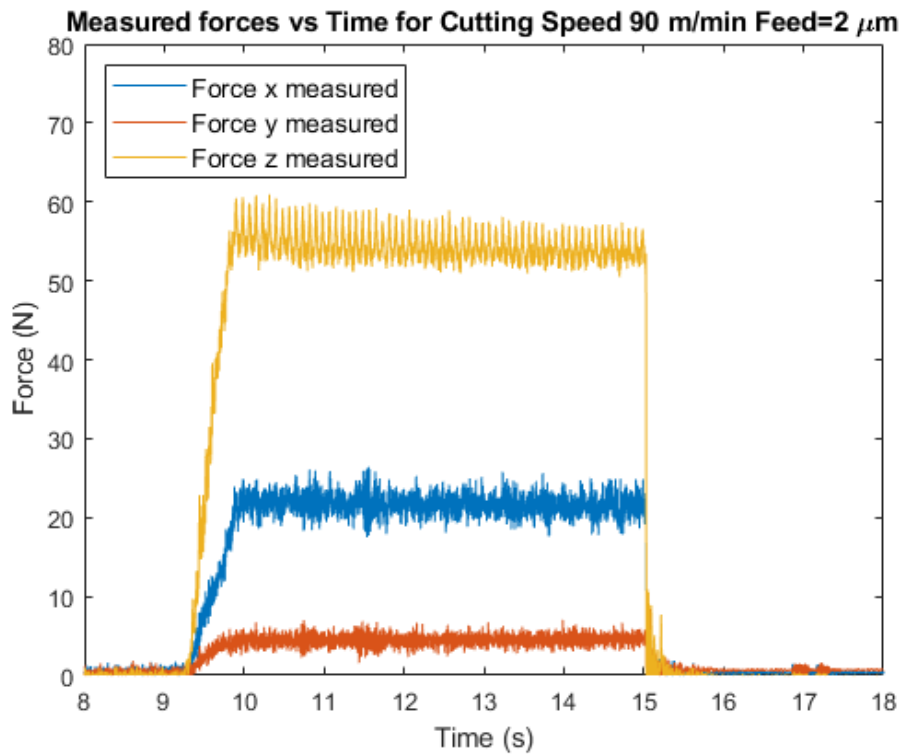


Figure 145: Typical cutting forces (RPM = 720, Cutting speed= 90 m/min, feed = 0.002 mm/rev OR Feed rate of mm/min = N. $F = 720 * 0.002 \text{ mm/rev} = 1.44 \text{ mm/min}$).

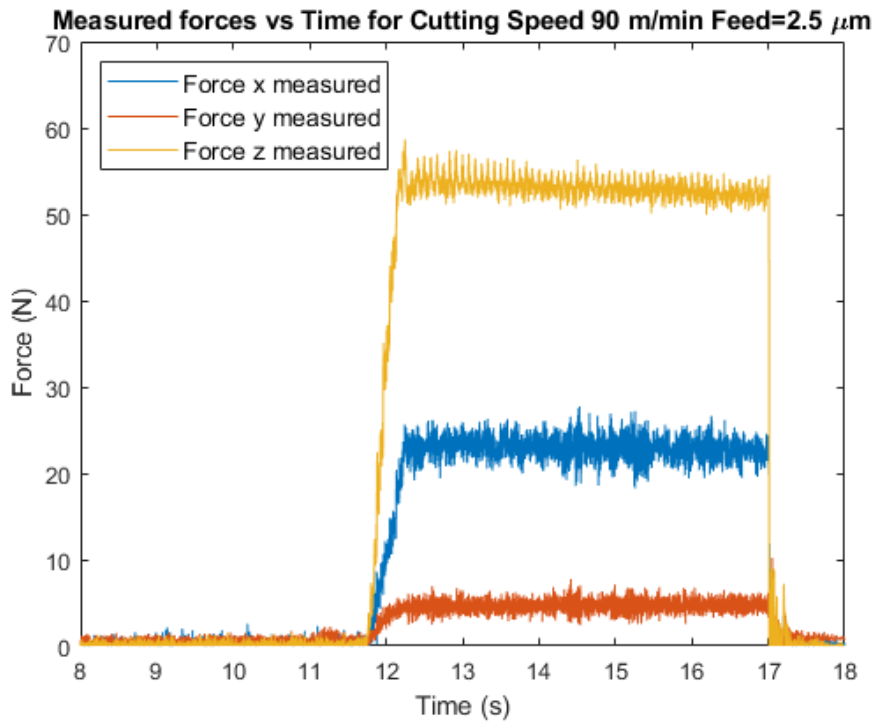


Figure 146: Typical cutting forces (RPM = 720, Cutting speed= 90 m/min, feed = 0.0025 mm/rev OR Feed rate of mm/min = N. $F = 720 * 0.0025 \text{ mm/rev} = 1.8 \text{ mm/min}$).

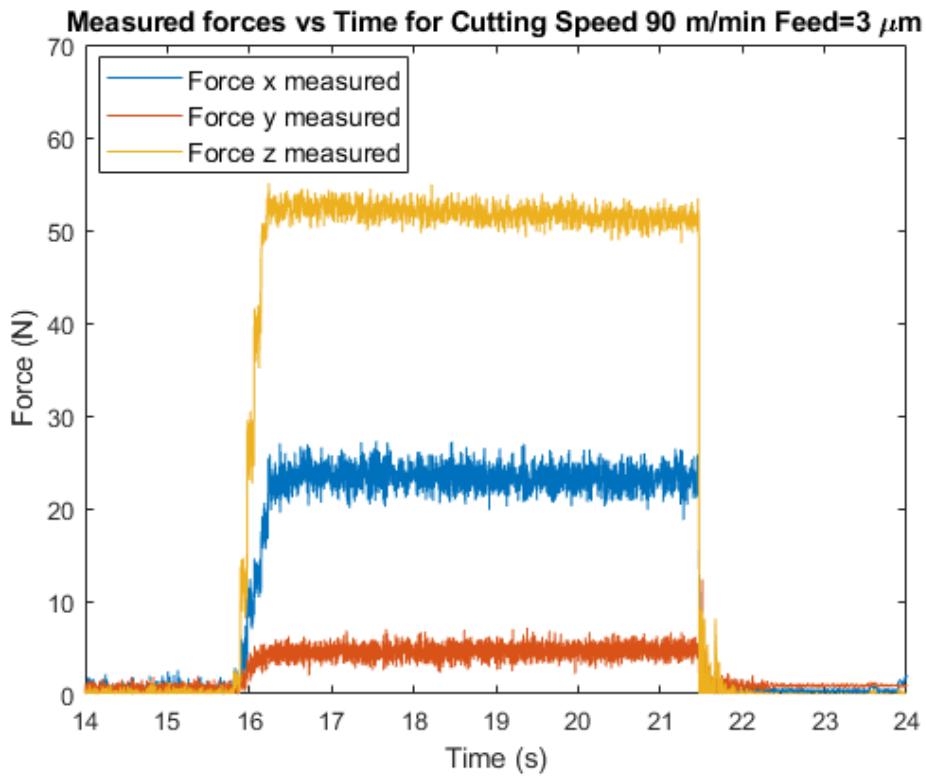


Figure 147: Typical cutting forces (RPM = 720, Cutting speed= 90 m/min, feed = 0.003 mm/rev OR Feed rate of mm/min = N. $F = 720 * 0.002 \text{ mm/rev} = 2.16 \text{ mm/min}$).

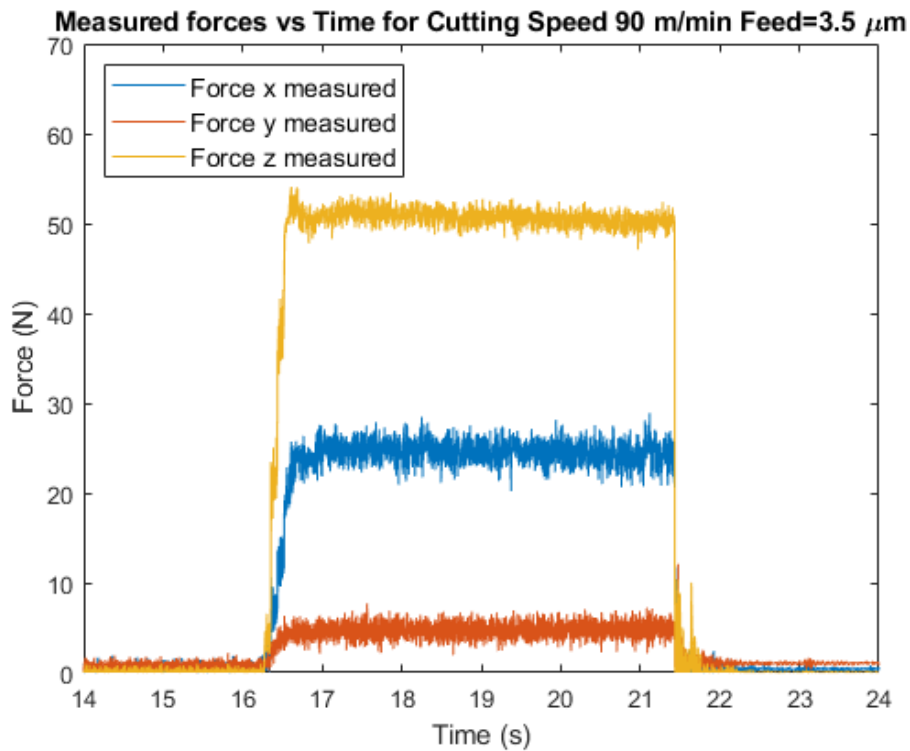


Figure 148: Typical cutting forces (RPM = 720, Cutting speed= 90 m/min, feed = 0.0035 mm/rev OR Feed rate of mm/min = N. $F = 720 * 0.0025 \text{ mm/rev} = 2.52 \text{ mm/min}$).

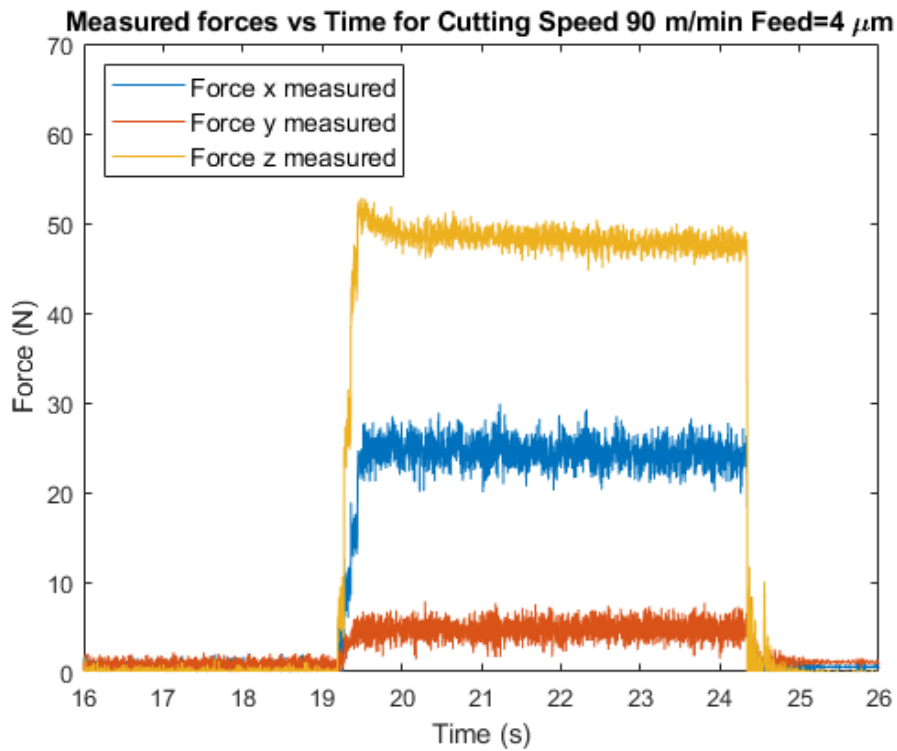


Figure 149: Typical cutting forces (RPM = 720, Cutting speed= 90 m/min, feed = 0.004 mm/rev OR Feed rate of mm/min = N. $F = 720 * 0.004 \text{ mm/rev} = 2.88 \text{ mm/min}$).

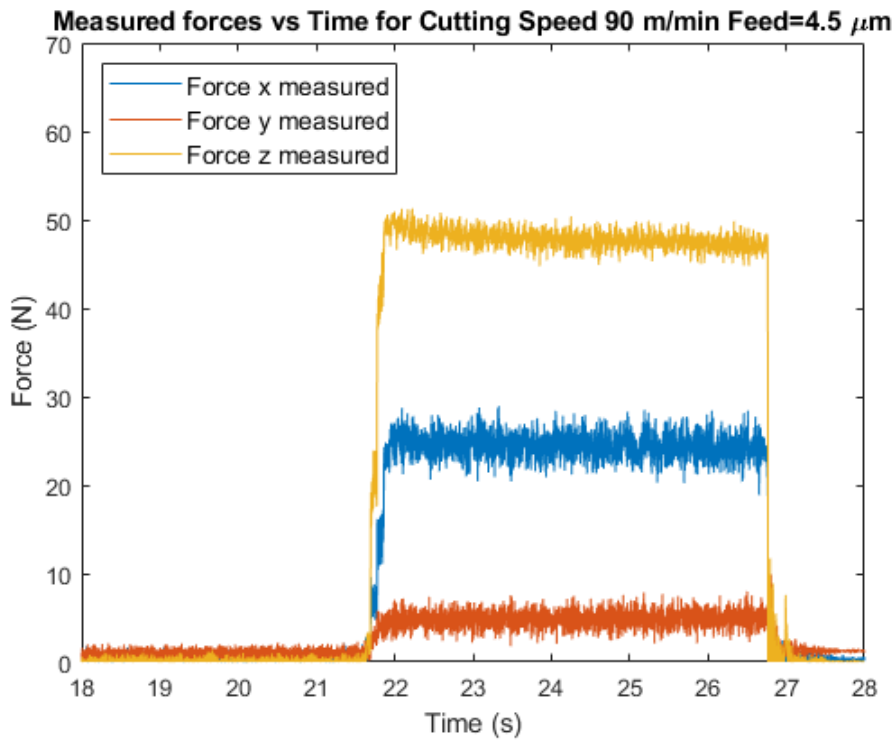


Figure 150: Typical cutting forces (RPM = 720, Cutting speed= 90 m/min, feed = 0.0045 mm/rev OR Feed rate of mm/min = N. $F = 720 * 0.0045 \text{ mm/rev} = 3.24 \text{ mm/min}$).

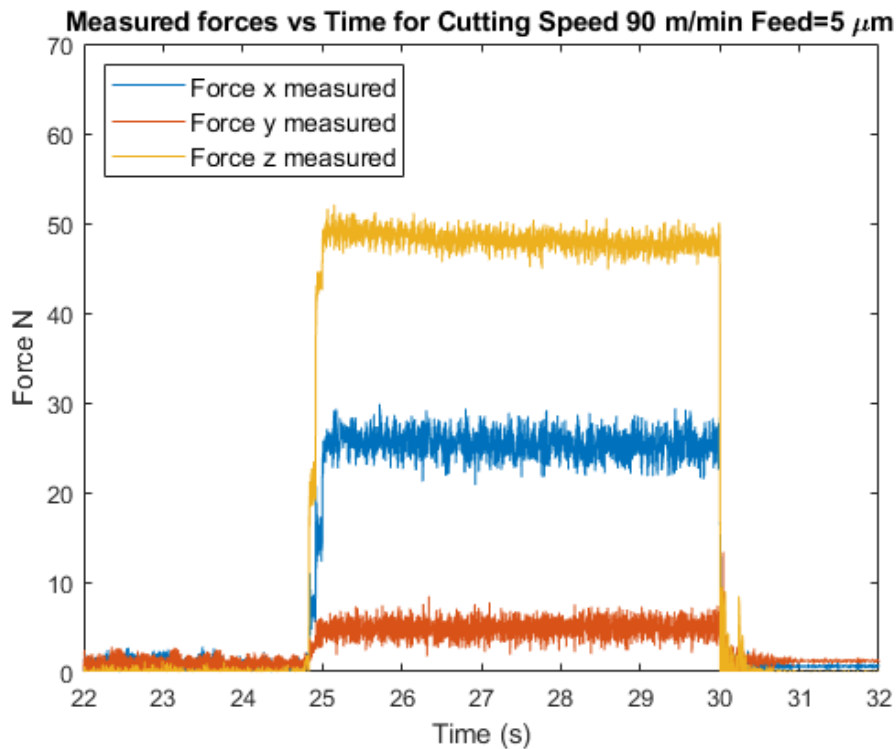


Figure 151: Typical cutting forces (RPM = 720, Cutting speed= 90 m/min, feed = 0.005 mm/rev OR Feed rate of mm/min = N. $F = 720 * 0.005 \text{ mm/rev} = 3.6 \text{ mm/min}$).

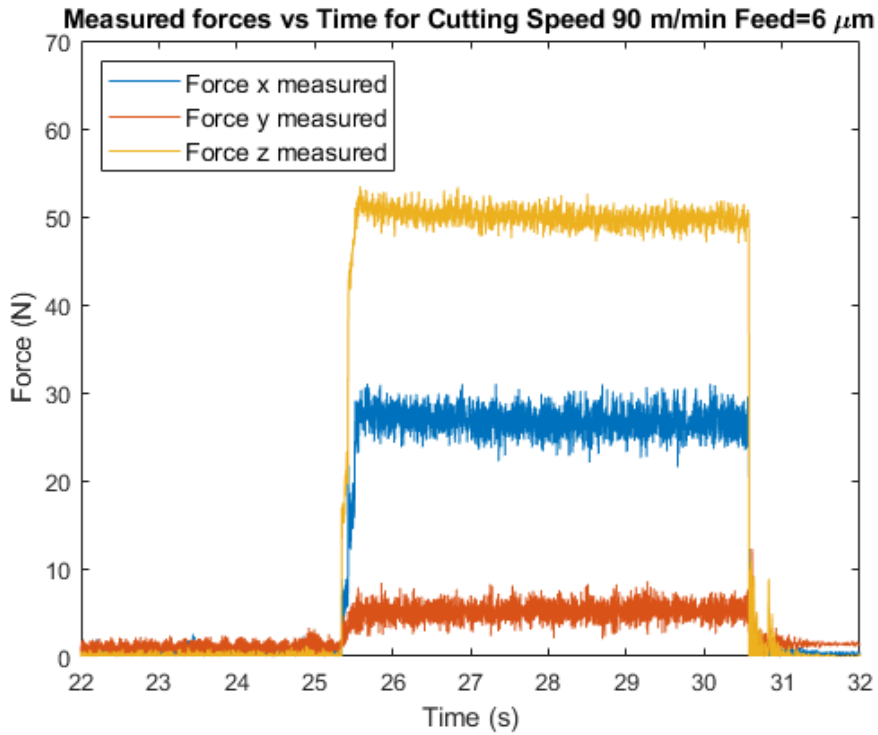


Figure 152: Typical cutting forces (RPM = 720, Cutting speed= 90 m/min, feed = 0.006 mm/rev OR Feed rate of mm/min = $N \cdot F = 720 * 0.006 \text{ mm/rev} = 4.32 \text{ mm/min}$).

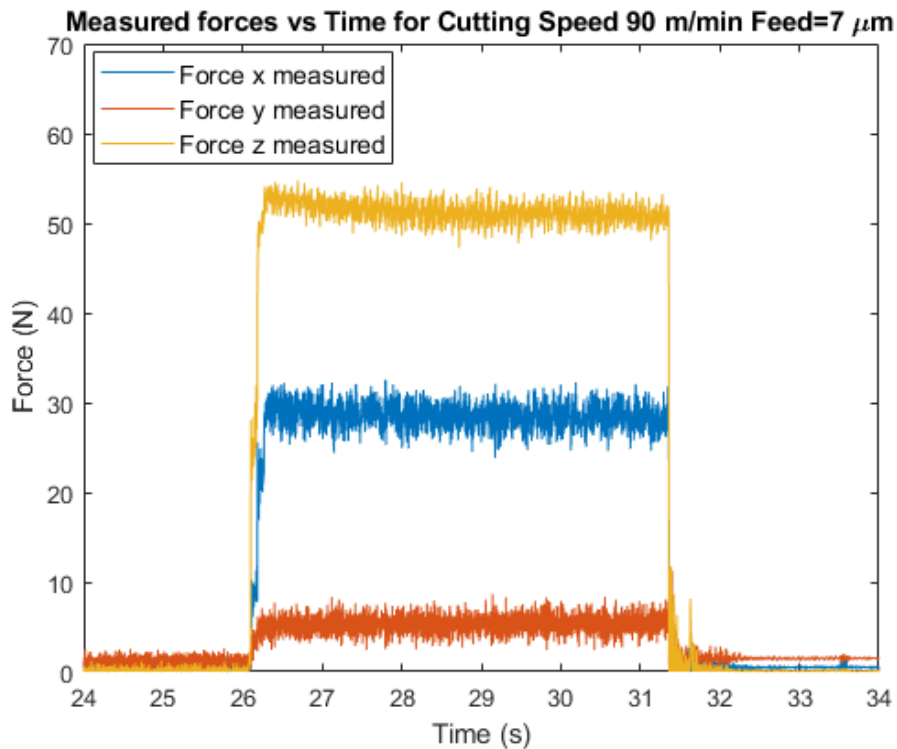


Figure 153: Typical cutting forces (RPM = 720, Cutting speed= 90 m/min, feed = 0.007 mm/rev OR Feed rate of mm/min = $N \cdot F = 720 * 0.007 \text{ mm/rev} = 5.04 \text{ mm/min}$).

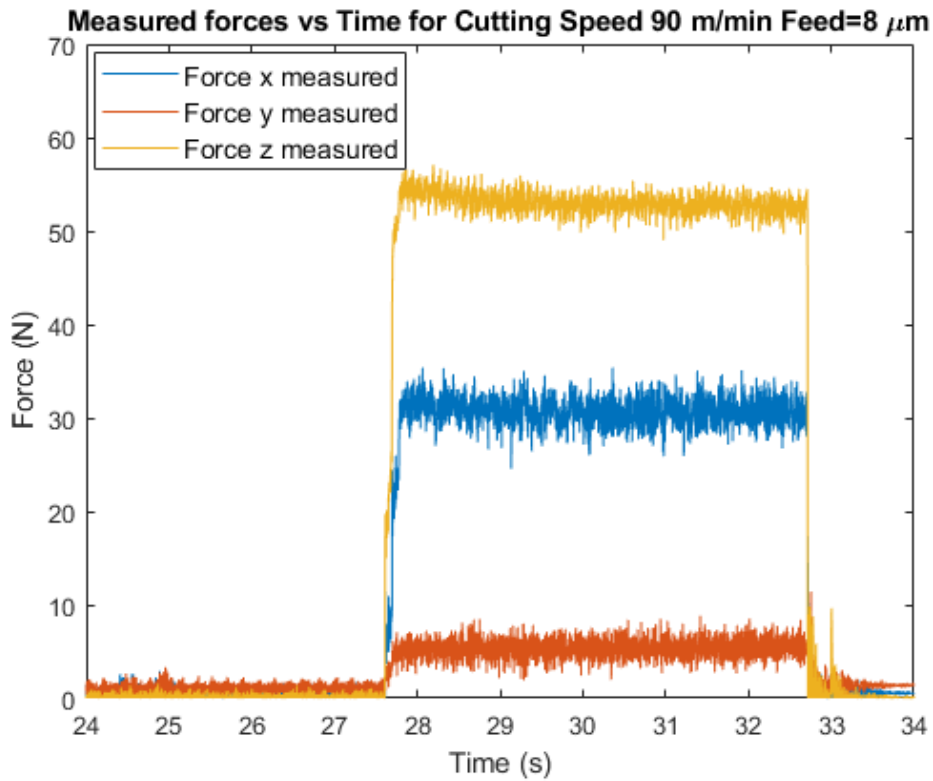


Figure 154: Typical cutting forces (RPM = 720, Cutting speed= 90 m/min, feed = 0.008 mm/rev OR Feed rate of mm/min = N. $F = 720 * 0.008 \text{ mm/rev} = 5.76 \text{ mm/min}$).

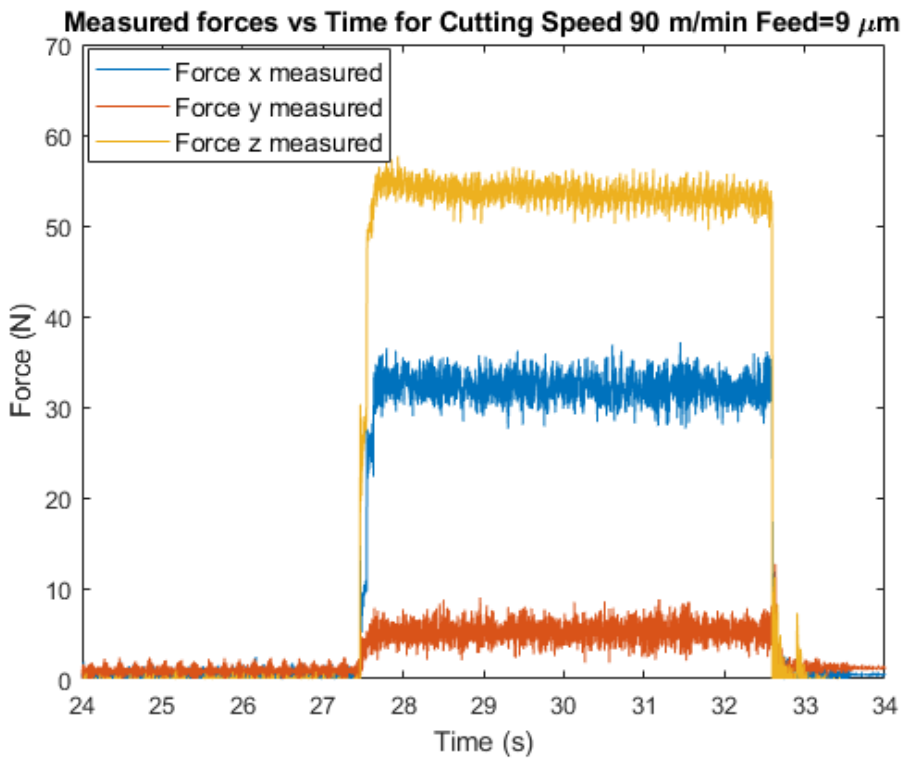


Figure 155: Typical cutting forces (RPM = 720, Cutting speed= 90 m/min, feed = 0.009 mm/rev OR Feed rate of mm/min = N. $F = 720 * 0.009 \text{ mm/rev} = 6.48 \text{ mm/min}$).

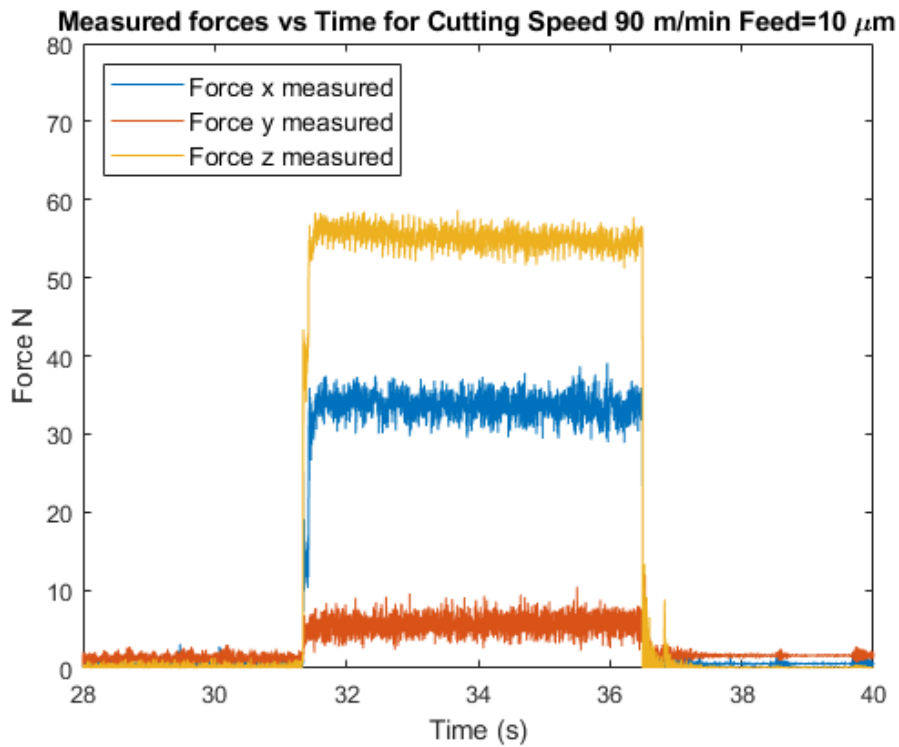


Figure 156: Typical cutting forces (RPM = 720, Cutting speed= 90 m/min, feed = 0.01 mm/rev OR Feed rate of mm/min = $N \cdot F = 720 * 0.001 \text{ mm/rev} = 7.2 \text{ mm/min}$).

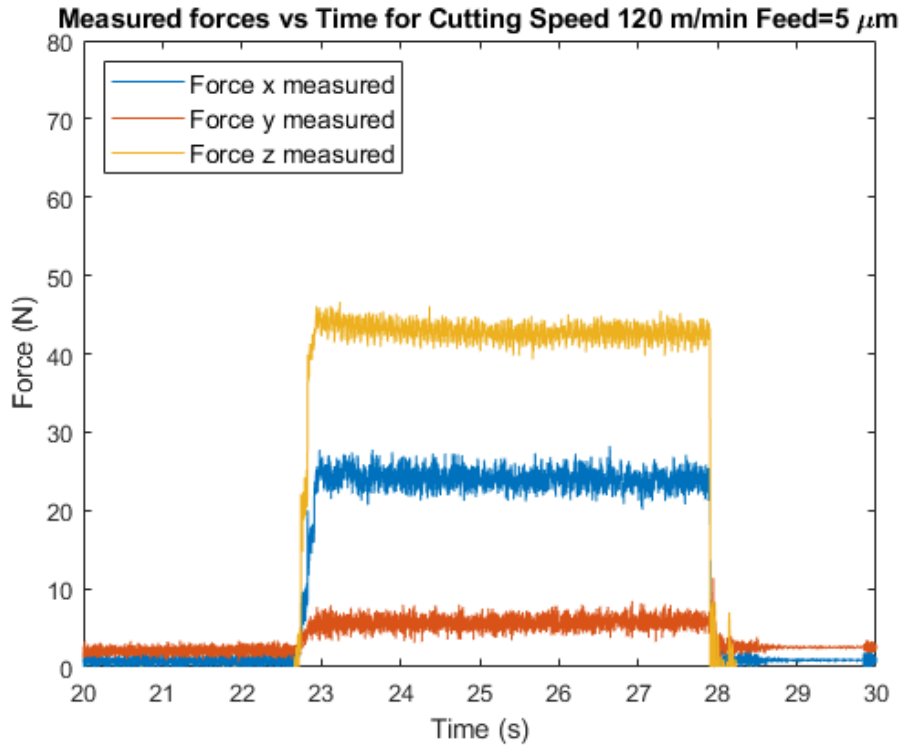


Figure 157: Typical cutting forces (RPM = 720, Cutting speed= 120 m/min, feed = 0.0005 mm/rev OR Feed rate of mm/min = $N \cdot F = 720 * 0.0005 \text{ mm/rev} = 0.36 \text{ mm/min}$).

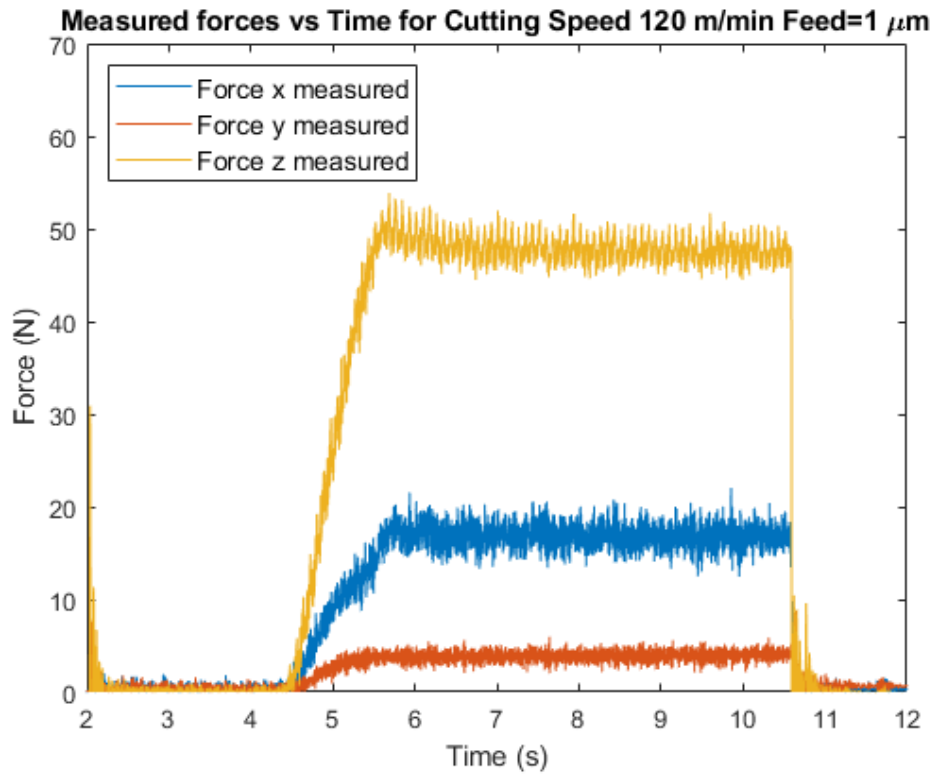


Figure 158: Typical cutting forces (RPM = 720, Cutting speed=120 m/min, feed = 0.001 mm/rev OR Feed rate of mm/min = N. F = 720 * 0.001 mm/rev = 0.72 mm/min).

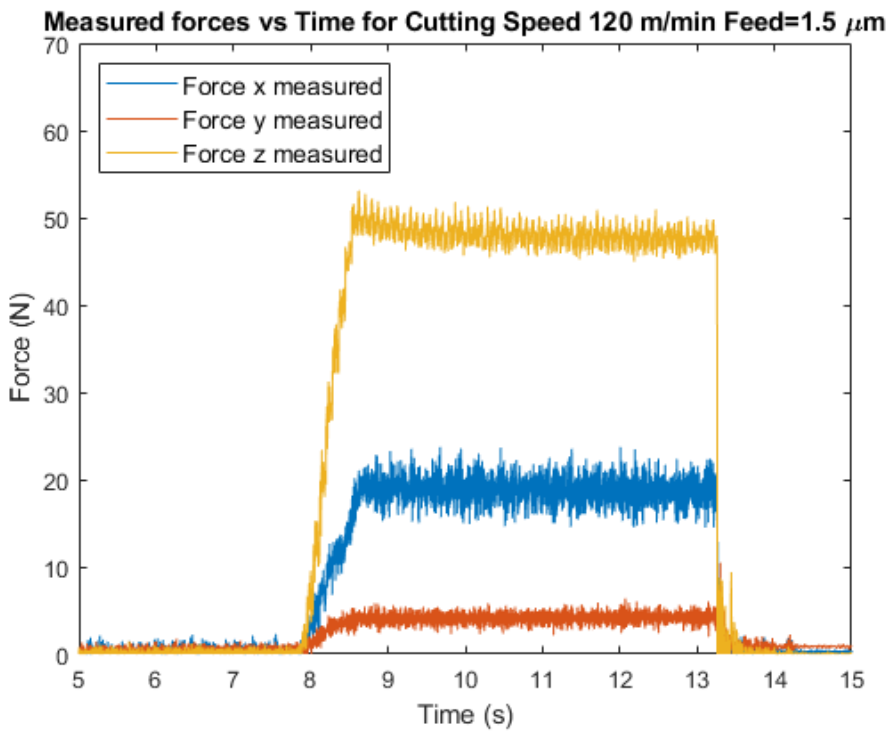


Figure 159: Typical cutting forces (RPM = 720, Cutting speed=120 m/min, feed = 0.0015 mm/rev OR Feed rate of mm/min = N. F = 720 * 0.0015 mm/rev = 1.08 mm/min).

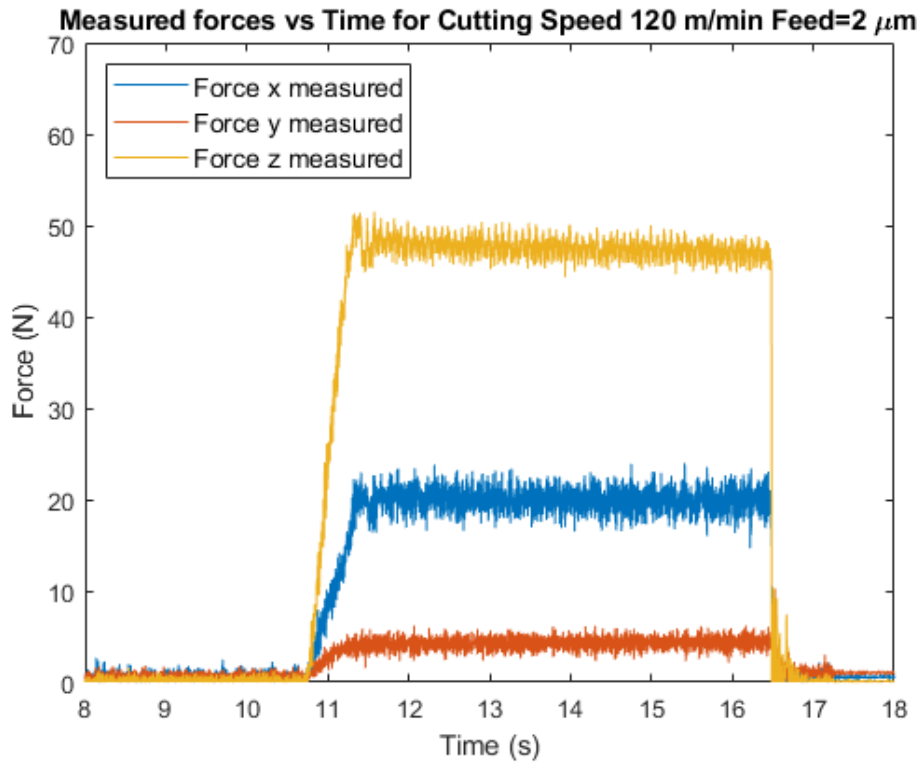


Figure 160: Typical cutting forces (RPM = 720, Cutting speed=120 m/min, feed = 0.002 mm/rev OR Feed rate of mm/min = $N \cdot F = 720 * 0.002 \text{ mm/rev} = 1.44 \text{ mm/min}$).

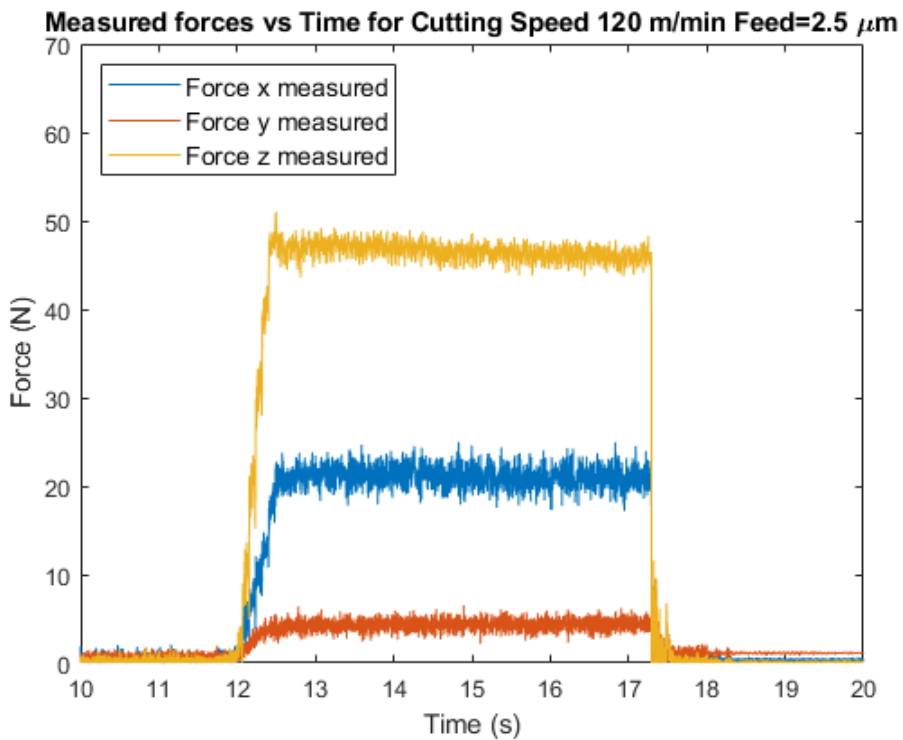


Figure 161: Typical cutting forces (RPM = 720, Cutting speed=120 m/min, feed = 0.0025 mm/rev OR Feed rate of mm/min = $N \cdot F = 720 * 0.0025 \text{ mm/rev} = 1.8 \text{ mm/min}$).

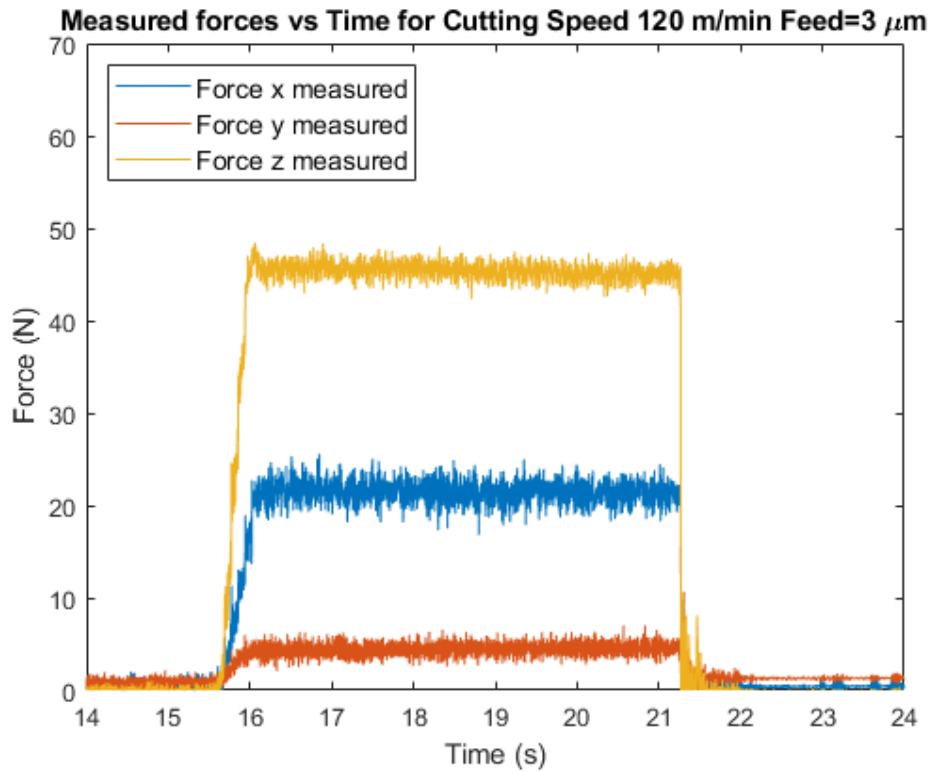


Figure 162: Typical cutting forces (RPM = 720, Cutting speed=120 m/min, feed = 0.003 mm/rev OR Feed rate of mm/min = $N \cdot F = 720 * 0.003 \text{ mm/rev} = 2.16 \text{ mm/min}$).

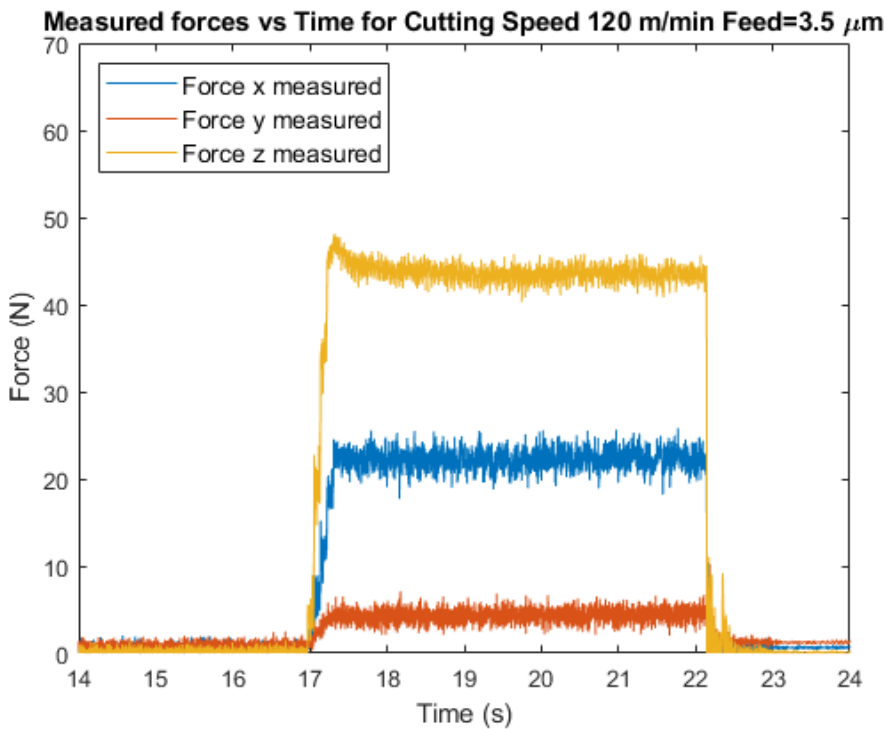


Figure 163: Typical cutting forces (RPM = 720, Cutting speed=120 m/min, feed = 0.0035 mm/rev OR Feed rate of mm/min = $N \cdot F = 720 * 0.0035 \text{ mm/rev} = 2.52 \text{ mm/min}$).

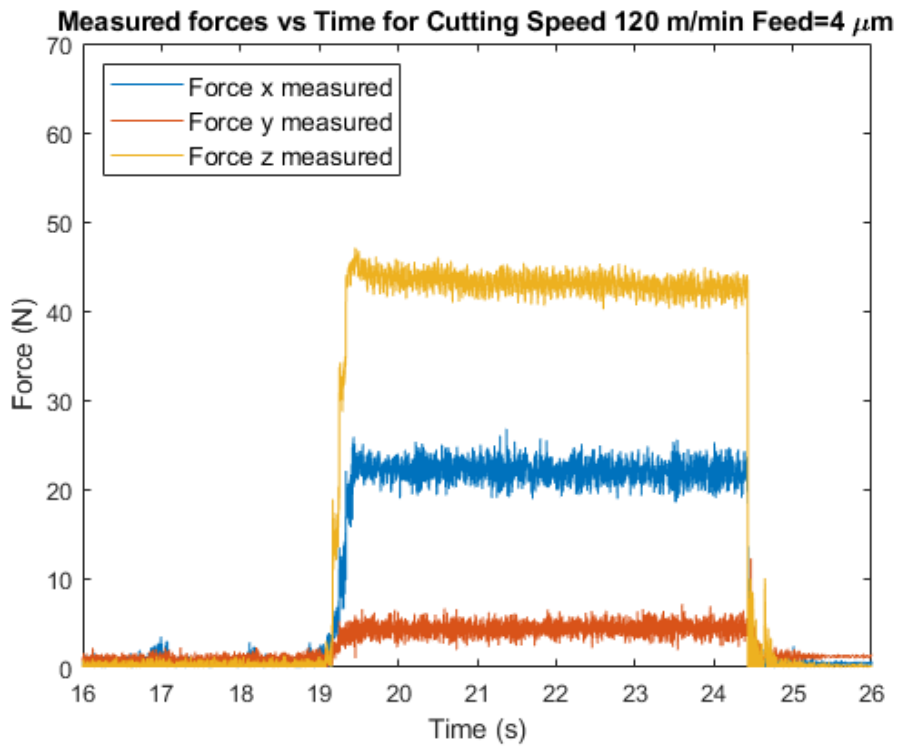


Figure 164: Typical cutting forces (RPM = 720, Cutting speed=120 m/min, feed = 0.004 mm/rev OR Feed rate of mm/min = N. $F = 720 * 0.004 \text{ mm/rev} = 2.88 \text{ mm/min}$).

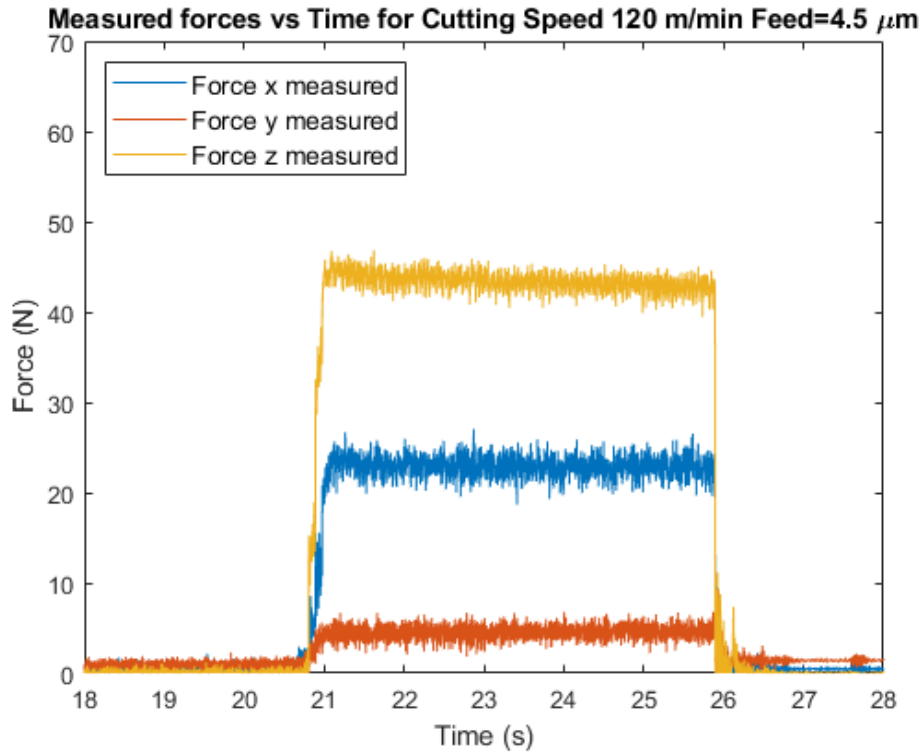


Figure 165: Typical cutting forces (RPM = 720, Cutting speed=120 m/min, feed = 0.0045 mm/rev OR Feed rate of mm/min = N. $F = 720 * 0.0045 \text{ mm/rev} = 3.24 \text{ mm/min}$).

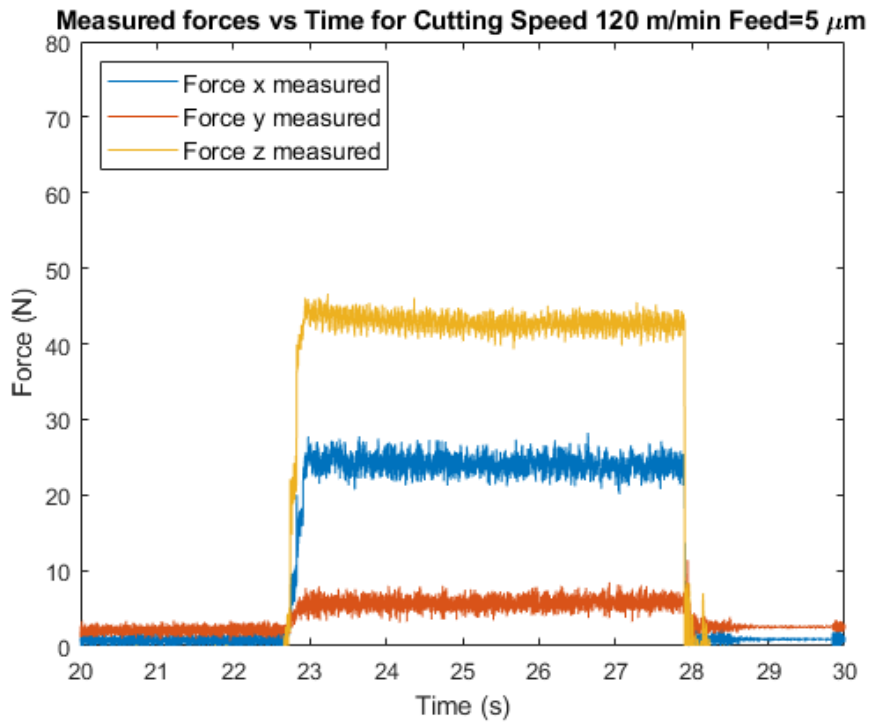


Figure 166: Typical cutting forces (RPM = 720, Cutting speed=120 m/min, feed = 0.005 mm/rev OR Feed rate of mm/min = N. $F = 720 * 0.005 \text{ mm/rev} = 3.6 \text{ mm/min}$).

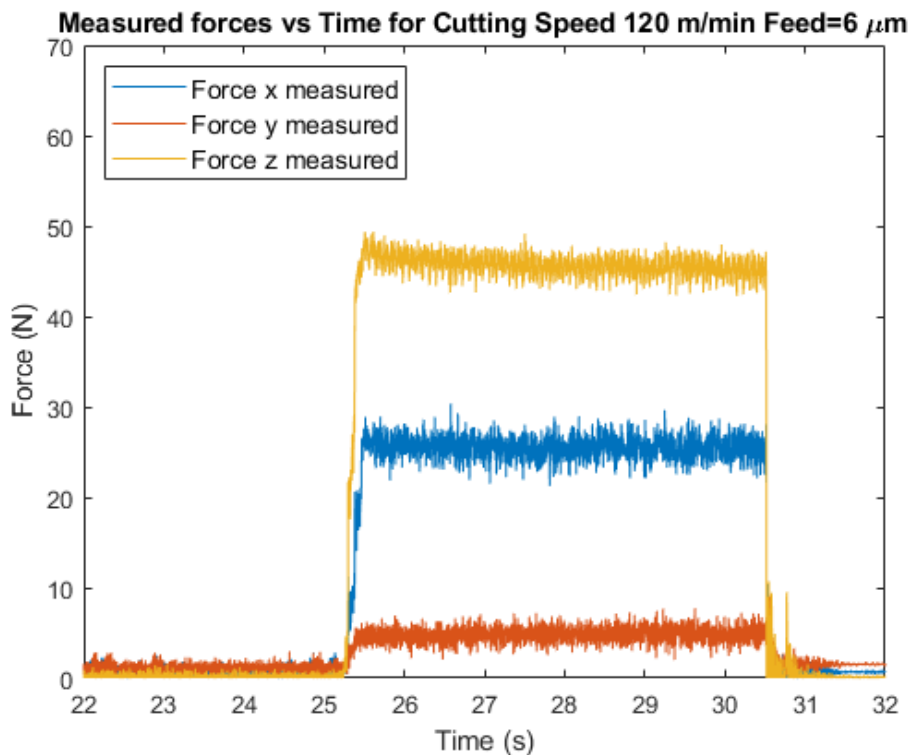


Figure 167: Typical cutting forces (RPM = 720, Cutting speed=120 m/min, feed = 0.006 mm/rev OR Feed rate of mm/min = N. $F = 720 * 0.006 \text{ mm/rev} = 4.32 \text{ mm/min}$).

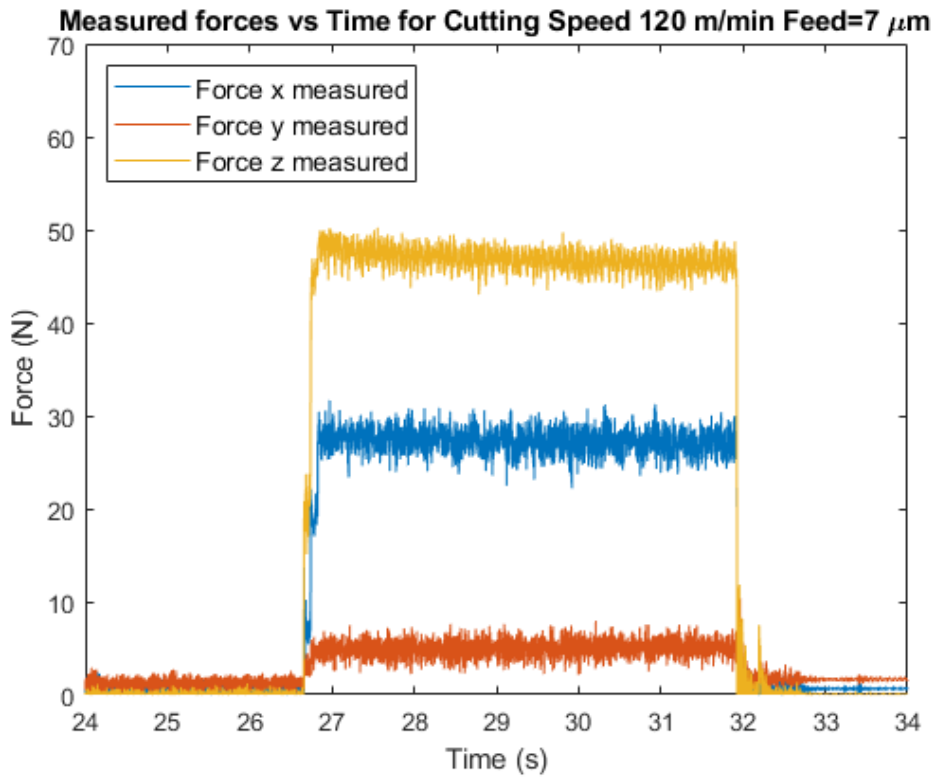


Figure 168: Typical cutting forces (RPM = 720, Cutting speed=120 m/min, feed = 0.007 mm/rev OR Feed rate of mm/min = $N \cdot F = 720 * 0.007 \text{ mm/rev} = 5.04 \text{ mm/min}$).

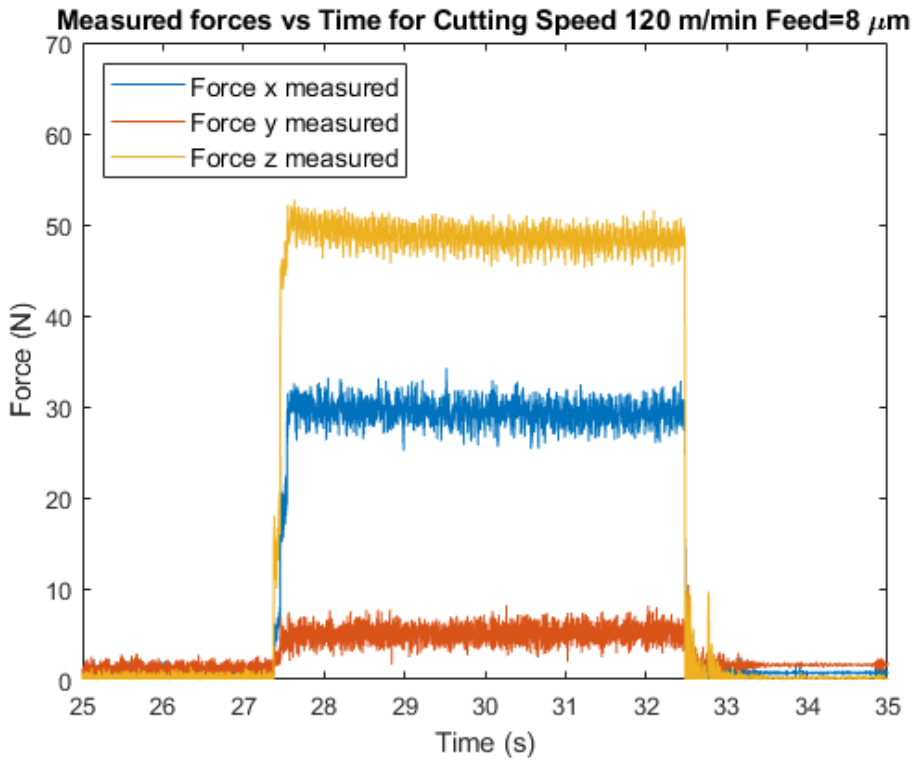


Figure 169: Typical cutting forces (RPM = 720, Cutting speed=120 m/min, feed = 0.008 mm/rev OR Feed rate of mm/min = $N \cdot F = 720 * 0.008 \text{ mm/rev} = 5.76 \text{ mm/min}$).

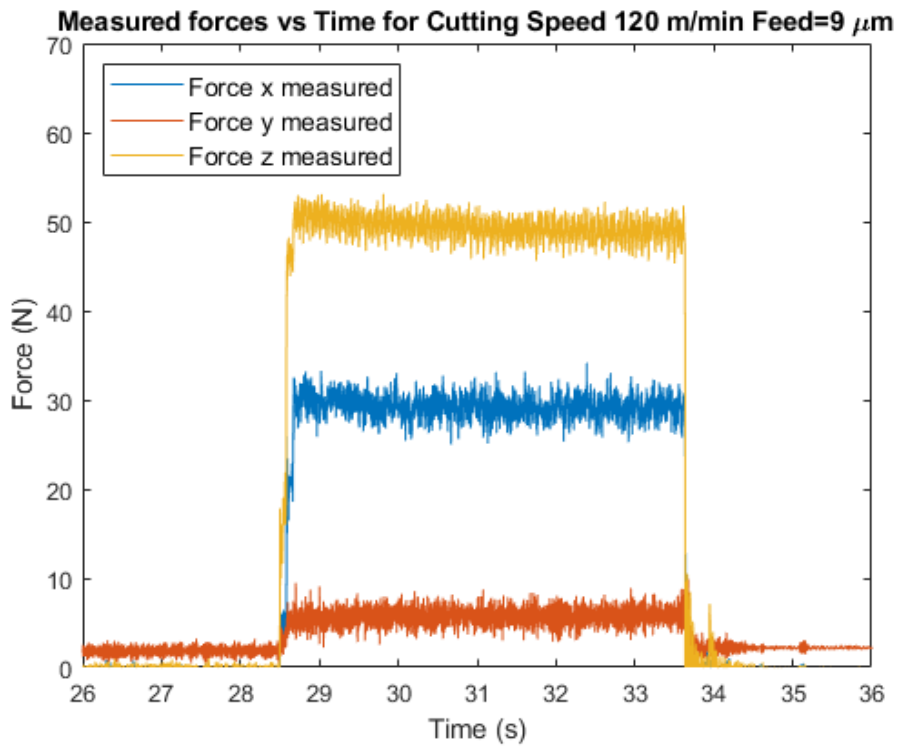


Figure 170: Typical cutting forces (RPM = 720, Cutting speed=120 m/min, feed = 0.009 mm/rev OR Feed rate of mm/min = N. $F = 720 * 0.009 \text{ mm/rev} = 6.48 \text{ mm/min}$).

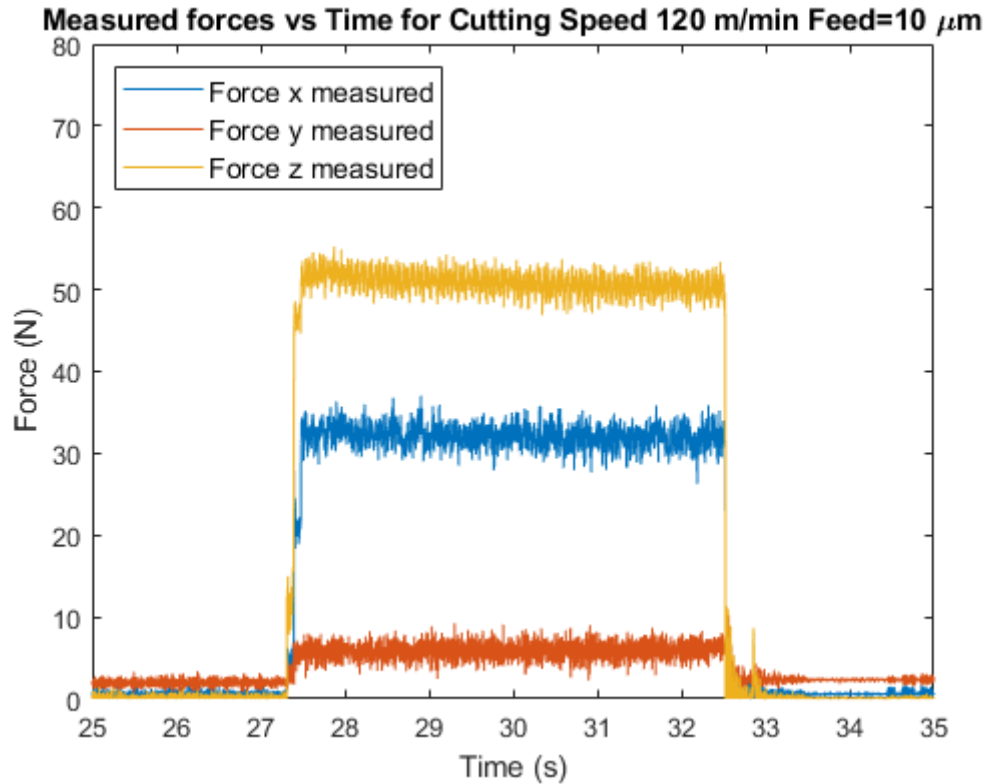


Figure 171: Typical cutting forces (RPM = 720, Cutting speed=120 m/min, feed = 0.01 mm/rev OR Feed rate of mm/min = N. $F = 720 * 0.01 \text{ mm/rev} = 7.2 \text{ mm/min}$).

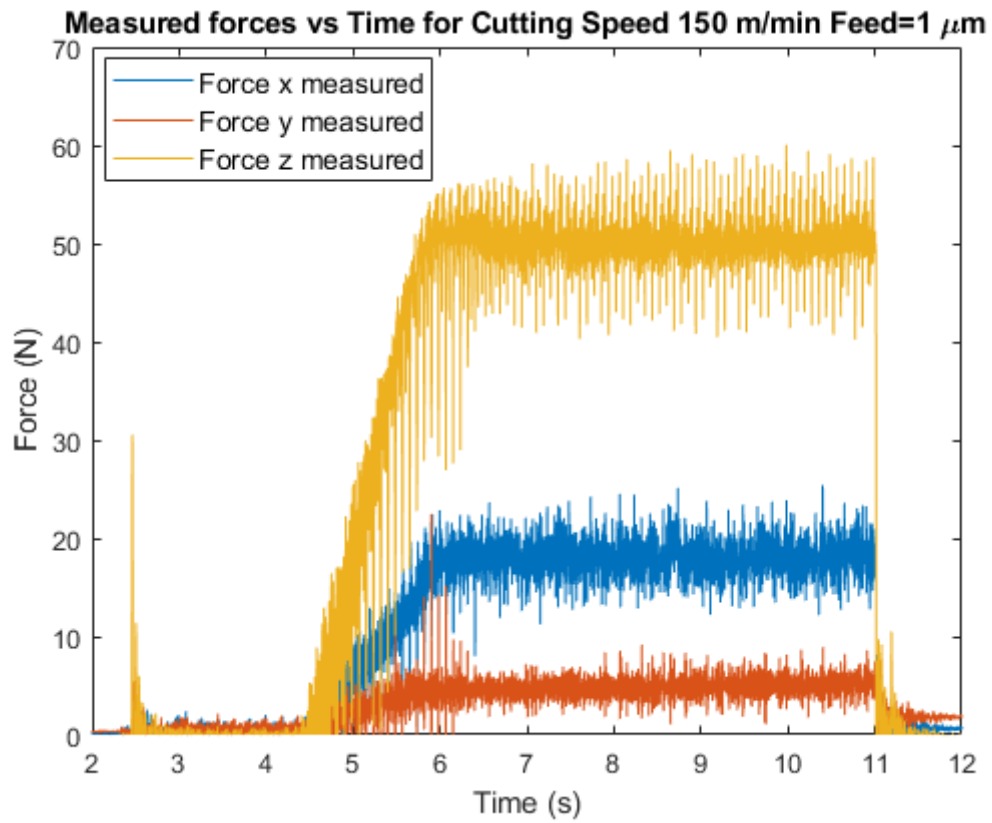


Figure 172: Typical cutting forces (RPM = 720, Cutting speed=150 m/min, feed = 0.0005 mm/rev OR Feed rate of mm/min = $N \cdot F = 720 * 0.0005$ mm/rev = 0.36 mm/min).

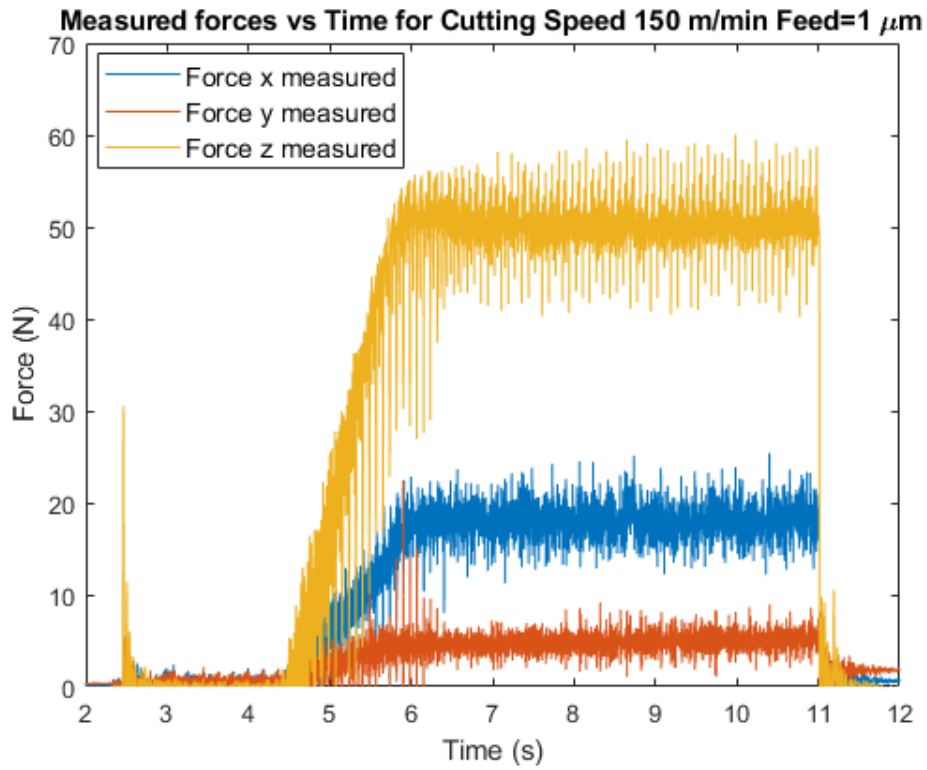


Figure 173: Typical cutting forces (RPM = 720, Cutting speed=150 m/min, feed = 0.001 mm/rev OR Feed rate of mm/min = $N \cdot F = 720 * 0.001 \text{ mm/rev} = 0.72 \text{ mm/min}$).

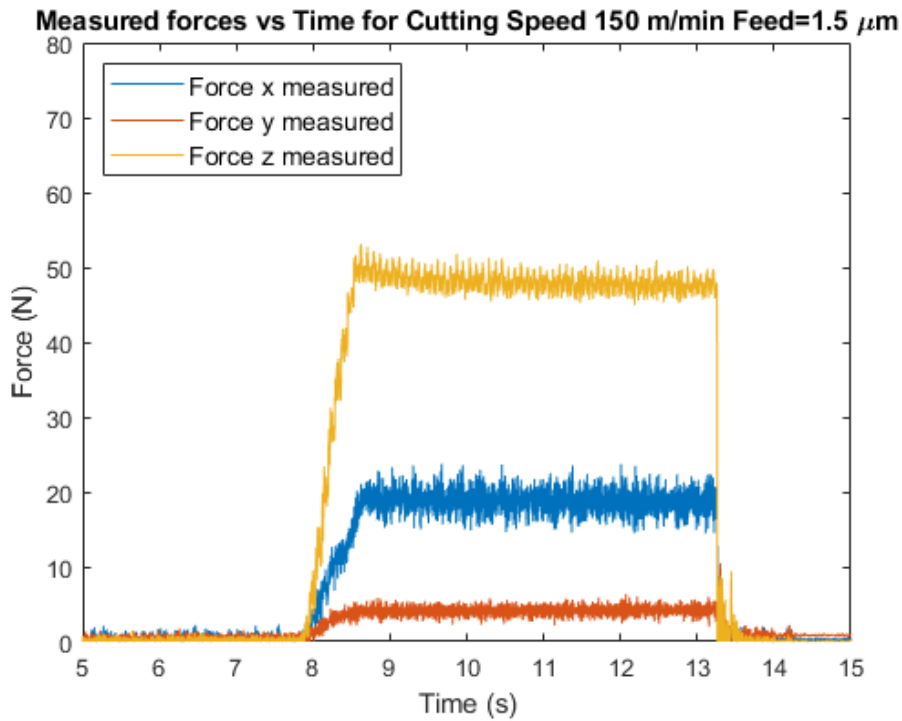


Figure 174: Typical cutting forces (RPM = 720, Cutting speed=150 m/min, feed = 0.0015 mm/rev OR Feed rate of mm/min = $N \cdot F = 720 * 0.0015 \text{ mm/rev} = 1.08 \text{ mm/min}$).

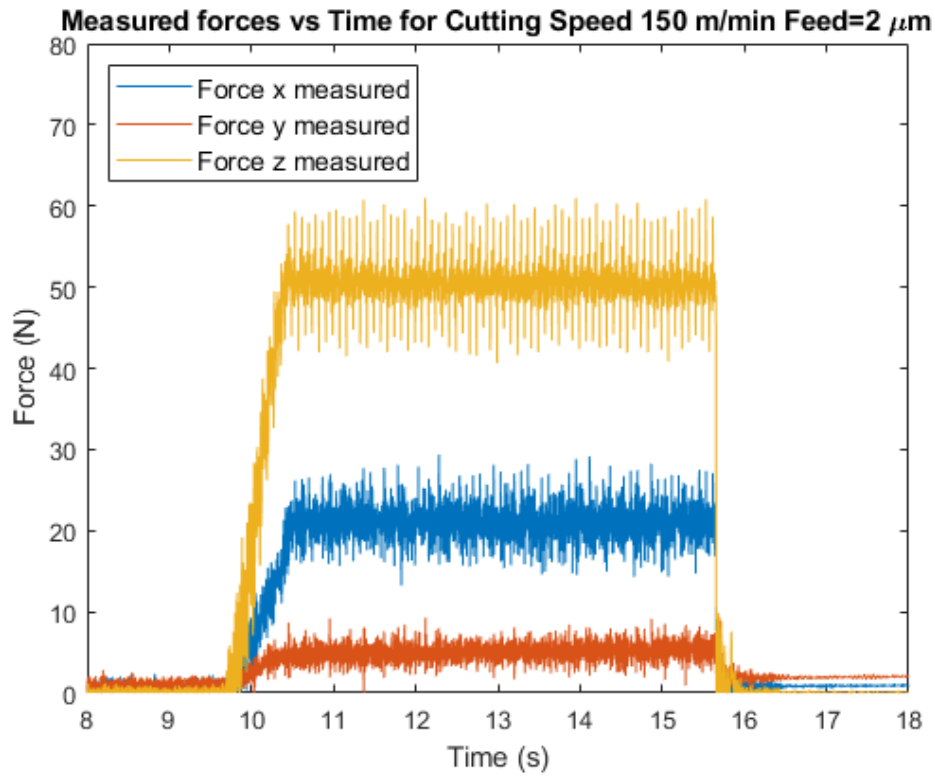


Figure 175: Typical cutting forces (RPM = 720, Cutting speed=150 m/min, feed = 0.002 mm/rev OR Feed rate of mm/min = $N \cdot F = 720 * 0.002 \text{ mm/rev} = 1.44 \text{ mm/min}$).

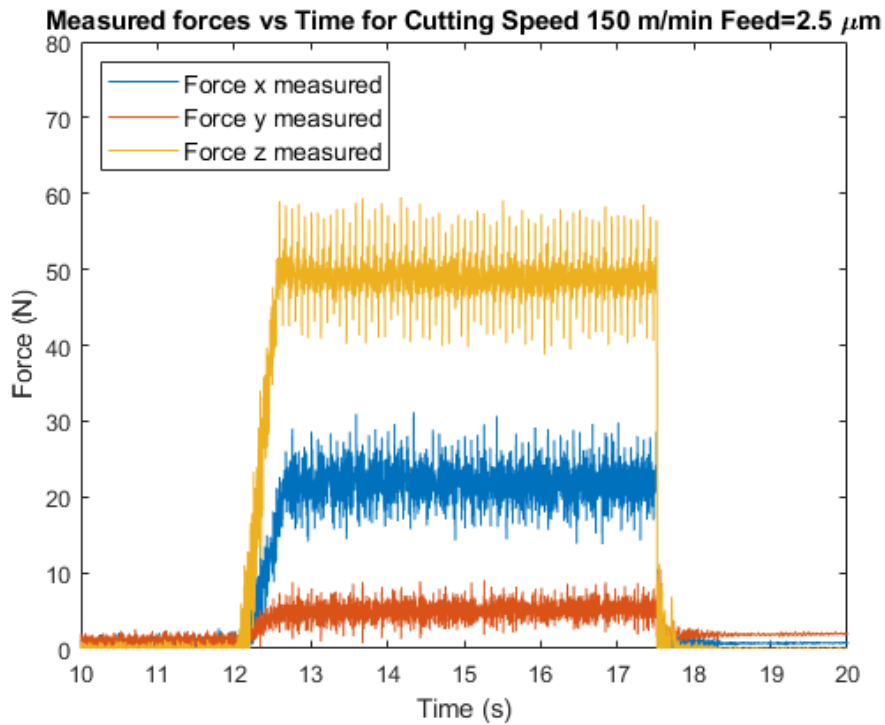


Figure 176: Typical cutting forces (RPM = 720, Cutting speed=150 m/min, feed = 0.0025 mm/rev OR Feed rate of mm/min = $N \cdot F = 720 * 0.0025 \text{ mm/rev} = 1.8 \text{ mm/min}$).

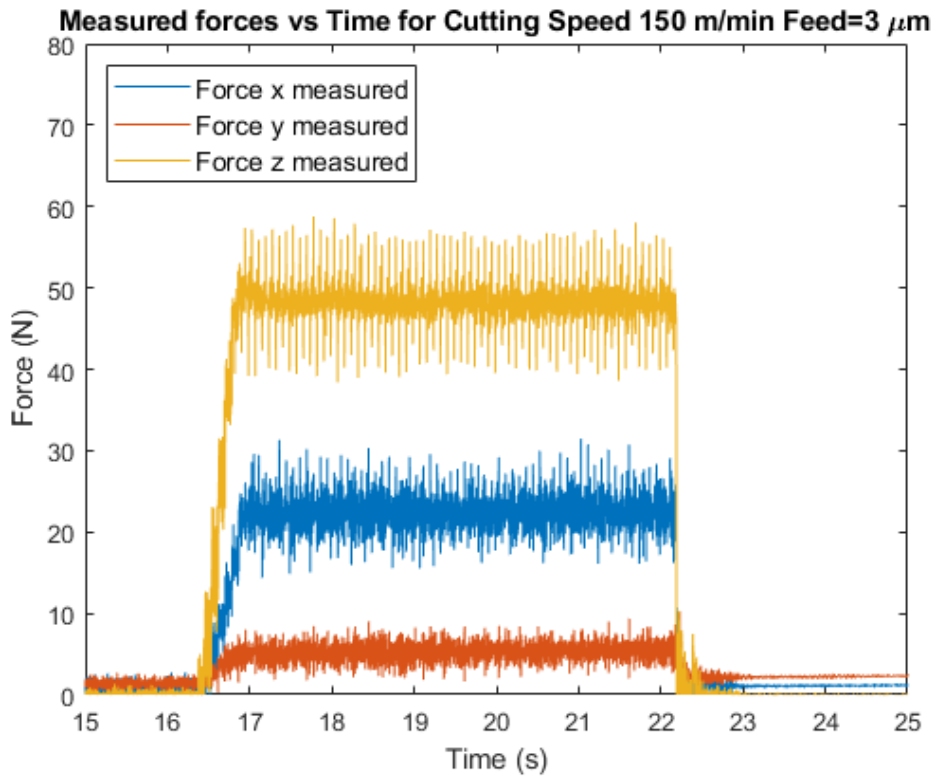


Figure 177: Typical cutting forces (RPM = 720, Cutting speed=150 m/min, feed = 0.003 mm/rev OR Feed rate of mm/min = N. F = 720 * 0.003 mm/rev = 2.16 mm/min).

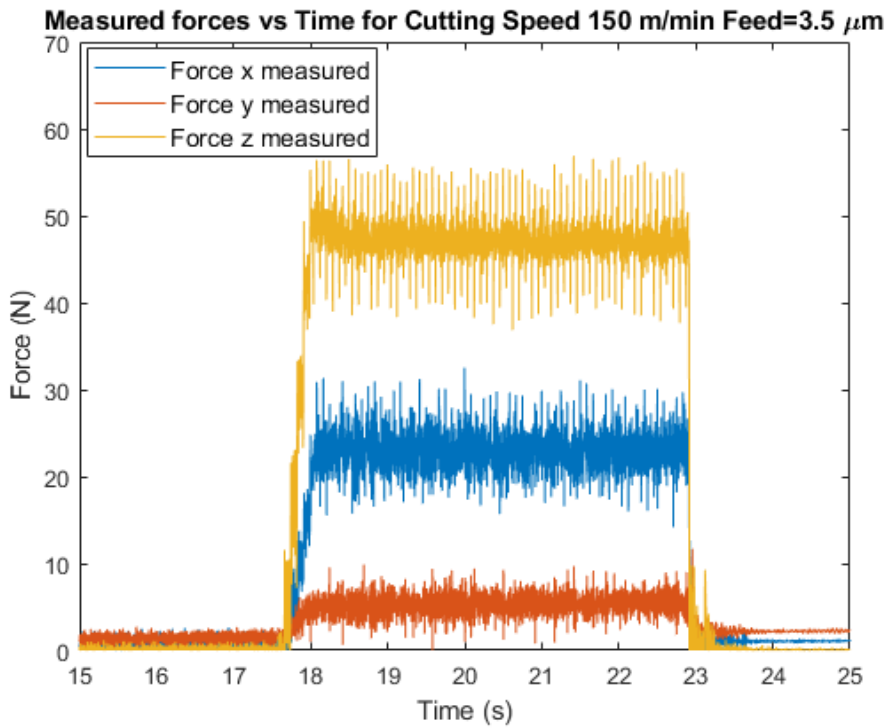


Figure 178: Typical cutting forces (RPM = 720, Cutting speed=150 m/min, feed = 0.0035 mm/rev OR Feed rate of mm/min = N. F = 720 * 0.0035 mm/rev = 2.52 mm/min).

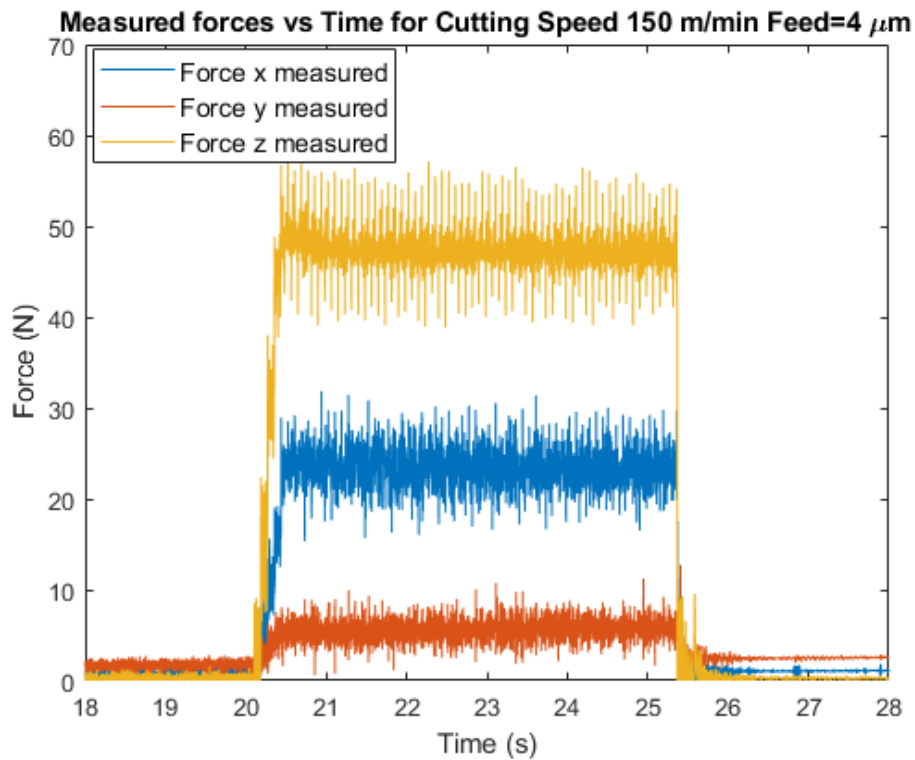


Figure 179: Typical cutting forces (RPM = 720, Cutting speed=150 m/min, feed = 0.004 mm/rev OR Feed rate of mm/min = N. $F = 720 * 0.004 \text{ mm/rev} = 2.88 \text{ mm/min}$).

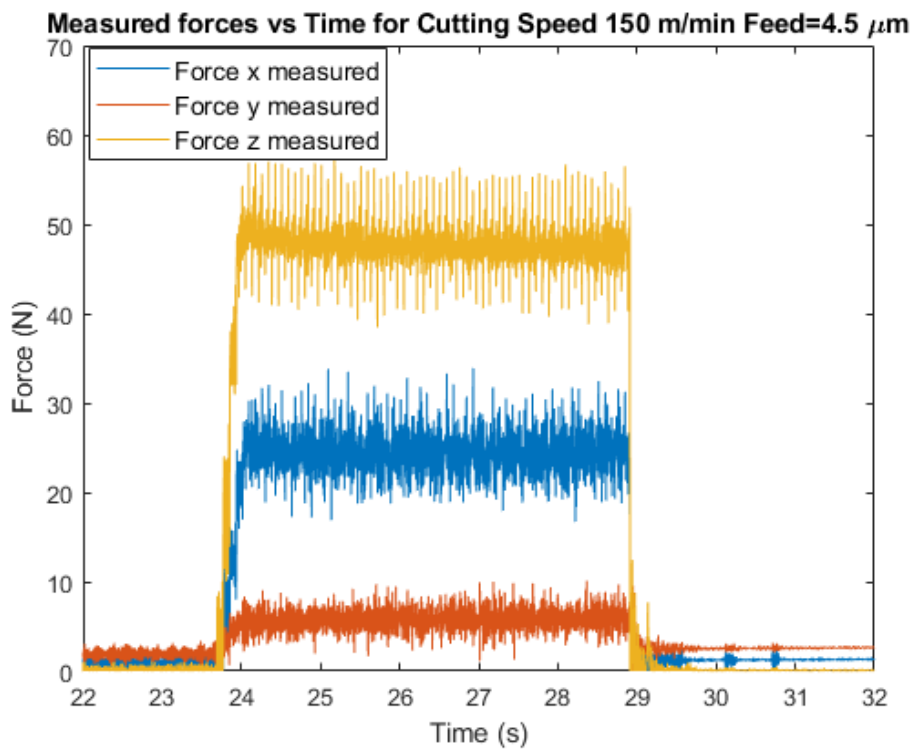


Figure 180: Typical cutting forces (RPM = 720, Cutting speed=150 m/min, feed = 0.0045 mm/rev OR Feed rate of mm/min = N. $F = 720 * 0.0045 \text{ mm/rev} = 3.24 \text{ mm/min}$).

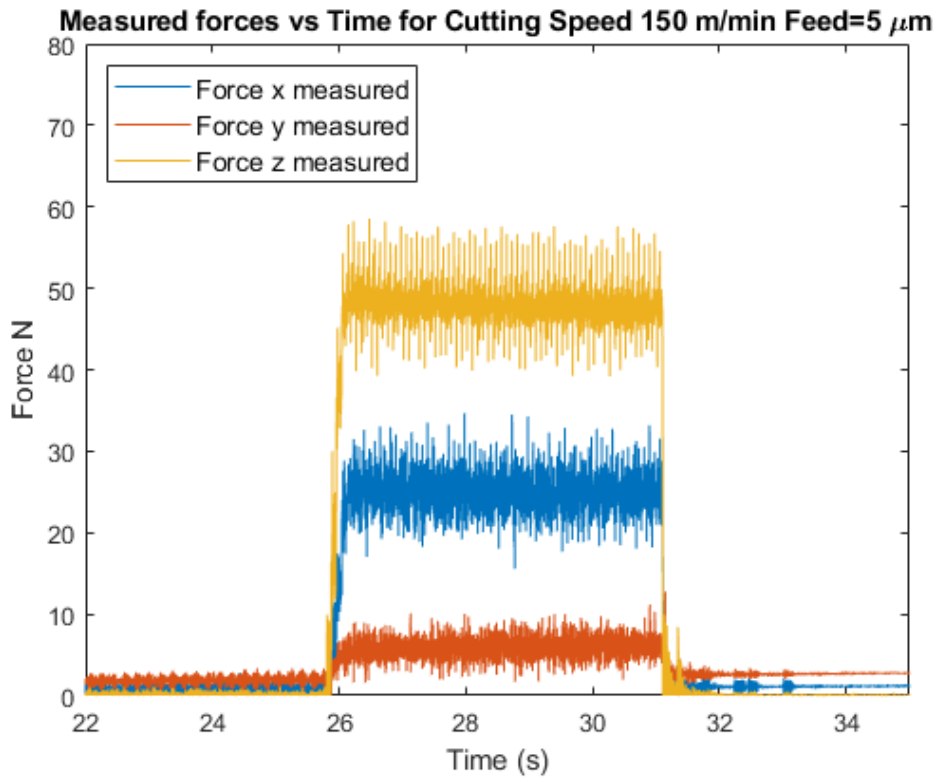


Figure 181: Typical cutting forces (RPM = 720, Cutting speed=150 m/min, feed = 0.005 mm/rev OR Feed rate of mm/min = N. $F = 720 * 0.005 \text{ mm/rev} = 3.6 \text{ mm/min}$).

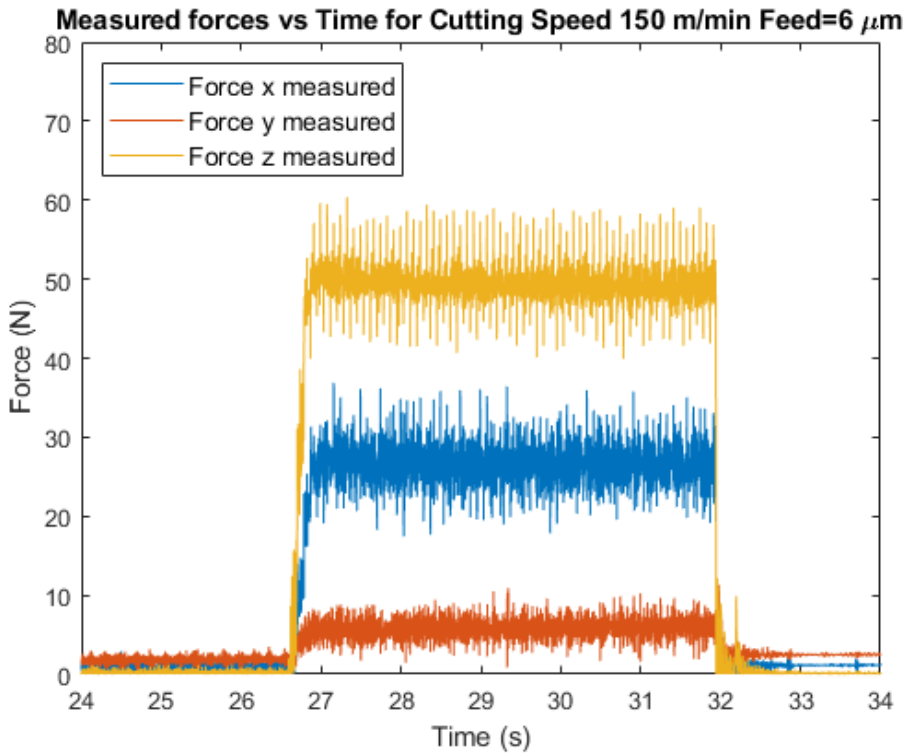


Figure 182: Typical cutting forces (RPM = 720, Cutting speed=150 m/min, feed = 0.006 mm/rev OR Feed rate of mm/min = N. $F = 720 * 0.006 \text{ mm/rev} = 4.32 \text{ mm/min}$).

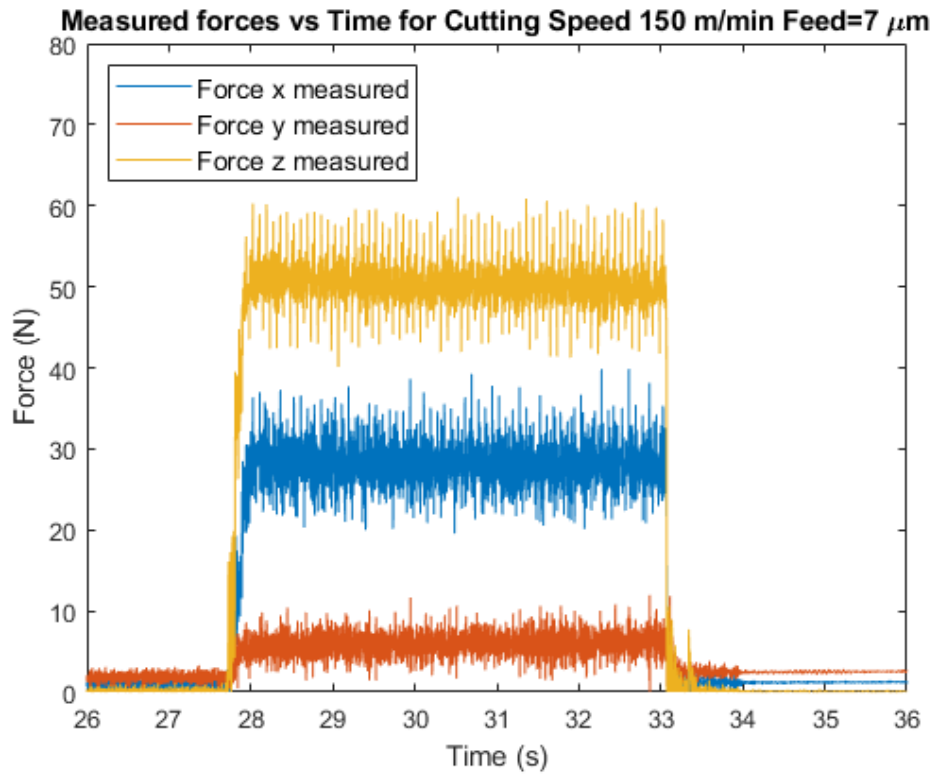


Figure 183: Typical cutting forces (RPM = 720, Cutting speed=150 m/min, feed = 0.007 mm/rev OR Feed rate of mm/min = $N \cdot F = 720 \cdot 0.007 \text{ mm/rev} = 5.04 \text{ mm/min}$).

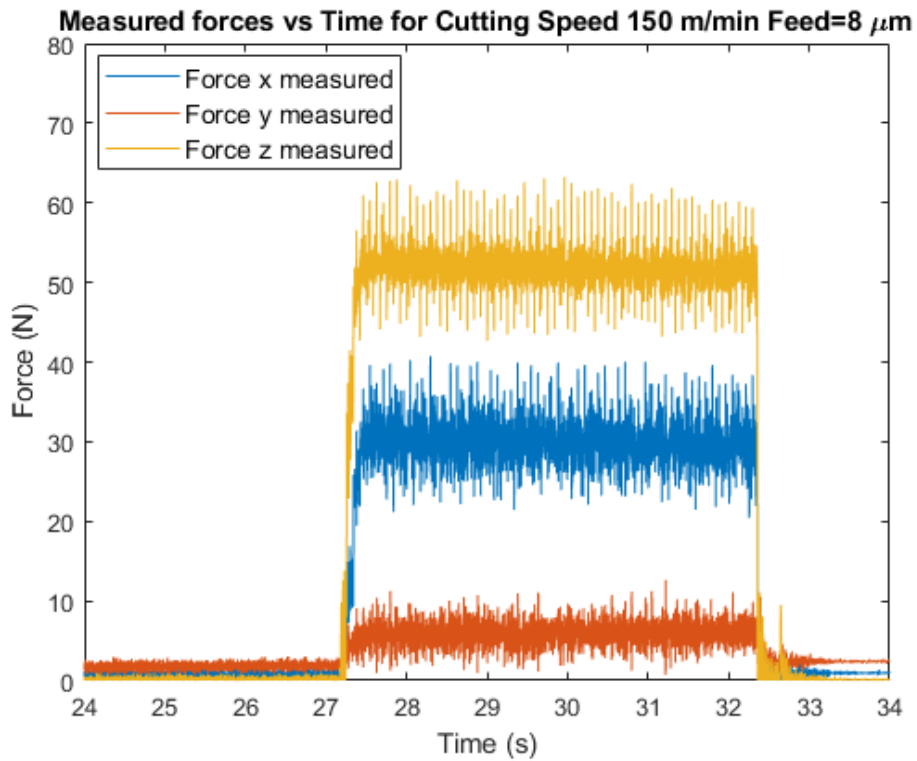


Figure 184: Typical cutting forces (RPM = 720, Cutting speed=150 m/min, feed = 0.008 mm/rev OR Feed rate of mm/min = $N \cdot F = 720 \cdot 0.008 \text{ mm/rev} = 5.76 \text{ mm/min}$).

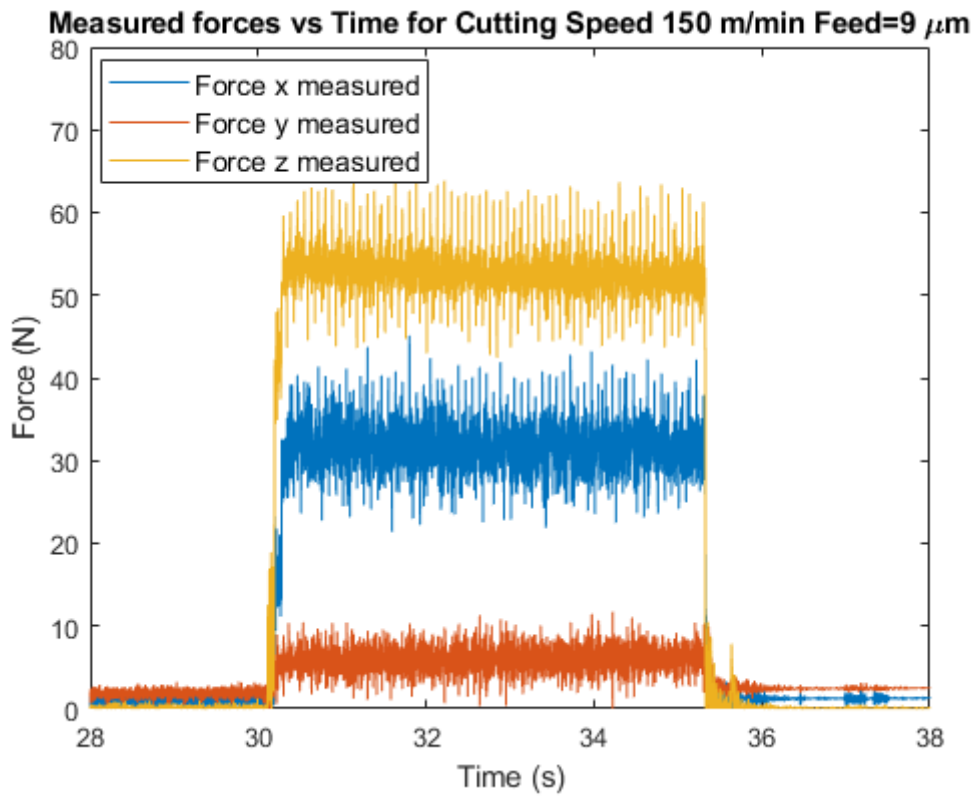


Figure 185: Typical cutting forces (RPM = 720, Cutting speed=150 m/min, feed = 0.009 mm/rev OR Feed rate of mm/min = N. $F = 720 * 0.009 \text{ mm/rev} = 6.48 \text{ mm/min}$).

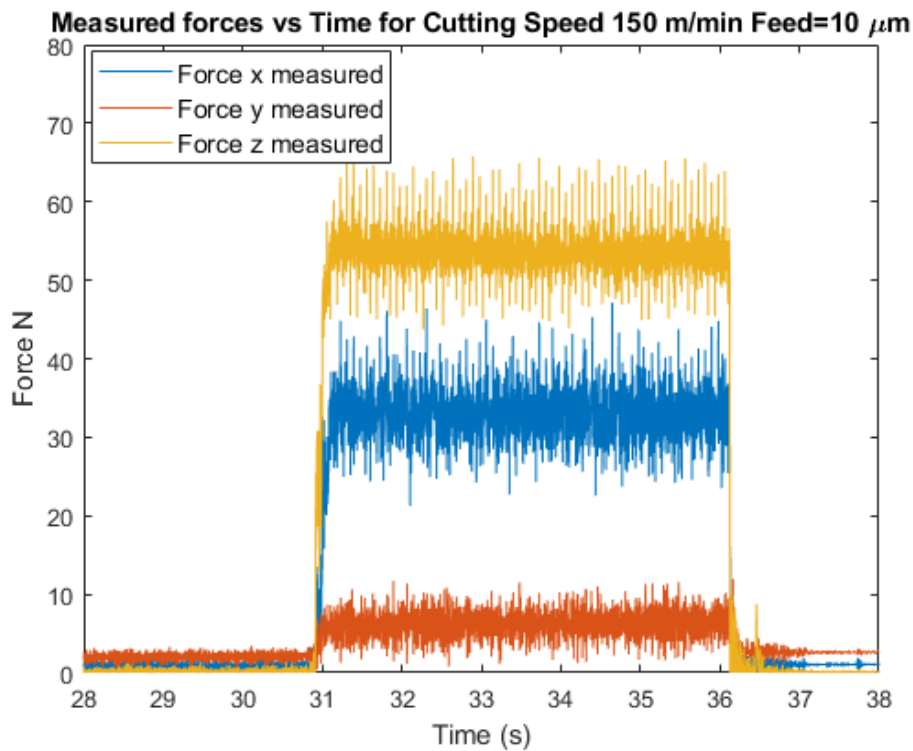


Figure 186: Typical cutting forces (RPM = 720, Cutting speed=150 m/min, feed = 0.01 mm/rev OR Feed rate of mm/min = N. $F = 720 * 0.01 \text{ mm/rev} = 7.2 \text{ mm/min}$).

